



University *of* Glasgow

Harmonic Domain Modelling of Wind-based Micro-grids

Majid Mumtaz

Submitted in fulfilment of the requirements for
the degree of Doctor of Philosophy (Ph.D)

School of Engineering
College of Science and Engineering
University of Glasgow

September 2012

© Majid Mumtaz

Abstract

Power quality problems have been identified with wind generation sites and their connection with the distribution network. The main aim of this research is to put forward and develop models for the conventional components in a power system, but with provision for the representation of wind farms. To develop the necessary tools and computational methods that can be embedded in programmes in such a way that economic and security assessments can be carried out on present and future wind-based networks that are likely to be highly decentralized in future. The goal has been accomplished using M_{ATLAB} programming and the ‘power library’ tools.

In the early chapters, the main challenges associated with the power quality problems in micro-grid connected wind power plants have been investigated and possible approaches to solve the problem have been quantified and assessed. Assessing the frequency response of an electrical power system, with conventional generation and with wind generators, has been identified as a likely way forward to gaining a fundamental understanding of the impact of ‘harmonic currents’ and ‘harmonic voltages’ in such power networks.

A starting point was to develop a ‘transformer model’ in the ‘harmonic domain’, and this has been key to progressing harmonic domain models of other elements found in systems with wind-power generation, such as synchronous generators and induction generators. The various non-linear effects found in transformer magnetic cores have been explored, with emphasis placed on the effect of core saturation as it leads to high harmonic current generation. As magnetic core saturation can be presented by means of ‘polynomial functions’ the work has focused on ‘harmonic studies’. This approach is amenable to very speedy harmonic evaluation, using repeated convolution and several efficient algorithms have been researched and reported on here.

Harmonic domain models of a synchronous generator have been developed using the ‘Hartley’ and the ‘Fourier transform’ approach. In these models it has been assumed that the ‘damper winding’ is short circuited and only the DC component of the field excitation has been taken into account. The admittance matrices of the synchronous generator in the $dq0$ and the $\alpha\beta\gamma$ axis are derived and used to obtain the admittance in abc coordinates by means of the

transformation matrices. These admittance matrices illustrate, rather well, the frequency conversion effect present in the synchronous generator.

Also, owing to its extensive use in wind farms, modelling of an induction generator has been performed. Because this generator's rotor-shaft is coupled to a wind turbine, importance has also been attached to the modelling of its mechanical input part. When used in a load flow programme, the model for the induction generator provides a 'new' simulation facility allowing analyses now of electrical power systems in which wind is an important basic source of energy.

Finally, a harmonic analyses of the penetration of the harmonic currents generated by the various models has been used to determine the effect of wind generated power on the network at the point of common coupling (PCC). This has provided an insight as to the requirements of the network to accept wind generated power, without exceeding G5/4-1 recommendations.

And in conclusion the final part of the research points toward the future with suggestions of further useful work that could be undertaken.

Acknowledgement

I would like to acknowledge those who have played an important part during my stay at the University of Glasgow; in particular I wish to thank Dr. Leslie C. Campbell, Professor Margaret Lucas and Professor Enrique Acha for their support and help during the preparation of this research work.

Deep from my heart, I say thanks to my friends and all the members of my family whose encouragement gave me strength to progress towards a more successful life.

To my wife and my little daughters, Maryam and Sarah; please excuse me for I have been too busy to give you time you all deserved. You are a great blessing to me.

Finally, I greatly appreciate the financial support provided by *MUST* and *HEC*, without which this project might not have been possible.

Contents

Abstract	i
Acknowledgements	iii
Contents	iv
Acronyms and Nomenclature	ix
List of Figures	xv
List of Tables	xix
1. Introduction	1
1.1 An overview of power system harmonics	1
1.1.1 Causes of harmonic distortion in power systems	2
1.1.2 Impact of harmonics on power system	5
1.1.3 Elimination of harmonics	9
1.1.4 Measurement and simulation of harmonics	13
1.1.5 Standards	17
1.2 Grid-connected wind-power plants and power quality issues	22
1.2.1 Frequency change, harmonics and inter-harmonics	22
1.2.2 Cost of quality supply	24
1.2.3 Lack of control over source	24
1.2.4 Quality and reliability	24
1.2.5 Voltage flickers	25
1.2.6 Fault protection system	25
1.3 Micro-grids	26
1.3.1 Definition and overview	26
1.3.2 Contemporary and future micro-grids	29
1.4 The modelling	32
1.5 Thesis outline	34
1.6 References	36

2. Harmonic Impedance at The Point of Common Coupling (PCC)	40
2.1 Introduction	40
2.2 Measurement of system's harmonic impedance	41
2.2.1 High pre-existing harmonic voltage	41
2.2.2 Powerful harmonic current source	42
2.3 System response characteristics	42
2.3.1 Parallel resonance	44
2.3.2 Effect of parallel resistive load	52
2.3.3 System response referred to LV side (400V)	53
2.4 Harmonic resonance due to wind power plants	56
2.4.1 Collector and transmission cable	56
2.4.2 Reactors and capacitor banks	57
2.5 System response with an induction generator added	57
2.5.1 Impact of VAR compensation, power factor correction apparatus and starting capacitor on frequency response	64
2.6 Calculation of total harmonic distortion (THD)	65
2.7 Harmonics out of an inverter	70
2.7.1 Calculation of THD based on an inverter output	74
2.8 Summary	75
2.9 References	76
3. Harmonic Domain Algebra	80
3.1 Introduction	80
3.2 Orthogonal functions	80
3.3 Periodic functions	81
3.4 The Fourier series	82
3.5 The Fourier transform	84
3.5.1 Discrete Fourier transform (DFT)	85
3.5.2 Fast Fourier transform (FFT)	87
3.6 Polynomial evaluation using Fourier	88

3.7	The Hartley transforms	94
3.7.1	Discrete Hartley transform (DHT)	95
3.7.2	Fast Hartley transform (FHT)	95
3.7.3	Polynomial evaluation using Hartley	95
3.8	A critical comparison of the Fourier and Hartley series amid at harmonic domain applications	98
3.9	Summary	103
3.10	References	104
4.	Modelling of Power Transformer in Harmonic Domain	105
4.1	Introduction	105
4.2	Nonlinear effects in the transformer core	106
4.2.1	Saturation	106
4.2.2	Eddy currents	107
4.2.3	Hysteresis	107
4.3	Polynomial fitting of the hysteresis curve	110
4.4	Norton equivalent for the magnetization branch in harmonic domain	117
4.5	Full transformer model in harmonic domain	120
4.6	Case study	121
4.7	Generalization to 3-phase transformer	124
4.8	Case study	127
4.9	Harmonic domain iterative solution	131
4.10	Summary	132
4.11	References	132
5.	Harmonic Domain Modelling of Synchronous Generator	137
5.1	Introduction	137
5.2	Synchronous generator under harmonic conditions in the Fourier harmonic domain	142
5.2.1	Machine's Fourier harmonic admittance matrix model in $dq0$	143

axis	
5.2.2 Machine's Fourier harmonic admittance matrix model in $\alpha\beta\gamma$ axis	145
5.2.3 Machine's Fourier harmonic admittance matrix model in abc axis	149
5.3 Synchronous generator's harmonic equivalents	151
5.3.1 Machine's Norton's harmonic equivalent	151
5.3.2 Machine's Thevnin's harmonic equivalent	152
5.4 Synchronous generator under harmonic conditions in the Hartley harmonic domain	153
5.4.1 Machine's Hartley harmonic admittance matrix model in $dq0$ axis	154
5.4.2 Machine's Hartley harmonic admittance matrix model in $\alpha\beta\gamma$ axis	157
5.4.3 Machine's Hartley harmonic admittance matrix model in abc axis	162
5.5 Case study	164
5.6 A comparison of the Fourier and the Hartley based admittance matrix models of synchronous generator	167
5.7 Summary	171
5.8 References	172
6. Induction Generator Model for Wind-farm Applications	177
6.1 Introduction to wind-based power	177
6.1.1 Types of wind turbines	179
6.1.1.1 Horizontal axis wind turbines	179
6.1.1.2 Vertical axis wind turbines	180
6.1.2 Anatomy of wind turbine	181
6.1.3 Modelling of wind turbine	192
6.2 Induction generator modelling	193

6.2.1	Reference frame transformation of induction generator	201
6.2.2	Flux linkages	204
6.2.3	Equations of an induction machine in arbitrary reference frame	205
6.2.4	Induction machine in synchronous rotating reference frame	206
6.2.5	The dynamic equations of induction generator	207
6.2.6	The model	208
6.3	Summary	210
6.4	References	211
 7. Conclusions and Future Work		
7.1	Conclusions	215
7.2	Future Work	216
 APPENDICES		
Appendix I	M _{ATLAB} functions for harmonic domain model of a single-phase transformer	219
Appendix II	M _{ATLAB} functions for harmonic domain model of a three-phase transformer	225
Appendix III	M _{ATLAB} functions for synchronous generator model in the Fourier harmonic domain	232
Appendix IV	M _{ATLAB} functions for synchronous generator model in the Hartley harmonic domain	237
Appendix V	M _{ATLAB} functions for wind turbine model using an induction generator	241

Acronyms and Nomenclature

Acronym/Symbol	Description	Unit
AC	Alternating Current	
DC	Direct Current	
DFIG	Doubly Fed Induction Generator	
DFT	Discrete Fourier Transform	
DG	Distributed Generation	
DHT	Discrete Hartley Transform	
D-VAR	Dynamic-Volt Ampere Reactive	
EHV	Extra High Voltage	
EMC	Electro-Magnetic Compatibility	
ENA	Energy Network Association	
ES	Energy Source	
FACTS	Flexible AC Transmission System	
FDTD	Finite Difference Time Domain	
FFT	Fast Fourier Transform	
FHT	Fast Hartley Transform	
FT	Fourier Transform	
GTO	Gate Turn-off	
HT	Hartley Transform	
HV	High Voltage	
HVDC	High Voltage DC	
IEC	International Electro-technical Commission	
IEEE	Institute of Electronics and Electrical Engineers	
IG	Induction Generator	
IGBT	Insulated Gate Bi-polar Transistor	
IU	Inverter Unit	
LC	Load Controller	
LV	Low Voltage	
LSC	Local Supervisory Controller	
MMF/mm ^f	Magneto Motive Force	<i>A/mA</i>
MV	Mega Volt	

MVA	Mega Volt Ampere	
MVAR/MVAr	Mega Volt Ampere Reactive	
MW	Mega Watt	
PC	Personal Computer	
PCC	Point of Common Coupling	
pf	Power Factor	
PV	Photovoltaic	
PWM	Pulse Width Modulated	
RES	Renewable Energy Source	
RMS/rms	Root Mean Square	
SC	Source Controller	
SCR	Silicon Control Rectifier	
SG	Synchronous Generator	
SVC	Static VAR Compensator	
TDD	Total Demand Distortion	
THD	Total Harmonic Distortion	
TF	Transformer	
TV	Television	
VAR	Volt Ampere Reactive	
VSC	Voltage Source Converter	
WT	Wind Turbine	
$(a+jb)$	Complex number with 'a' real and 'b' imaginary part	
\hat{i}_N	Harmonic Norton equivalent current, three phase	A/mA
A_0	DC component	
A_n	Magnitude of the nth harmonic term	
C_n	Coefficient of the Fourier series in complex form	
L_{Gen}	Generator inductance	H/mH
L_d	d axis self inductance	H/mH
L_{lfd}	Field winding leakage inductance (reflected to the stator)	H/mH
L_{lkd}	d axis damper leakage inductance (reflected to the stator)	H/mH
L_{lkq}	q axis damper leakage inductance (reflected to the stator)	H/mH
L_{ls}	Armature phase leakage inductance	H/mH

L_{md}	d axis coupling inductance	H/mH
L_{mq}	q axis coupling inductance	H/mH
L_{mq}	q axis coupling inductance	H/mH
M_{df}	Field d axis coupling inductance	H/mH
M_{ds}	Damper d axis coupling inductance	H/mH
M_{fs}	Field winding and damper winding mutual inductance	H/mH
M_{qt}	Damper q axis coupling inductance	H/mH
P_w	Wind source power	W
R_{fd}	Field winding resistance (reflected to the stator)	$\Omega/k\Omega$
R_{Gen}	Generator resistance	$\Omega/k\Omega$
R_{kd}	d axis damper wining resistance (reflected to the stator)	$\Omega/k\Omega$
R_{kq}	q axis damper winding resistance (reflected to the stator)	$\Omega/k\Omega$
R_s	Armature phase resistance	$\Omega/k\Omega$
V_{fd}	Field winding terminal voltage (reflected to the stator)	V
V_h	Harmonic voltage	V
V_d, v_d	Armature d axis terminal voltage	V
V_q, v_q	Armature q axis terminal voltage	V
X_C	Capacitive reactance	$\Omega/k\Omega$
X_{Gen}	Generator reactance	$\Omega/k\Omega$
X_L	Inductive reactance	$\Omega/k\Omega$
X_{SC}	Short circuit reactance	$\Omega/k\Omega$
X_t	Transformer reactance	$\Omega/k\Omega$
Z_h	Harmonic impedance	$\Omega/k\Omega$
i_{fd}	Field winding terminal current (reflected to the stator)	A/mA
i_h	Harmonic current	A/mA
i_d	Armature d axis terminal current	A/mA
i_{kd}	d axis damper winding current (reflected to the stator)	A/mA
i_{kq}	q axis damper winding current (reflected to the stator)	A/mA

i_{kq}	q axis damper winding current (reflected to the stator)	A/mA
i_q	Armature q axis terminal current	A/mA
i_t, i_s	Damper winding current	A/mA
v_s, v_r	Stator, rotor respective voltage	V
v_s, v_t	Damper respective winding voltage	V
θ_n	Phase angle of the n th harmonic term	rad
λ_d	Total armature flux in d axis	Wb/mWb
λ_q	Total armature flux in q axis	Wb/mWb
$[X]$	The matrix X	
$[X]^{-1}$	Inverse of the matrix X	
$[X]^t, [X]'$	Transpose of the matrix X	
ΔT	Interval between two consecutive steps in sampling function	
Δi	Incremental magnetization current	
$\Delta \phi$	Incremental flux	
A	Area of wind parcel	m^2
$a_0, a_n, b_n,$	Coefficients of the Fourier series	
B	Flux density\Susceptance	$tesla$
C	Capacitance\ Connection matrix	
C_p	Power coefficient	
D	Diagonal matrix\ Derivative matrix	
$d, q; \alpha, \beta; x, y$	Co-ordinate axis	
E	Peak amplitude of the excitation	
f	Frequency of supply	Hz
F	Magneto motive force (mmf)	A/mA
$F(k)$	Notation used for the Fourier transform	
F_{AB}	The difference between mmf at 'A' and 'B'	
F_n	Incremental mmf	
G	Magnetic conductance	$Wb-A^{-1}$
Gen	Short for Generator	
G_{rr}	Rotor self inductance, rotating	H/mH
G_{rs}	Rotor-stator mutual inductance	H/mH

G_{sr}	Satator-rotor mutual inductance	H/mH
G_{ss}	Stator self inductance, stationary	H/mH
h	Harmonic order	
H	Magnetizing force	Am^{-1}
$H(k)$	Notation used for the Hartley transform	
H_g	Norton harmonic admittance vector for generator	
I	Current	A/mA
I_g	Norton harmonic current vector for generator	
I_N	Harmonic Norton equivalent current, single phase	
j	$\sqrt{(-1)}$	
L	Inductance	H/mH
m	Slope	
N	Total numer of samples\ Number of turns	
$N(E, \omega)$	Gain of non-linearity, a function of E and ω	
P	Power (Watts)/Active power	$W/kW/MW$
p	d/dt	
$P_{per-phase}$	Per-phase power in watts	W/kW
Q	Quality factor\Reactive power	W/kW
R	Resistance	$\Omega/k\Omega$
\mathcal{R}	Reluctance	H^{-1}
R_m	Equivalentr Resistance responsible for certain losses	$\Omega/k\Omega$
R_r	Rotor resistance	$\Omega/k\Omega$
R_s	Stator resistance	$\Omega/k\Omega$
s	Fractional slip, s_0, s_1, s_2 , respectively for zero, positive and negative sequenc	
S_h	Slip at hrmonic frequency h	
T	Transformation matrix	
t	time	sec
TN	Notation for transformer N	
V	Voltage	V
V	Speed of the wind	mph
V_{AB}	Potential difference between point A and point B	V

W	Energy	$J/Watt-hr$
$x(t), y(t)$	Periodic variables	
X_m	Magnetizing reactance	$\Omega/k\Omega$
X_r	Rotor reactance	$\Omega/k\Omega$
X_s	Stator reactance	$\Omega/k\Omega$
Y	Harmonic Norton admittance	
$Y_{abc}, Y_{dq0} \dots$	Admittance matrices in respective frame of reference	
Z	Impedance	$\Omega/k\Omega$
ω_r	Rotor speed	rpm
ω_s	Synchronous speed	rpm
β	Blade pitch angle	$degree$
δ	Filter detuning factor\ Impulse function	
θ	Angle(Electrical degrees\Degrees\radians)	
λ	Tip speed ratio for wind turbine	
ρ	Air density	$kg-m^{-3}$
τ	Time constant	
φ, λ	Magnetic flux linkage	$Wb-t$
ω	Angular velocity of supply voltage vector	$rad-sec^{-1}$
$\omega(t)$	Window function	
ϕ	Magnetic flux	Wb

List of Figures

Fig. 1.1	Types of harmonic voltage distortion	3
Fig. 1.2	Flow of harmonic currents in the network	6
Fig. 1.3	An installation circuit	7
Fig. 1.4	Equivalent phase circuit for the arrangement shown in Fig. 1.3	8
Fig. 1.5	Harmonic filter characteristics	10
Fig. 1.6	A balancer and filter group schematic diagram.	11
Fig. 1.7	Detuned capacitors for power factor correction	13
Fig. 1.8	Typical current waveform of a DC drive	15
Fig. 1.9	The frequency response characteristics	16
Fig. 1.10	Serious harmonic voltage distortion	16
Fig. 1.11	Internal and external grid connection of a wind farm	23
Fig. 1.12	A micro-grid configuration for low and medium voltage levels	27
Fig. 1.13	Micro-grid, and example	29
Fig. 1.14	A schematic of the UK electricity system	31
Fig. 1.15	Schematic of a power system with various forms of wind turbines	33
Fig. 2.1	Thevenin harmonic equivalent of a system.	42
Fig. 2.2	Determination of harmonic impedance Z_h .	42
Fig. 2.3	Frequency response of an assumed purely inductive system.	43
Fig. 2.4	Cable capacitance in the inductive system and equivalent circuit.	45
Fig. 2.5	Frequency response of circuit shown in Fig. 2.4, Case 1 and 2, Table 2.1	47
Fig. 2.6	Frequency response of circuit in Fig. 2.4, Case 4, 5 and 6, Table 2.1	49
Fig. 2.7	Frequency response of circuit in Fig. 2.4, Case 7, 8 and 9, Table 2.1	50
Fig. 2.8	Frequency response of circuit in Fig. 2.4, Case 1, 5 and 9, Table 2.1	51
Fig. 2.9	Effect of parallel load on the frequency response characteristics	52
Fig. 2.10	Frequency response of circuit in Fig. 2.4 with reference to low voltage side, Case 1, 6 and 9, Table 2.2	55
Fig. 2.11	A wind based induction generator connected to the system of Fig 2.4 and its per-phase equivalent electrical circuit	58
Fig. 2.12	Response of the circuit in Fig 2.11, case 2, data from Table 2.3	60

List of Figures

Fig. 2.13	Response of the circuit shown in Fig. 2.11, Case 3, data from Table 2.3	61
Fig. 2.14	Response of the circuit shown in Fig. 2.11, Case 5, data from Table 2.3	62
Fig. 2.15	Response of the circuit shown in Fig. 2.11, Case 6, data from Table 2.3	63
Fig. 2.16	Impact of power factor correction and VAR compensation on system response, data from Table 2.3, Case 1.	65
Fig. 2.17	A typical distribution system and its equivalent circuit diagram	66
Fig. 2.18	Frequency response of the system shown in Fig 2.17	68
Fig. 2.19	Harmonic currents out of 6-pulse thyristor inverter	71
Fig. 2.20	Harmonic currents out of 6-pulse PWM drive	72
Fig. 2.21	DFIG with a rotor, a gear box and a converter	73
Fig. 2.22	A full scale converter configuration	74
Fig. 3.1	An example of a periodic function	81
Fig. 3.2	Fourier series of a square wave.	83
Fig. 3.3	A sample waveform and its discrete Fourier transform	87
Fig. 4.1	Hysteresis loop for three different magnetic materials	108
Fig. 4.2	An assumed nonlinear system	108
Fig. 4.3	Hysteresis loop; flux linkage and excitation current plot, schematic	109
Fig. 4.4	A sample hysteresis loop approximated by four line sections	110
Fig. 4.5	Sampled points on the magnetization curve	111
Fig. 4.6	Variation in magnetization curve with a change in a , b and n	114
Fig. 4.7	Recorded magnetizing characteristics of the transformer	116
Fig. 4.8	Relation between flux, supply voltage and no-load magnetizing current	117
Fig. 4.9	An idealized flux-current characteristic curve	117
Fig. 4.10	Change in flux with change in magnetizing current near operating point	118
Fig. 4.11	Harmonic Norton equivalent for the magnetization branch	119
Fig. 4.12	Harmonic representation of a single-phase transformer	120
Fig. 4.13	Test circuit	121
Fig. 4.14	Harmonic Voltage at Node 1, Fig. 4.13	122
Fig. 4.15	Harmonic Voltage at Node 2, Fig. 4.13	122
Fig. 4.16	4.16: Harmonic Voltage at Node 3, Fig. 4.13	123

List of Figures

Fig. 4.17	Analogy of electric and magnetic circuit	124
Fig. 4.18	Harmonic Voltage at Node 1. Phase <i>a</i> , Fig. 4.13	128
Fig. 4.19	Harmonic Voltage at Node 1. Phase <i>b</i> , Fig. 4.13	128
Fig. 4.20	Harmonic Voltage at Node 1. Phase <i>c</i> , Fig. 4.13	128
Fig. 5.1	Cross-section of a simple synchronous generator	138
Fig. 5.2	Synchronous generator's equivalent circuit in rotor frame of reference	140
Fig. 5.3	Ggenerator circuit in rotor frame of reference, no damper winding	141
Fig. 5.4	(a)The shape of admittance matrix Y_{dq0} (b) Y_{dq0} , Surface plot	144
Fig. 5.5	(a)The shape of admittance matrix $Y_{\alpha\beta\gamma}$ (b) $Y_{\alpha\beta\gamma}$, Surface plot	148
Fig. 5.6	(a)Structure of admittance matrix Y_{abc} (b) Y_{abc} , Surface plot	150
Fig. 5.7	The Norton's harmonic equivalent of synchronous generator	152
Fig. 5.8	The Thevenin's harmonic equivalent of synchronous generator	153
Fig. 5.9	Machine's <i>abc</i> and <i>dq0</i> axes	154
Fig. 5.10	(a)The structure of admittance matrix Y_{dq0} in Hartley harmonic domain (b) Y_{dq0} in Hartley harmonic domain Harmonic order Vs Magnitude	156
Fig. 5.11	(a)Structure of admittance matrix in $\alpha\beta\gamma$ reference frame (b) $Y_{\alpha\beta\gamma}$, in Hartley harmonic domain, Harmonic order Vs Magnitude	161
Fig. 5.12	(a)Structure of Hartley admittance matrix in <i>abc</i> frame of reference (b) Y_{abc} , in Hartley harmonic domain, Harmonic order Vs Magnitude	163
Fig. 5.13	Circuit arrangement for case study	164
Fig. 5.14	Voltage waveform across unbalanced load (Fig. 5.13)	165
Fig. 5.15	Current waveform across unbalanced load (Fig. 5.13)	165
Fig. 5.16	The harmonic voltage content across load (with frequency conversion effect)	166
Fig. 5.17	The harmonic currents across the load (frequency conversion effect included)	166
Fig. 5.18	The harmonic voltages in <i>phase a</i> , <i>b</i> and <i>c</i> , (Fig. 5.13)	169
Fig. 5.19	The harmonic currents in <i>phase a</i> , <i>b</i> and <i>c</i> , (Fig. 5.13)	170
Fig. 6.1	A schematic of a wind energy conversion, Wind turbine generator output	178
Fig. 6.2	The horizontal axis wind turbine arrangements	179
Fig. 6.3	The vertical axis wind turbine arrangements	180
Fig. 6.4	Main parts and different controls of a wind-turbine	182

List of Figures

Fig. 6.5	Direct drive synchronous generators	188
Fig. 6.6	Fixed-speed squirrel cage induction generators	188
Fig. 6.7	Variable speed double-fed (wound rotor) induction generators	189
Fig. 6.8	A general per phase equivalent circuit of an induction generator	194
Fig. 6.9	An induction generator feeding to local load and grid	196
Fig. 6.10	Equivalent circuit for the model system shown in Fig.6.8	197
Fig. 6.11	Relative position of rotor and stator in an induction machine	199
Fig. 6.12	Transformation of reference frame in an induction machine	202
Fig. 6.13	Induction generator in synchronous rotating frame	207
Fig. 6.14	A steady state equivalent circuit of a wound rotor induction machine	208

List of Tables

Table 1.1	IEEE Table 10.3, Current distortion limits	18
Table 1.2	IEEE Table 11.1, Voltage distortion limits	19
Table 1.3	G5/4-1 Harmonic limits for voltage distortion at 415V and 11kV	21
Table 2.1	Data for different parameters in Fig. 2.4, used for plots	46
Table 2.2	Data for different curves in Fig. 2.9	54
Table 2.3	Data for different components in Fig. 2.10	59
Table 2.4	Data for different components of the system shown in Fig. 2.17	67
Table 3.1	Elements of multiplication matrix	100
Table 3.2	Number of operations using complex Fourier	101
Table 3.3	Number of operations using Hartley	103
Table 4.1	Harmonic contents in the current given by Equation (4.31)	116
Table 4.2	Harmonic voltages at Node 2, Fig. 4.13	129
Table 4.3	Harmonic voltages at Node 3, Fig. 4.13	130
Table 6.1	Comparison: horizontal axis and vertical axis wind turbine generators	181
Table 6.2	Techniques for the generation of synchronous power from wind	185
Table 6.3	Results of induction generator model	210

1. INTRODUCTION

1.1 An overview of power system harmonics

Harmonics in an electric power system are the components of a distorted periodic waveform whose frequencies are integral multiples of the fundamental frequency. An electrical power system should be completely balanced and with a specific frequency during normal operation. The waveform of the network should be purely sinusoidal with pre-defined amplitude. However, this is only imagined as an ideal condition. Practically all the components in the power system network have their unique characteristics and for some reason these components in the power system cause distortion of the ideal sinusoidal waveshape leading to adverse impacts to the whole system and also to individual components in the network. To limit these components is an extremely difficult task as these are mainly the non-linear loads. Probably these non-linear loads will remain as an active source of harmonics for ever in the power system.

The harmonic currents, generated by any nonlinear load, flow from the load into the main system. These currents always tend to flow to ground through the paths of minimum impedance causing a distortion in the applied voltage. The distorted voltage now results in new harmonic currents for some other loads in the network and the process is repeated. The wave shape starts deviating from the original by a significant factor. The effects of harmonics vary depending upon the nature and type of load. A resistive heating load may not be affected by the harmonic voltage. However, in many cases it causes unwanted heat in the equipments and machines. The rise in temperature can seriously damage any sensitive instruments, protection circuits and control circuits.

The level of total harmonic distortion (THD) in the power system network must be limited and both supplier and consumer should take respective measures to keep the level of total harmonic distortion within the limits. There are different standards set by different organizations and regulatory authorities in the form of mature documents to provide a guide on how different

installations should be constructed. They provide the information on the manner in which the design should be made to allow the utility to manage the harmonics [1-2].

Since the potential of adopting corrective measures increases directly with an increase in the problem and because the corrective measures are expensive as well these measures are avoided whenever possible. Preventive actions generally cost less than the corrective measures therefore preventive actions are preferred to maintain harmonic distortion level within limits for a smooth operation of power system. Many of the preventive actions depend upon the prediction of harmonic distortion made on the basis of the models as well as on the basis of information of relevant network parameters at harmonic frequencies. There has always been an issue of correctness and lack of information provided by the manufacturer.

Based on an in depth research work and wide practical experience on the diverse aspects of harmonic distortion in electric power systems many books have been published under the subject of power quality or specifically under the subject of harmonics e. g [3-5]. The following is a very short summary of the key points in these aspects.

1.1.1 Causes of harmonic distortion in power systems

The main causes of harmonic distortion in the power system are:

a) Non-linear loads

Harmonic distortion is usually defined either in terms of ‘current distortion’ or ‘voltage distortion’. Non-linear loads draw a non-sinusoidal current from a sinusoidal voltage supply. The distortion to the normal incoming sinusoidal current wave results from the load emitting harmonic currents that distort the incoming current. These emitted harmonic currents, like any generated current, will circulate via available paths and return to the other pole of the non-linear load causing harmonic voltage drops in all the impedances through which they pass hence distorting the normal supply sinusoidal voltage.

The nonlinear load is present in all industrial, commercial and domestic categories and their type varies from a desktop computer to an induction motor. Fig. 1.1 shows different types of

harmonic voltage distortion while Fig. 1.2 shows some nonlinear loads causing harmonic distortion and how harmonic currents flow in the power system network.

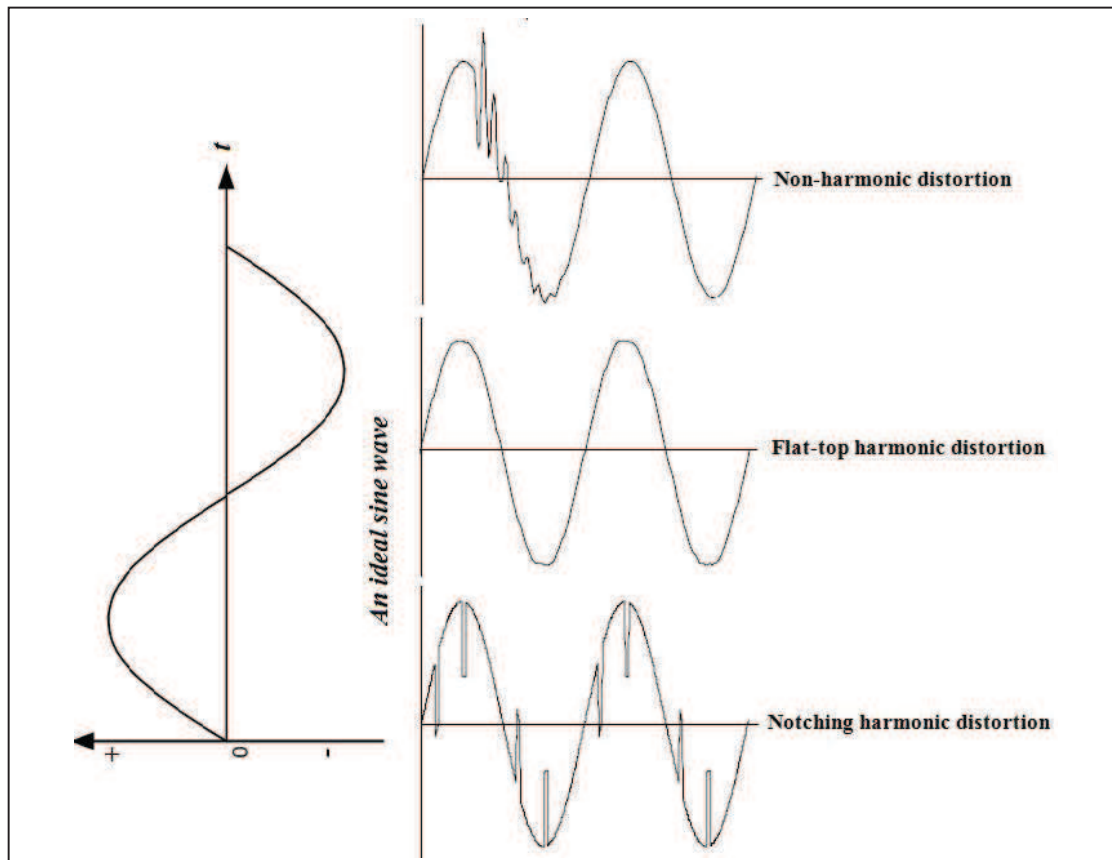


Fig. 1.1: Types of harmonic voltage distortion

b) Transformers

The magnetic circuit in transformers and rotating machines operating under varying conditions of saturation is a source to produce power system harmonics. Typically a transformer magnetizing current contains small 3rd, 5th and 7th harmonic components. Normally transformers are designed to operate up to the knee point of their magnetizing curve, but under conditions of magnetic saturation the harmonic content of the magnetizing current can increase dramatically. Equipment containing saturable reactors, which deliberately exploit the magnetic saturation phenomenon, will therefore probably require harmonic filtering. Residual flux in transformer

core (caused for example by circuit breaker interruption of a fault when there is still a significant DC component) can persist for long durations and, by displacing the B-H curve can result in magnetizing asymmetry and even harmonics in the magnetizing current. (Note it gets removed once it is loaded up after the fault DC shift.)

c) Rotating machines

Rotating machines are also considered a source of harmonics in power system network [6-7] because usually their windings are embedded which are not perfectly sinusoidally distributed and *mmf* is distorted. This problem is present in almost all sort of rotating machines. Induction motor behaves as a nonlinear load and is heavily used in the industry with its application from small to a large scale.

d) Convertors

Converter is the generic name given to rectifier and inverter systems. These systems range from simple rectifiers through to AC–DC–AC systems for the interconnection of major power networks such as the UK/France cross Channel power link and frequency changer systems for soft start and speed control of AC machine drives. In addition, particularly with the advent of the gate turn off thyristor (GTO), Flexible AC Transmission Systems (FACTS) of great technical and operational sophistication are gaining widespread use for the control and conditioning of power systems. All these systems can produce significant harmonics. The principal harmonic numbers may be filtered out on site but significant harmonic currents may still emanate from these systems onto the power network.

e) Thyristor bridge

Thyristor rectifier – inverter bridges are the basis of all the systems described in the previous section.

f) Static VAR compensators

The ability to control voltage by compensating for rapid changes in reactive power loading has resulted in widespread use of VAR compensators as elements in power transmission systems.

They typically include in their assembly thyristor control equipment that inevitably generates its own harmonic currents which are very sensitive to the thyristor firing angle delay. The static VAR compensators also contain capacitor banks, which are often split into sub units that double as the necessary harmonic filters.

1.1.2 Impact of harmonics on power system

a) Heating effect

Harmonic currents flowing into rotating machines cause heating effects both in the conductors as well as in the iron circuit. In particular, eddy current losses are proportional to the square of the frequency. Further, some harmonics are negative phase sequence in nature and these give rise to additional losses by inducing higher frequency currents and negative torques in machine rotors. Harmonic currents will tend to flow into the system capacitance and this can give rise to overloading of power factor correction capacitors and to the derating of cables. The only meaningful way to sum harmonic currents is by their heating effect, that is, by their root mean square (rms) value. Thus the effectiveness of, say, a group of harmonic currents and the fundamental current is given in terms of their rms values as follows:

$$I_{rms} = \sqrt{\left\{ \frac{I_1^2}{2} + \frac{I_2^2}{2} + \frac{I_3^2}{2} + \dots + \frac{I_n^2}{2} \right\}} \quad (1.1)$$

Where I is the peak value of the waveform and subscripts indicate the respective harmonic term.

b) Over voltages

Small over voltages are caused by harmonic currents flowing against impedance to the harmonic. Such effects are known to cause equipment failures, and capacitors are particularly susceptible. These overvoltages can be enhanced by system resonances whereby a given harmonic current may generate a disproportionately large harmonic voltage. Since, from the point of view of

electric stress, the peak value of applied voltage is important, it is not appropriate in this case to take the rms value of a given harmonic voltage spectra. It is not possible to be certain of the changing phase relationship of the harmonics to the fundamental voltage. Therefore it is recommended that the arithmetic sum of the peaks of the fundamental and harmonic voltages are calculated when assessing the stresses placed on equipment due to harmonics. Such a pessimistic approach will ensure that the equipment, particularly capacitors, are generously rated and be less susceptible to overvoltage and over-current failure.

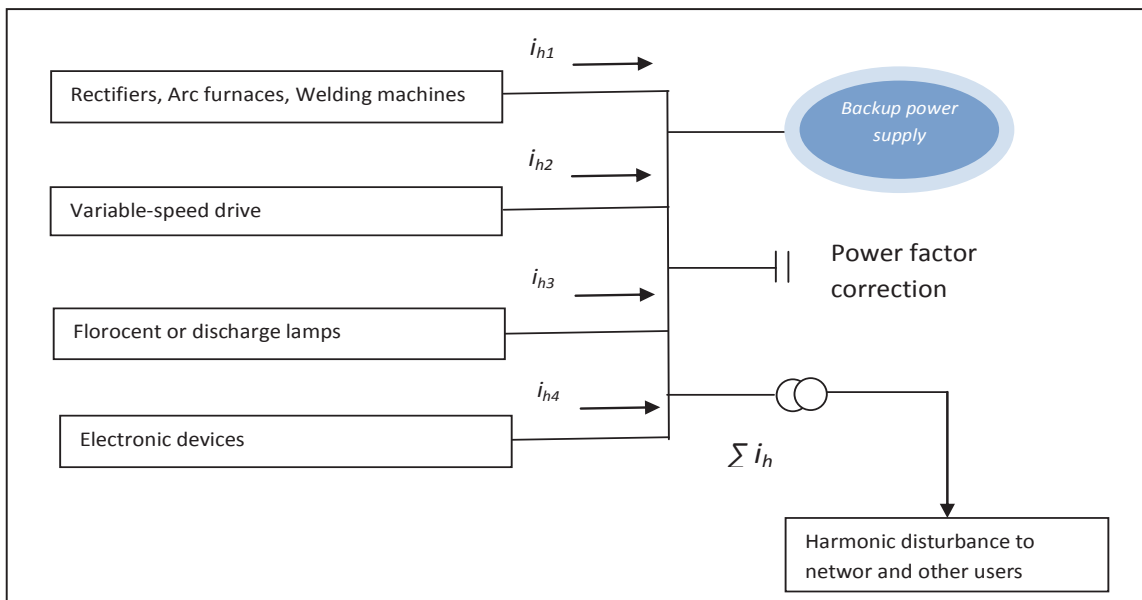


Fig. 1.2: Flow of harmonic currents in the network

c) Resonance

The simultaneous use of capacitive and inductive devices in distribution networks results in parallel or series resonance manifested by very high or very low impedance values respectively. The variations in impedance modify the current and voltage in the distribution network. At harmonic frequencies, from the perspective of harmonic sources, shunt capacitors appear to be in parallel with the equivalent system inductance. That is why, only parallel resonance phenomena, the most common, will be discussed here. Consider Fig. 1.3 representing an installation made up of a supply transformer, linear loads, non-linear loads drawing harmonic currents and power factor correction capacitors.

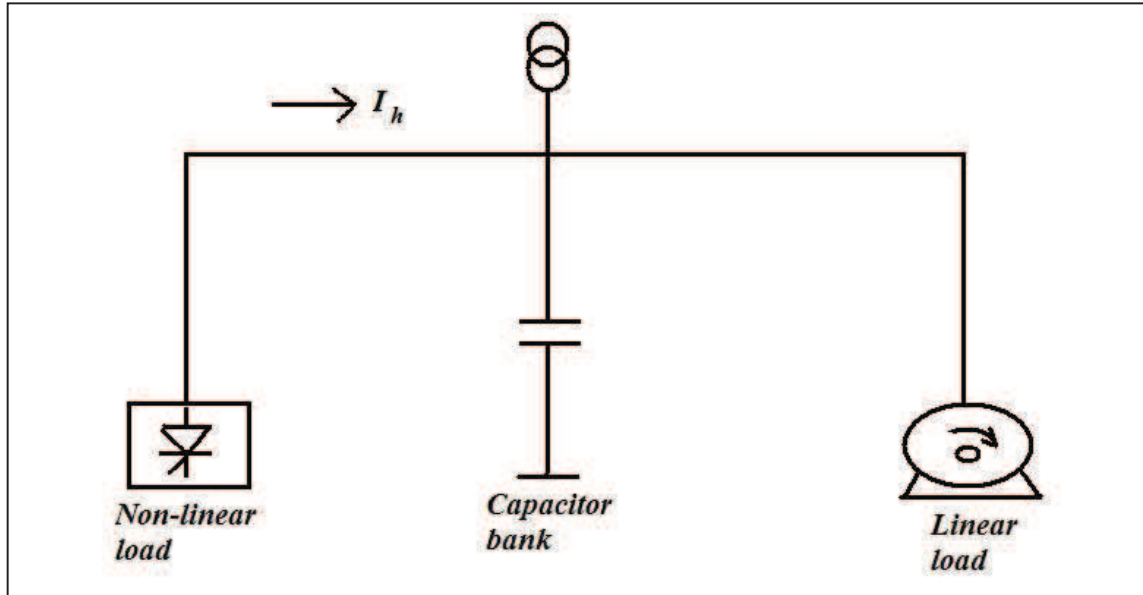


Fig. 1.3: An installation circuit

For harmonic analysis, the phase equivalent diagram is shown in Fig. 1.4. The impedance Z is calculated by:

$$Z = \frac{j\omega L_s}{1 - \omega^2 CL_s} \quad \Omega \quad (1.2)$$

$$\omega = 2\pi f$$

Neglecting R and where:

L_s = Supply inductance (upstream network + transformer + line)

C = Capacitance of the power factor correction capacitors

R = Resistance of the linear loads (neglected)

I_h = Harmonic current

Resonance occurs when the denominator $1 - L_s C \omega^2$ in equation (1.2) tends toward zero. The corresponding frequency is called the resonance frequency of the circuit. At that frequency, impedance is at its maximum and high amounts of harmonic voltages appear with the resulting major distortion in the voltage. The voltage distortion is accompanied, in the $L_s + C$ circuit, by the

flow of harmonic currents greater than those drawn by the loads. The distribution network and the power factor correction capacitors are subjected to high harmonic currents and the resulting risk of overloads. To avoid resonance, anti-harmonic coils can be installed in series with the capacitors.

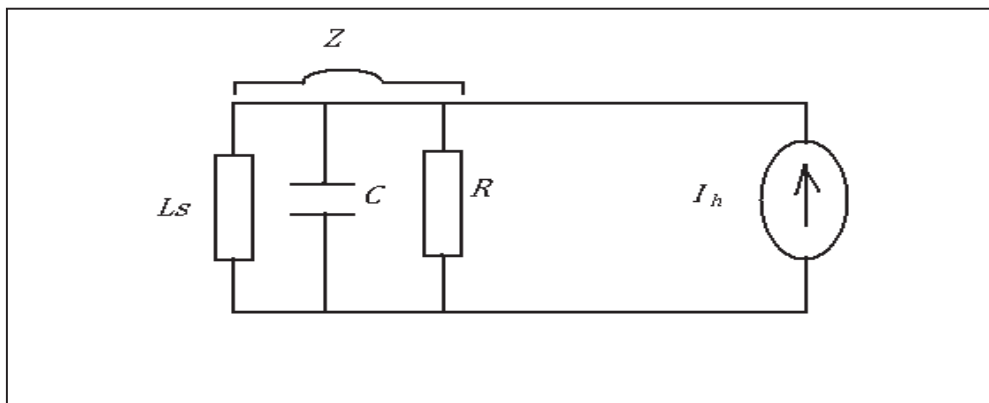


Fig. 1.4: Equivalent phase circuit for the arrangement shown in Fig. 1.3.

d) Interference

Harmonics in power system can cause interference with communication, signaling, metering, control and protection systems either by electromagnetic induction or by the flow of ground currents. However, systems such as signaling circuits whose correct function is essential to safety should have any sensitivity to harmonic interference designed out of them at the outset. Also, standby earth fault relays connected in the neutral of transformer circuits may employ 3rd harmonic filters.

Filters are designed to prevent anomalous relay operation from large discharge lighting loads which may generate triplen harmonics flowing in the neutral conductor. Incorrect earth fault residual current relay element operation may also be prevented by connecting the supply transformers to converter equipment in a delta configuration thus blocking the flow of zero sequence currents from converters to the power system. Other adverse effects of harmonics include overstressing and heating of insulation, machine vibration, the destruction by overheating of small auxiliary components, e.g. small capacitors and motors and malfunctioning of electronic devices.

1.1.3 Elimination of harmonics

The process of elimination of harmonics mainly comprises of two different techniques

a) Harmonic filters

With the increase of harmonic currents and voltages in present-day power systems, the installation of passive, active, and hybrid filters gains in importance. In the future, recommended practices further increased use of filters within the distribution system is expected. There is a great variety in filter configurations. Classification of filters can be based on different criteria such as supply type, filter connection, number of filter elements, power rating, compensation type, speed of response, and control technique. Proper selection of filter configurations depends primarily on the properties of nonlinear loads, type of supply, and system ratings.

Harmonic filters are series or parallel resonant circuits designed to shunt or block harmonic currents. They reduce the harmonic currents flowing in the power system from the source and thereby reduce the harmonic voltage distortion in the system. Such devices are expensive and should only be used when other methods to limit harmonics have also been assessed. The application of filters in a given situation is not always straightforward. The filters themselves may interact with the system or with other filters to produce initially unsuspected resonances. Hence in all but the simplest cases harmonic studies should be used to assist with the determination of the type, distribution and rating of the filter group. Classical shunt filter circuits and their associated characteristics are shown in Fig. 1.5. Note that when the filter forms the capacitive section of an SVC, it is essential for it to be capacitive at fundamental frequency so it will produce the reactive power required. The selectivity or tuning response of the simple single resonant frequency filter circuit is defined by its Q or quality factor:

$$Q = \frac{\omega L}{R} \quad (1.3)$$

A high Q factor gives good selectivity (narrow frequency response) but the filter tuned circuit may be prone to drifting in its tuned frequency owing to changes in temperature or component ageing. Since slight changes in system frequency will cause detuning a less peaky filter response with a lower Q factor is more desirable to accommodate these changes. The tuned resonance frequency of a series LCR circuit is given by:

$$f = \frac{1}{2\pi} \sqrt{[1/LC]} \quad (1.4)$$

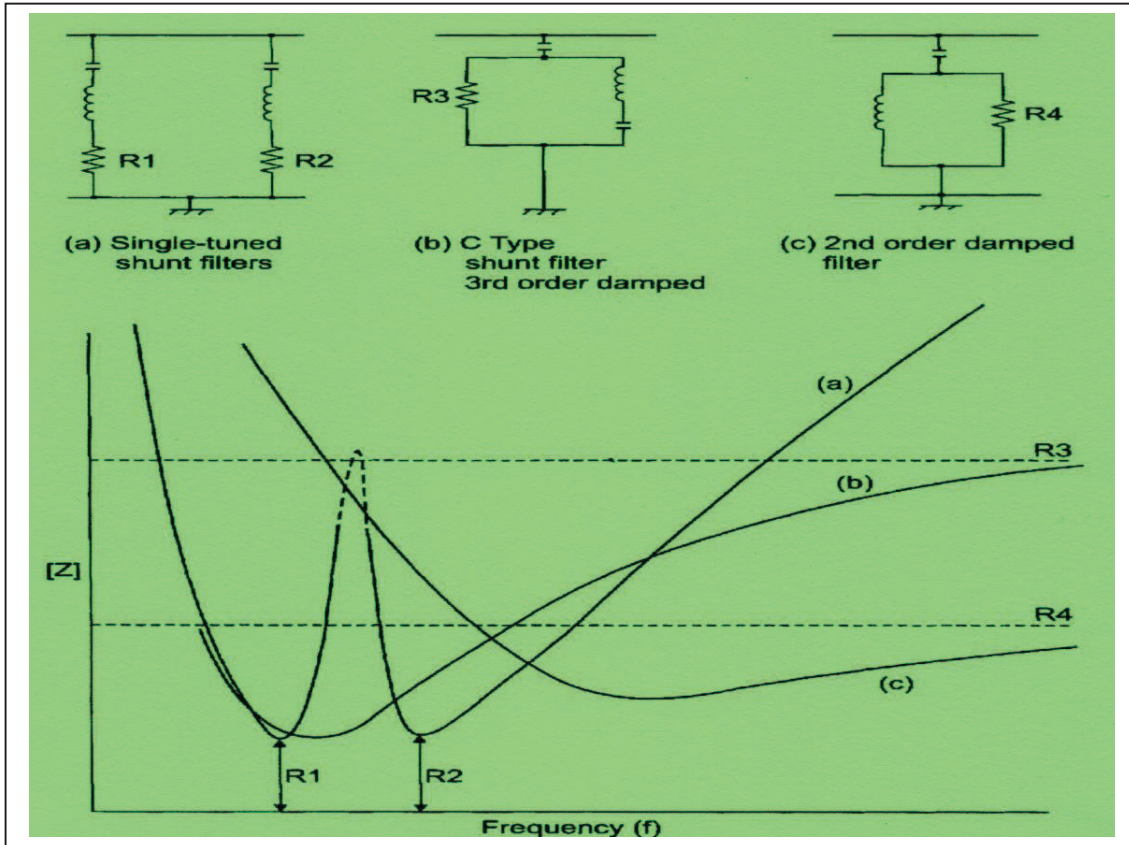


Fig. 1.5: Harmonic filter characteristics [36]

And the impedance at resonance is simply the residual reactor resistance, R . The detuning of filters for changes in harmonic frequency can be expressed as:

$$\delta = \frac{\omega - \omega_n}{\omega_n} = \frac{\Delta f}{f_n} \quad (1.5)$$

If changes in capacitance and inductance, due to temperature change and ageing are included, the detuning factor becomes:

$$\delta = \frac{\Delta f}{f_n} + \frac{1}{2} \left\{ \frac{\Delta L}{L_n} + \frac{\Delta C}{C_n} \right\} \quad (1.6)$$

Active filters may be employed to overcome such effects such that the filter is constantly kept in tune by automatically varying the reactor by means of a control system to keep the inductor and

capacitor voltages equal. It is often the case that more than one harmonic is exceeding the harmonic limits set by the supply authority. Therefore more than one filter is necessary. However, as the number of shunt filters increases there is a tendency for these circuits to interact with the power system impedance to produce unwanted resonances involving other frequencies, if such harmonic frequencies exist on the system. A solution is to use a high pass shunt or *C* type filter arrangement whereby all frequencies above a certain harmonic are shunted to ground. A typical filter group is shown in Fig. 1.6. The required optimum selectivity of the tuned filters depends upon the system impedance angle, θ , at the point of filter connection, and the detuning factor, δ .

An approximation for a possible optimum Q value [8] derived from a graphical construction is given by the expression:

$$Q = \frac{1 + \cos \theta}{2\delta \sin \theta} \quad (1.7)$$

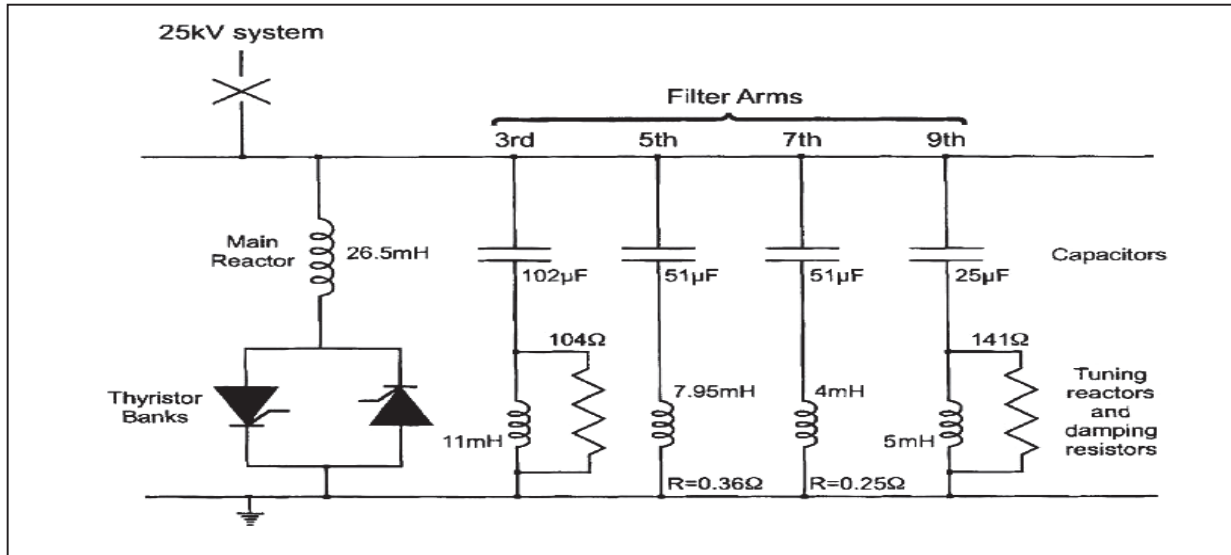


Fig. 1.6: A balancer and filter group schematic diagram.

Consider a converter connected to a 33 kV system with a 50Hz +1% frequency supply where studies have shown that there is a need for 5th and 7th harmonic filters. Suppose also that these studies show the need for 2MVar of reactive compensation for the converter. This could be

conveniently split into two 1MVA units to form the filters; the 1MVA capacitors being more than adequate for the filter duty. Assume that the temperature variation for the inductors and capacitors is 0.01% per degree Celsius and 0.04% per degree Celsius respectively with a possible ambient temperature variation of 20°C above normal. Then from equation (1.6):

$$\delta = \frac{\Delta f}{f_n} + \frac{1}{2} \left\{ \frac{\Delta L}{L_n} + \frac{\Delta C}{C_n} \right\} = 0.015$$

Now if the system impedance angle is 70 degrees, from equation (1.7):

$$Q = \frac{1 + \cos 70}{2(0.015) \sin 70} = 47.6$$

then for each capacitor

$$MVA_r = \frac{V^2}{X_c} \quad \text{and} \quad X_c = \frac{10^6}{2\pi f C} \Omega$$

$$C = \frac{MVA_r}{2\pi f V^2} \times 10^6 = 10^6 \mu F$$

Based on this for the 5th harmonic 0.0584 μF , 0.0694H and 22.9 Ω is respectively the value of C , L and R .

b) Capacitor detuning

It is possible for power factor correction capacitors, particularly on thyristor-controlled drives, to form a low impedance path or ‘sink’ for harmonics or to inadvertently resonate with one of the harmonics produced by the non-linear load. Symptoms are typically capacitor overheating, capacitor fuse protection operation or failure due to overstressing. A solution is to detune the capacitors from high harmonics by the insertion of a series reactor forming a tuned circuit with the resonant frequency typically around the fourth harmonic. The capacitor circuit then looks inductive to all harmonics above the fourth harmonic and resonance is quenched. This is a sufficiently common problem that power factor correction capacitor banks may be specified for installation with these detuning components at the outset. Examples of detuned power correction capacitor networks are shown in Fig. 1.7.

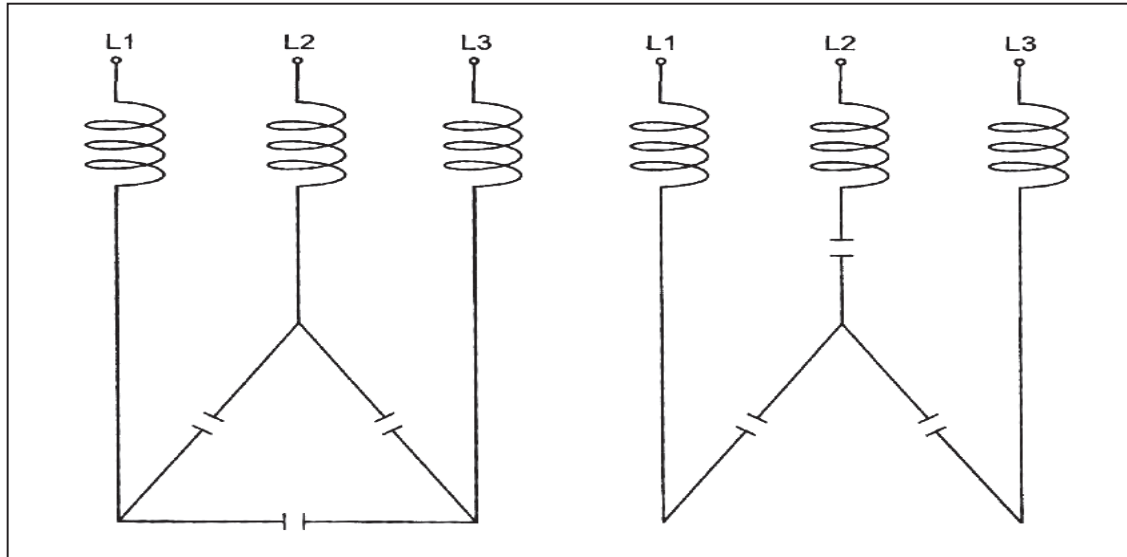


Fig. 1.7: Detuned capacitors for power factor correction

1.1.4 Measurement and simulation of harmonics

There are different methods of simulation for the modeling and analysis of power systems with nonlinear and time-varying components to achieve accurate results. These methodologies have been developed in the time, frequency and hybrid time and frequency domain frames of reference. The application to the computation of the periodic steady state solution of different test systems is different depending upon the advantage, limitation in terms of efficiency, computer requirement and accuracy.

Bearing in mind that the effect of the many distorting sources feeding into a supply network is to cause a rapidly fluctuating mix of harmonic spectra, it is necessary to undertake accurate measurements to determine the true maximum levels of harmonic pollution present. The technology of harmonic measuring equipment is undergoing rapid development, and it is wise to check the market and compare with the requirements of the project, before choosing instrumentation. Fast Fourier transforms have been used [9] to calculate the harmonic currents and voltages. Analysis of readings over a significant period enabled the worst levels of pollution to be selected as the basis for system studies. Further testing was undertaken to check performance after connection of the new loads, both to ensure limits were maintained and to

check the accuracy of the computer predictions of the design studies. Some more developments in this area are presented by [10-11]. Guidance on measuring techniques is provided in IEC 61000-4 and IEEE 1159.

Since the potential for harmonic distortion problems is dependent on the level of harmonic generation which can be associated with loads in the plant. Harmonic currents are generated by loads which have nonlinear voltage-current characteristics. The number and sizes of these devices at a given bus determines the level of harmonic current generation. Another factor on which the potential for harmonic distortion depends is the system frequency response characteristics. The frequency response at a given bus is dominated by the application of capacitors at that bus. Series reactors for transient control or harmonic control significantly change the frequency response.

Problems occur when the system response exhibits a parallel resonance near one of the harmonic components (usually the 5th or 7th harmonic) generated by the loads on the system. Resistive load provides damping near these resonant frequencies. Measurement of harmonic distortion is important for a number of reasons. Most importantly, the measurement must be used to characterize the level of harmonic generation for the existing nonlinear loads. Voltage and current harmonic distortion level is measured at different locations to accomplish this. It is also important to accurately document system conditions at the time of the measurement so that the results can be used to verify analytical results.

The harmonic generation characteristics of the nonlinear loads are determined by performing current measurement at a variety of locations within the facility. For example the wave form of a DC drive is shown in Fig. 1.8. Three-phase measurement is also made so that characteristic and non-characteristic (triplen) harmonic components can be determined. Then the system response characteristics are determined for particular conditions. Voltage measurement is used in conjunction with the current measurements to characterize system response for specific system conditions. These conditions provide the basis of harmonic domain analysis.

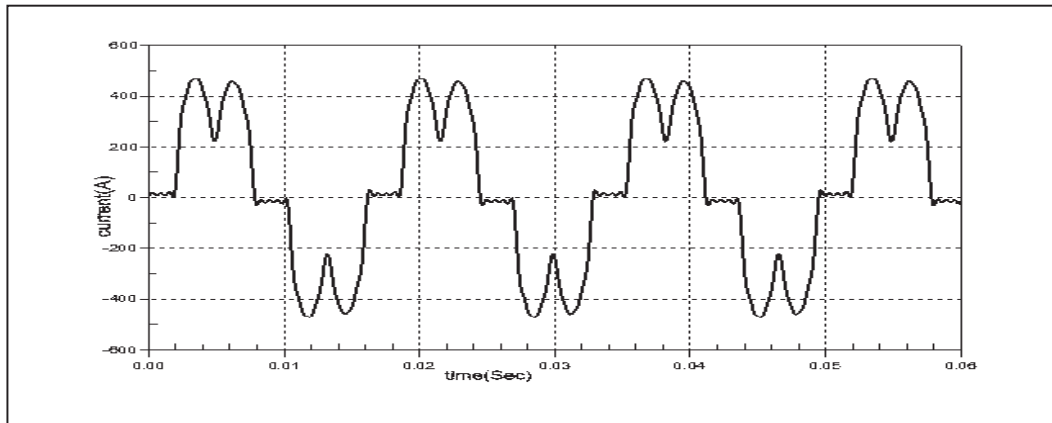


Fig. 1.8: Typical current waveform of a DC drive

Research has been carried out to analyze and configure nonlinear loads like welding loads, traction loads, SCR bridge rectifiers and lighting loads. To determine frequency response characteristics of the system, simulations are performed either by looking into or looking from the nominal voltage bus bar. Magnitude and phase angle of driving point impedance are obtained.

The impact of different nonlinear components is evaluated and risk for resonance condition is calculated. If results based on these calculations indicate any serious risk, the filters are designed and arranged for the circuit. Such an example is shown in Fig. 1.9; the results are based upon a simulation with 480V nominal bus voltage. The frequency response identifies different conditions which may cause severe consequences if resonance occurs due to harmonic distortion. These system conditions must be safely tackled when the level of harmonic distortion caused by different components is calculated.

The calculations and measurements should include the individual harmonic distortion level of different components, bus voltage distortion levels, current distortion levels, RMS voltage and current levels, and important waveforms.

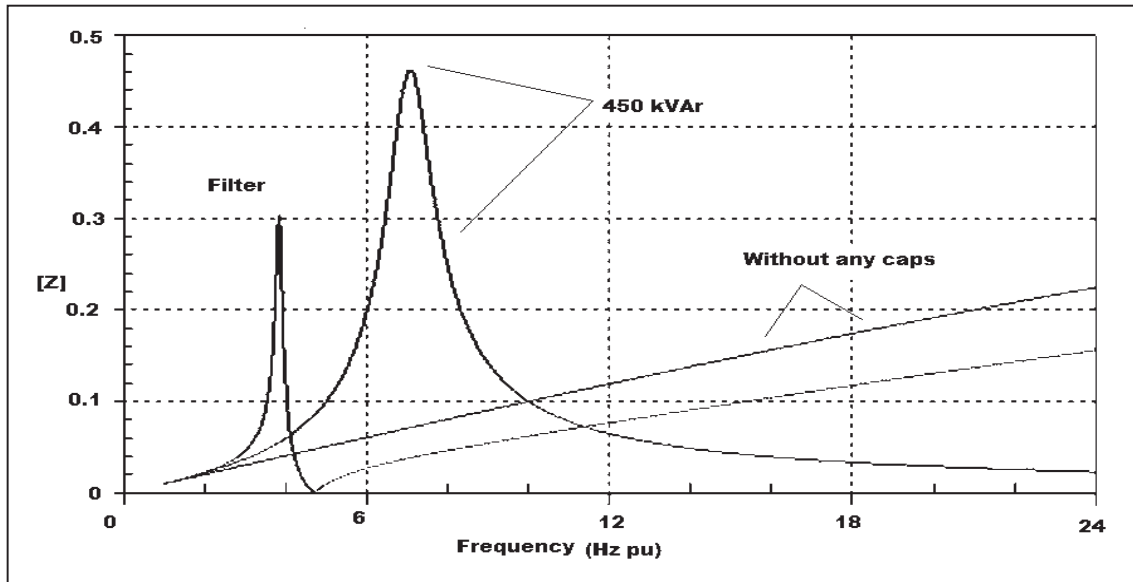


Fig. 1.9: The frequency response characteristics (with 480V nominal bus voltage).

One of bad effects of the harmonic currents generated by nonlinear loads and system resonances is that there temperature rise due to increased heating in system equipment hence creating the efficiency problems.

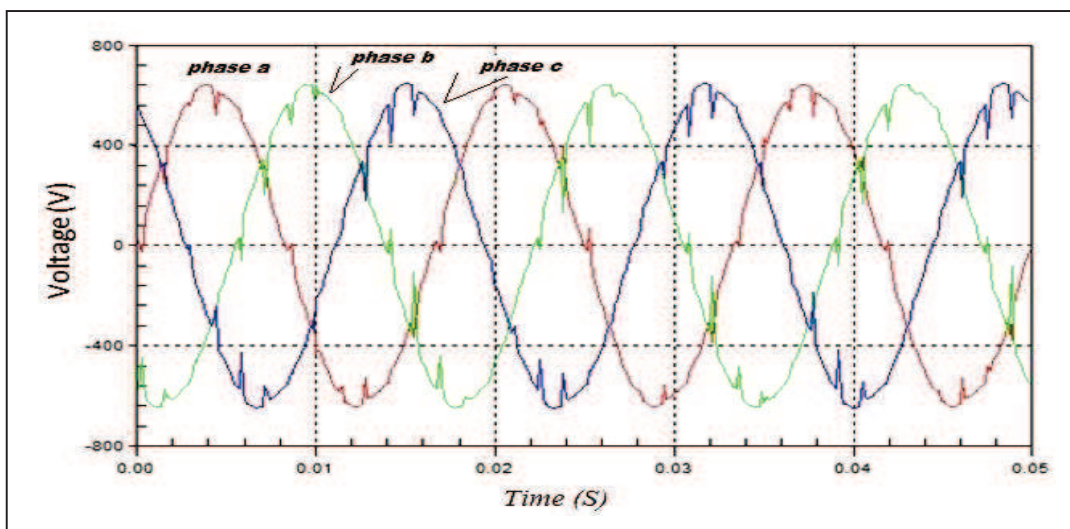


Fig. 1.10: An example of serious harmonic voltage distortion

1.1.5 Standards

Different standards have been prepared from time to time by IEEE, IEC and ENA which provide guidelines for power quality usages and practices. Harmonic standards mainly address the following issues:

1. Description and characterization of the phenomenon
2. Major sources of harmonic problems
3. Impact on other equipment and on the power system
4. Indices and statistical analysis to provide a quantitative assessment and its significance
5. Measurement techniques and guidelines
6. Emission limits of quality degradation for different types and classes of equipment
7. Immunity or tolerance level of different types of equipment
8. Testing methods and procedures for compliance with limits
9. Mitigation guidelines

a) IEEE Standards

IEEE 519-1981, “IEEE Guide for Harmonic Control and Reactive Compensation of Static Power Converters”, originally established levels of voltage distortion acceptable to the distribution system for individual non-linear loads. With the rising increase usage of industrial non-linear loads, such as variable frequency drives, it became necessary to revise the standard. The IEEE working groups of the Power Engineering Society and the Industrial Applications Society prepared recommended guidelines for power quality that the utility must supply and the industrial user can inject back onto the power distribution system.

The revised standard was issued on April 12, 1993 and titled “IEEE Recommended Practices and Requirements for Harmonic Control in Electrical Power Systems”. The revisions to IEEE 519-1992 establish recommended guidelines for harmonic voltages on the utility distribution system as well as harmonic currents within the industrial distribution system. According to the standard, the industrial system is responsible for controlling the harmonic currents created in the industrial workplace. Since harmonic currents reflected through distribution system impedances generate

harmonic voltages on the utility distribution systems, the standard proposes guidelines based on industrial distribution system design. Table 10.3 from IEEE 519-1992 defines level of harmonic currents that an industrial user can inject onto the utility distribution system.

Table 1.1: IEEE Table 10.3[12]

IEEE Table 10.3 Current Distortion Limits for General Distribution System (120 V through 69kV)						
Maximum harmonic current distortion in % of I_L Individual harmonic order (Odd Harmonics) ^(1,2)						
Isc/I_L	< 11	11 ≤ h ≤ 17	17 ≤ h ≤ 23	23 ≤ h ≤ 35	35 ≤ h	TDD
<20 ⁽³⁾	4.0	2.0	1.5	0.6	0.3	5.0
20<50	7.0	3.5	2.5	1.0	0.5	8.0
50<100	10.0	4.5	4.0	1.5	0.7	12.0
100<1000	12.0	5.5	5.0	2.0	1.0	15.0
>1000	15.0	7.0	6.0	2.5	1.4	20.0
<p>(1) Even harmonics are limited to 25% of the odd harmonic limits above.</p> <p>(2) Current distortion that result in a DC offset e.g. , half-wave converters are not allowed</p> <p>(3) All power generation equipment is limited to these values of current distortion, regardless of actual Isc/I_L. Where Isc. is maximum short circuit current at PCC and I_L is maximum demand load current (fundamental frequency component) at PCC</p>						

Table 11.1 of IEEE 519-1992 defines the voltage distortion limits that can be reflected back onto the utility distribution system. Usually if the industrial user controls the overall combined current distortion according to Table 10.3, this will help them meet the limitations set forth in the guidelines. IEEE Table 10.3 Current Distortion Limits for General Distribution Systems.

Table 1.2: IEEE Table 11.1[13]

IEEE Table 11.1 Voltage Distortion Limits		
Bus Voltage at PCC	Individual Voltage (%)	Total Harmonic Voltage Distortion THD (%)
69kV and below	3.0	5.0
69.0001 kV- to- 161 kV	1.5	2.5
161.001 kV and above	1.0	1.5
High Voltage systems can have up to 2.0% total harmonic distortion(THD) where the cause is an HVDC terminal that will attenuate by the time it is tapped for a user		

Some important concepts and terms associated with a harmonic analysis involve PCC, TDD and THD. The Point of Common Coupling (PCC) is the location of the harmonic voltage and current distortion to be calculated or measured. PCC can be measured or calculated on the primary or secondary of a utility transformer or at the service entrance of the facility. In some cases, PCC can be measured or calculated between the non-linear loads and other loads of an industrial plant. Total Demand Distortion (TDD) is the percentage of total harmonic current distortion calculated or measured at PCC. Total Harmonic Distortion (THD) is the total harmonic voltage distortion calculated or measured at PCC. In the future, a task force will be created to develop an application guide for IEEE 519 to help users and utilities in cooperate and understand how to solve potential problems related to power system harmonics.

b) IEC Standards

Geneva based International Electro-technical Commission or Commission Electro-technique Internationale (IEC) is the widely recognized organization as the curator of electric power quality standards. IEC has introduced a series of standards, known as Electro-Magnetic Compatibility (EMC) standards, to deal with power quality issues. Integer and inter harmonics are included in IEC61000 series as one of the conducted low-frequency electro-magnetic

phenomena. The series also provides internationally accepted information and guideline for the control of power system harmonic as well as inter-harmonic distortion [14].

IEC 61000 1-4: It provides the rationale for limiting power frequency conducted harmonic and inter-harmonic current emissions from equipment in the frequency range up to 9 kHz.

IEC 61000 2-1: Power system equipment, industrial loads and residual loads as considered here as three major sources of harmonics in this series. The series consider HVDC converters, FACTS devices as main power system equipment for harmonic distortion originating in the transmission system. Static power converters and electric arc furnaces are included as harmonics sources in the industrial category. Appliances powered by rectifiers with smoothing capacitors like PCs, TV receivers, etc are considered as the main distorting components in the residential category.

IEC 61000 2-2: Compatibility levels of the harmonic and inter-harmonic voltage distortion in public low-voltage power industry systems are discussed in this section.

IEC 61000 2-4: Compatibility levels of harmonic and inter-harmonic for industrial plant with the main effects of inter-harmonics are discussed in this section.

IEC 61000 2-12: This section covers compatibility levels for low-frequency conducted disturbances related to medium voltage power supply systems and injected signals such as those used in ripple control equipment.

IEC 61000 3-2 and 3-4: this section gives the guideline for limiting harmonic current emissions by equipment with input currents of 16 A and below per phase along with measurement circuit, supply source and testing conditions as well as the requirements for the instrumentation for harmonics monitoring.

IEC 61000 3-6: This section deals with the capability levels for harmonic voltages in low and medium voltage networks as well as planning levels for MV, HV and EHV power systems indicating emission limits for distorting loads in MV and HV power systems.

IEC 61000 3-12: Limits for the harmonic currents produced by equipment connected to low voltage systems with input currents equal to and below 75A per phase are discussed in this section.

IEC 61000 4-7: This section deals with testing and measurement techniques.

IEC 61000 4-13: Testing and measurement techniques with reference to harmonics and inter-harmonics, including mains signaling at AC power ports as well as low-frequency immunity tests are covered in this section.

c) ENA Standards

In the UK, levels for harmonic voltage distortion and connection of nonlinear equipment to the transmission and distribution network are managed by ENA according to ER G5/4-1 recommendations [15].

Table 1.3: G5/4-1 Harmonic limits for voltage distortion

Odd harmonics (non-multiple of 3)					Odd harmonics (multiple of 3)					Even Harmonics				
h	%Voltage				h	%Voltage				h	%Voltage			
	400V	6.6kV 11kV 20kV	>20kV and <145kV	275kV and 400kV		400V	6.6kV 11kV 20kV	>20kV and <145kV	275kV and 400kV		400V	6.6kV 11kV 20kV	>20kV and <145kV	275kV and 400kV
5	4.0	3.0	2.0	2.0	3	4.0	3.0	2.0	1.5	2	1.6	1.5	1.0	1.0
7	4.0	3.0	2.0	1.5	9	1.2	1.2	1.0	0.5	4	1.0	1.0	0.8	0.8
11	3.0	2.0	1.5	1.0	15	0.3	0.3	0.3	0.3	6	0.5	0.5	0.5	0.5
13	2.5	2.0	1.5	1.0	21	0.2	0.2	0.2	0.2	8	0.4	0.4	0.4	0.4
17	1.6	1.6	1.0	0.5	>21	0.2	0.2	0.2	0.2	10	0.4	0.4	0.4	0.4
19	1.2	1.2	1.0	0.5						12	0.2	0.2	0.2	0.2
23	1.2	1.2	0.7	0.5						>12	0.2	0.2	0.2	0.2
25	0.7	0.7	0.7	0.5										
>25	0.2+0.5(25/h)													

The harmonic limits for voltage distortion at 415V and 11kV are extracted in Table 1.3. The limit for total harmonic current distortion allowed at 415V is five percent while only four percent is permissible at 11kV.

1.2 Grid-connected wind-power plants and power quality issues

Due to an increase in energy demand and fossil fuel shortage, renewable energy supplies have become an essential to fulfil the energy demand in the age of technology. Together with hydro and solar power plants, wind based power plants also make a huge contribution to the production of renewable energy.

A wind farm may have a number of wind turbines depending upon the total output power delivered to substation and individual size of the wind turbine. Fig. 1.11 shows how power is collected from individual wind turbines and a schematic of the connection to grid. On average a wind turbine in an ideal location can deliver an annual electrical power output of about 850 kWh per square meter of rotor surface area. A simple rule to estimate the annual energy output on a site with average wind speed is that, the output is equivalent to about two thousand full load hours and at high wind sites approximately three thousand hours. For instance, a 1.5 MW wind turbine [16] produces 3×10^6 kWh on the average, for a 1500 kW for 2000 hours. The capacity factor of this wind turbine is nearly 23%. Overall capacity factor for wind system is 20% to 40%, whereas in the U. K it has varied from 24% to 31% reaching an average of 27% in 2005 [37].

Although wind power plants have a major contribution in renewable energy, the power generated by wind turbines over time is uneven due to the unpredictable nature of their primary source of power which increases the problems inherent to the integration of a great number of wind turbines into power networks. Therefore the contribution of wind power plants faces certain challenges like voltage and frequency regulation and wind-farm operation.

1.2.1 Frequency change, harmonics and inter-harmonics

If a wind turbine operates at a variable speed, the electric frequency of the coupled generator also varies. Therefore the generator has to be decoupled from the frequency of the grid. This is usually achieved by an inverter system.

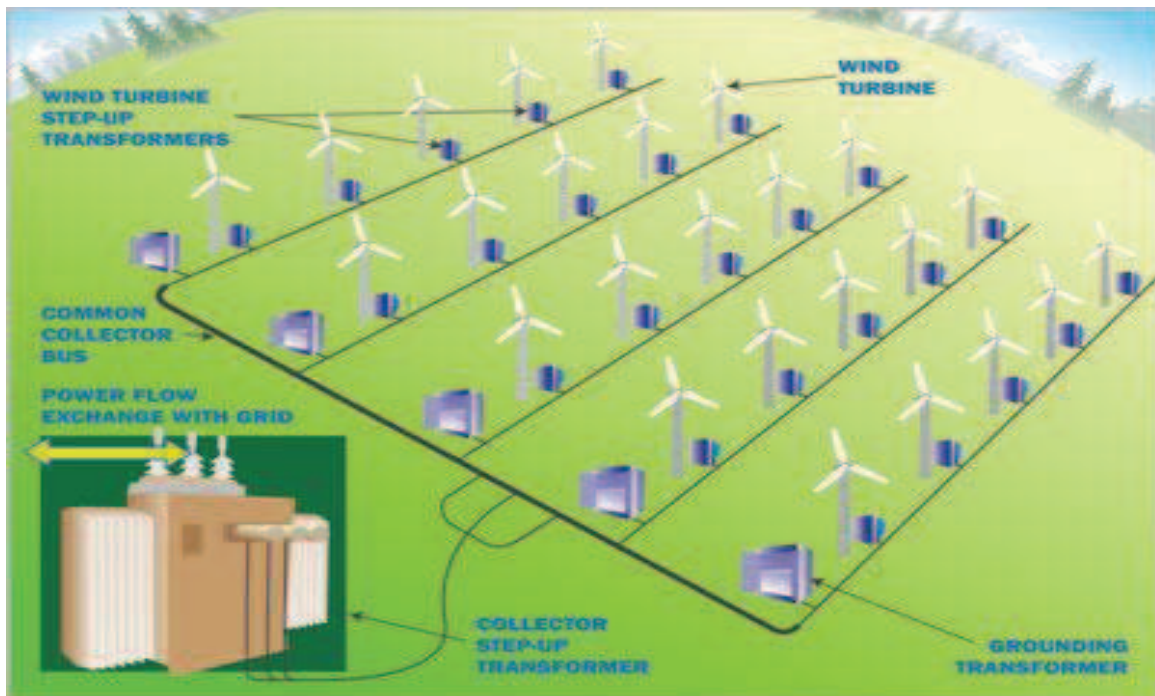


Fig. 1.11: Grid connection of a wind farm [35]

There are two kinds of inverter systems, the first one is grid-commutated and the second one self-commutated inverter system. The grid-commutated inverter is a thyristor inverter. This kind of inverter produces integral harmonics for example the 5th, 7th, 11th and 13th order harmonics. These harmonics in general must be filtered by harmonic filters.

Thyristor inverter is not able to control the reactive power at its own. The behavior of this inverter concerning reactive power is very much similar to the behavior of an induction generator. Both of them consume inductive reactive power. Self-commutated inverter is mainly pulse width modulated (PWM) inverter in which IGBTs (Insulated Gate Bipolar Transistor) is used. This inverter has the advantage that in the reactive power is controllable however an associated disadvantage is the production of interharmonics. In general these interharmonics are generated by the inverter in the range of some kHz. Therefore filters are extremely important to eliminate the interharmonic distortion. Because of the fact that the frequencies are quite high, the design and construction of the filters is not a big problem. Modern wind turbines generally use thyristor based inverter systems only.

1.2.2 Cost of quality supply

Wind farms and utility transmission grids present each other with a host of voltage and power quality related challenges. To prevent problems for the utility grid, the wind farm must typically adhere to strict interconnection requirements for output power factor, voltage regulation, low and high voltage ride through, flicker and harmonics.

There is concern that the latest generation of wind generators and coupled directly to the wind turbine shaft, may be producing inter-harmonics. In addition, a wind farm must protect itself from events occurring on the utility grid that would otherwise cause damage, tripping or result in increased maintenance or lost revenues.

1.3.2 Lack of control over source

The electricity supply network these days is a complex system. In the last fifteen years, a steadily increasing number of renewable energy resources such as wind and solar power generation plants have been added to the existing electrical networks. All renewable resources generate electricity when the source is available. For wind power, this characteristic is of little importance if the amount of wind power is modest compared to the total installed and spinning capacity of controllable power plant. If not, there is a big technical issue as the renewable part grows to cover a large part of the total demand for electric energy in the system.

1.2.4 Quality and reliability

The existence of wind power plant as a cogeneration is recognized as practical solution and provides a healthy option to cope with the increasing energy demand. However; vertically integrated utilities are cautious to integrate dispersed generating units into their system. An electrical utility is characterized as vertically integrated when the generated electric power flows only in one direction and power generation, transmission, and distribution sectors are owned and operated by a single authority.

Depending on the grid size and its topology, a low power grid-connected wind farm may not affect the power quality and disrupt the reliability of the main system; however, as the injected power of grid-connected wind-based plant increases, the power quality and overall reliability of the network is reduced. This reduction in power quality and reliability can appear in the network

in the form of voltage rise, voltage flicker, and voltage harmonics. Voltage rise effect is one of the issues that would also surface as a result of increasing wind power plant interconnection given during the low demand season. Voltage rise can be handled through the control of power-factor and ring-operated distribution network with respect to the wind farm interconnection [18].

1.2.5 Voltage flickers

Wind power plants may cause voltage flicker as a result of the surrounding and environmental changes which would have resulted in a significant voltage change on the feeder. The output fluctuates as the intensity of the wind's currents. These voltage flickers are also caused by switching operations in the wind power plant installation. Rapid voltage changes occur within the 10 min average interval used in the definition of slow voltage variations, typically on a time scale between half a period (10 ms at 50 Hz) and a time of few seconds [19].

1.2.6 Fault protection system

As already mentioned wind farms use voltage- source converter technology. These converters introduce harmonics in the network to which it is interconnected. Furthermore, wind-based system, which depends on uncontrollable variable wind speed, is bound to affect the generated power quality.

Voltage and current distortion are highly expected as a result of grid-connected wind plants. When wind-based plant is interconnected in parallel with the utility distribution system, some operating conflicts might arise that could affect the system's reliability. The utility breakers and reclosers are set to see certain distance down the radial feeder referred to as the reach of the device. The device reach is determined by minimum fault current that the device would detect. The minimum fault current could be degraded with the presence of grid-connected wind power plant that is injecting power into the grid. All the afore mentioned challenges are anticipated if a wind based power plant is directly or indirectly connected to the main system.

1.3 Micro-grids

1.3.2 Definition and overview

In an electric power system micro-grid is the name given to a group of electric loads and power generation sources (e.g., wind power plant) operating as a controllable system that inject electric power to its local area and regional grid e.g., [20–22].

A micro-grid plays an important role to enhance local reliability, increase efficiency, support local voltages, voltage sag correction, or provide uninterruptible power supply functions [23-24]. A micro-grid can be operated either in an interconnected mode or in an islanded mode [24].

Micro-grid schemes are usually intended more for low voltage level grid. This concept can also be applied to medium and high voltage interconnection levels. Fig. 1.12 shows a basic micro-grid connection scheme that can pertain to low as well as medium and high voltage level connections. All the energy sources (ESs) are connected to the grid through inverter units (IUs), source controllers (SCs) and local supervisory controllers (LSCs). The loads are managed through a load controller (LCs) which make or break the load from the network according to the grid's safety.

Most of the renewable energy sources including wind energy source, are not suitable for direct connection with the electrical network due to the characteristics of the produced electric power (i.e., voltage and frequency levels).

Power electronic interfaces (DC/AC or AC/DC/AC converters) or IUs are required to synchronize the output power of these units with the grid's power characteristics. The IU conversion method depends on the renewable energy source (RES) technology. A photovoltaic (PV) system for example, produces direct current (DC) and direct voltage signal profile outputs like a battery. The IU is configured to convert direct steady output to alternating one with frequency matching the grid's frequency.

The inverter unit (IU) also helps synchronizing the voltage level and waveform with the grid's voltage. Where as a wind turbine produces alternating electric output features with frequency and

voltage levels that not be compatible with the grid's frequency and voltage levels. Here, an IU converts the turbine's alternating output power to direct power signal, and then converts the direct power to alternating power signal that is compatible with the grid's voltage and frequency characteristics. This converted power output from renewable energy source is fed into the grid through SC. SC is essentially a protection system unit and consists of protection instruments like circuit breakers, relays, filters and communication modules.

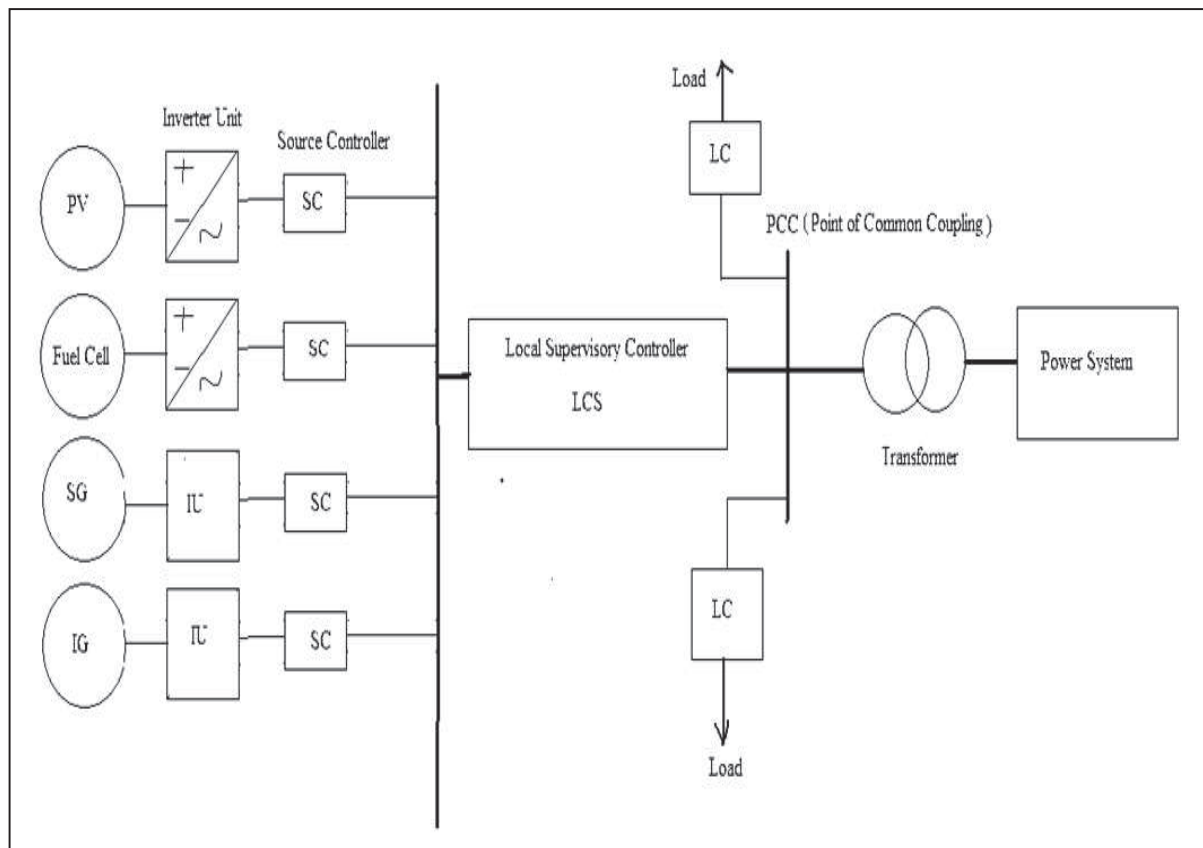


Fig. 1.12: A schematic of controls for a micro-grid (low and medium voltage levels)

SCs are monitored and controlled by LSC. LSC possesses key functions like cost managing function, optimization, and control functionalities. The design and operation of micro-grids based on renewable energy resources has received considerable research attraction all over the world e.g., Europe [25], USA [26], and Asia [27].

Micro-grids are relatively new concept which refers to a small-scale power system with loads and distributed generators operate with energy management in a safe and reliable mode. There are devices like the flexible AC transmission system (FACTS) control devices such as power flow controllers and voltage regulators as well as protective relays and circuit breakers. In simple words, a micro-grid is a collection of loads and micro-generators along with some local storage and behaves just like a model-citizen from grid side thanks to intelligent control [28]. Although a micro-grid may itself be composed of many generators and loads, it appears as a net load or a net generator to the broader grid with well-behaved characteristics [29].

Another sample microgrid architecture is shown in Fig. 1.13. The micro-grid is a very versatile concept as it can accommodate various types of the micro generators (wind turbine, photovoltaic (PV) array, diesel generator, and wave generator), local storage elements (capacitors, flywheel) and loads. A distributed generator might be a diesel generator which can be coupled to the grid directly, or a PV array which needs direct current (DC)/alternating current (AC) inverter interface or an asynchronous wind-turbine which requires AC–DC–AC inversion for proper grid connection. The storage devices used in the system may or may not require an inverter interface as in the case of capacitor banks and flywheel, respectively.

The micro-grids can be a DC [30], AC or even a high frequency AC grid [31]. It can be a single or a three phase system or it may be connected to low voltage or medium power distribution networks. The microgrids could be operating in either grid connected or islanded operation mode. For each operating mode operational requirements are different and distinct control schemes are required. The ground-breaking feature of micro-grids is their ability to operate independently when there is a power failure in the main grid. This operation mode is called islanded operation as the micro-grid disconnects from the grid and becomes an island with local generators and loads. The consumers may receive continuous service even when there is power outage in the grid due to a fault or maintenance. If there are voltage sags, frequency drops, or faults in the main grid then the microgrid can be easily disconnected, i.e. islanded from the rest of the grid and the users can be isolated from those problems. So, a microgrid not only helps in providing uninterrupted supply but also contributes to maintain service quality.

The small electrical networks manage distributed generators, loads, storage and protection devices within their own grid. If each micro-grid is operating as a model citizen, i.e. either as a load receiving power with acceptable electrical characteristics or as a power supply supplying power with acceptable electrical characteristics, then the overall utility grid can be operated properly.

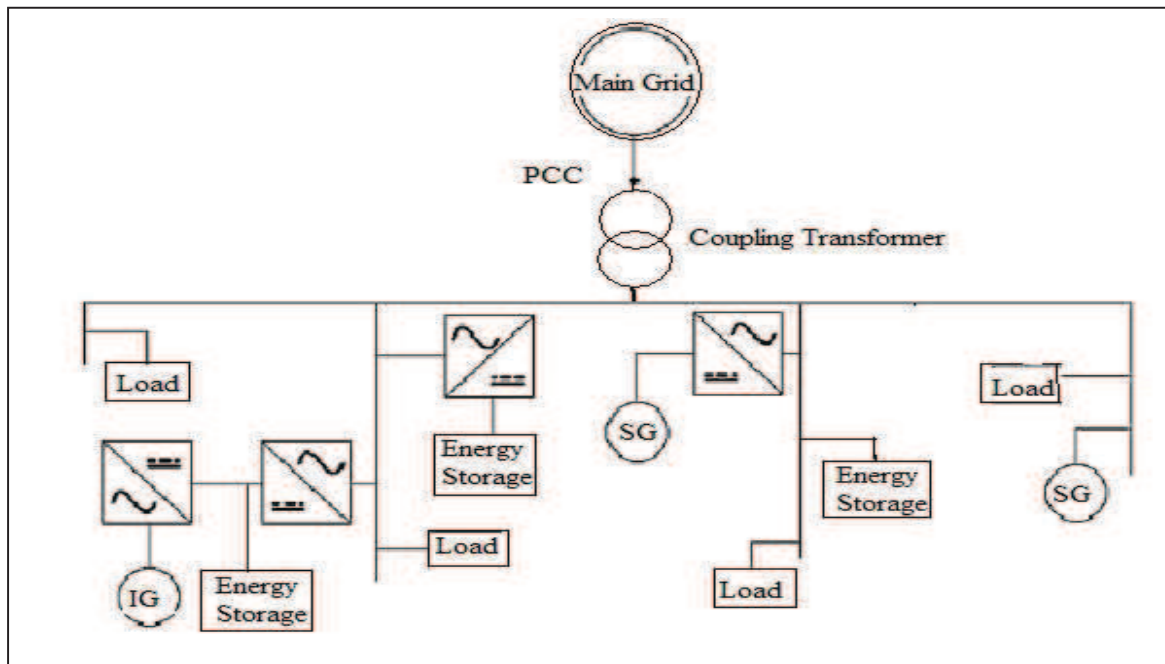


Fig. 1.13: An example of a micro-grid with various types of generators

Higher penetration levels of distributed generators, especially those requiring power electronics interfaces, alter the grid structure and badly affect the safety and reliability of operation. The micro-grid concept is introduced to manage these generators in small quantities rather than trying to tackle the whole network. In this way, the side-effects on the main grid operation can be eliminated and more distributed generators can be employed in the main grid.

2.3.2 Contemporary and future micro-grids.

Owing to their energy efficiency, minimization of the overall energy consumption, improved environmental impact, improvement of energy system reliability, network benefits and cost

efficient electricity infrastructure management, microgrids offer the solution to almost all major energy problems in the future.

This however demands a proper steps towards energy management within and outside of the distributed power system, control philosophies for example hierarchical or distributed, islanding and interconnected operation philosophy, type of networks ac or dc, fixed or variable frequency, management of power flow constraints, voltage and frequency device and interface response and intelligence requirements, protection options for the networks of variable configurations, next-generation communications infrastructure and standardization of technical and commercial protocols and hardware. The concept of integration of distributed energy sources in particular renewable energy resources heavily depends upon the growth of microgrids.

A properly planned and designed micro-grid produces sufficient energy to meet the power needs of the users within the micro-grid. A micro-grid may be any specific area where groups of consumers are present. A microgrid is the most economical way to manage and deliver electric power to a local group of users. Economic and environmental benefits to well designed micro-grid users are maximized while minimizing energy loss due to transmission over long distances. In future one will be able to regulate energy use in a real-time model which enables one to save energy by managing consumer demand, cost, harmonic distortion control and spinning reserve which can result in massive revenue increases. In future microgrids will support revenue streams from distributed power generation.

Future microgrids will be more and more reliable hence helping consumers and businesses save money lost to due to power outages and other power quality problems. Local generation minimizes peak load costs and in future microgrids may allow consumers to procure power in real-time at low expenditures. Local power generation shall be more efficient and transmission losses will be reduced, giving a hope of reduction in electricity bills. From environmental point of view, a local power plant can be renewable or natural gas/coal or oil fuelled. Micro-grids will be able reuse waste heat from the burnt fuel for other uses such as heating buildings, cooling.

Microgrids have enough flexibility to use a range of energy sources such as wind and solar. These efficiencies will save the natural atmosphere around the planet. Microgrids these days,

can feed the larger power grid when power demand and cost is highest by supplying electricity from renewable sources. Local power generation and storage allows the microgrids and critical facilities to operate independent of the larger grid when required. New technologies will be able to automatically adjust and even anticipate power disturbances.

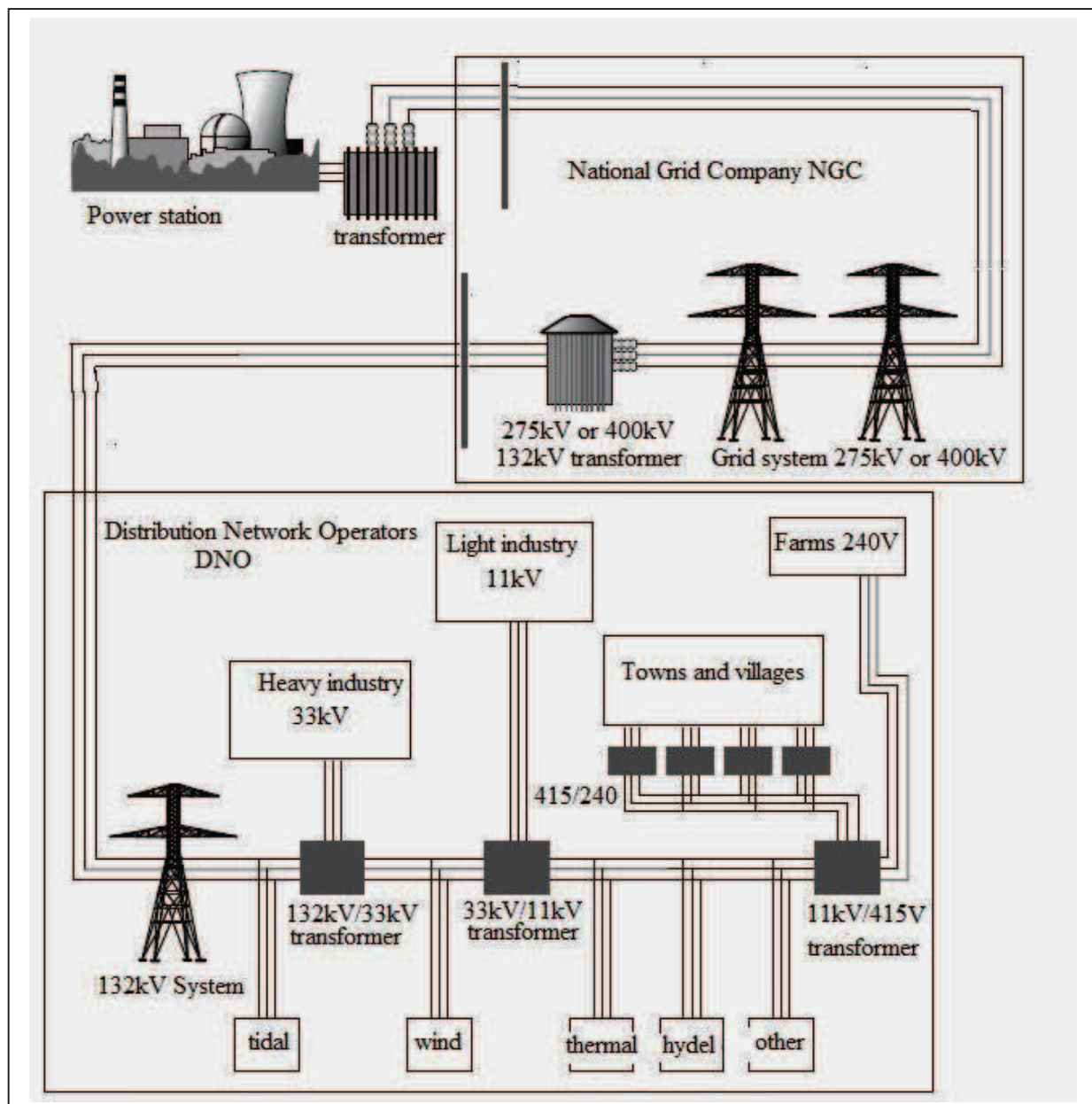


Fig. 1.14: A schematic of the UK electricity system [17]

A supreme benefit of micro-grids is that they can have a better location than the major grid to deal with known and unknown future problems arising due to local population expansion. Rather than having to wait for power companies to build centralized power plants, microgrids can increase the overall electricity supply reasonably fast and efficiently through relatively small local power stations.

1.4 The modelling

There are many problems on the distribution side of power systems due to waveform unbalance and harmonic distortion caused by the single phase nature of the domestic loads and large number of electrical appliances within a household. With growing energy demand, an ample model of each of individual component in a conventional power distribution system with provisions for the representation of wind-based micro-grids is indispensable. The development of tools and methods embedded in software with which to carry out economic and security assessments of contemporary and future wind-based power distribution networks is the need of today.

The modelling of all components in the micro-network is carried out in harmonic domain using different tools available in Matlab and Matlab programming in particular. The harmonic domain models of transformer, synchronous generator and induction generator are prepared.

The individual micro-grids may contain a mix of conventional and renewable generation and may or may not be connected to the local utility grid. A comprehensive representation would enable realistic studies of distribution system to be carried out and following economic and technical justifications, a mean for assessing the optimal development of multifunction power electronics compensator with load balancing, power factor correction and harmonic capabilities in order to improve the overall efficiency of power network.

Fig 1.15 illustrates a future power system with a blend of conventional synchronous generation using any of the many forms of fossil fuels and synchronous and induction generators driven by wind turbines.

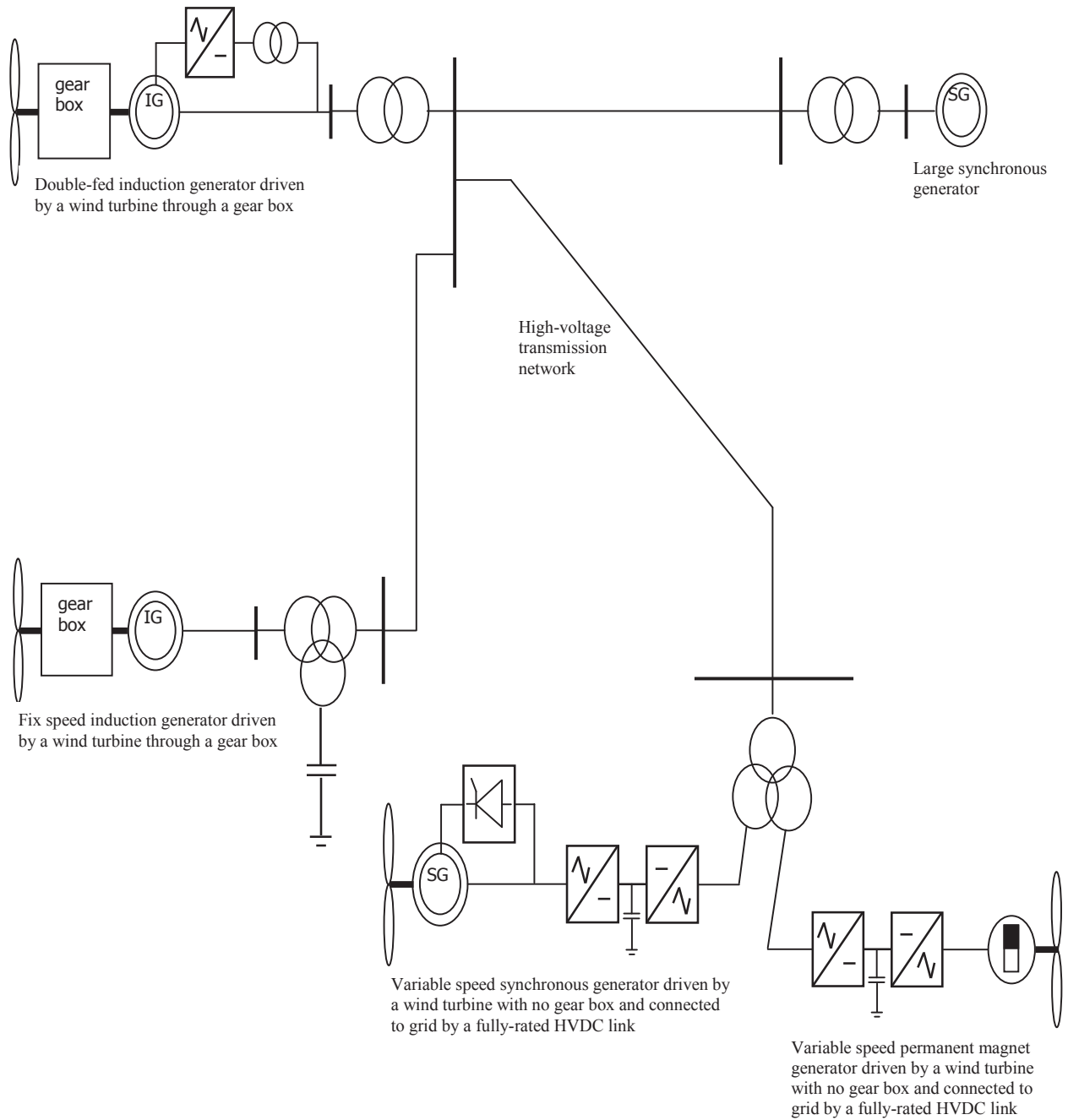


Fig. 1.15: Schematic diagram of a power system with various forms of wind turbines

1.5 Thesis outline

Chapter 1. This chapter has described different causes and effects of harmonic distortion in power system. The importance and necessity of accurate simulation models for the prediction of harmonic distortion in power system network is explained. The importance and role of the micro-grids in today's electricity market has been highlighted and technical issues associated with the development of micro-grids have been discussed. After a concise overview the aims of this research work are presented.

Chapter 2. The importance of the measurement of harmonic impedance and the methods to measure harmonic impedance at PCC are brought to light. An attention is drawn to different aspects of system response characteristics where parallel resonance is emphasized. A representative study system is devised and cases have been studied for frequency response characteristics. Imperative factors affecting parallel resonance are underlined. The impact of connecting a wind turbine generator to an existing substation is also analyzed.

Chapter 3. An overview of orthogonal series expansion is presented. Both the Fourier and Hartley analysis are discussed in short. A portion of the chapter has been dedicated to Hartley transforms and their importance is discussed. A unique computational comparison between the two discussed analysis methods is made to demonstrate the practical importance of the Hartley transforms.

Chapter 4. Historic developments in harmonic domain modelling of transformer are summerazed in chapter 4. A new model in harmonic domain for the magnetization branch of the transformer is derived and presented. The various non-linear effects found in transformer magnetic cores are outlined, with the emphasis on saturation due to its high impact on harmonic generation. The harmonic balance method is used for frame of reference to asses the harmonic behaviour of power transformer. Due to the fact that magnetic core saturation is well presented by polynomial functions and that these are open to to speedy harmonic evaluations with repeated convolution, an organized algorithm have been given in this chapter.

Chapter 5. Aiming at developing a flexible and comprehensive harmonic domain programme for the study of the periodic steady-state of electrical power systems, two new algorithms for harmonic domain models of a synchronous generator are developed. First using famous Fourier transforms and second using to an extent lesser popular Hartley's Transform. The derivations make the very practical assumption that damper windings are short circuited. The DC component of the excitation is taken into account and the harmonic admittance matrices of the synchronous generator in $dq0$ and $\alpha\beta\gamma$ axes are derived and used to obtain the admittance in abc coordinates by means of transformation metrics. Hartley's transform uses only real function and it shows efficiency advantage over a comparable module developed using the complex Fourier in some specific cases, however; the priority has been given to the Fourier transform owing to their popularity and other advantages.

Chapter 6. After a short description of the history and fundamentals of the wind based electrical power systems, different types of wind turbines has been compared and advantages and disadvantages of specific sets have been tabulated. Anatomy of wind turbine is briefly viewed and the possible methods to obtain synchronous power from wind based electrical generators are shown in this chapter. A new three-phase model of an induction generator is derived for wind-based electrical power system. The model includes wind turbine model as a sub model and has the compatibility with unbalanced three-phase distribution systems. The model also covers an analytical representation of its major components, mainly the wind turbine and the wound-rotor induction generator.

Chapter 7. This chapter draws an overall conclusion of this research. The suggestions have been made for the future research work.

A detailed list of references is also given at the end of appropriate subdivision which should be of great help in acquiring the understanding of relevant topic.

1.6 References

- [1] International Electrotechnical Commission (IEC), IEC 61000-3-6, IEC 61000-3-7, IEC 61000-3-13.
- [2] Institute of Electronics and Electrical Engineers (IEEE), IEEE 519-1992
- [3] J. W. George. “Power System Harmonics: fundamentals, analysis and filter design” Springer, 2001
- [4] C. Sankaran. “Power Quality” CRC Press LLC, 2002
- [5] J. Arrillaga, D. A. Bradley, P. S. Bodger. “Power System Harmonics” Wily, 1985
- [6] B. Drury; “The control techniques drives and controls hand book”, IET. 2nd Edition, 2009
- [7] R. C. Dugan, M. F. McGranaghan and H. W. Beaty; “Electrical Power Systems Quality”. McGraw-Hill, 1996
- [8] Arrillaga, Smith, Watson and Wood, “Power System Harmonic Analysis”, John Wiley & Sons, 1997
- [9] Ponsonby and Hardy, “Power Quality on London Underground’s Power system – a survey of recent work”. Recent Developments in Railway Electrification IEE Conference Publication /10458, p. 58, 2004
- [10] H. C. Lin, “Power system harmonics measurement using graphical programming tool”, Proceedings of the IEEE Conference on Cybernetics and Intelligent System, Singapore, 1-3, pp.885-889,2004
- [11] J. Arrillaga, Watson N.R.: Power System Harmonics. Wiley, Chichester, 2003
- [12] Persistent Link IEEE: <http://ieeexplore.ieee.org/servlet/opac?punumber=2227>. Recommended Practices and Requirements for Harmonic Control in Electrical Power Systems, 1993, revised 2002

- [13] Link: <http://ieeexplore.ieee.org/servlet/opac?punumber=2227>. IEEE Recommended Practices and Requirements for Harmonic Control in Electrical Power Systems, 1993, revised 2002
- [14] Julio Barros, Ramón I. Diego “A new method for measurement of harmonic groups using wavelet analysis in the IEC standard framework”; Science Direct, Electric Power Systems Research, vol.76, iss. 4, pp.200-208, 2006
- [15] ENA, Engineering Recommendations G5/4-1, www.ena-eng.org, 2005
- [16] Fred Wien, Power Quality and Utilization Guide, distribution generation and renewables, KEMA Nederland BV, 2006
- [17] DTI, Sustainable energy programmes, wind energy and electricity networks, 2001
- [18] Repo S, Laaksonen H, Jarventausta P, Huhtala O, Mickelsson M. A case study of a voltage rise problem due to a large amount of distributed generation on a weak distribution network. IEEE Power Tech Conference Proceedings, Bologna, Italy, vol. 4, pp. 1–6, 2003
- [19] Papathanassiou S. A technical evaluation framework for the connection of DG to the distribution network. Electric Power Syst RES, 77, pp-24–34, 2007
- [20] Dvorsky E, Hejtmankova P, Skorpil J. Control of micro-grids with renewable power sources. IEEE, PES transmission and distribution conference and exposition, pp. 1–4. 2008
- [21] Jiayi H, Chuanwen J, Rong X. A review on distributed energy resources and microgrid. Renew Sust Energy Rev, pp.2472-2483, 2007
- [22] Lasseter R. H. MicroGrids. In: IEEE power eng soc transm distrib conf, pp. 305–308. 2002

- [23] Marnay C, Venkataramanan G. Microgrids in the evolving electricity generation and delivery infrastructure. In: IEEE power eng soc gen meet; pp. 18–22, 2006
- [24] Pecas Lopes J. A, Moreira C. L, Madureira A. G. Defining control strategies for microgrids islanded operation. IEEE Trans Power Syst. pp. 916–24, 2006
- [25] Buchholz B, Engler A, Hatziargyriou N, Scholtes J, Schluecking U, Furones Fartos I. Lessons learned: European pilot installations for distributed generation. An overview by the IRED cluster. In: CIGRE, 2006
- [26] Hatziargyriou N, Asano H, Iravani R, Marnay C. Microgrids. IEEE Power and Energy Magazine, pp. 78–94, 2007
- [27] Fujioka Y, Maejima H, Nakamura S, Kojima Y, Okudera M, Uesaka S. Regional power grid with renewable energy resources: a demonstrative project in Hachinohe. In: CIGRE 2006
- [28] Mike BARNES. Real-world microgrids – an overview. IEEE International Conference on System of Systems Engineering. 2007
- [29] Lasseter B. Microgrids [distributed power generation]. IEEE, Power Engineering Society Winter Meeting, vol.1, pp.146-149, 2001
- [30] Xialing X, Xiaoming Z. Overview of the researches on distributed generation and microgrid. IPEC , Power Engineering Conference, pp. 966–971. 2007
- [31] Sudipta C. Distributed intelligent energy management system for a singlephase high-frequency AC microgrid. IEEE Transactions on Industrial Electronics , pp. 97-109, 2007
- [32] Dodge, D. M; ‘Illustrated History of Wind Power Development’, Littleton, Colorado, 2009

- [33] Marnay, C. and Venkataramanan, G.; ‘Microgrids in the evolving electricity generation and delivery infrastructure’ IEEE, Power Engineering Society General Meeting, 2006
- [34] G. T. Heydt; “Electric Power Quality” Stars in a circle Publications, 1991
- [35] Google images, www.google.com
- [36] Colin Bayliss and Brian Hardy; “Transmission and Distribution Electrical Engineering”, 4th Edition, Newnes, 2012
- [37] Graham Sinden; “Wind power and the UK wind resource” report by Environmental Change Institute, Oxford University, 2005

2. HARMONIC IMPEDANCE AT THE POINT OF COMMON COUPLING (PCC)

2.1 Introduction

The analysis of a power system component such as generators, transmission lines and transformers, rely on harmonic voltage and current distortion levels. The harmonic distortion in voltage and current is usually calculated by means of load flow studies with an assumption that power generation and transmission system is perfectly linear. In practice however, the transformer magnetising current harmonics will cause the generator to produce harmonic voltages and currents as harmonic interaction takes place between the rotor and stator circuit of the generator. The process of harmonic conversion changes the waveform of the transformer flux which produces distortion in the magnetising spectrum. This new magnetising spectrum results in repetition of the harmonic conversion process at the synchronous generator. Apart from this, any harmonic contribution from any other network component like transmission line, triggers the harmonic interaction between these two nonlinear power system components.

It is hard to analyse the effect of harmonic cross coupling by using a time domain method. However this is an important characteristic of harmonic formulation and its relevance is evident from harmonic studies. The dynamic analysis of the power system components often needs a detailed model for a certain part of the network, while the rest of the network can be considered an equivalent circuit. In this way the computation efforts required for simulation of the whole network is considerably reduced and simplified.

Short circuit impedance is probably the simplest equivalent model approach at the fundamental frequency. For studies such as fault analysis, this approach is good enough. However for studies where system response should be reproduced at harmonic frequencies, this model can not approximate the system's behaviour. Harmonic generating equipment, coupled with system resonance condition effects are cumulative and can be severe on system operations, if not mitigated. Capacitor banks for reactive power compensation, power converters in variable speed controls of wind turbine generators, FACTS devices and other

high power electronic devices used for power system control; are all major causes of harmonic penetration in the system.

The level of harmonic penetration is determined with the help of harmonic measurements and simulations. An option to achieve this is the programming of typical steady-state power flow software to compute the system frequency response. Frequency response at some typical operating conditions, parallel resonance situations and total harmonic distortion under these conditions are discussed in rest of this chapter.

2.2 Measurement of system's harmonic impedance

Modelling of systems under harmonic conditions involves the determination of the impedance of the system at harmonic frequencies, as well as the representation of the harmonic sources. The former is determined on the basis of the value of the different elements at power frequency of 50 Hertz. The model depends upon a number of things, for instance the accuracy of data and the range of frequency. It is hard to represent the complete system in full in all harmonic studies. The dimensions of the system are therefore reduced to minimum possible scale using the equivalent impedance representing the behaviour of the component to harmonic disturbances. The impedance varies over time and from one point to the other within the system. This variation depends upon the cable length, short circuit power of the system, the VAR compensation and the load level in the system. The measurement of the harmonic impedance of the system is quite difficult to implement. It necessitates the presence of a powerful harmonic current source or a relatively high pre-existing harmonic voltage at the node where the impedance is to be measured [1-2]

2.2.1 High pre-existing harmonic voltage

The pre-existing harmonic or inter-harmonic voltage V_h causes an inter-harmonic current to flow in load Z , as shown in Fig. 2.1.

The harmonic impedance Z_h is given by:

$$Z_h = \frac{V_{h_1} - V_{h_2}}{i_h} \quad (2.1)$$

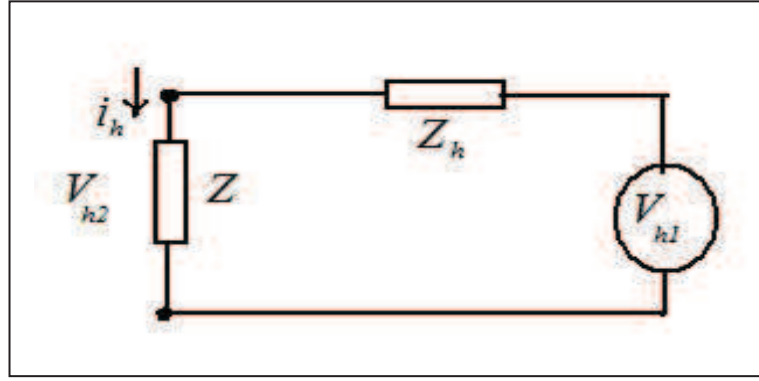


Fig. 2.1: Thevenin harmonic equivalent of a system.

2.2.2 Powerful harmonic current source

If there is not any harmonic voltage in the system before the injection of harmonic currents by equipment or by use of equipment; the injection will produce a harmonic voltage V_h .

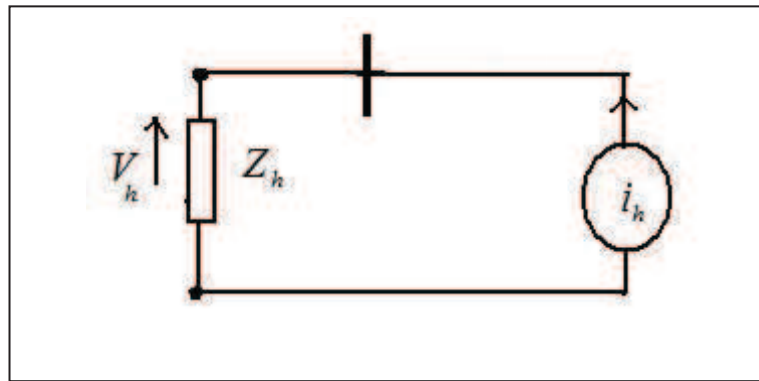


Fig. 2.2: Determination of harmonic impedance Z_h .

The harmonic impedance Z_h of stream system viewed from injection point is:

$$Z_h = \frac{V_h}{i_h} \quad (2.2)$$

2.3 System response characteristics

In power systems, the system response is equally as important as the source of harmonics. Identification of a source of harmonics is only half the job in harmonic analysis. The response of power system at each harmonic frequency determines the true impact of nonlinear loads on harmonic voltage distortion.

The impedance of the system can be determined by means of analytical computations as long the size of the system is not too large. The impedance of a system is formed of succession of resonances and any resonances which take place mainly due to the cable/transmission line capacitance. If the capacitance is high, these resonances are there at low frequencies (sometimes even at power frequencies). They are also present due to high installed load for VAR compensation.

At the fundamental frequency the power systems are primarily inductive and equivalent impedance is sometimes called simply the short-circuit reactance. The capacitive effects are normally neglected on utility distribution systems and industrial power systems. The inductive reactance of the system changes linearly with the frequency. In power systems, generally do not change significantly with frequency before 9th harmonic.

For lines and cables the resistance varies by square root of the frequency once skin effect becomes significant in the conductor at higher frequencies. At utilization voltages the equivalent system reactance is normally dominated by the in service transformer impedance. An approximation for X_{SC} , based on transformer impedance only is [3]:

$$X_{SC} \cong X_t \quad (2.3)$$

where
$$X_t = \frac{(kV)^2}{MVA} \times \%Z \quad (2.4)$$

The equivalent reactances of some of the ten percent transformers are given in the table. A plot of impedance vs. frequency for an inductive system without any capacitors installed would look like that shown in Fig. 2.3. However the real power systems rarely behave like this. Here the capacitance is neglected which can not be done for the harmonic analysis.

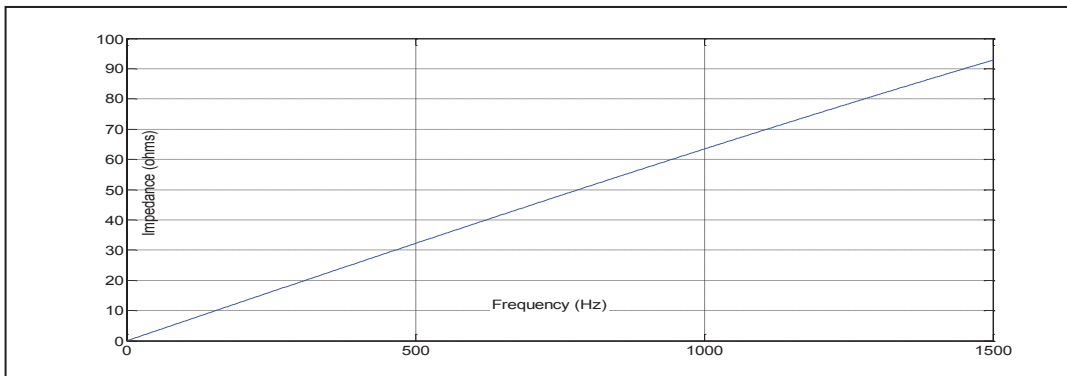


Fig. 2.3: Frequency response of an assumed purely inductive system.

Shunt capacitance either due to cable or due to capacitors at the customer locations for power factor correction on the utility distribution system, dramatically vary the systems impedance with frequency. A severe harmonic distortion can sometimes be endorsed due to their presence. The capacitive reactance X_c is given by:

$$X_c = \frac{1}{2\pi f C} \quad (2.5)$$

Where C is the capacitance. The equivalent line-to-neutral capacitive reactance can be determined by:

$$X_c = \frac{kV^2}{MVAR} \quad (2.6)$$

2.3.1 Parallel resonance

One particular worry with harmonics is the resonance condition in the power system. The existence of both inductive components and capacitive components in the system at certain frequencies can cause resonance conditions at point of common coupling or any other bus. If the resonance occurs at a bus where a harmonic current is injected into the system, an overvoltage condition may be observed.

All the circuits containing both inductances and capacitances have one or more natural frequencies. When one of these frequencies, is lined-up with a frequency that is being produced on the power system, resonance can develop in which voltages and currents in the system persist very high values. This is the root of many problems with harmonic distortion in power systems.

At harmonic frequencies, from the perspective of harmonic sources, shunt capacitors appear to be in parallel with equivalent system inductance as shown in Fig. 2.4. At frequencies other than fundamental frequency, the power system generation appears to be as short circuit. When X_c and total system reactance are equal (the difference between X_L and X_c becomes zero), the harmonic currents becomes extremely large. The resonant for a parallel combination of an inductive and capacitive element is:

$$f_{Resonance} = \frac{1}{2\pi\sqrt{LC}} \quad (2.7)$$

Where L is the inductance and C is the capacitance of the network [4]. At high voltages the resistance of a network is more often than not small compared with capacitance and

inductance. Therefore, the impedance can change radically. The situation becomes harsh when the resonance frequency matches with the frequency of any harmonic current or voltage. The harmonic current or voltage is amplified, which can cause damage of network components. At this point it is essential to remark that very often resonant frequencies are present between harmonic frequencies (inter harmonic resonance) [5].

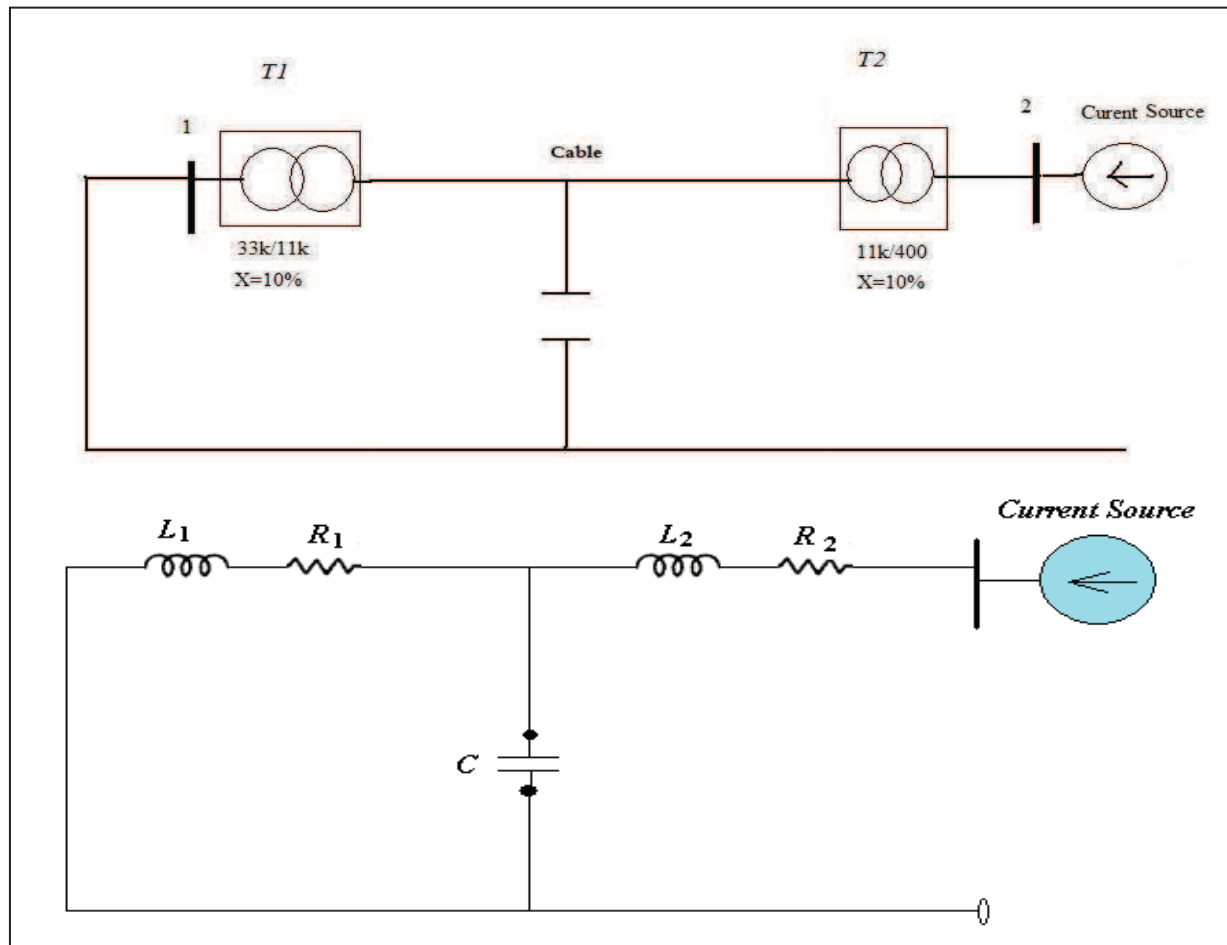


Fig. 2.4: Cable capacitance in the inductive system and equivalent circuit.

Same system may have several resonance frequencies depending upon the grid configuration. A relatively small distortion at a resonance frequency can lead to overwhelming consequences, which emphasizes the importance of the advance analysis of harmonics. There are two different types of resonances which may occur in the network; parallel resonance and series resonance [6-7], here the emphasis has been given on parallel resonance.

In parallel a resonance, the impedance of a circuit is usually high. In an ideal resonance (the circuit does not have any resistance) impedance becomes infinitely high, which leads to enormously high overvoltage. At parallel resonance frequency, the voltage obtains its uppermost possible value at a given current [8].

Table 2.1: Data for different parameters in Fig. 2.4, used for plots

Case /Plot	T1 MVA	T2 MVA	X1 Ω	X2 Ω	L1 mH	L2 mH
	X=10%	X=10%	$\left(\frac{V_L^2}{MVA}\right) \times 10\%$	$\left(\frac{V_L^2}{MVA}\right) \times 10\%$	$X_1/2\pi f$	$X_2/2\pi f$
1	5	0.5	2.42	24.2	7.7	77
2	5	1	2.42	12.1	7.7	38.5
3	5	5	2.42	2.42	7.7	7.7
4	10	0.5	1.21	24.2	3.9	77
5	10	1	1.21	12.1	3.9	38.5
6	10	5	1.21	2.42	3.9	7.7
7	15	0.5	0.81	24.2	2.6	77
8	15	1	0.81	12.1	2.6	38.5
9	15	5	0.81	2.42	2.6	7.7

Parallel resonance can occur when a source of a harmonic current is connected to the electrical circuit that can be simplified as a parallel connection of inductive and capacitive component. In an extreme case, even a relatively small harmonic current can cause destructively high voltage peaks at resonance frequency. Parallel resonance is common when there are capacitor banks or long AC lines or cables are connected with large transformers. In this case, large capacitances and inductances start to resonate with each other [4].

Simulation is performed based on the data presented in Table 2.1 for two different cable lengths. The cables are assumed of twenty five kilometres and fifty kilometres lengths at a

capacitance of $0.4 \mu\text{F}/\text{km}$. Therefore, $10 \mu\text{F}$ and $20 \mu\text{F}$ capacitance corresponds to $X_c = 320 \text{ Ohms}$ and $X_c = 160 \text{ Ohms}$ respectively. The resistance R_1 and R_2 in the circuit of Fig. 2.4 are assumed small (0.01 Ohms) and correspondingly transferred to 400V . The transformer is usually a very efficient machine and operates at an efficiency of about 98%; therefore its winding resistance is usually small and so is the case assumed in this discussion.

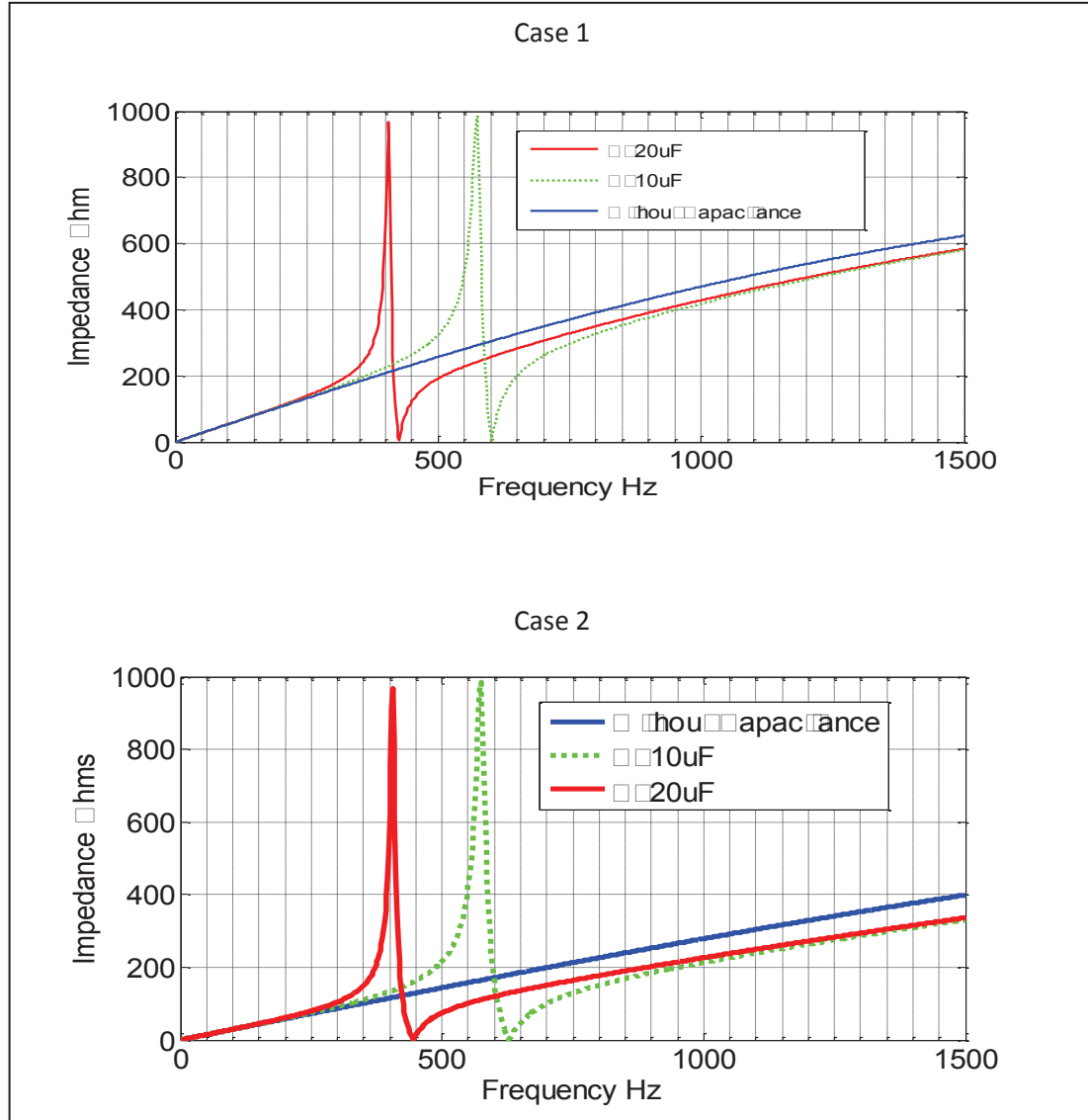


Fig. 2.5: Frequency response of circuit shown in Fig. 2.4, Case 1 and 2, Table 2.1

The parallel resonance in both the cases shown in Fig. 2.5 is occurring in the same region, 400 Hz and 575 Hz respectively for 50 km and 25 km cable lengths. This indicates that

transformer's rating as well as its physical location are the important factors and have significant effect in determining the resonance frequency.

Case 3, in the Table 2.1; is not considered as it can be seen from the transformer ratings that the system with such an arrangement will be un-economical and un-necessary.

Fig. 2.6 shows the frequency response of circuit shown in Fig 2.4. The graphs correspond to Case 4, Case 5 and Case 6 in the data Table 2.1. Unlike first three cases the transformer used from 33 kV to 11 kV is a 10 MVA transformer, which indicates a smaller value of inductive reactance.

Consequently the inductance in the circuit shown in Fig 2.4 has shifted to the new position determined by the size of the transformer. This is repeated for a 15MVA transformer in three following cases.

The resonance frequency also varies with cable capacitance. The longer is the length of cable, lower is the resonance frequency. It is also important to notice that the deviation from blue line in Fig. 2.6 as well as Fig. 2.7, starts quite earlier than actual peak occurs and continues after the the peak has occurred.

This explains that the real interval for which harmonic distortion is produced in the system can not be specified only by the spike due to parallel resonance. For instance in Case 9 of Fig. 2.7, the resonance curve starts moving away from the reference line at about 500 Hz and difference is present even beyond 1.5 kHz, which can cause severe impact on the quality of the supply voltage.

Moreover a comparsion of all the graphs from Cas 1 through to Case 9 shed light on the fact that the resonant frequency also depends upon the inductance value. For example the resonant frequency in Case1 for a $20\mu\text{F}$ capacitance is around 400Hz (Fig. 2.5), in Case 9 the resonance frequency has shifted to 700Hz for the same value of capacitance (Fig. 2.7). This factor is higly important and must be kept in mind while selecting the size of the transformer.

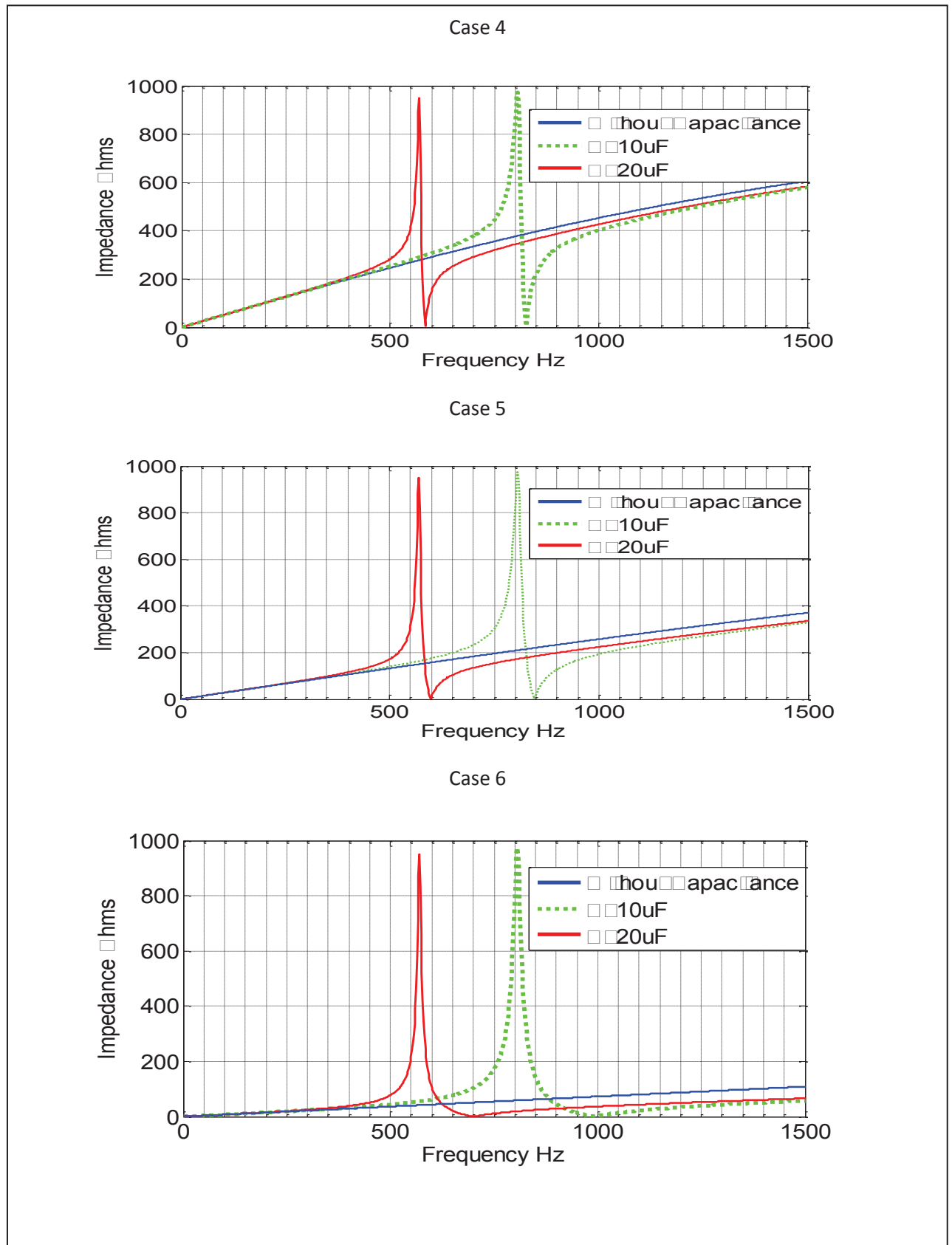


Fig. 2.6: Frequency response of circuit in Fig. 2.4, Case 4, 5 and 6, Table 2.1

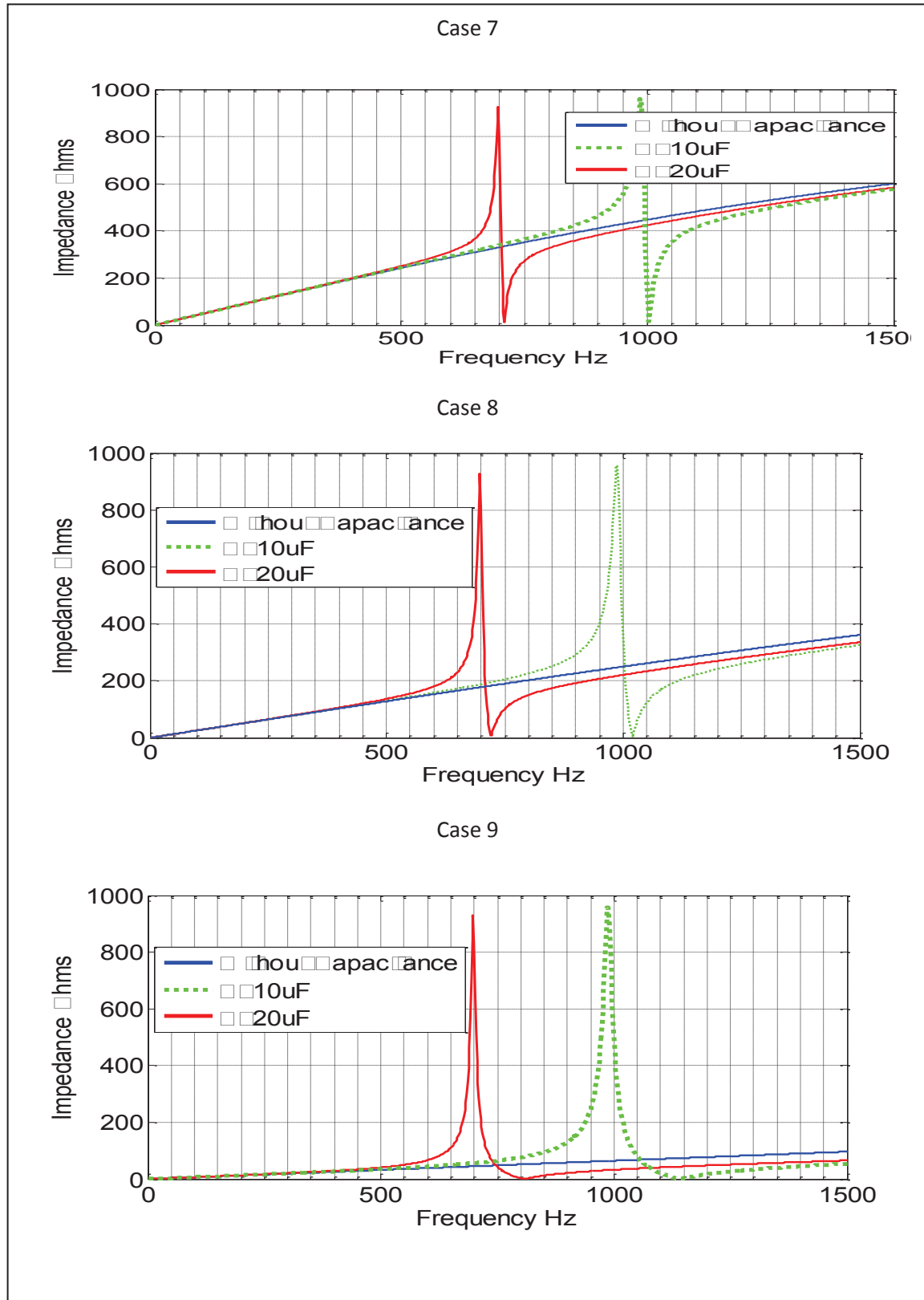


Fig. 2.7: Frequency response of circuit in Fig. 2.4, Case 7, 8 and 9, Table 2.1

For a certain known resonant condition, given the value of either inductive reactance or capacitive reactance, the value of unknown component can be evaluated. For example, if the resonant frequency is assumed at 500 Hz for Parallel combination of L_1 and C ;

$$C = \frac{1}{(2\pi \times 500)^2} \times \frac{1}{L_1} \quad (2.8)$$

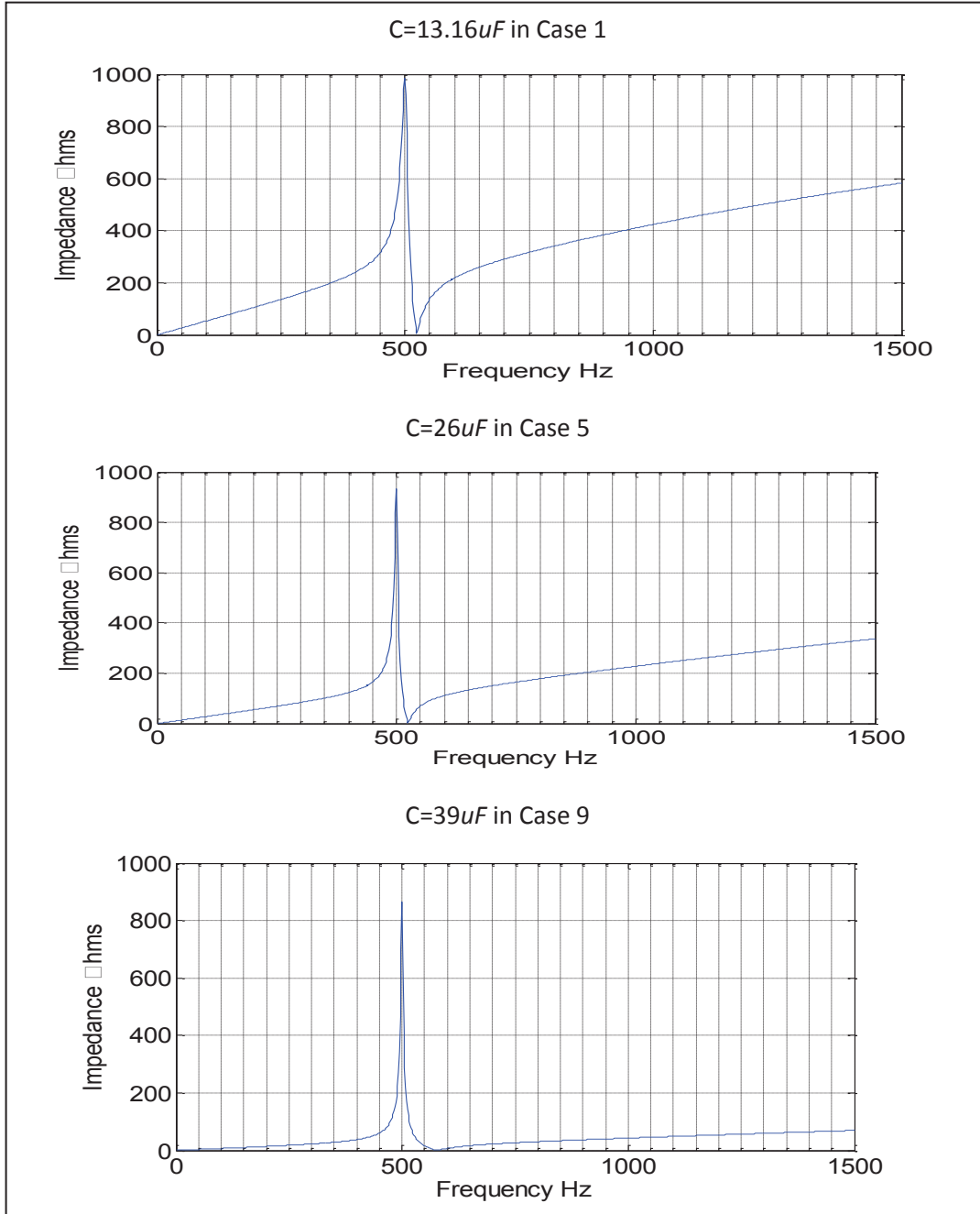


Fig. 2.8: Frequency response of circuit shown in Fig. 2.4, case 1, 5 and 9, Table 2.1; with pre-calculated fixed values of capacitances.

For three values of L_1 ; 7.7mH, 3.9mH and 2.6mH corresponding to for 5, 10 and 15 MVA transformers and an assumed resonance frequency of 500 Hz, the relevant capacitances are:

$$C_{5MVA} = \frac{1}{(2\pi \times 500)^2} \times \frac{1}{7.7 \times 10^{-3}} = 13.16\mu F$$

$$C_{10MVA} = \frac{1}{(2\pi \times 500)^2} \times \frac{1}{3.9 \times 10^{-3}} = 26\mu F$$

$$C_{15MVA} = \frac{1}{(2\pi \times 500)^2} \times \frac{1}{2.6 \times 10^{-3}} = 39\mu F$$

All three plots in Fig. 2.8, demonstrate good agreement with afore calculated respective values of resonant frequencies which substantiate the correctness of simulation process.

2.3.2 Effect of parallel resistive load

Determining that the resonant harmonic aligns with a common harmonic source is not always cause of alarm. The damping provided by the resistance in the system is often sufficient to prevent disastrous voltages and currents.

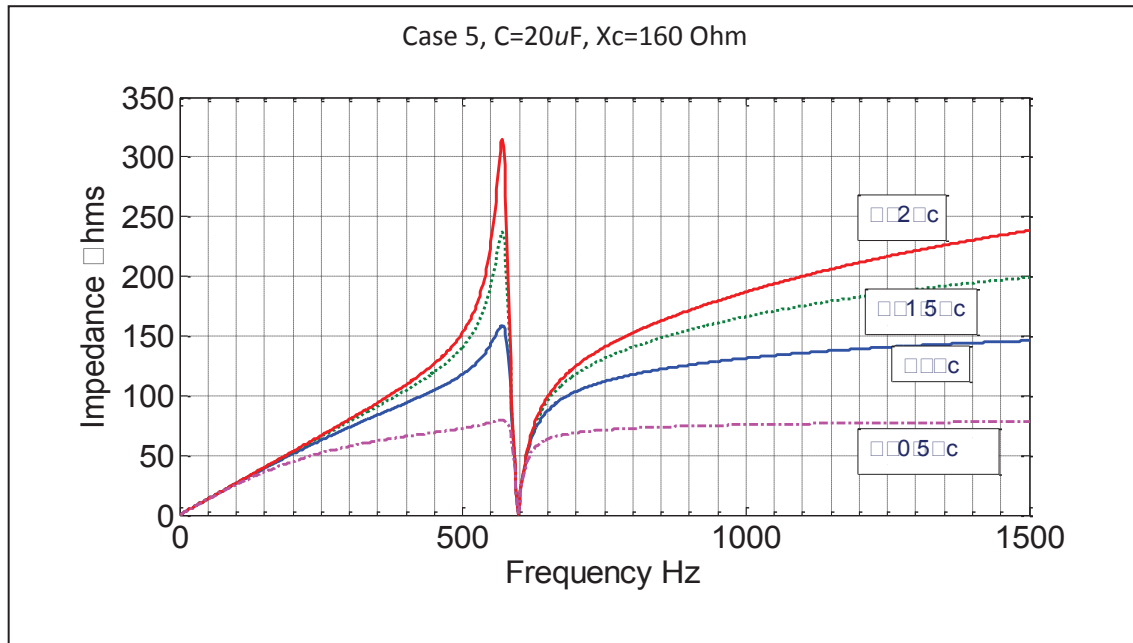


Fig. 2.9: Effect of parallel load resistance on the frequency response characteristics

Fig. 2.9 depicts the impact of three different parallel resistances in the same case of parallel resonance in system response characteristics. As little as ten percent resistor loading can have a noteworthy and valuable impact on peak impedance. The most troublesome resonant conditions evolve when capacitors are installed on substation buses where the transformer dominates the system impedance and has a high X/R ratio. The relative resistance is low and corresponding parallel resonant impedance peak is very sharp and high. This is a common cause of capacitor failure, transformer failure or the failure of other load equipment. It is a misunderstanding that resistive load damp harmonics as in the absence of resonance, load will have little impact on the harmonic currents and the resulting voltage distortion. Most of the current will flow back in the power source. Nevertheless it is appropriate to say the resistive loads damp the resonance hence considerably reducing the harmonic distortion. Motor loads are primarily inductive and provide little damping, rather they may cause an increase in the problem by shifting the resonant frequency closer to a significant harmonic. However some small fractional horsepower motors may help in damping because their X/R ratio is lower than large three phase motors

2.3.3 System response referred to LV side (400V)

At the receiving end or from consumer's point of view, the affect of parallel resonance discussed in section 2.3.2 can be better understood. When referred to low voltage side (400 V), the inductance representing transformers is given as:

$$\frac{L_{11kv}}{L_{400V}} = \left(\frac{11kV}{400V}\right)^2 \quad (2.9)$$

or

$$L_{1new} = \frac{L1}{\left[\frac{11kV}{400V}\right]^2}$$

Similarly the cable capacitance affcet can be transferred to low voltage side. When referred to 400 V, the equivalent to cable capacitance becomes:

For 25 km long cable

$$C = 10\mu F \times \left(\frac{11}{0.4}\right)^2 = 0.0076F$$

And for 50 km cable length

$$C = 20\mu F \times \left(\frac{11}{0.4}\right)^2 = 0.0151F$$

Table 2.2: Data for curves in Fig. 2.10

Case /Plot	T1 MVA	T2 MVA	X1 Ω	X2 Ω	L1 _{11kV} mH	L1 _{400V} mH	L2 _{11kV} mH	L2 _{400V} mH
	X=10%	X=10%	$\left(\frac{V_L^2}{MVA}\right) \times 10\%$	$\left(\frac{V_L^2}{MVA}\right) \times 10\%$	$X_1/2\pi f$	Base 400V	$X_2/2\pi f$	400V Base
1	5	0.5	2.42	24.2	7.7	0.0102	77	0.102
2	5	1	2.42	12.1	7.7	0.0102	38.5	0.051
6	10	5	1.21	2.42	3.9	0.00516	7.7	0.0102
9	15	5	0.81	2.42	2.6	0.0034	7.7	0.0102

More practical cases from Table 2.1 have been picked and set again in Table 2.2 with values of L1 and L2 referred to 400 V base correspondingly. The response of the circuit with these inductances and above calculated values of capacitances at a base voltage of 400 V is shown in Fig 2.10. If we compare results from this figure to those shown in Fig 2.5, we observe a vital difference; since the peak of the resonance is controlled by the resistive elements in the circuit, the curve is widened out. The percentage of harmonic distortion however remains the same. The parallel resonance in case 1, Table 2.2 occurs at:

$$f_{Resonance} = \frac{1}{2\pi\sqrt{LC}} = \left\{ \frac{1}{(2 \times \pi) \times \sqrt{((1.02e - 5) \times (0.0076))}} \right\}$$

$$= 571 \text{ Hz}$$

And for a cable length of 50 km

$$f_{Resonance} = \frac{1}{2\pi\sqrt{LC}} = \left\{ \frac{1}{(2 \times \pi) \times \sqrt{((1.02e - 5) \times (0.0151))}} \right\}$$

$$= 405 \text{ Hz}$$

This is matching with both the graphs shown in Fig 2.10 and Fig 2.5. Same is the case with rest of the contents of Fig. 2.10 and Table 2.2 which signify exactness of the analysis.

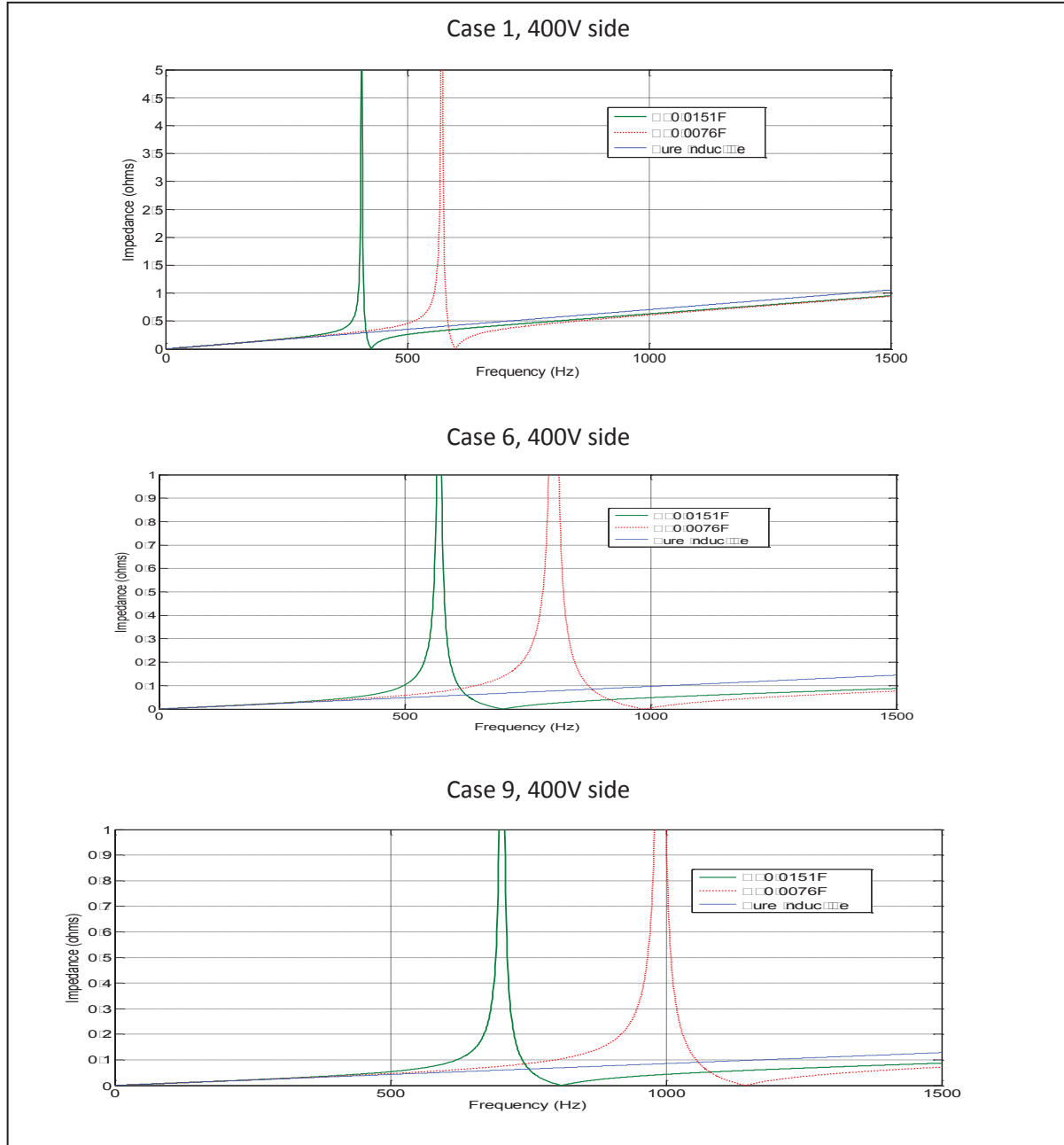


Fig. 2.10: Frequency response of circuit shown in Fig. 2.4 with reference to low voltage side, Case 1, 6 and 9, Table 2.2

Notice that the graphs in Fig. 2.10 are going out of the scale due to the deliberate selection of small scale along impedance axis. When referred to LV side the the total pure inductance of the system becomes very small and response line drops below recognizable point on normal

scale. The small scale has to be selected to visualise the distortion due to resonance and to compare it with the response of purely inductive circuit. Therefore peak of the curve is given lesser importance and more attention is paid to the clarity in reference line.

2.4 Harmonic resonance due to wind power plants

Wind power plants introduce a great number of non-linear power electronic devices like full scale frequency converters into the grid. The switching operations of the pulse width modulation (PWM) controlled converters are the main sources of both harmonic and inter harmonic currents. Generally speaking, converters create harmonics in the range of a few kilohertz. [16] Measuring and controlling these harmonics is one of the greatest challenges of the power quality in wind power plants [17]. A large number of non-linear power electronic devices can have significant effect on the harmonic emissions. These harmonics can form a serious threat for power quality. That is why harmonic analysis has to be developed and taken as an integrated part of wind power plant design. Because every power network is unique and has different characteristics, the effect of the harmonics on every power system varies. Nevertheless, some common features can be found. Even if the percentage of the harmonics seems small, the harmonic emission becomes a significant issue when the capacity of a wind power plant is hundreds of megawatts.

The wind power plants have their own resonance frequencies that are dependent on the grid topology, associated generators and reactive power apparatus used [9]. Furthermore the impedance and the resonance points of a wind park change all the time when the number of turbines and capacitor banks in operations changes or when there are changes in the connections of collector cables [10]. The more turbines the wind park has, the more the impedance can vary. The topic is especially important in large off shore wind parks, where the number of turbines in function can vary from a few to many hundreds. Moreover, off shore wind farms are connected with long cables that have large capacitance [11]. Summarised below are some of the most important components due to impedance changes.

2.4.1 Collector and transmission cables

An internal collector cable system of a wind power plant is one that connects the turbines of the wind park with each other and a transmission cable is one that connects the wind park to substation, many times located on shore. The total length of the collector cable system varies

in different kinds of off shore wind power plants from a few kilometres to tens of kilometres. The widespread submarine collector cable network can bring a large capacitance in the system. Underwater cables have to be resistant, and consequently well armoured [12]. The armouring affects a lot the impedance and the frequency response of underwater cables. The connection cable is another large capacitance that can magnify harmonic currents or voltages that are near the resonance frequency. The connection may be an AC or a DC cable depending on transferred distance. Naturally, these two options have different effect on resonance frequencies. The DC connection cable can also have tens of kilometres long distances. Harmonic resonance is one of the main technical challenges in the design and operation of off shore distribution system [13].

2.4.2 Reactors and capacitor banks

Capacitor banks are commonly used to compensate reactive power and to help improving the power factor in the power system network. Many times, there is a capacitor bank at each turbine as well as at the point of common coupling (PCC) [14]. The capacitor banks in the individual turbines are used also to support the voltage in sudden dips that may occur in harsh wind conditions. Starting capacitors are also in use in induction generators driven by wind turbines. Large wind power plants with even hundreds of turbines have a great number of different switching options for the capacitor banks.

There can also be shunt reactors connected to transmission cable terminations to compensate the high capacitance of the cables. These reactors are inductive components that may be adjustable and equipped with a tap changer. The reactors can be connected to the same switch together with the cable connection [15].

2.5 System response with an induction generator added

The induction generator is most widely used machine in wind-based power plants. Depending upon the size and location of wind power station, many times they are connected to 11kV bus bar in the main network. Therefore the system's response has been investigated with the addition of an induction generator and its effect on parallel resonance is analysed.

The generator is assumed to be a, 500 kVA, 440V, 50Hz and $X_{per-phase} = 0.8 \text{ Ohm}$. It is also assumed that the machine is not a self start one and uses a capacitor bank to start i.e. $C_{starting} = 200\mu\text{F}$. The generator is connected to 11kV bus through a cable of relatively

small length and a transformer with rating similar to transformer T2 in data Table 2.3. The whole arrangement and its equivalent circuit diagram are shown in Fig. 2.11. As the effect of starting capacitor when transferred to the secondary side of the transformer is small; the corresponding capacitance in the circuit is rounded of to a small value of $0.5 \mu\text{F}$ together with cable capacitance feeding generator power to the grid.

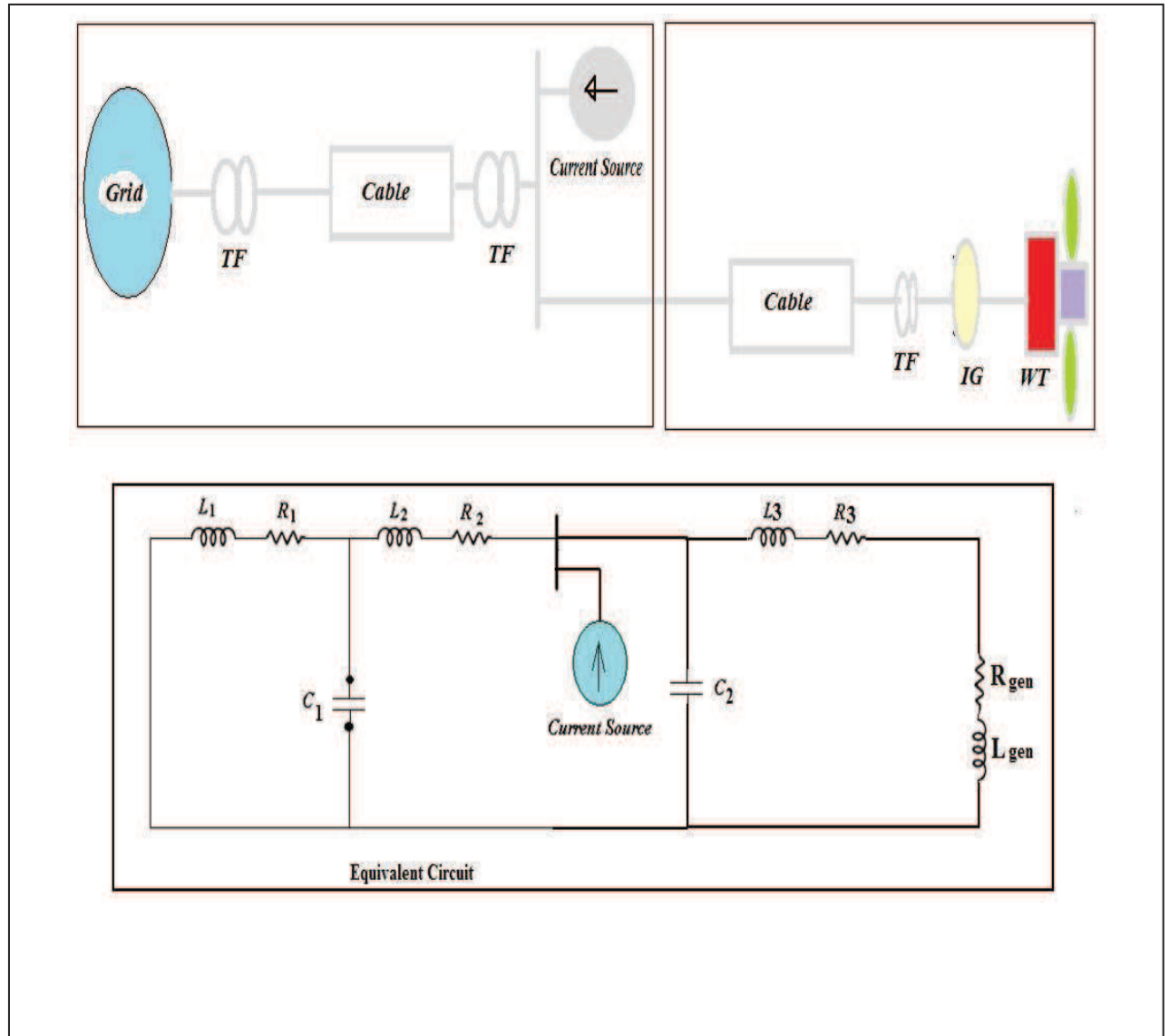


Fig. 2.11: A wind based induction generator connected to the system of Fig 2.4 and its per-phase equivalent electrical circuit

Two different situations arise when the generator is connected. First the wind-generator side of the Fig. 2.10 is referred to 11 kV bus as a whole; and second is that the already-existing equivalent part is referred to low voltage (400 V) side. The response of the circuit in both the situations under 4 different circumstances of Table 2.3 is given in Fig. 2.12-15.

Notice that cable capacitances represented by $C1$ and $C2$ are referred to $11kV$; when referred to low voltage side these values increase according to following relation:

$$C_{400V} = C_{11kV} \times \frac{(11kV)^2}{(400V)^2}$$

Also the $2.5mH$ inductance for the representation of generator when referred to $11kV$ is given by:

$$L_{Gen_{11kV}} = L_{Gen_{400V}} \times \frac{(11kV)^2}{(400V)^2} = 1.89 H$$

The resistances R_1 , R_2 and R_3 in the circuit are assumed to be small and when transferred to low voltage side are further dropped off, that is why, the skin effect has been ignored here.

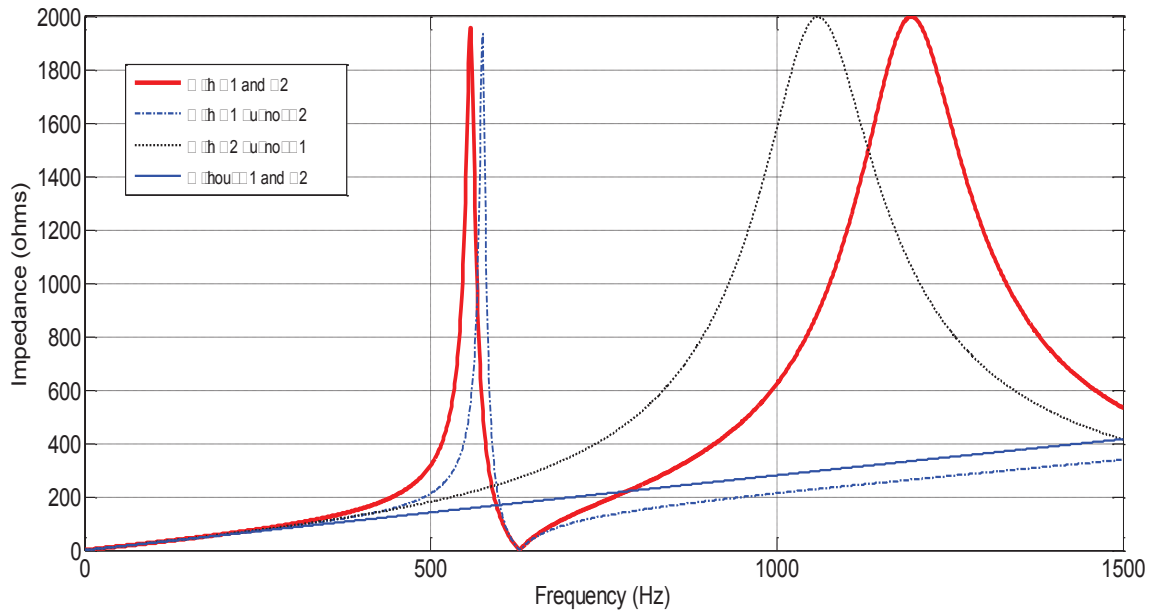
The generator resistance however when transferred to $11kV$, increases significantly i.e.

$$R_{Gen_{11kV}} = R_{Gen_{400V}} \times \frac{(11kV)^2}{(400V)^2}$$

Table 2.3: Data for components in Fig. 2.11.

Case /Plot	T1 MVA	T2 MVA	X1 Ω	X2 Ω	L1 mH	L1 _{400V} mH	L2 mH	L2 _{400V} mH
	X=10%	X=10%	$\left(\frac{V_L^2}{MVA}\right) \times 10\%$	$\left(\frac{V_L^2}{MVA}\right) \times 10\%$	$X_1/2\pi f$	Base 400V	$X_2/2\pi f$	400V Base
2	5	1	2.42	12.1	7.7	0.0102	38.5	0.051
3	10	1	1.21	12.1	3.9	0.00516	38.5	0.051
5	15	5	0.81	2.42	2.6	0.0034	7.7	0.0102
6	10	5	1.21	2.42	3.9	0.00516	7.7	0.0102

Case 2: $L_3 = L_2$, $R_3 = R_2$, $X_{gen} = 0.8 \text{ ohm}$, $L_{gen} = 2.5 \text{ mH}$, $R_{gen} = 0.1 \text{ ohm}$, $C_1 = 20 \mu\text{F}$, $C_2 = 0.5 \mu\text{F}$



Case 2 referred to 400V Side

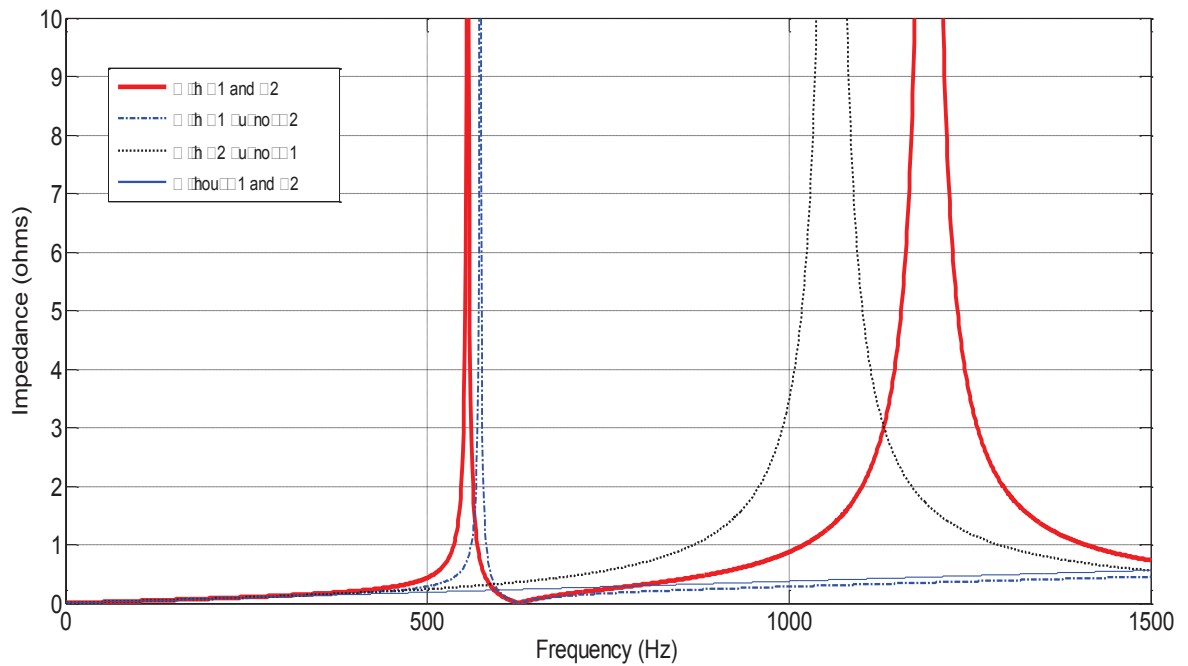
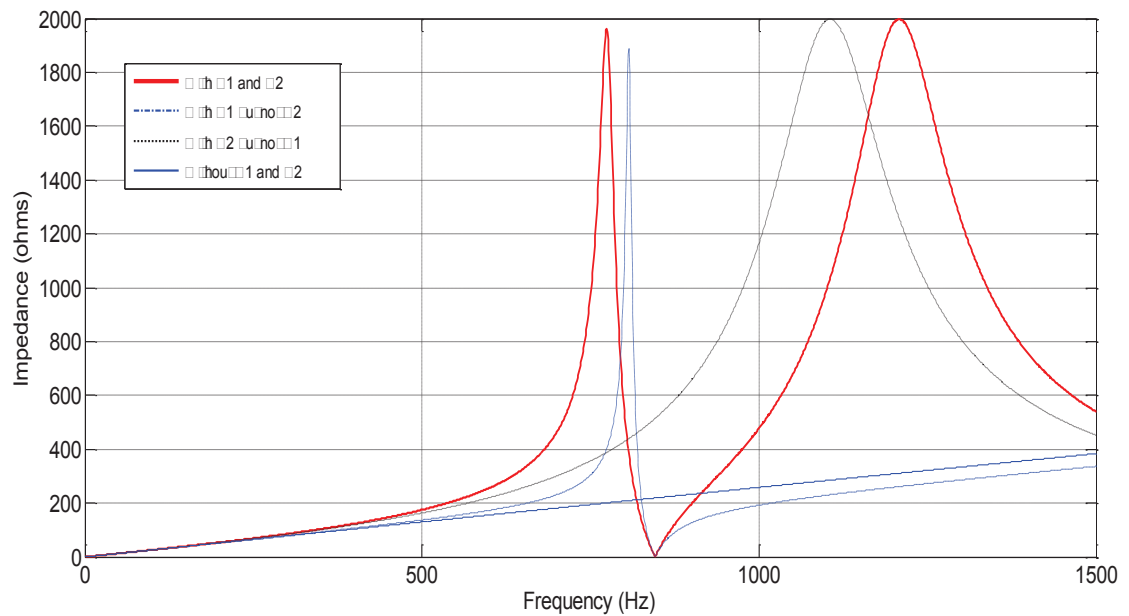


Fig. 2.12: Response of the circuit shown in Fig 2.11, Case 2, data from Table 2.3

Case 3: $L_3 = L_2$, $R_3 = R_2$, $X_{gen} = 0.8 \text{ ohm}$, $L_{gen} = 2.5 \text{ mH}$, $R_{gen} = 0.1 \text{ ohm}$, $C_1 = 20 \mu\text{F}$, $C_2 = 0.5 \mu\text{F}$



Case 3 referred to 400V Side

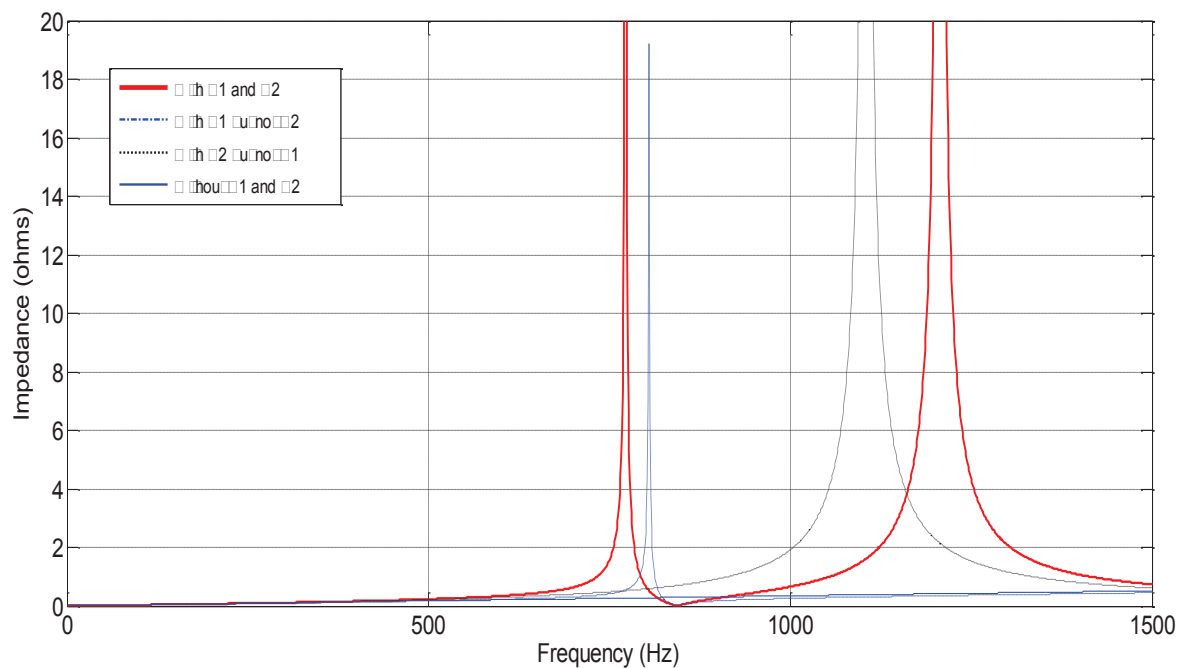
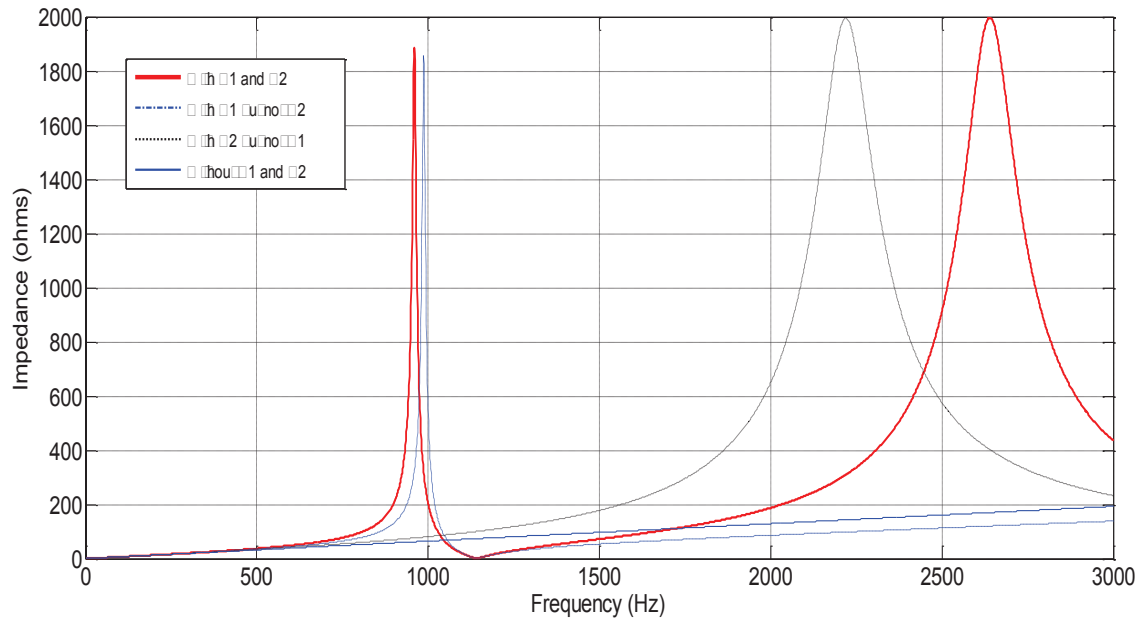


Fig. 2.13: Response of the circuit shown in Fig. 2.11, Case 3, data from Table 2.3

Case 5: $L_3 = L_2$, $R_3 = R_2$, $X_{gen} = 0.8 \text{ ohm}$, $L_{gen} = 2.5 \text{ mH}$, $R_{gen} = 0.1 \text{ ohm}$, $C_1 = 20 \mu\text{F}$, $C_2 = 0.5 \mu\text{F}$



Case 5 referred 400V Side

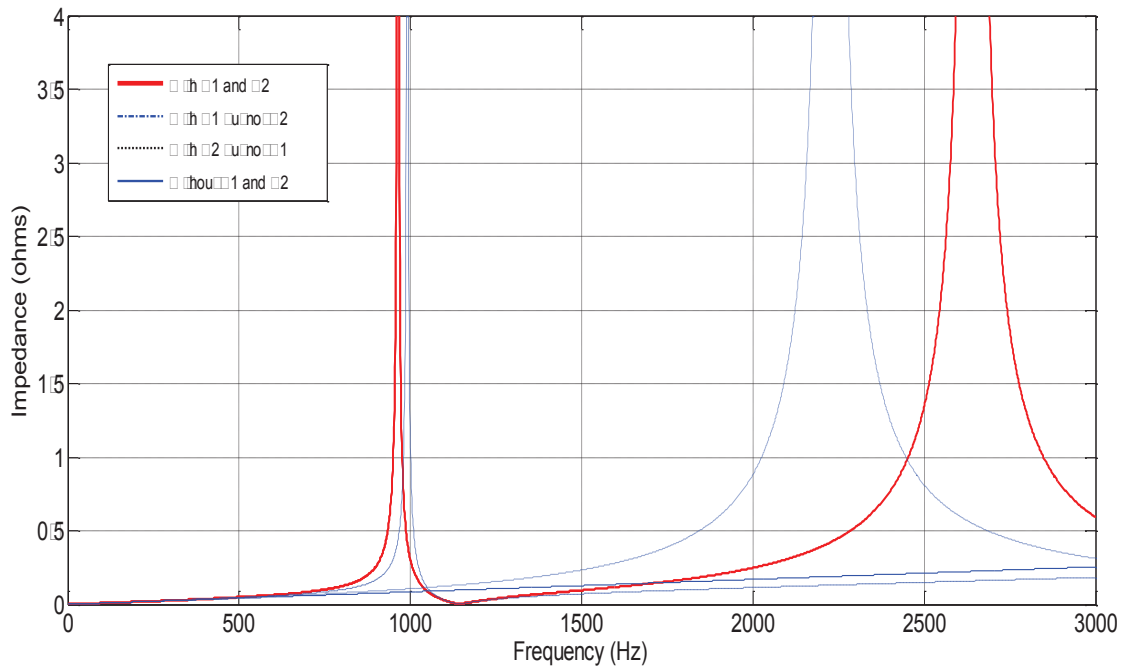


Fig. 2.14: Response of the circuit shown in Fig. 2.11, Case 5, data from Table 2.3

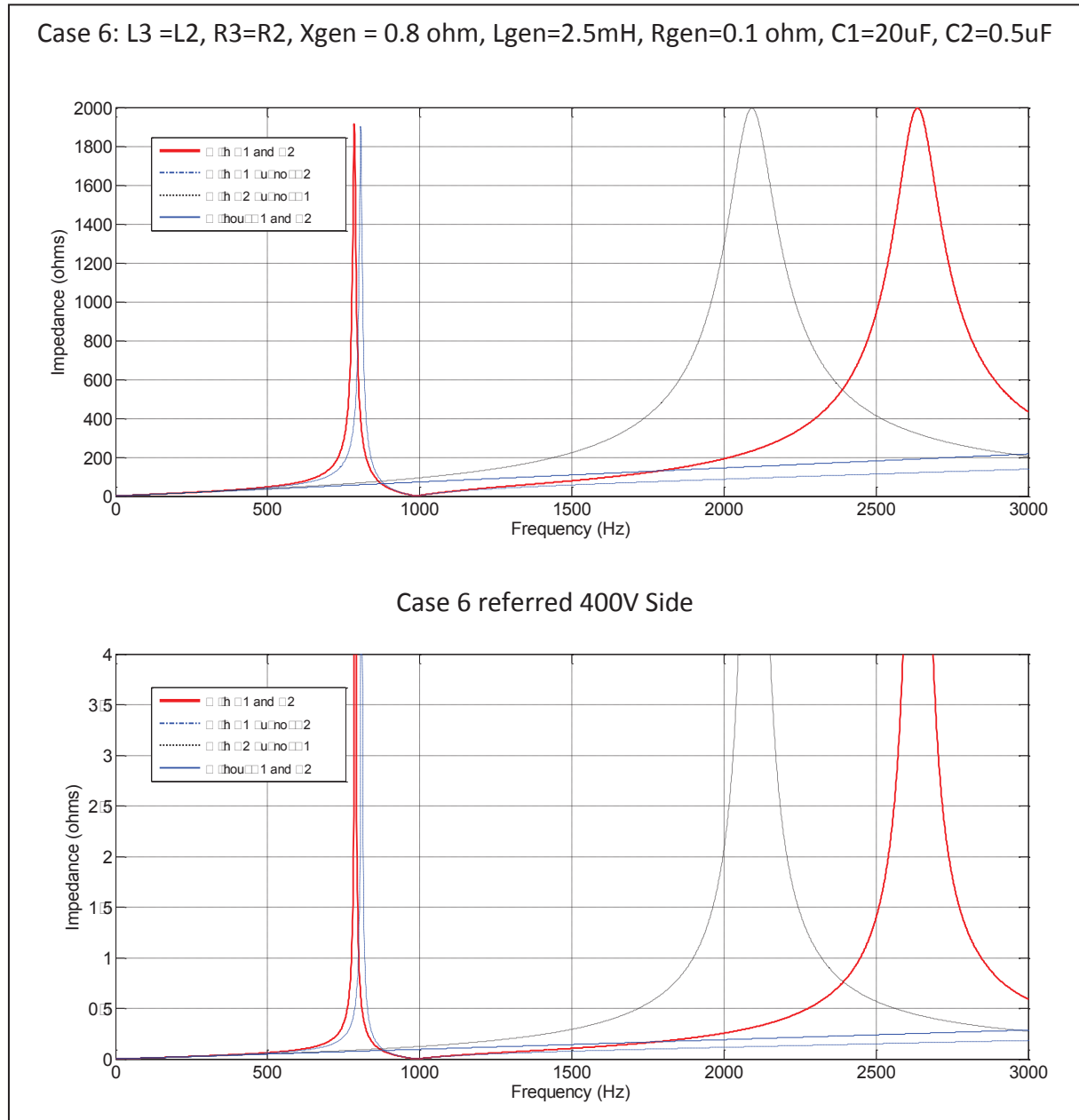


Fig. 2.15: Response of the circuit shown in Fig. 2.11, Case 6, data from Table 2.3

A comparison of waveshapes of all the cases shown in Fig. 2.12-15 with the corresponding case given in Fig. 2.5-6 shows that there is a huge distortion in waveform beyond about 600Hz. This is an indication of the impact of connecting a wind generator with main system due to parallel resonance because of the presence of collector cable and feeding step up transformer.

2.5.1 Impact of VAR compensation, power factor correction apparatus and starting capacitor on frequency response

The power factor correction and VAR compensation instruments usually consist of the capacitor banks, installed on substations and other locations in electrical power network. Fig. 2.16 shows such a capacitor installed with or near the induction generator unit and the frequency response of the circuit demonstrating the impact of a power factor correction or VAR compensation on the system when analysed with reference to 11kV bus. The values of different components are referred to case 1 of the Table 2.2. Notice that the peaks of resonance curves are being controlled by the small resistances present in the circuit. These resistances widen up the waveshape and do not allow the impedance value go beyond a certain magnitude depending upon their size.

In many cases wind power plants use induction generators which are not self start and use a large capacitor bank installed with them for the start up. These starting capacitor depend upon the size of the induction generator and can be up to 300 μF or even larger. Fig. 2.16 also shows the frequency response of the circuit demonstrating the impact of a 150 μF capacitor on the system when analysed with reference to 11kV bus. The values of different components are referred to case 1 of the Table 2.2. Again please notice that the peaks of resonance curves are being controlled by the small resistances present in the circuit. An equivalent capacitance of 151 μF is assumed to present instead of only 1 μF capacitor in circuit of Fig. 2.16.

Fig. 2.16 not only indicates that resonance occurs at very low frequencies but also shows that the starting capacitors and other such equipment can cause a significant shift in the resonance frequency. Although the starting capacitor may not continuously remain in the circuit and should be disconnected from the circuit as soon as the generator starts but even then the shift in resonance frequency is a matter of concern. The response of the circuit with both the cable capacitance and pf correction arrangements show that the deviation of red curve from the reference line unmistakably displays how power factor correction and VAR compensation equipment can cause harmonics and of what order these harmonics can be.

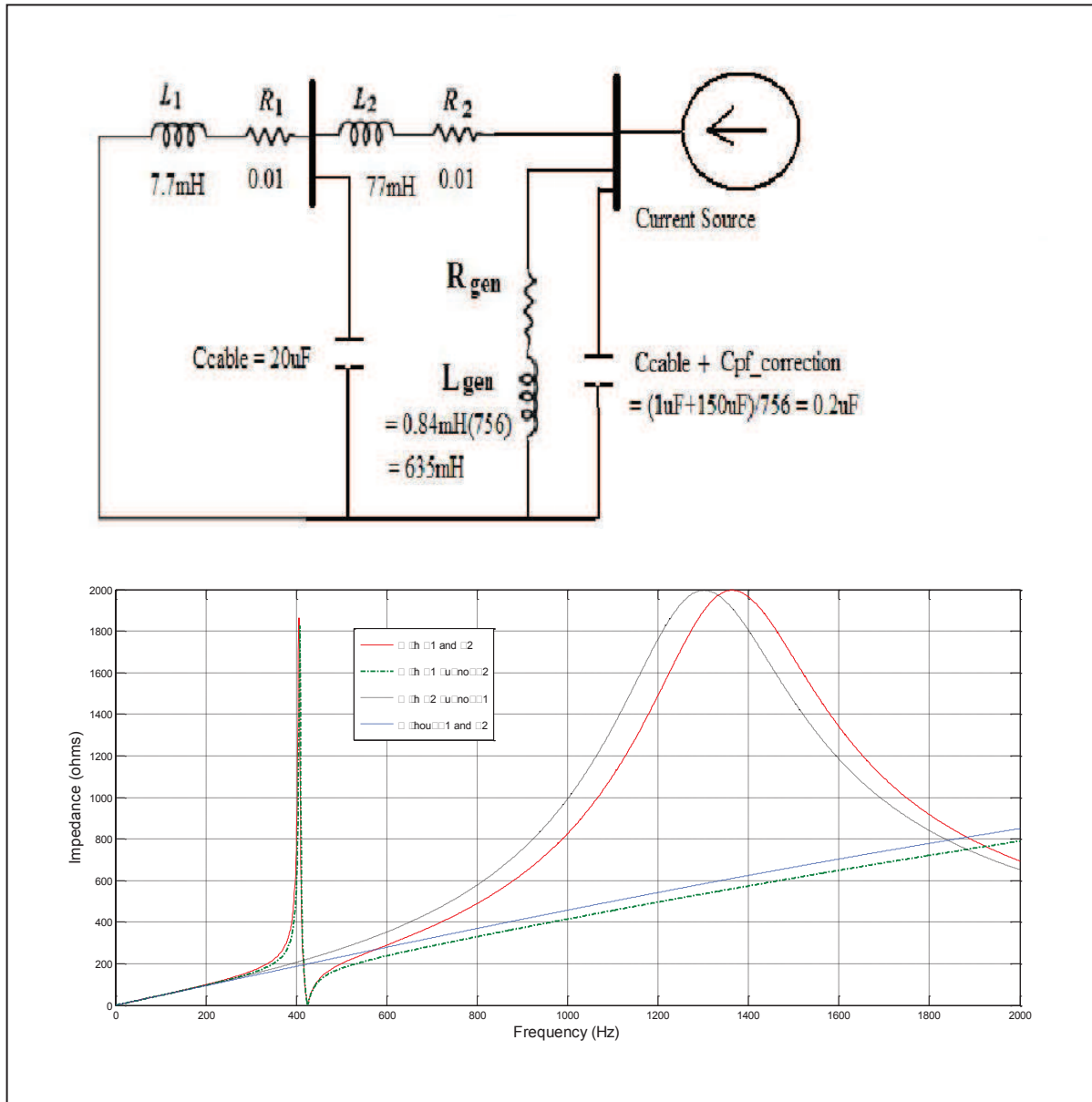


Fig. 2.16: Impact of power factor correction and VAR compensation

on system response, data from Table 2.3, Case 1.

2.6 Calculation of total harmonic distortion (THD)

The transformer used (T3 in Table 2.4) is a 60MVA one, depending upon voltage transformation level. 132kV to 66kV transformation is rarely practiced. The value of X has been calculated on 11kV base. Since skin effect has a significant effect on AC resistance and as in practice the skin effect may not be avoidable and should be a part of calculations, here it

is not ignored and value of the resistance is considered increased ten times the original value. Considered here is only the left hand side resonance area in the Fig. 2.18 to calculate THD.

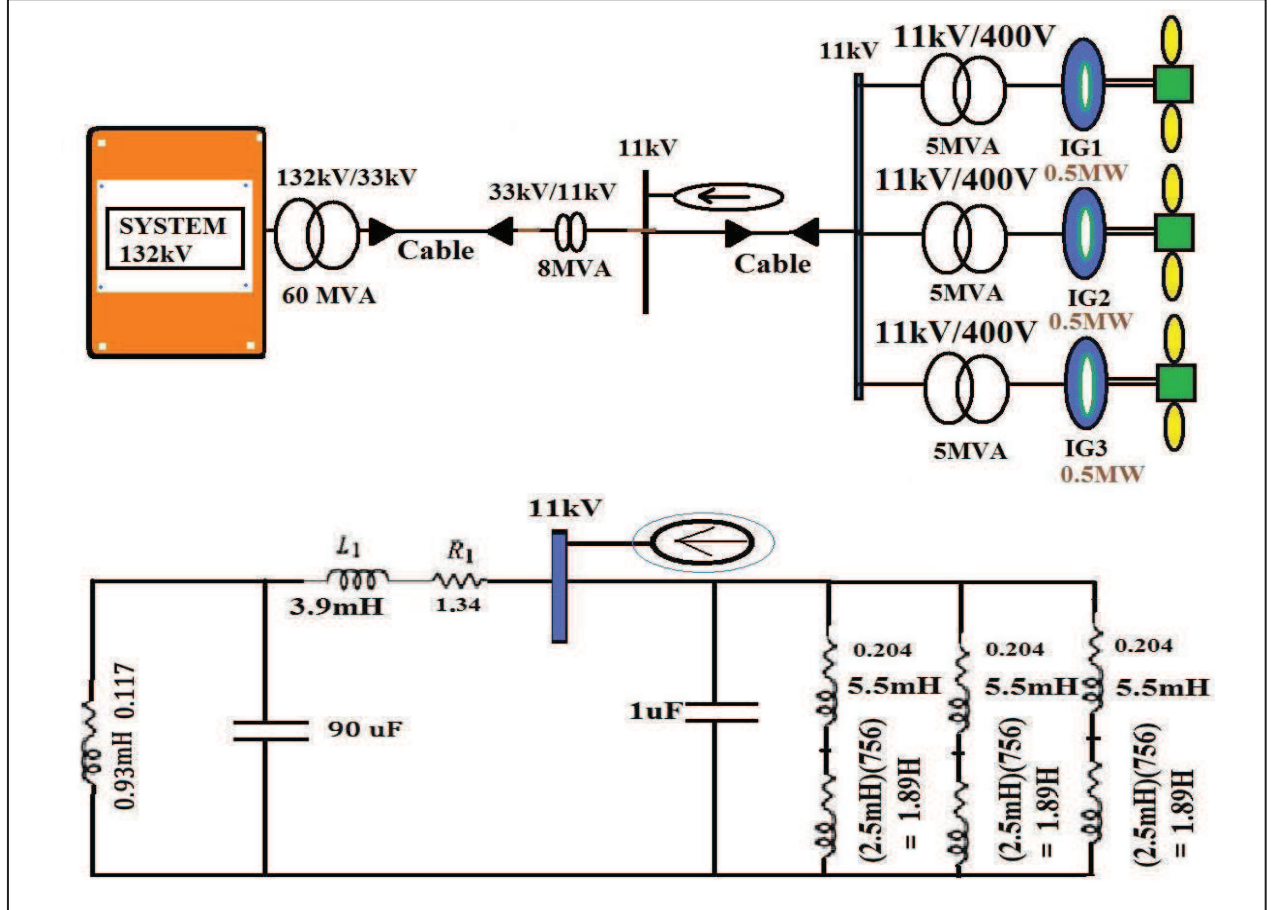


Fig. 2.17: A typical distribution system and its equivalent circuit diagram

For a cable length of an equivalent to 10 μ F capacitance on 33 kV, when referred to 11 kV side the equivalent capacitance will be:

$$C_{11kV} = \frac{C_{33kV}}{(11/33)^2} = 90 \mu F$$

And the parallel resonance occurs at:

$$f_{Resonance} = \frac{1}{2\pi\sqrt{LC}} = \left\{ \frac{1}{(2 \times \pi) \times \sqrt{((0.93 \times 10^{-3}) \times (90 \times 10^{-6}))}} \right\}$$

$$= 550.12 \text{ Hz}$$

The above calculated value of resonance frequency is in good approximation with simulation results as demonstrated by Fig. 2.18.

Table 2.4: Data for different components of the system shown in Fig. 2.17

T1 = 8 MVA	T2 = 5 MVA	T3 = 60 MVA	Gen = 0.5 MW
Z=8% ; X/R=9	Z=7.15% ; X/R=8.5	Z = 14.5% ; X/R = 25	X per-phase = 0.8
$X1 = \left(\frac{V_L^2}{MVA} \right) \times 8\%$ =1.21Ω	$X2 = \left(\frac{V_L^2}{MVA} \right) \times 7.15\%$ =1.73Ω	$X3 = \left(\frac{V_L^2}{MVA} \right) \times 14.5\%$ =0.29 Ω	$L_{gen} = X / 2\pi f$
R1 = X/9 = 0.1344 Ω Including skin effect R1= 1.344 Ω	R2 = X/8.5 = 0.204 Ω	R3 = X/25 = 0.0117 Ω Including skin effect R3= 0.12 Ω	Rgen = 0.01 Ω
$L1 = X / 2\pi f = 3.9 \text{ mH}$	$L2 = X / 2\pi f = 5.5 \text{ mH}$	$L3 = X / 2\pi f = 0.93 \text{ mH}$	Lgen = 2.5 mH

Fig. 2.18 shows the frequency response of the system shown in Fig 2.17 and a zoomed view for the calculation of total harmonic distortion. As mentioned earlier the emphasis is given only on non-tripline odd harmonics and studies has been limited to 5th, 7th and 11th harmonic terms. For star-delta configuration the tripline harmonics (3rd, 9th, 15th and 21st) are circulated inside the delta connected winding and do not propagate to the system. With the assumption that there will be no even harmonics present, rest of the analysis is performed for only 5th, 7th and 11th harmonic terms. Assuming that our 500 kVA, 440V, 50Hz induction generators is operating at a power factor of 0.85; total active power of the individual machine is given by

$$P = 0.85 \times kVA$$

$$= 0.85 \times 500$$

$$= 425 \text{ kW}$$

$$\text{or } P_{per-phase} = \frac{425}{3} \cong 140 \text{ kW}$$

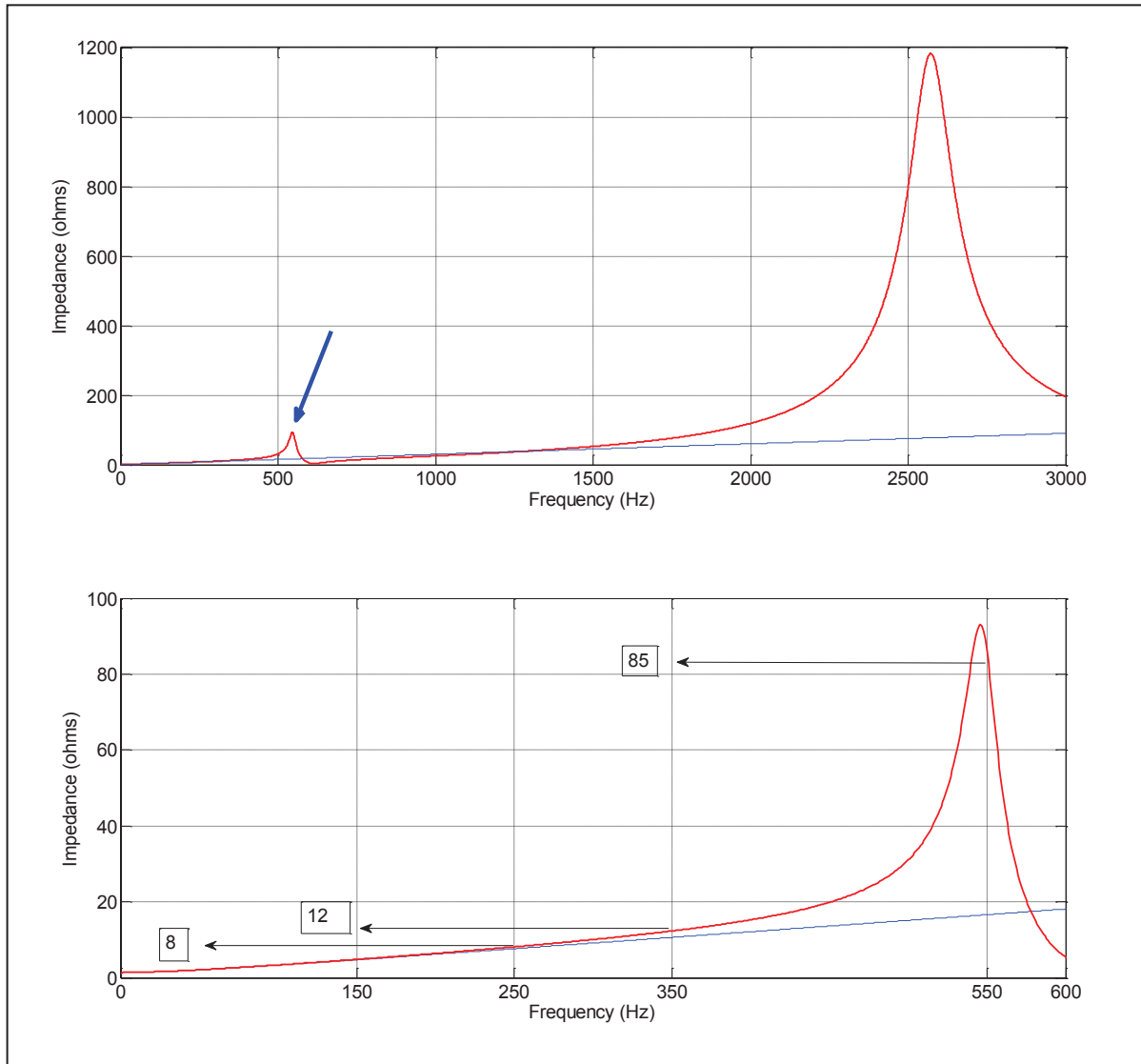


Fig. 2.18: Frequency response of the system shown in Fig 2.17

On the assumption that the machine is operating at unity power factor and rounding the induction generator power to $0.5MW$

$$P_{Gen} = 0.5MW$$

$$or \ P_{Gen \ per-phase} = \frac{0.5}{3} \cong 166kW$$

At a phase voltage of 11kV, the fundamental current is

$$I = \frac{166kW}{11kV/\sqrt{3}} \cong 26A$$

For 50Hz fundamental frequency

$$5^{th} \Rightarrow 50 \times 5 = 250 \text{ Hz}$$

$$7^{th} \Rightarrow 50 \times 7 = 350 \text{ Hz}$$

$$11^{th} \Rightarrow 50 \times 11 = 550 \text{ Hz}$$

The impedance values are 8Ω , 12Ω and 85Ω for corresponding 5^{th} , 7^{th} and 11^{th} harmonic frequencies, obtained from the frequency response of the circuit and shown in the graphs with arrows.

With 5^{th} harmonic @ 60% $\Rightarrow I_5 = 26 \times 0.6 = 15.6A$

$$7^{th} \text{ harmonic @ } 45\% \Rightarrow I_7 = 26 \times 0.45 = 11.7A$$

$$11^{th} \text{ harmonic @ } 40\% \Rightarrow I_{11} = 26 \times 0.4 = 10.4A$$

$$I_{THD} = \frac{\sqrt{(15.6)^2 + (11.7)^2 + (10.4)^2}}{26} \times 100 = 85\%$$

For harmonic voltage distortion

$$V_5 = I_5 \times X_5 = 15.6 \times 8 = 124.8 \text{ V}$$

$$V_7 = I_7 \times X_5 = 11.7 \times 12 = 140.4 \text{ V}$$

$$V_{11} = I_{11} \times X_5 = 10.4 \times 85 = 884 \text{ V}$$

$$V_{THD} = \frac{\sqrt{(124.8)^2 + (140.4)^2 + (884)^2}}{\left[11kV/\sqrt{3}\right]} \times 100 = 14.23\%$$

Which is way beyond the tolerable limit. In order to reduce THD to a permissible range and to add more wind based units, the transformer used should be a larger one with low value of %X. For example, instead using 60MVA if we install an 80MVA transformer in the system shown in Fig. 2.16, total harmonic distortion in voltage is lowered to about 5%. Another way to maintain total harmonic distortion within acceptable range is that filters have to be arranged so that 11^{th} harmonic in particular does not penetrate more than ten percent in the system. If we assume a lower rate of 11^{th} harmonic in above system, say 10%; then:

$$I_{11} = 26 \times 0.1 = 2.6A$$

And total harmonic distortion in current becomes

$$I_{THD} = \frac{\sqrt{(15.6)^2 + (11.7)^2 + (2.6)^2}}{26} \times 100 = 75\%$$

Similarly

$$V_{11} = I_{11} \times X_5 = 2.6 \times 85 = 221 V$$

So total harmonic distortion in voltage will be

$$V_{THD} = \frac{\sqrt{(124.8)^2 + (140.4)^2 + (221)^2}}{\left[11kV/\sqrt{3}\right]} \times 100 = 4.57\%$$

2.7 Harmonics out of an inverter

If the WT operates at variable rotational speed, the electric frequency of the generator varies and must therefore be decoupled from the frequency of the grid. This can be achieved by an inverter system. There are two different types of inverter systems:

1. Grid-commutated inverter systems
2. Self-commutated inverter systems

The grid-commutated inverters are mainly thyristor inverters, e. g. 6 or 12 pulse. This type of inverter produces integer harmonics like the 5th, 7th, 11th and 13th order etc (frequencies of 250, 350, 550, 650 Hz), which may be reduced by harmonic filters. On the other hand thyristor inverters are not able to control the reactive power. Their behaviour concerning reactive power is similar to the behaviour of an induction generator they consume inductive reactive power.

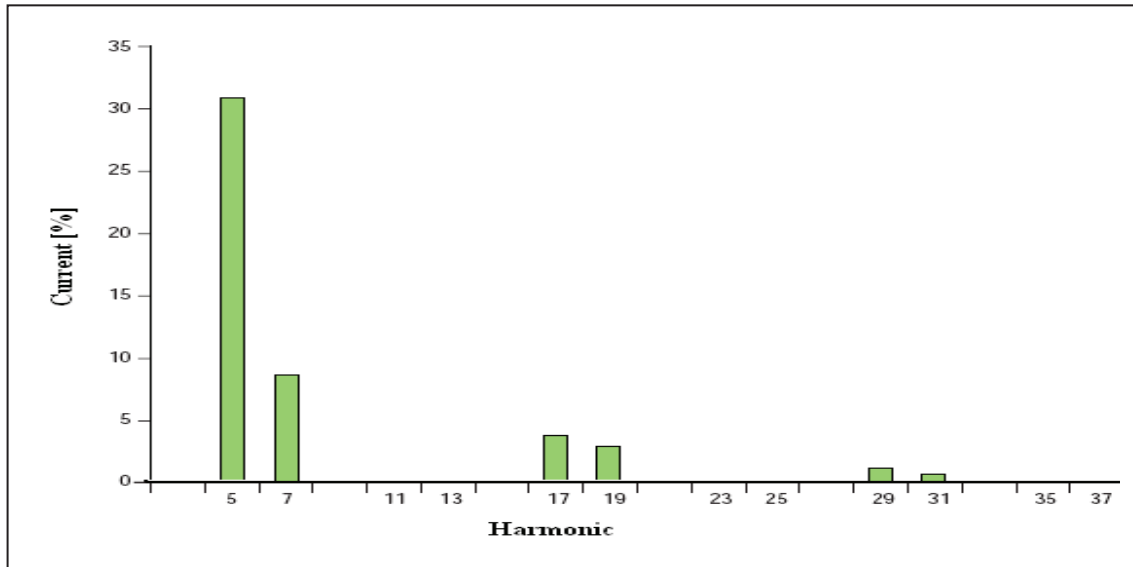


Fig. 2.19: Harmonic currents out of 6-pulse thyristor inverter [18]

Self-commutated inverter systems are mainly pulse width modulated (PWM) inverter, where IGBTs (Insulated Gate Bipolar Transistors) are used. This type of inverter gives the advantage that in addition to the control of the active power the reactive power is also controllable. That means the reactive power demand of the generator can be delivered by the PWM-inverter. One disadvantage is the production of interharmonics. In general these interharmonics are generated by the inverter in the range of some kHz. Thus filters are necessary to reduce the interharmonics. But due to the high frequencies, in general the construction of the filters is easier.

Highly distorting loads are older un-filtered frequency converters based on thyristor technology and similar types of equipment. It is characteristic for this type that it switches one time in each half period and it may generate large amounts of the lower harmonic orders, i.e. up to $N=40$. Newer transistor based designs are used in most variable speed WT today. The method is referred to as Pulse Width Modulation (PWM). It switches many times in each period and typically starts producing harmonics where the older types stop, that is around 2 kHz. Their magnitude is smaller and they are easier to remove by filtering than the harmonics of lower order. IEC 1000-3-6 put forward guidelines on compatibility and planning levels for MV and HV networks and presents methods for assessing the contribution from individual installations to the overall disturbance level.

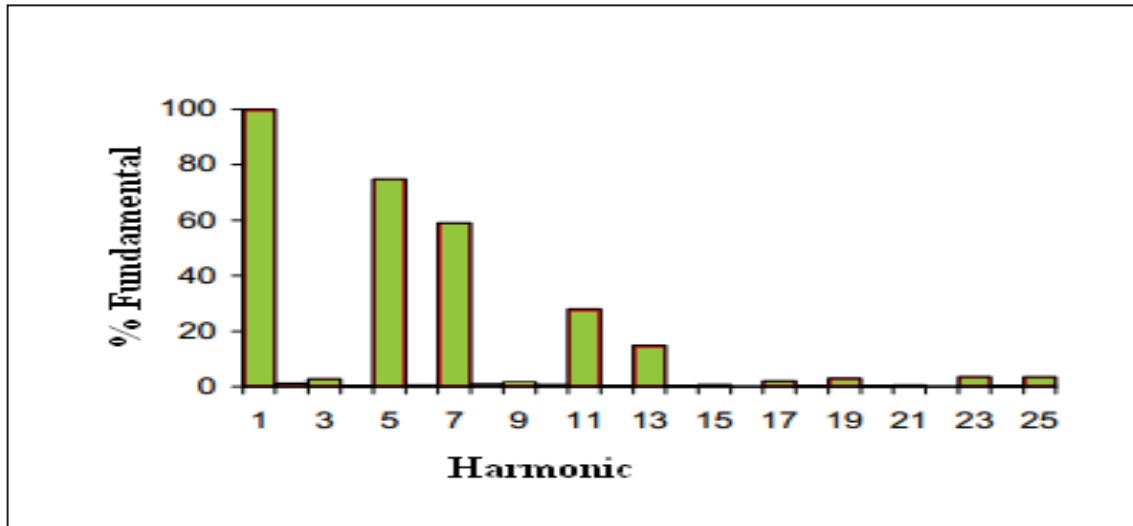


Fig. 2.20: Harmonic currents out of 6-pulse PWM drive [19]

In modern wind power plants a number of different power electronic apparatus is installed, which is the core reason for harmonics in the wind power plants. The switching operations of the pulse width modulation (PWM) controlled converters are the main sources of harmonic and inter harmonic currents, but not the only ones. Generally speaking, converters create harmonics in the range of a few kilohertz. Measuring and controlling these harmonics is one of the greatest challenges of the power quality in wind power plants.

Wind turbine and induction generator set using power electronic equipment when connected to the electrical system has to be checked concerning harmonics. The harmonic current emission of such wind turbine with power electronics are usually given in the power quality data sheet. Limits for harmonic emissions are often given only for harmonic voltages, not for harmonic currents. Thus harmonic voltages must be calculated from the harmonic current emission of the wind turbine. But the grid impedances vary with frequency, where the utilities often can not give the frequency dependency of the grid impedances, which makes calculations difficult [18].

Nowadays new wind turbines are variable speed wind turbines that are connected either partly or totally to the internal medium voltage network of a wind power plant through a power electronic converter [20]. In the both types, the power converter actually has two parts,

the rotor side converter and the grid side converter that are jointed together by parallel capacitance. This kind of converter is called back-to-back converter [21].

Most common types of wind turbines are:

a) Doubly fed induction generator (DFIG). It offers the flexibility to operate at the maximum power output over a wide range of wind speed without the necessity of having a full rated converter [22]. The main idea of a doubly fed induction generator turbine is shown in Fig. 2.21. The rotor side converter handles the active and reactive power control of the generator and the grid side converter keeps the voltage of the DC link constant [23].

b) The second type of wind turbines is the full scale converter, where all the power from the generator and flows through the converter. The generator can be either an induction generator or a synchronous generator. In the latter case the generator is usually a permanent magnet synchronous generator that is the most widely used type of synchronous generators.

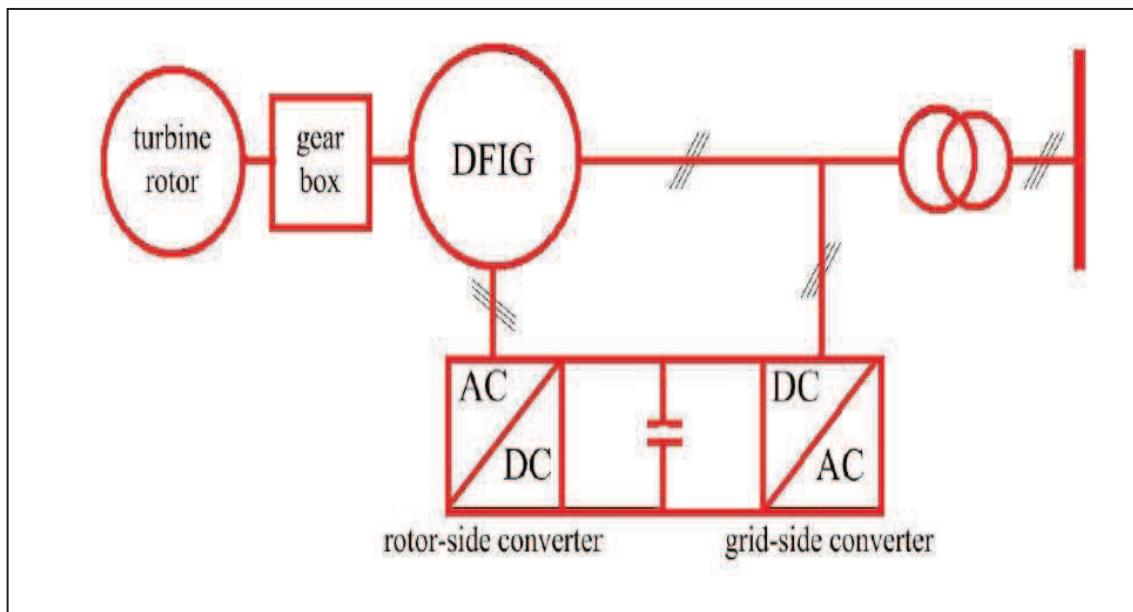


Fig. 2.21: DFIG with a rotor, a gear box and a converter [24].

Permanent magnet synchronous generator becomes more and more feasible option along the development of the technology [25-26]. The arrangement of using a synchronous generator with a full scale converter provides a lot of flexibility in the operation as it can support the network offering reactive power even if there was not wind at all [27]. An arrangement of a

synchronous generator with a full scale converter is shown in Fig. 2.22. The harmonic emissions of wind turbines can be classified as characteristic and noncharacteristic harmonics.

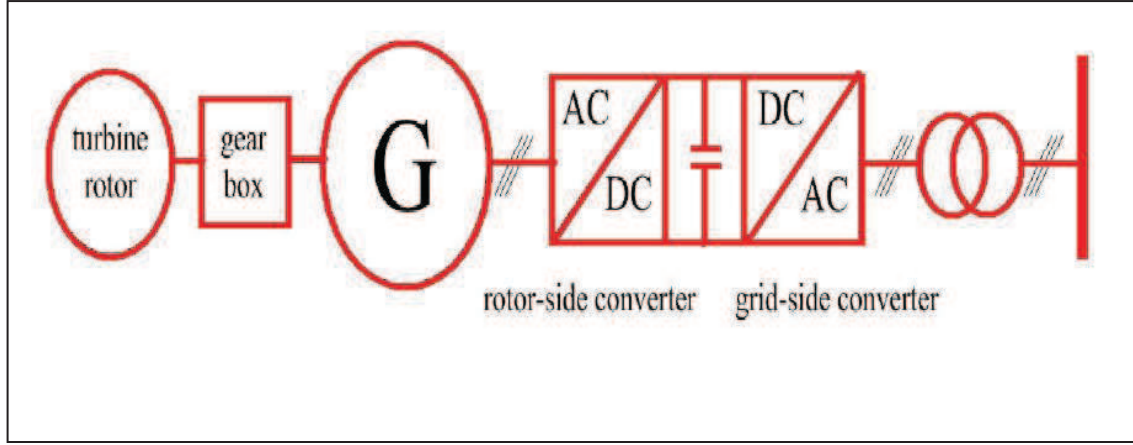


Fig. 2.22: A full scale converter configuration with a turbine rotor, a gear box, a generator (G) and a back-to-back converter [10].

The characteristic harmonics depend on the converter topology and switching strategy used during an ideal operation (with no disturbances). For a six-pulse converter, the characteristic harmonics are the harmonics of the harmonic order $6n \pm 1$, where n is a positive integer [28]. Similarly for a twelve-pulse converter the characteristic harmonics are of the order $12n \pm 1$. The non-characteristic harmonics are not dependant upon the converter topology, but the operating point of the converter [29]. This type of harmonics can be as large and as significant as the characteristic harmonics [30].

2.7.1 Calculation of THD based on an inverter out put

For harmonic current out of a 6-pulse thyristor invertor as shown in Fig. 2.18 and based on previously determined THD in section 2.6, for a fundamental frequency of 50Hz:

With 5^{th} harmonic @ 30% $\Rightarrow I_5 = 26 \times 0.3 = 7.8A$

7^{th} harmonic @ 10 $\Rightarrow I_7 = 26 \times 0.1 = 2.6A$

11^{th} harmonic @ 0% $\Rightarrow I_{11} = 26 \times 0.0 = 0.0A$

THD in voltage is given as:

$$V_5 = I_5 \times X_5 = 7.8 \times 8 = 62.4 \text{ V}$$

$$V_7 = I_7 \times X_5 = 2.6 \times 12 = 31.2 \text{ V}$$

$$V_{11} = I_{11} \times X_5 = 10.4 \times 0 = 0.0 \text{ V}$$

$$V_{THD} = \frac{\sqrt{(62.4)^2 + (31.2)^2 + (0.0)^2}}{\left[11kV/\sqrt{3}\right]} \times 100 = 1.1\%$$

Notice that 11th and 13th harmonic are not present in the inverter current and higher harmonic terms are neglected in these calculations. Nevertheless, including 17th, 19th, 29th and 31st harmonic term, has an impact on the calculated THD value but the value is still well within the permissible limit.

2.8 Summary

The importances of the measurement of harmonic impedance and the methods to measure harmonic impedance at the PCC have been brought to light. Attention has been drawn to different aspects of the system response characteristic and parallel resonance is emphasised. A representative study system was devised and cases have been studied for the frequency response characteristics. Important factors affecting parallel resonance are underlined.

Electrical resonance in a power network can be a complex phenomenon, where several components participate. However, it is clear that shunt capacitance of an underground cable system is the dominating element in the resonances of a wind power plant. A change in the length of the collector cables moves the resonance frequencies. As a general rule, the greater the capacitance of a capacitive element is, the lower are the resonance frequencies. What must be considered is that the cables do not resonate alone since they need an interaction with an inductive element to create a resonance. Typically this element is a (electrically) local transformer due to its large inductance. The number of resonances is likely equal to the number of physical and equivalent capacitors (cables, capacitor banks etc). The effect of capacitive elements on resonance appears to be decoupled. Each capacitive element contributes to a resonance. There are no “joint” resonances.

In the end, the effect of adding wind based units at the PCC is surveyed and ways to lessen THD are ascertained. Presently, most variable speed wind turbines are connected to the PCC through power electronic converters which act as a source of harmonic injection. Fixed speed wind units on the other hand, use power factor correction capacitors which can shift previously calculated resonance frequency values, hence causing severe distortion in current as well as voltage waveforms.

2.9 References

- [1] A. Robert; "Guide for assessing the network harmonic impedance", Working group CC02, Cigre 36.05/Cired 2, 1992.
- [2] M. Lemoine; "Methods of measuring harmonic impedances", IEE, International Conference on Electricity Distribution, 1977.
- [3] Roger Dugan, "Electric power system harmonic design guide" report for the US department of energy.
- [4] H. K. Lukasz, J. Hjerrild and C. L. Bak, "Harmonic Models of a Back-to-Back Converter in Large Offshore Wind Farms Compared with Measurement Data", Nordic Wind Power Conference, 2009.
- [5] E. W. Gunther, "Interharmonics in Power Systems", IEEE Power Engineering Society Summer Meeting, pp. 813–817 vol. 2, 2001.
- [6] D. Patel, "Impact of Wind Turbine Generators on Network Resonance and Harmonic Distortion," Electrical and Computer Engineering, Canada, 2010.
- [7] G. J. Wakileh, "Power System Harmonics - Fundamentals, Analysis and Filter Design", Springer, 2001.
- [8] H. D. Young and R.A. Freedman, "Sears and Zemansky's University Physics with Modern Physics", San Francisco: Addison-Wesley, 2011.

- [9] Fox. B, Flynn. D, Malley.O. M, Bryans .L and Watson. R; "Wind Power Integration Connection and System Operational Aspects", Stevenage: Institution on Engineering and Technology, 2007.
- [10] H. K. Lukasz, J. Hjerrild and C. L. Bak, "Harmonic Analysis of Offshore Wind Farms with Full Converter Wind Turbines", 8th International Conference on Large- Scale Integration of Wind Power into Power Systems, Bremen, Germany, 2009.
- [11] H. K. Lukasz, J. Hjerrild and C. L. Bak, "Wind Farm Structures, Impact on Harmonic Emission and Grid Interaction", European Wind Energy Conference, Warsaw, Poland, 2010.
- [12] C. H. Chien and R. Bucknall, "Harmonic Calculations of Proximity Effect on Impedance Characteristics in Subsea Power Transmission Cables", IEEE Transactions on Power Delivery, vol. 24, pp. 2150–2158, 2009.
- [13] L. Xiaodong and W. M. Jackson, "Influence of Subsea Cables on Offshore Power Distribution Systems", IEEE Transactions on Industry Applications, vol. 45, pp. 2136-2144, 2009.
- [14] S. Heier, "Grid Integration of Wind Energy Conversion Systems", Chichester, Wiley, 2006.
- [15] F. Shewarega, I. Erlich and J. L. Rueda, "Impact of Large Offshore Wind Farms on Power System Transient Stability" IEEE/PES, Power Systems Conference and Exposition, pp. 1–8, 2009.
- [16] S. Tentzerakis, S. Papathanassiou, P. Papadopoulos, D. Foussekis and P. Vionis, "Evaluation of Wind Farm Harmonic Current Emissions", European Wind Energy Conference, Milan, Italy, 2007.
- [17] T. Ackermann, "Wind Power in Power Systems", England, John Wiley, 2005.

- [18] Richard H. Osman; "Medium voltage variable frequency drives for induction and synchronous motors", ASI Robicon. www.asirobicon.com , 2002.
- [19] Control of harmonics in electrical power system; www.eagle.org , ABS, 2006.
- [20] Jun Li, N. Samaan and S. Williams, "Modeling of Large Wind Farm Systems for Dynamic and Harmonics Analysis", Transmission and Distribution Conference and Exposition, T&D, IEEE/PES , pp. 1–7, 2008.
- [21] M. Chaves, E. Margato, J. F. Silva, S. F. Pinto and J. Santana, "Fast Optimum-Predictive Control and Capacitor Voltage Balancing Strategy for Bipolar Back-to-Back NPC Converters in High-Voltage Direct Current Transmission Systems", Generation, Transmission & Distribution, The Institution of Engineering and Technology (IET), vol. 5, pp. 368–375, 2011.
- [22] S. Liang, Q. Hu and W. Lee, "A Survey of Harmonic Emissions of a Commercial Operated Wind Farm", Industrial and Commercial Power Systems Technical Conference (I&CPS), IEEE, pp. 1–8. 2010.
- [23] B. Baby Priya, A. Chilambuchelvan. "Modelling and Analysis of DFIG Wind Turbine Harmonics Generated in Grids", International Journal of Engineering and Technology (IJET), ISSN: 0975-4024, 2(3), pp. 185–189, 2010.
- [24] J. Hu, H. Nian, H. Xu and Y. He, "Dynamic Modeling and Improved Control of DFIG Under Distorted Grid Voltage Conditions", Energy Conversion, IEEE Transactions on, vol. 26, pp. 163–175, 2011.
- [25] D. D. Banham-Hall, G. A. Taylor, C. A. Smith and M. R. Irving, "Towards Large-Scale Direct Drive Wind Turbines with Permanent Magnet Generators and Full Converters", Power and Energy Society General Meeting, 2010 IEEE, ISSN: 1944-9925, Minneapolis, USA, pp. 1–8, 2010.
- [26] A. T. Alexandridis and G. E. Marmidis, "Modeling Wind Generators with Full-Scale Frequency Converters: Stability and Passivity Properties", Power Generation,

- Transmission, Distribution and Energy Conversion (MedPower 2010), 7th Mediterranean Conference and Exhibition on, Agia Napa, Cyprus, pp. 1–5, 2010
- [27] L. Kocewiak, L. Bak and J. Hjerrild, "Harmonic Aspects of Offshore Wind Farms", PhD Seminar on Detailed Modelling and Validation of Electrical Components and Systems 2010, Fredericia, Denmark, p. 40–45, 2010.
- [28] M. H. J. Bollen, S. Cundeva, S. K. Rönnerberg, M. Wahlberg, Kai Yang and Liangzhong Yao, "A Wind Park Emitting Characteristic and Non-Characteristic Harmonics", Power Electronics and Motion Control Conference (EPE/PEMC) 14th International, pp. S14–22–S14–26, 2010.
- [29] L. Kocewiak, J. Hjerrild and L. Bak., "The Impact of Harmonics Calculation Methods on Power Quality Assessment in Wind Farms", ISBN: 978-1-4244-7244-4, Bergamo, Italy, pp. 1–9, 2010.
- [30] S. Tentzerakis, N. Paraskevopoulou, S. Papathanassiou and P. Papadopoulos, "Measurement of Wind Farm Harmonic Emissions", IEEE Power Electronics Specialists Conference (PESC 2008), Rhodes, Greece, pp. 1769-1775, 2008.

3. HARMONIC DOMAIN ALGEBRA

3.1 Introduction

The understanding of orthogonal series expansion is important in understanding the concept of harmonic domain modelling. Orthogonal series expansion is widely used by engineers to solve differential equations. The cyclic convolution is revised in this chapter due to its key role in harmonic domain solutions. The periodic functions can be analysed into their fundamental and harmonic components. This approximate analysis is performed using trigonometric functions of different wave shapes by adding more and more functions together. These special trigonometric functions together make up the Fourier series. Since the Fourier series is extremely popular and has been also extensively applied in waveform analysis, its two forms (trigonometric and exponential) are reviewed here.

Orthogonal series expansion is used to provide a generalised frame of reference for all linear and non-linear elements and either Fourier or Hartley may be used [1] for this purpose. That is why a comparison is made between these two transforms at the end of this chapter.

3.2 Orthogonal functions

Functions $f_x(t)$ and $f_y(t)$ are considered orthogonal over the time period $0 < t < T_0$ if following conditions are met [2]

$$\text{a) } \int_0^{T_0} f_x(t)f_y(t)dt = 0 \quad \forall x \neq y \quad (3.1)$$

$$\text{b) } \int_0^{T_0} f_x(t)f_y(t)dt \neq 0 \quad \forall x = y \quad (3.2)$$

For example

$$\int_0^{T_0} \cos xt \sin xt \, dt = \frac{1}{2} \int_0^{T_0} \sin 2xt \, dt$$

$$\begin{aligned}
 &= \frac{1}{4x} \cos 2xt \\
 &= 0
 \end{aligned}$$

Therefore $\cos xt$ and $\sin xt$ are orthogonal functions.

3.3 Periodic functions

A function $f(t)$ is called periodic function if

$$f(t) = f(t + T_0) \quad (3.3)$$

Where $T_0 = \frac{1}{f}$ is the time period. In general periodic function is a function which repeats its values after a certain regular interval of time [3]. Fig. 3.1 shows a common example of periodic function.

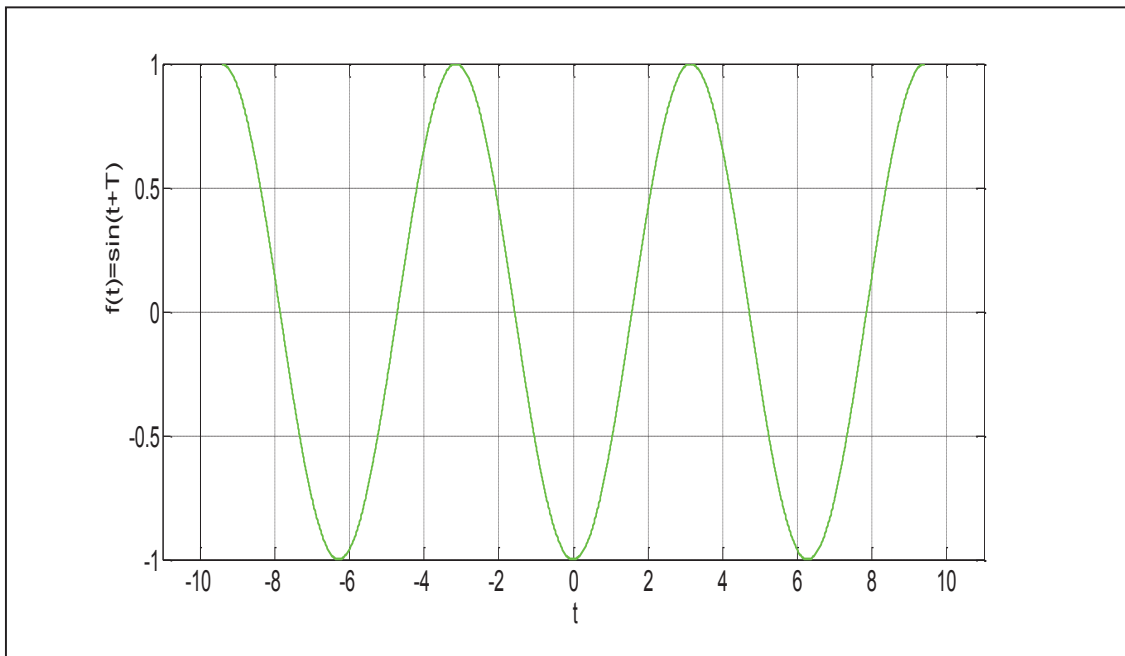


Fig. 3.1: An example of a periodic function

3.4 The Fourier series

The Fourier series is basically the decomposition of a signal into the sums of sines and cosines of different frequencies [4]. A periodic function $f(t)$ with time period T_0 can be written in the form of a Fourier series as:

$$f(t) = \frac{1}{2}a_0 + \sum_{n=1}^{\infty}(a_n \cos n\omega t + b_n \sin n\omega t) \quad (3.4)$$

where

$$\omega = 2\pi f$$

$$a_0 = \frac{2}{T_0} \int_{-\frac{T_0}{2}}^{\frac{T_0}{2}} f(t) dt \quad (3.5)$$

$$a_n = \frac{2}{T_0} \int_{-\frac{T_0}{2}}^{\frac{T_0}{2}} \cos n\omega t dt \quad (3.6)$$

$$b_n = \frac{2}{T_0} \int_{-\frac{T_0}{2}}^{\frac{T_0}{2}} \sin n\omega t dt \quad (3.7)$$

Equation (3.4) can be written as:

$$f(t) = A_0 + \sum_{n=1}^{\infty} A_n \cos(n\omega t + \theta_n) \quad (3.8)$$

In equation (3.8)

$$A_0 = \frac{1}{2}a_0 \quad (3.9)$$

$$A_n = A_{-n} = \sqrt{a_n^2 + b_n^2} \quad (3.10)$$

$$\theta_n = -\theta_{-n} = \arctan \frac{-b_n}{a_n} \quad (3.11)$$

In electrical analysis A_0 referred to as *dc* component while A_n and θ_n are respectively the magnitude and phase angle of the harmonic term. Also A_n is the even part and θ_n is the odd part of the n^{th} harmonic term.

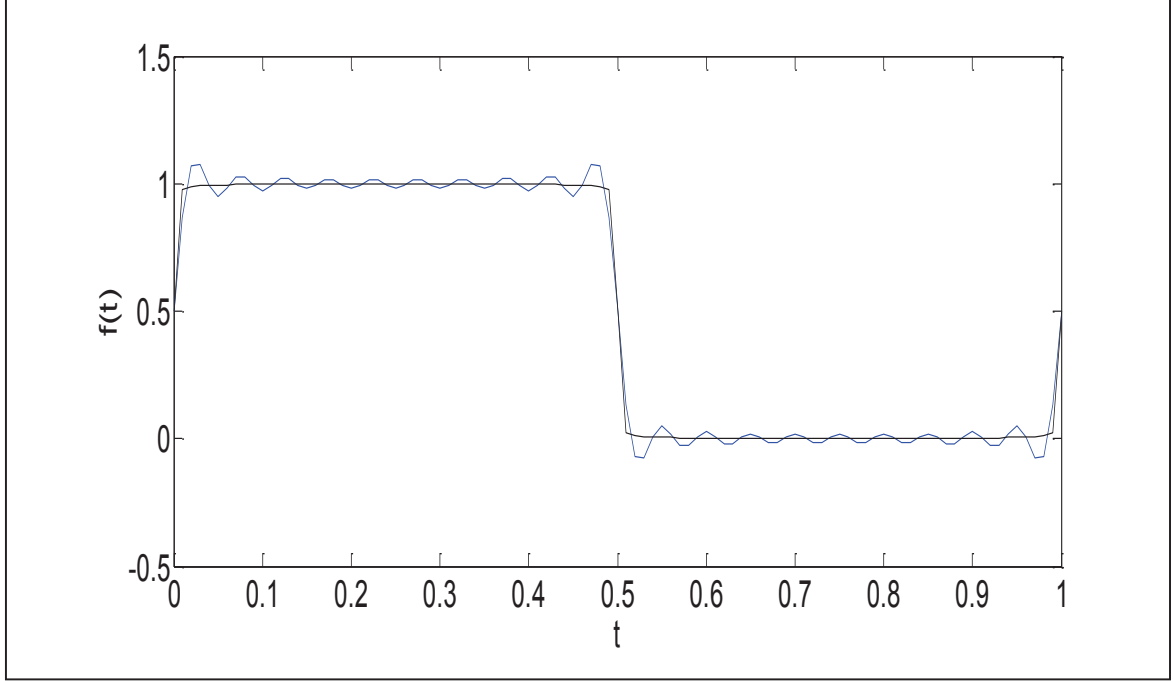


Fig. 3.2: Fourier series of a square wave.

The harmonic terms in equation (3.4) can be expressed with the help of its coefficients a_n and b_n

$$f_n(t) = a_n \cos n\omega t + b_n \sin n\omega t \quad (3.12)$$

Equation (3.12) can be written in exponential form as:

$$f_n(t) = \frac{a_n}{2} (e^{jn\omega t} + e^{-jn\omega t}) - j\frac{b_n}{2} (e^{jn\omega t} - e^{-jn\omega t}) \quad (3.13)$$

$$= \frac{1}{2} (a_n - jb_n)e^{jn\omega t} + \frac{1}{2} (a_n + jb_n)e^{-jn\omega t}$$

$$f_n(t) = C_n e^{jn\omega t} + C_{-n} e^{-jn\omega t} \quad (3.14)$$

where

$$C_n = \frac{1}{2} (a_n - jb_n) \quad (3.15)$$

$$C_{-n} = C_n^* \quad C_n^* \Rightarrow \text{Conjugate of } C_n$$

For $n = 0$

$$C_0 = \frac{a_0}{2}$$

The n th harmonic index in equation (3.14) can also be expressed as:

$$\begin{aligned} C_n &= |C_n| \angle \theta_n \\ &= \frac{1}{2} A_n \angle \theta_n \end{aligned}$$

Equation (3.12) can now be written as:

$$f_n(t) = \sum_{n=-\infty}^{\infty} C_n e^{jn\omega t} \quad (3.16)$$

This leads to a Fourier series in the complex form, a discrete frequency representation of a continuous periodic function $f(t)$. The complex coefficient can be found by solving the integral

$$C_n = \frac{1}{T_0} \int_{-T_0/2}^{T_0/2} f(t) e^{-jn\omega t} dt \quad (3.17)$$

3.5 The Fourier transform

In equation (3.16), when under the limit T_0 approaches infinity, an infinite number of infinitesimally close frequency components are generated. At this point $n\omega$ becomes a function $F(\omega)$ of the continuous frequency variable ω , and Fourier transform is obtained.

$$F(\omega) = \int_{-\infty}^{\infty} f(t) e^{-j\omega t} dt \quad (3.18)$$

The inverse Fourier transform is:

$$f(t) = \frac{1}{2\pi} \int_{-\infty}^{\infty} F(\omega) e^{j\omega t} d\omega \quad (3.19)$$

For example assuming a simple rectangular waveform given by

$$f(t) = A \Pi\left(\frac{t}{T}\right) = \begin{cases} A & \text{if } |t| < \frac{T}{2} \\ 0 & \text{otherwise} \end{cases}$$

Using the definition of Fourier transform

$$\begin{aligned}
 F(\omega) &= \int_{-T/2}^{T/2} A e^{j2\pi\omega t} dt \\
 &= A \left[\frac{e^{-j2\pi\omega t}}{-j2\pi\omega} \right]_{-T/2}^{T/2} \\
 &= AT \left[\frac{\sin \pi \omega t}{\pi \omega t} \right]
 \end{aligned}$$

Notice that the value of $F(0)$ is equal to the area under the graph of $f(t)$. Similarly, the value of $f(0)$ is equal to the area under $F(\omega)$. These are general results which follow immediately from the definitions and are useful for checking.

$$f(0) = \int_{-\infty}^{\infty} F(\omega) d\omega \quad \text{and} \quad F(0) = \int_{-\infty}^{\infty} f(t) dt$$

3.5.1 Discrete Fourier transform (DFT)

Consider the sample waveform shown in Fig. 3.3. The product of $f(t)$ and $S_T(t)$ is $f_s(t)$.

$$f_s(t) = \Delta T \sum_{n=-\infty}^{\infty} f(t) \delta(t - n\Delta T) \quad (3.20)$$

δ here is the impulse function.

The Fourier transform of equation (3.20) is:

$$\begin{aligned}
 F[k\omega] &= \frac{1}{T_0} \int_0^{T_0} f_s(t) e^{-jk\omega t} dt \\
 &= \frac{\Delta T}{T_0} \int_0^{T_0} \sum_{n=-\infty}^{\infty} f(t) \delta(t - n\Delta T) e^{-jk\omega t} dt
 \end{aligned}$$

$$F[k\omega] = \frac{\Delta T}{T_0} \int_0^{T_0} \int_{-\infty}^{\infty} g(t) \delta(t - \tau) dt \quad (3.21)$$

where $\tau = n\Delta T$ and $g(t) = f(t)e^{-jk\omega t}$

The infinite summation is expressed as an integral in equation (3.21). From this equation since

$$\int_{-\infty}^{\infty} g(t) \delta(t - \tau) dt = g(\tau)$$

Therefore

$$\begin{aligned} F[k\omega] &= \frac{\Delta T}{T_0} \int_0^{T_0} g(\tau) d\tau \\ F[k\omega] &= \frac{\Delta T}{T_0} \int_0^{T_0} f[n\Delta T] e^{-jk\omega n\Delta T} dt \end{aligned} \quad (3.22)$$

As shown in Fig. 3.3, the product of $f_s(t)$ and $\omega(t)$ is given by $f_d(t)$.

$$f_d(t) = f_s(t) \omega(t)$$

Where $\omega(t)$ is known as window function, gives the specifications of the wave form of the signal for the transform while $\frac{1}{[\Delta T/T_0]} = N$ is the total number of samples. Equation (3.22) in the form of summation is given as:

$$F[n\Delta T] = N \sum_{k=0}^{N-1} f[n\Delta T] e^{-jk\omega n\Delta T} \quad k = 0, 1, 2, 3, \dots, N-1 \quad (3.23)$$

Equation (3.23) is known as the discrete Fourier transform (DFT) of $f(n\Delta T)$. The inverse will be

$$f(n\Delta T) = N \sum_{k=0}^{N-1} F[k\omega] e^{-jk\omega n\Delta T} \quad n = 0, 1, 2, 3, \dots, N-1 \quad (3.24)$$

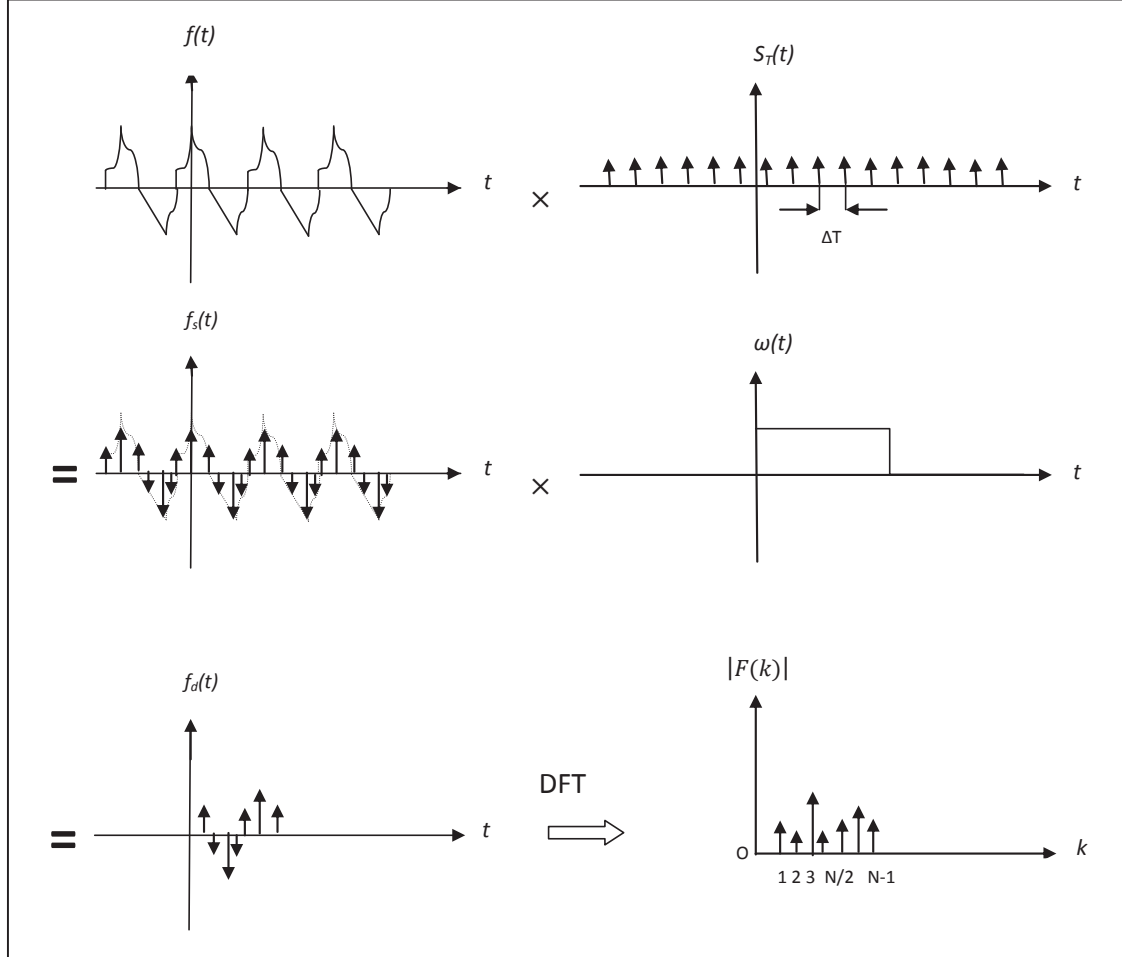


Fig. 3.3: A sample waveform and its discrete Fourier transform

3.5.2 Fast Fourier transform (FFT)

Fast Fourier transform (FFT) is the name given to algorithms used to solve discrete Fourier transforms (DFTs). Computing discrete Fourier transform (DFT) from the definition is often very slow and time consuming. Fast Fourier transform (FFT) gives the same result within short time.

In equation (3.23) if $\omega = 2\pi/T_0$, $\Delta T = T_0/N$ and $W = e^{-j2\pi/N}$ then

$$F[k] = \frac{1}{N} \sum_{n=0}^{N-1} f[n] W^{kn}$$

$$k = 0, 1, 2, \dots, N-1$$

In compact matrix form

$$\mathbf{F} = \mathbf{W}\mathbf{f} \quad (3.25)$$

where

$$\mathbf{F} = \begin{bmatrix} F[0] \\ F[1] \\ F[2] \\ \vdots \\ F[N-1] \end{bmatrix}, \quad \mathbf{W} = \begin{bmatrix} W^0 & W^0 & W^0 & \dots & W^0 \\ W^0 & W^1 & W^2 & \dots & W^{(N-1)} \\ W^0 & W^2 & W^4 & \dots & W^{2(N-1)} \\ \vdots & \vdots & \vdots & \ddots & \vdots \\ W^0 & W^{(N-1)} & W^{2(N-1)} & \dots & W^{(N-1)(N-1)} \end{bmatrix} \text{ and } \mathbf{f} = \begin{bmatrix} f[0] \\ f[1] \\ f[2] \\ \vdots \\ f[N-1] \end{bmatrix}$$

FFT is generally faster than DFT, however there are some applications where a DFT is faster than FFT. Such an example is finite difference time domain (FDTDs) solutions. If N^2 multiplications are required to produce a result of Fourier transform of a discrete function using equation (3.23), only $\frac{1}{2}N \log_2 N$ multiplications will produce the same result using an FFT.

3.6 Polynomial evaluation using the Fourier series

To explain the procedure of polynomial evaluation using Fourier, a simple polynomial is evaluated below by use of repeated convolution and complex Fourier series.

$$\text{Let } u = f(x) = \sum_{q=0}^3 b_q (x_{(t)})^q$$

$$f(x) = b_0 x^0 + b_1 x^1 + b_2 x^2 + b_3 x^3 \quad (3.26)$$

In equation (3.26), x_0 represents the *dc* component with unit magnitude. In harmonic domain it is written as:

$$X^0 = \begin{bmatrix} 0 \\ 0 \\ 0 \\ 1 \\ 0 \\ 0 \\ 0 \end{bmatrix} \quad (3.27)$$

Now assuming that x contains only *dc* terms and fundamental terms

$$x(t) = \sum_{h=-1}^1 X_h e^{jhwt} \quad (3.28)$$

$$x^2(t) = \sum_{h=-1}^1 X_h e^{jhwt} \sum_{h=-1}^1 X_h e^{jhwt} \quad (3.29)$$

In harmonic domain

$$\begin{aligned} x^2(t) &= X^2 \\ &= X \otimes X \\ &= \begin{bmatrix} 0 \\ X_{-1} \\ X_0 \\ X_1 \\ 0 \end{bmatrix} \otimes \begin{bmatrix} 0 \\ X_{-1} \\ X_0 \\ X_1 \\ 0 \end{bmatrix} \\ X^2 = x^2(t) &= \begin{bmatrix} X_{-1}X_{-1} \\ X_{-1}X_0 + X_0X_{-1} \\ X_{-1}X_1 + X_0X_0 + X_{-1}X_{-1} \\ X_1X_0 + X_0X_1 \\ X_1X_1 \end{bmatrix} \end{aligned} \quad (3.30)$$

Since X is a vector, X^2 is the convolution of X by itself, i.e. self convolution. Equation (3.30) can be expressed as:

$$\begin{aligned} X^2 &= \begin{bmatrix} X_0 & X_{-1} \\ X_1 & X_0 & X_{-1} \\ & X_1 & X_0 & X_{-1} \\ & & X_1 & X_0 \end{bmatrix} \begin{bmatrix} 0 \\ X_{-1} \\ X_0 \\ X_1 \\ 0 \end{bmatrix} \\ X^2 &= \begin{bmatrix} X_{-2}^{(2)} \\ X_{-1}^{(2)} \\ X_0^{(2)} \\ X_1^{(2)} \\ X_2^{(2)} \end{bmatrix} \end{aligned} \quad (3.31)$$

The cubic term in equation (3.26) is obtained by mutual convolution of X and X^2

$$\begin{aligned}
 X^3 &= X \otimes X^2 \\
 X^3 &= \begin{bmatrix} X_0 X_{-1} X_{-1} \\ X_1 X_0 X_0 X_{-1} \\ X_1 X_1 X_0 X_{-1} X_{-1} \\ X_1 X_1 X_0 X_{-1} X_{-1} X_{-1} \\ X_1 X_1 X_0 X_{-1} X_{-1} X_{-1} X_{-1} \end{bmatrix} \times \begin{bmatrix} 0 \\ X_{-1} X_{-1} \\ X_{-1} X_0 + X_0 X_{-1} \\ X_1 X_{-1} + X_0 X_0 + X_{-1} X_{-1} \\ X_1 X_0 + X_0 X_1 \\ X_1 X_1 \\ 0 \end{bmatrix} \\
 X^3 &= \begin{bmatrix} X_{-3}^{(3)} \\ X_{-2}^{(3)} \\ X_{-1}^{(3)} \\ X_0^{(3)} \\ X_1^{(3)} \\ X_2^{(3)} \\ X_3^{(3)} \end{bmatrix}
 \end{aligned} \tag{3.32}$$

Now evaluating the polynomial equation (3.26), using equations (3.27-32)

$$\begin{bmatrix} Y_{-3} \\ Y_{-2} \\ Y_{-1} \\ Y_0 \\ Y_1 \\ Y_2 \\ Y_3 \end{bmatrix} = b_0 \begin{bmatrix} 0 \\ 0 \\ 0 \\ 1 \\ 0 \\ 0 \\ 0 \end{bmatrix} + b_1 \begin{bmatrix} 0 \\ 0 \\ X_{-1} \\ X_0 \\ X_1 \\ 0 \\ 0 \end{bmatrix} + b_2 \begin{bmatrix} 0 \\ X_{-2}^{(2)} \\ X_{-1}^{(2)} \\ X_0^{(2)} \\ X_1^{(2)} \\ X_2^{(2)} \\ 0 \end{bmatrix} + b_3 \begin{bmatrix} X_{-3}^{(3)} \\ X_{-2}^{(3)} \\ X_{-1}^{(3)} \\ X_0^{(3)} \\ X_1^{(3)} \\ X_2^{(3)} \\ X_3^{(3)} \end{bmatrix}$$

Similar procedure can be adopted for evaluating rational polynomials. In practice this harmonic domain evaluation is applicable to only the static parts but not to the dynamic elements of the nonlinear polynomial relations.

Now assuming

$$x = \sum_{p=0}^{\infty} (X_p^s \sin p\omega t + X_p^c \cos p\omega t) \tag{3.33}$$

and

$$y = \sum_{q=0}^{\infty} (Y_q^s \sin q\omega t + Y_q^c \cos q\omega t) \tag{3.34}$$

two periodic real variables. In real Fourier harmonic domain, the product of equation (3.33) and equation (3.34) produces another periodic variable.

$$\begin{aligned} \sum_{r=0}^{\infty} (Z_r^s \sin r\omega t + Z_r^c \cos r\omega t) &= \sum_{p=0}^{\infty} (X_p^s \sin p\omega t + X_p^c \cos p\omega t) \\ &\times \sum_{q=0}^{\infty} (Y_q^s \sin q\omega t + Y_q^c \cos q\omega t) \end{aligned} \quad (3.35)$$

In compact form

$$\begin{bmatrix} Z^s \\ Z^c \end{bmatrix} = \begin{bmatrix} X^s \\ X^c \end{bmatrix} \otimes \begin{bmatrix} Y^s \\ Y^c \end{bmatrix} \quad (3.36)$$

where

$$\begin{bmatrix} X^s \\ X^c \end{bmatrix} = \begin{bmatrix} X_1^s \\ X_2^s \\ X_3^s \\ \vdots \\ - \\ X_0^c \\ X_1^c \\ X_2^c \\ X_3^c \\ \vdots \end{bmatrix}; \begin{bmatrix} Y^s \\ Y^c \end{bmatrix} = \begin{bmatrix} Y_1^s \\ Y_2^s \\ Y_3^s \\ \vdots \\ - \\ Y_0^c \\ Y_1^c \\ Y_2^c \\ Y_3^c \\ \vdots \end{bmatrix}; \begin{bmatrix} Z^s \\ Z^c \end{bmatrix} = \begin{bmatrix} Z_1^s \\ Z_2^s \\ Z_3^s \\ \vdots \\ - \\ Z_0^c \\ Z_1^c \\ Z_2^c \\ Z_3^c \\ \vdots \end{bmatrix}$$

To solve equation (3.36), convolution operation is replaced by matrix operation as:

$$\begin{bmatrix} Z^s \\ Z^c \end{bmatrix} = \frac{1}{2} \begin{bmatrix} X^{ss} & X^{sc} \\ X^{cs} & X^{cc} \end{bmatrix} \begin{bmatrix} Y^s \\ Y^c \end{bmatrix}$$

Where the matrices X^{ss} , X^{sc} , X^{cs} and X^{cc} consist of the product of the elements corresponding to the respective term of Y in equation (3.35). For instance Y_q^s

$$\begin{aligned} &\sum_{p=0}^{\infty} (X_p^s \sin p\omega t + X_p^c \cos p\omega t) Y_q^s \sin q\omega t \\ &= \frac{1}{2} \sum_{p=0}^{\infty} \{ \cos(p-q)\omega t - \cos(p+q)\omega t \} X_p^s X_q^s \\ &+ \frac{1}{2} \sum_{p=0}^{\infty} \{ -\sin(p-q)\omega t + \sin(p+q)\omega t \} X_p^c X_q^s \end{aligned}$$

and for Y_q^c ;

$$\begin{aligned}
 & \sum_{p=0}^{\infty} (X_p^s \sin p\omega t + X_p^c \cos p\omega t) Y_q^s \cos q\omega t \\
 &= \frac{1}{2} \sum_{p=0}^{\infty} \{ \sin(p-q)\omega t - \sin(p+q)\omega t \} X_p^s X_q^c \\
 &+ \frac{1}{2} \sum_{p=0}^{\infty} \{ -\cos(p-q)\omega t + \cos(p+q)\omega t \} X_p^c X_q^c
 \end{aligned}$$

After considering each term Y^s and Y^c the matrices X^{ss} , X^{sc} , X^{cs} and X^{cc} are identified as:

$$\begin{aligned}
 X^{ss} &= \begin{bmatrix} 2X_0^c - X_2^c & X_1^c - X_3^c & X_2^c - X_4^c & X_3^c - X_5^c & \dots \\ X_1^c - X_3^c & 2X_0^c - X_4^c & X_1^c - X_5^c & X_2^c - X_6^c & \dots \\ X_2^c - X_4^c & X_1^c - X_5^c & 2X_0^c - X_6^c & X_1^c - X_7^c & \dots \\ X_3^c - X_5^c & X_2^c - X_6^c & X_1^c - X_7^c & 2X_0^c - X_8^c & \dots \\ \vdots & \vdots & \vdots & \vdots & \ddots \end{bmatrix} \\
 X^{sc} &= \begin{bmatrix} 2X_1^s & X_2^s & -X_1^s + X_3^s & -X_2^s + X_4^s & -X_3^s + X_5^s & \dots \\ 2X_2^s & X_1^s + X_3^s & X_4^s & -X_1^s + X_5^s & -X_2^s + X_6^s & \dots \\ 2X_3^s & X_2^s + X_4^s & X_1^s + X_5^s & X_6^s & -X_1^s + X_7^s & \dots \\ 2X_4^s & X_3^s + X_5^s & X_2^s + X_6^s & X_1^s + X_7^s & X_8^s & \dots \\ \vdots & \vdots & \vdots & \vdots & \vdots & \ddots \end{bmatrix} \\
 X^{cs} &= \begin{bmatrix} X_1^s & X_2^s & X_3^s & X_4^s & \dots \\ X_2^s & X_1^s + X_3^s & X_2^s + X_4^s & X_3^s + X_5^s & \dots \\ X_1^s + X_3^s & X_4^s & X_1^s + X_5^s & X_2^s + X_6^s & \dots \\ X_2^s + X_4^s & -X_1^s + X_5^s & X_6^s & X_1^s + X_7^s & \dots \\ X_3^s + X_5^s & -X_2^s + X_6^s & -X_1^s + X_7^s & X_8^s & \dots \\ \vdots & \vdots & \vdots & \vdots & \ddots \end{bmatrix} \\
 X^{cc} &= \begin{bmatrix} 2X_0^c & X_1^c & X_2^c & X_3^c & X_4^c & \dots \\ 2X_1^c & 2X_0^c + X_2^c & X_1^c + X_3^c & X_2^c + X_4^c & X_3^c + X_5^c & \dots \\ 2X_2^c & X_1^c + X_3^c & 2X_0^c + X_4^c & X_1^c + X_5^c & X_2^c + X_6^c & \dots \\ 2X_3^c & X_2^c + X_4^c & X_1^c + X_5^c & X_0^c + X_6^c & X_1^c + X_7^c & \dots \\ 2X_4^c & X_3^c + X_5^c & X_2^c + X_6^c & X_1^c + X_7^c & X_0^c + X_8^c & \dots \\ \vdots & \vdots & \vdots & \vdots & \vdots & \ddots \end{bmatrix}
 \end{aligned}$$

The evaluation of dynamic terms in real Fourier harmonic domain is carried out by means of simple algebraic operations. Consider $z = x$, the fundamental dynamic relation, where z and x are two periodic variables given by:

$$x = \sum_{p=0}^{\infty} (X_p^s \sin p\omega t + X_p^c \cos p\omega t) \quad (3.37)$$

and

$$z = \sum_{r=0}^{\infty} (Z_r^s \sin r\omega t + Z_r^c \cos r\omega t) \quad (3.38)$$

The dynamic relation between x and z may be represented as:

$$\sum_{r=0}^{\infty} (z) = \frac{d}{dt} \sum_{p=0}^{\infty} x$$

Using equation (3.37) and equation (3.38) in above equation

$$\begin{aligned} \sum_{r=0}^{\infty} (Z_r^s \sin r\omega t + Z_r^c \cos r\omega t) &= \frac{d}{dt} \sum_{p=0}^{\infty} (X_p^s \sin p\omega t + X_p^c \cos p\omega t) \\ &= \sum_{p=0}^{\infty} (p\omega X_p^s \cos p\omega t - p\omega X_p^c \sin p\omega t) \end{aligned}$$

In terms of harmonic coefficients

$$\begin{bmatrix} Z_1^s \\ Z_2^s \\ Z_3^s \\ \vdots \\ - \\ Z_0^c \\ Z_1^c \\ Z_2^c \\ Z_3^c \\ \vdots \end{bmatrix} = \begin{bmatrix} 0 & \cdots & \cdots & 0 & | & 0 & -\omega & 0 & \cdots & 0 \\ \vdots & \ddots & & \vdots & | & \vdots & \ddots & -2\omega & \ddots & \vdots \\ \vdots & & \ddots & \vdots & | & \vdots & & \ddots & -3\omega & 0 \\ 0 & \cdots & \cdots & 0 & | & 0 & \cdots & \cdots & 0 & \ddots \\ - & - & - & - & | & - & - & - & - & - \\ 0 & \cdots & \cdots & 0 & | & 0 & \cdots & \cdots & \cdots & 0 \\ \omega & \ddots & & \vdots & | & \vdots & \ddots & & & \vdots \\ 0 & 2\omega & \ddots & \vdots & | & \vdots & & \ddots & & \vdots \\ \vdots & \ddots & 3\omega & 0 & | & \vdots & & & \ddots & \vdots \\ 0 & \cdots & 0 & \ddots & | & 0 & \cdots & \cdots & \cdots & 0 \end{bmatrix} \begin{bmatrix} X_1^s \\ X_2^s \\ X_3^s \\ \vdots \\ - \\ X_0^c \\ X_1^c \\ X_2^c \\ X_3^c \\ \vdots \end{bmatrix} \quad (3.39)$$

Equation (3.39) can be expressed in compact form as:

$$\begin{bmatrix} Z^s \\ Z^c \end{bmatrix} = \begin{bmatrix} 0 & D(-p\omega) \\ D(p\omega) & 0 \end{bmatrix} \begin{bmatrix} X^s \\ X^c \end{bmatrix}$$

and

$$\begin{bmatrix} X^s \\ X^c \end{bmatrix} = \begin{bmatrix} 0 & D(1/p\omega) \\ D(-1/p\omega) & 0 \end{bmatrix} \begin{bmatrix} Z^s \\ Z^c \end{bmatrix}$$

3.7 The Hartley transforms

R. V. L. Hartley introduced an alternative to Fourier transform in 1942. The Hartley transform have the advantage of transforming the real functions to real functions and of being its own inverse over the well known Fourier transform. Hartley transform of a function $f(t)$ is defined as:

$$H[v] = \int_{-\infty}^{\infty} f(t) \text{cas } vtdt \quad (3.40)$$

where

$$\text{cas } vt = \cos vt + \sin vt \quad (3.41)$$

and

$$v = 2\pi\omega$$

The *cas* (cosine-and-sine) is known as the Hartley's kernal. The Hartley transform also has the convenient property of being its own inverse. Equation (3.40) can be written as:

$$\begin{aligned} H[v] &= \int_{-\infty}^{\infty} f(t) \cos vtdt + \int_{-\infty}^{\infty} f(t) \sin vtdt \\ H[v] &= \left[\int_{-\infty}^{\infty} f_{\text{even}}(t) \cos vtdt + \int_{-\infty}^{\infty} f_{\text{odd}}(t) \cos vtdt \right] \\ &\quad + \left[\int_{-\infty}^{\infty} f_{\text{even}}(t) \sin vtdt + \int_{-\infty}^{\infty} f_{\text{odd}}(t) \sin vtdt \right] \\ &= \left[\int_{-\infty}^{\infty} f_{\text{even}}(t) \cos vtdt + \int_{-\infty}^{\infty} f_{\text{even}}(t) \sin vtdt \right] \\ &\quad + \left[\int_{-\infty}^{\infty} f_{\text{odd}}(t) \cos vtdt + \int_{-\infty}^{\infty} f_{\text{odd}}(t) \sin vtdt \right] \\ H[v] &= H_{\text{even}}[v] + H_{\text{odd}}[v] \end{aligned} \quad (3.42)$$

This *even* and *odd* nature of the Hartley transform provides a great deal of ease in calculation.

3.7.1 Discrete Hartley transform (DHT)

Discrete Hartley transform (DHT) is defined as:

$$H[k] = \frac{1}{N} \sum_{n=0}^{N-1} f[n] \text{cas} \left(nk \frac{2\pi}{N} \right) \quad k = 0, 1, 2, \dots, n-1 \quad (3.43)$$

The inverse is given by:

$$f[n] = \sum_{k=0}^{N-1} H[k] \text{cas} \left(nk \frac{2\pi}{N} \right) \quad k = 0, 1, 2, \dots, n-1 \quad (3.44)$$

Notice that the inverse transformation to achieve original function $f[n]$ from $H[k]$, differs the transform by only factor $1/N$. That is, the discrete Hartley transform (DHT) is its own inverse and exhibits the property of involution.

3.7.2 Fast Hartley transform (FHT)

Fast Hartley transform (FHT) is the name given to the algorithms used to solve above mentioned discrete Hartley transform (DHT). FHT algorithms resemble FFT algorithms, however FHT algorithms have the advantage of using fewer memory space compared to FFT algorithms. The total number of operations for both FHT and FFT is $\frac{1}{2}N \log_2 N$. The only difference is that in case of FFT the operations are complex, where as for FHT all the operations are real.

3.7.3 Polynomial evaluation using Hartley

Both self convolution and mutual convolution operations can be performed in the same way in Hartley harmonic domain as these two operations are carried out in complex Fourier and real Fourier harmonic domain.

Consider three vectors X , Y and Z , of Hartley harmonic coefficients corresponding respectively to periodic variables x , x^2 and x^3 . Then

$$X \otimes X = Y \quad (3.45)$$

known as the self convolution in Hartley and

$$Y \otimes X = Z \quad (3.46)$$

is given the name of mutual convolution in Hartley harmonic domain. Supposing the periodic variables in Hartley harmonic domain

$$x(t) = \sum_{i=-\infty}^{\infty} X_i \text{cas } ivt \quad (3.47)$$

and

$$y(t) = \sum_{h=-\infty}^{\infty} Y_h \text{cas } hvt \quad (3.48)$$

Similar to real Fourier harmonic domain the product of equation (3.47) and equation (3.48) gives rise to another periodic variable i. e

$$\sum_{k=-\infty}^{\infty} Z_k \text{cas } kvt = \sum_{i=-\infty}^{\infty} X_i \text{cas } ivt \ y(t) \sum_{h=-\infty}^{\infty} Y_h \text{cas } hvt \quad (3.49)$$

Equation (3.49) can be expressed in vector form using harmonic coefficients as:

$$\begin{bmatrix} \vdots \\ Z_{-1} \\ Z_0 \\ Z_1 \\ \vdots \end{bmatrix} = \begin{bmatrix} \vdots \\ X_{-1} \\ X_0 \\ X_1 \\ \vdots \end{bmatrix} \otimes \begin{bmatrix} \vdots \\ Y_{-1} \\ Y_0 \\ Y_1 \\ \vdots \end{bmatrix} \quad (3.50)$$

Using Hartley identity

$$\text{cas } \alpha \text{cas } \beta = \frac{1}{2} \{ \text{cas}(\alpha + \beta) + \text{cas}(\alpha - \beta) + \text{cas}(-\alpha + \beta) - \text{cas}(-\alpha - \beta) \}$$

Manipulating equation (3.49) yields

$$\begin{aligned} & \sum_{k=-\infty}^{\infty} Z_k \text{cas } kvt \\ &= \frac{1}{2} \sum_{i=-\infty}^{\infty} X_i Y_h \{ \text{cas}(i + h)vt + \text{cas}(i - h)vt + \text{cas}(-i + h)vt - \text{cas}(-i - h)vt \} \end{aligned} \quad (3.51)$$

The convolution operation of equation (3.50) is better expressed and understood in matrix form. This matrix form is obtained by considering one term of equation (3.51) at a time, for instance h

$$\begin{bmatrix} \vdots \\ Z_{-2} \\ Z_{-1} \\ Z_0 \\ Z_1 \\ Z_2 \\ \vdots \end{bmatrix} = \frac{1}{2} \left\{ \begin{bmatrix} \vdots \\ X_{-2+h} \\ X_{-1+h} \\ X_{0+h} \\ X_{1+h} \\ X_{2+h} \\ \vdots \end{bmatrix} + \begin{bmatrix} \vdots \\ X_{-2-h} \\ X_{-1-h} \\ X_{0-h} \\ X_{1-h} \\ X_{2-h} \\ \vdots \end{bmatrix} + \begin{bmatrix} \vdots \\ X_{2+h} \\ X_{1+h} \\ X_{0+h} \\ X_{-1+h} \\ X_{-2+h} \\ \vdots \end{bmatrix} - \begin{bmatrix} \vdots \\ X_{2-h} \\ X_{1-h} \\ X_{0-h} \\ X_{-1-h} \\ X_{-2-h} \\ \vdots \end{bmatrix} \right\} Y_h \quad (3.52)$$

or

$$\begin{bmatrix} \vdots \\ Z_{-2} \\ Z_{-1} \\ Z_0 \\ Z_1 \\ Z_2 \\ \vdots \end{bmatrix} = \frac{1}{2} \left\{ \begin{bmatrix} \vdots & \vdots \\ X_{-2+h} & X_{-2-h} \\ X_{-1+h} & X_{-1-h} \\ X_{0+h} & X_{0-h} \\ X_{1+h} & X_{1-h} \\ X_{2+h} & X_{2-h} \\ \vdots & \vdots \end{bmatrix} + \begin{bmatrix} \vdots & \vdots \\ X_{2+h} & X_{2-h} \\ X_{1+h} & X_{1-h} \\ X_{0+h} & X_{0-h} \\ X_{-1+h} & X_{-1-h} \\ X_{-2+h} & X_{-2-h} \\ \vdots & \vdots \end{bmatrix} \right\} Y_h \quad (3.53)$$

After considering all the terms of input Y , two matrices can be clearly identified.

$$\begin{bmatrix} \vdots \\ Z_{-2} \\ Z_{-1} \\ Z_0 \\ Z_1 \\ Z_2 \\ \vdots \end{bmatrix} = \frac{1}{2} \left\{ \begin{bmatrix} \ddots & & & & \\ 2X_0 & X_{-1} + X_1 & X_{-2} + X_2 & X_{-3} + X_3 & \\ X_1 + X_{-1} & 2X_0 & X_{-1} + X_1 & X_{-2} + X_2 & X_{-3} + X_3 \\ X_2 + X_{-2} & X_1 + X_{-1} & 2X_0 & X_{-1} + X_1 & X_{-2} + X_2 \\ X_3 + X_{-3} & X_2 + X_{-2} & X_1 + X_{-1} & 2X_0 & X_{-1} + X_1 \\ & X_3 + X_{-3} & X_2 + X_2 & X_1 + X_{-1} & 2X_0 \\ & & & & \ddots \end{bmatrix} + \begin{bmatrix} \ddots & & & & \\ X_{-3} - X_3 & X_{-2} - X_2 & X_{-1} - X_1 & 0 & \\ X_{-3} - X_3 & X_{-2} - X_2 & X_{-1} - X_1 & 0 & X_1 - X_{-1} \\ X_{-2} - X_2 & X_{-1} - X_1 & 0 & X_1 - X_{-1} & X_2 - X_{-2} \\ X_{-1} - X_1 & 0 & X_1 - X_{-1} & X_2 - X_{-2} & X_3 - X_{-3} \\ 0 & X_1 - X_{-1} & X_2 - X_{-2} & X_3 - X_{-3} & \\ & & & & \ddots \end{bmatrix} \right\} \begin{bmatrix} \vdots \\ Y_{-2} \\ Y_{-1} \\ Y_0 \\ Y_1 \\ Y_2 \\ \vdots \end{bmatrix} \quad (3.54)$$

Equation (3.54) can be written in compact form as:

$$Z = \frac{1}{2} \{X_I + X_{II}\} Y \quad (3.55)$$

In Hartley harmonic domain self and mutual convolution are performed using these equations. Similar to real Fourier Harmonic domain, the evaluation of dynamic elements in Hartley harmonic domain is carried out by simple algebraic operations.

Consider $z = x$, where z and x are two periodic variables given by following equations:

$$x_{(t)} = \sum_{n=-\infty}^{\infty} X_n \text{cas } nvt \quad (3.56)$$

$$z_{(t)} = \sum_{h=-\infty}^{\infty} Z_h \text{cas } hvt \quad (3.57)$$

The dynamic relation between $x_{(t)}$ and $z_{(t)}$ may be represented as:

$$\begin{aligned} \sum_{h=-\infty}^{\infty} Z_h \text{cas } hvt &= \frac{d}{dt} \sum_{n=-\infty}^{\infty} X_n \text{cas } nvt \\ &= \sum_{n=-\infty}^{\infty} nv X_n \text{cas}(-nvt) \end{aligned}$$

In harmonic coefficients

$$\begin{bmatrix} \vdots \\ Z_{-2} \\ Z_{-1} \\ Z_0 \\ Z_1 \\ Z_2 \\ \vdots \end{bmatrix} = \begin{bmatrix} & & & & & & \ddots \\ & & & & -2v_0 & & \\ & & & & -v_0 & & \\ & & & 0 & & & \\ & & v_0 & & & & \\ 2v_0 & & & & & & \\ & & & & & & \\ \ddots & & & & & & \end{bmatrix} \begin{bmatrix} \vdots \\ X_{-2} \\ X_{-1} \\ X_0 \\ X_1 \\ X_2 \\ \vdots \end{bmatrix} \quad (3.58)$$

Equation (3.58) can be written in compact form as:

$$Z = D(nv_0)X \quad (3.59)$$

3.8 A critical comparison of the Fourier and Hartley series amid at harmonic domain applications

The convolution theorem says that Fourier Transform (FT) of a convolution of two functions is proportional to the product of individual Fourier transforms, and vice versa. For instance if

$$f(x) = FT[f(t)]$$

$$\begin{aligned}
 &\text{and} & g(x) &= FT[g(t)] \\
 &\text{then} & f(x) g(x) &= FT[f(x) \otimes g(x)] \\
 &\text{and} & f(x) \otimes g(x) &= FT[f(x)g(x)]
 \end{aligned}$$

Now consider the function

$$x(t) = \sum_{h=-3}^3 X_h e^{jh\omega t}$$

The convolution of $x(t)$ is given by

$$x^2(t) = \sum_{h=-3}^3 X_h e^{jh\omega t} \otimes \sum_{h=-3}^3 X_h e^{jh\omega t}$$

In vector form

$$\begin{aligned}
 x^2(t) &= X \otimes X \\
 &= \begin{bmatrix} X_{-3} \\ X_{-2} \\ X_{-1} \\ X_0 \\ X_1 \\ X_2 \\ X_3 \end{bmatrix} \otimes \begin{bmatrix} X_{-3} \\ X_{-2} \\ X_{-1} \\ X_0 \\ X_1 \\ X_2 \\ X_3 \end{bmatrix} \\
 &= \begin{bmatrix} X_0 & X_{-1} & X_{-2} & X_{-3} & 0 & 0 & 0 \\ X_1 & X_0 & X_{-1} & X_{-2} & X_{-3} & 0 & 0 \\ X_2 & X_1 & X_0 & X_{-1} & X_{-2} & X_{-3} & 0 \\ X_3 & X_2 & X_1 & X_0 & X_{-1} & X_{-2} & X_{-3} \\ 0 & X_3 & X_2 & X_1 & X_0 & X_{-1} & X_{-2} \\ 0 & 0 & X_3 & X_2 & X_1 & X_0 & X_{-1} \\ 0 & 0 & 0 & X_3 & X_2 & X_1 & X_0 \end{bmatrix} \begin{bmatrix} X_{-3} \\ X_{-2} \\ X_{-1} \\ X_0 \\ X_1 \\ X_2 \\ X_3 \end{bmatrix} \\
 &= \begin{bmatrix} (X_0)(X_{-3}) + (X_{-1})(X_{-2}) + (X_{-2})(X_{-1}) + (X_{-3})(X_0) + (0)(X_1) + (0)(X_2) + (0)(X_3) \\ (X_1)(X_{-3}) + (X_0)(X_{-2}) + (X_{-1})(X_{-1}) + (X_{-2})(X_0) + (X_{-3})(X_1) + (0)(X_2) + (0)(X_3) \\ \vdots \\ (0)(X_{-3}) + (0)(X_{-2}) + (0)(X_{-1}) + (X_3)(X_0) + (X_2)(X_1) + (X_1)(X_2) + (X_0)(X_3) \end{bmatrix}
 \end{aligned}$$

All the elements of this matrix given according to corresponding subscript of X are as shown in Table 3.1

Table 3.1: Elements of multiplication matrix

$X_0 = a$	A real number only
$X_1 = (a_1 + jb_1)$	Complex number with both real and imaginary parts
$X_2 = (a_2 + jb_2)$	-do-
$X_3 = (a_3 + jb_3)$	-do-
$X_{-1} = (a_{-1} + jb_{-1})$	-do-
$X_{-2} = (a_{-2} + jb_{-2})$	-do-
$X_{-3} = (a_{-3} + jb_{-3})$	-do-

Replacing the respective values of X_h in the 1st row of the product matrix above and simplifying:

$$\{a \times (a_{-3} + jb_{-3})\} + \{(a_{-1} + jb_{-1}) \times (a_{-2} + jb_{-2})\} + \{(a_{-2} + jb_{-2}) \times (a_{-1} + jb_{-1})\} \\ + \{(a_{-3} + jb_{-3}) \times (a)\} + 0 + 0 + 0$$

It appears like there are four multiplications and three additions involved. But further simplification as shown below gives a clear view of the number of operations performed in practical.

$\{a * a_{-3}\} + \{a * jb_{-3}\}$	2 multiplications, 1 addition
$+ \{(a_{-1} * a_{-2}) + (a_{-1} * jb_{-2}) + (jb_{-1} * a_{-2}) + (jb_{-1} * jb_{-2})\}$	4 multiplications, 4 additions
$+ \{(a_{-1} * a_{-2}) + (a_{-1} * jb_{-2}) + (jb_{-1} * a_{-2}) + (jb_{-1} * jb_{-2})\}$	4 multiplications, 4 additions
$+ \{(a_{-3} * a) + (jb_{-3} * a)\}$	2 multiplications, 2 additions
Total Operations in First Row of Matrix.....	23, with 12 multiplications, 11 additions

Based on this we have the results shown in Table 3.2.

Table 3.2: Number of operations using complex Fourier

Number of total operations in first and last row	2(23)	46
Number of total operations in 2 nd and 2 nd -last row	2(31)	62
Number of total operations in 3rd and 3 rd -last row	2(39)	78
Number of total operations in middle row	1(47)	47
Number of total operations	(46 + 62 + 78 + 47)	233

Depending on the fact that a simple multiplication of any complex number of type $(a + ib)$ with another complex number of the same type involves as many as four multiplication operations $((a + ib) \times (a + ib) = (a \times a + a \times ib + ib \times a + ib \times ib))$ and three addition operations; if we assume all the numbers in above equation are complex of type $(a+ib)$, the total number of operations involved in the product matrix are worked out in Table 3.2 below.

Notice that, the operations which involve multiplication to zero are not counted hence not included in Table 3.2.

On the other hand if two functions, $f(x)$ and $g(x)$ have Hartley transforms $F(t)$ and $G(t)$, respectively, then their convolution $z(t) = f(x) \otimes g(x)$ has the Hartley transform

$$\begin{aligned} Z(t) &= [H(x \otimes y)] \\ &= \sqrt{\pi/2} \{X(t)[Y(t) + Y(-t)] + X(-t)[Y(t) - Y(-t)]\} \end{aligned}$$

Now consider once again

$$x(t) = \sum_{h=-3}^3 X_h e^{jh\omega t}$$

The convolution of $x(t)$ is given by:

$$x^2(t) = \sum_{h=-3}^3 X_h e^{jh\omega t} \otimes \sum_{h=-3}^3 X_h e^{jh\omega t}$$

In vector form

$$x^2(t) = X \otimes X$$

$$= \begin{bmatrix} X_{-3} \\ X_{-2} \\ X_{-1} \\ X_0 \\ X_1 \\ X_2 \\ X_3 \end{bmatrix} \otimes \begin{bmatrix} X_{-3} \\ X_{-2} \\ X_{-1} \\ X_0 \\ X_1 \\ X_2 \\ X_3 \end{bmatrix}$$

$$= \begin{bmatrix} X_0 & X_{-1} & X_{-2} & X_{-3} & 0 & 0 & 0 \\ X_1 & X_0 & X_{-1} & X_{-2} & X_{-3} & 0 & 0 \\ X_2 & X_1 & X_0 & X_{-1} & X_{-2} & X_{-3} & 0 \\ X_3 & X_2 & X_1 & X_0 & X_{-1} & X_{-2} & X_{-3} \\ 0 & X_3 & X_2 & X_1 & X_0 & X_{-1} & X_{-2} \\ 0 & 0 & X_3 & X_2 & X_1 & X_0 & X_{-1} \\ 0 & 0 & 0 & X_3 & X_2 & X_1 & X_0 \end{bmatrix} \begin{bmatrix} X_{-3} \\ X_{-2} \\ X_{-1} \\ X_0 \\ X_1 \\ X_2 \\ X_3 \end{bmatrix} \begin{matrix} cas(-) \\ \\ dc \\ cas(+) \end{matrix}$$

$$= \begin{bmatrix} (X_0)(X_{-3}) + (X_{-1})(X_{-2}) + (X_{-2})(X_{-1}) + (X_{-3})(X_0) + (0)(X_1) + (0)(X_2) + (0)(X_3) \\ (X_1)(X_{-3}) + (X_0)(X_{-2}) + (X_{-1})(X_{-1}) + (X_{-2})(X_0) + (X_{-3})(X_1) + (0)(X_2) + (0)(X_3) \\ \vdots \\ (0)(X_{-3}) + (0)(X_{-2}) + (0)(X_{-1}) + (X_3)(X_0) + (X_2)(X_1) + (X_1)(X_2) + (X_0)(X_3) \end{bmatrix}$$

Assuming all the numbers as real, the product matrix involves number of operations detailed in Table 3.3.

A total number of sixty-seven operations are involved; proving it much faster compared to complex Fourier. The number of operations can be further reduced in Hartley if even and odd functions in the series are treated separately.

Table 3.3: Number of operations using Hartley

Number of total operations in first and last row	2(7)	14
Number of total operations in 2 nd and 2 nd -last row	2(9)	18
Number of total operations in 3 rd and 3 rd -last row	2(11)	22
Number of total operations in middle row	1(13)	13
Number of total operations	(14 + 18 + 22 + 13)	67

The above example verifies that Hartley transforms have computational priority over Fourier transforms. However this depends upon which flavour of Fourier transform is in comparison. If we compare real Fourier transform with Hartley transform, Hartley transform may not be forward but if we compare complex Fourier transform with Hartley transform, then yes; Hartley transform is definitely faster as explained by the above example. Both types of the transforms will be used in Chapter 5, where modelling of a synchronous machine is presented.

3.9 Summary

An overview of orthogonal series expansion is presented. A characteristic definition of orthogonal functions and periodic functions has been given with appropriate examples. The Fourier and Hartley series are characterized and both Fourier and Hartley analysis are discussed in brief. Emphasis has been given to the process of polynomial evaluation using these transforms.

A portion of this chapter has been dedicated to Hartley transforms and their importance. In the end, a computational comparison between the two discussed analysis methods is made to demonstrate the computational importance of the Hartley transforms.

3.10 References

- [1] J. Arrillaga, N. R. Watson; “Power System Harmonics” John Willy & Sons, 2003
- [2] R. W. Hamming, “Numerical Methods for Scientists and Engineers” 1962, 1973
- [3] Pryymak, M.; Proshyn, S.; Karnaukhov, O.; “Periodic functions with variable periods and their properties”. IEEE, International workshop on ‘Intelligent Data Acquisition and Advanced Computing Systems’, pp. 347-350, 2009
- [4] R. N. Bracewell, “The Fourier Transform and its Applications” McGrahill, New York. 1965
- [5] K. J. Olejniczack and G.T. Heydt; “Special Section of the Hartley Transform”, IEEE proceedings, vol. 82, pp. 372-447, 1994
- [6] G.T. Heydt; “Systems Analysis Using Hartley Impedances”, IEEE Transactions on Power Delivery, vol. 7, no. 2, pp. 518-523, 1993
- [7] G.T. Heydt, K.J. Olejniczack, R. Spark and E. Viscinto; “Application of the Hartley Transform to the Analysis of the Propagation of Nonsinusoidal Waveforms in Power Systems”, IEEE Transactions on Power Delivery, vol. 6, no. 4, pp. 1862-1868, 1991

4. MODELLING OF POWER TRANSFORMER IN HARMONIC DOMAIN

4.1 Introduction

A power transformer is an essential part of any power network. During the last forty years intensive research efforts have been made to derive a suitable model of a transformer under steady state and transient conditions. A thorough knowledge of harmonics in power system networks requires an in-depth understanding and precise models for all the components of the power system. In many practical applications, the effect of non-linearity in the magnetization branch of transformer can be considered as negligible, research has been carried out to demonstrate its significance [1]. During the study of nonlinear systems [2], a number of transformer models in the harmonic domain have been put forward.

The transformer models were initially derived for load flow analysis [3], [4]. A full transformer model must include both electric and magnetic circuits. Several models have been developed, covering both the electrical and magnetic circuits of the transformer for the analysis of electromagnetic transients [5], [6].

Time domain procedures are usually used to determine steady state behaviour of the components in a power system, including the power transformer. The application of these procedures is however dependant upon information, which is not readily available, and results in an increased time required for computations. Harmonic phasors provide a fast and practical solution to this problem.

As already mentioned the harmonic domain frame, as a new frame for the analysis of the different components and the whole system, gives rise to more efficient models of these nonlinear components, like transformers and generators. Concerning the modelling of the transformer in the harmonic domain, several numerical procedures were proposed to simulate the nonlinearity of the transformer core.

The model that replaces nonlinearity of the transformer core with an equivalent circuit was presented in reference [7]. Norton harmonic equivalent for the magnetization branch of the single phase transformer was developed in the harmonic frame of reference [8]. The model was later extended and generalized to three phase networks, with multiple transformers [9], [10].

Harmonic domain modelling of transformer generally covers two aspects. First is the construction of the harmonic domain model, while the second aspect is the relation of the constructed model with harmonic frequencies. The harmonic model of a power transformer has been derived all is based on these two aspects [11]-[16]. Recently, a model for transformer nonlinearities including hysteresis is presented, which makes the use of describing functions and the harmonic balance method [17]. More recently, harmonic domain modelling of the single phase transformer core nonlinearities is derived and new computer algorithms are proposed [18]. Presented here is a full transformer model in the harmonic domain based on fundamental steps to derive a Norton equivalent for the magnetization branch of the transformer.

4.2 Nonlinear effects in the transformer core

Following nonlinear effects are present in a transformer core to a greater or lesser extent

4.2.1 Saturation

Saturation is a predominant effect in power transformers. Harmonics can be generated in all types of electrical machinery due to magnetic saturation in the core.

In order to avoid harmonics, the flux produced from the excitation current should always be proportional to it. However, as we know that magnetization curve is not linear, the magnetizing current is badly distorted after it enters the saturation region on the curve. Under normal conditions, the core operates in the linear region of the magnetization curve and does not usually saturate. In certain cases the transformer core enters the saturation region. For example, if a transformer is feeding to a converter load or an over-

excitation occurs due to a large rectifier plant connected to the transformer [19], harmonics in excitation current are caused.

4.2.2 Eddy Currents

Magnetic materials usually are good conductors of electricity. Potential difference provided by the winding turns across the core of transformer, allows Eddy currents to flow normal to the flux. These currents are a function of the supply frequency and generally their effect on power (low) frequency is not significant.

The core itself is usually made from laminated strips of the metal to minimize the effects of eddy currents. However, there is always a nonlinear effect present to some extent due to eddy currents and papers have been presented for modelling based on eddy currents e. g. [20]-[23] and more recently by [24] and [25]. Here eddy current currents are not a point of focus and it is assumed they are negligible.

4.2.3 Hysteresis

Hystereses depend upon the residual flux in the core. Residual flux varies with the type of magnetic material used in the core. Different materials have a different level of residual flux hence a different hysteresis loop. Fig. 4.1 shows the variation in the area of hysteresis loop for different materials.

Owing to efficiency requirements; transformer core should have a narrow hysteresis loop. Therefore they desire a material in which magnetization history is of minimum effect as they are usually subject to time varying magnetic fields. The materials with large residual flux are used in permanent magnets and memory devices. Based on the method of describing function, a model of for core nonlinearity caused by transformer has been presented by [26]. Similar procedure has been adapted by [27] for the representation of hysteresis loop and linearization of excitation current. The nonlinearity is a function of peak flux and applied frequency and can be given by:

$$N(E, \omega) = \frac{b_1 + ja_1}{E} \quad (4.1)$$

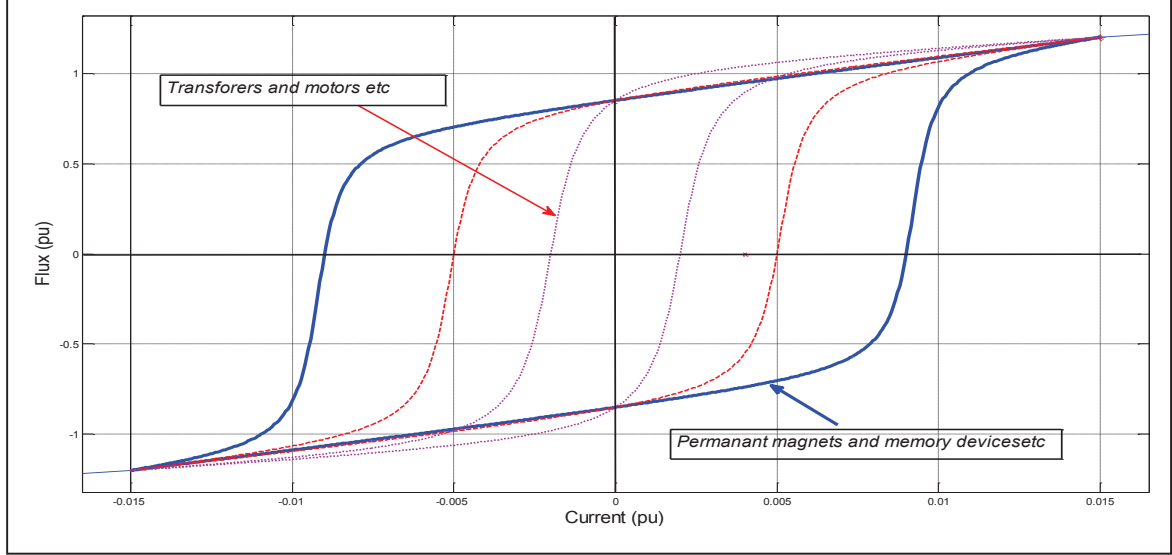


Fig. 4.1: Hysteresis loop for three different magnetic materials

Where b_1 and a_1 are the coefficients of the Fourier series. Consider the non linear system shown in Fig. 4.2 below



Fig. 4.2: An assumed nonlinear system

Where $\lambda(t)$ is the total flux linkage; given as:

$$\lambda(t) = E \sin(\omega t) \quad (4.2)$$

In equation (4.2) E is the amplitude and ω is the frequency of the input wave. The Fourier series of the function may be given as:

$$\lambda(t) = \frac{a_0}{2} + \sum_{n=1}^{\infty} a_n \cos(n\omega t) + \sum_{k=1}^{\infty} b_n \sin(k\omega t) \quad (4.3)$$

The experimental magnetizing characteristics of a small transformer may be recorded in a laboratory. The schematic for plot $i_e(t)$, the excitation current versus flux linkage λ , is shown in Fig. 4.3.

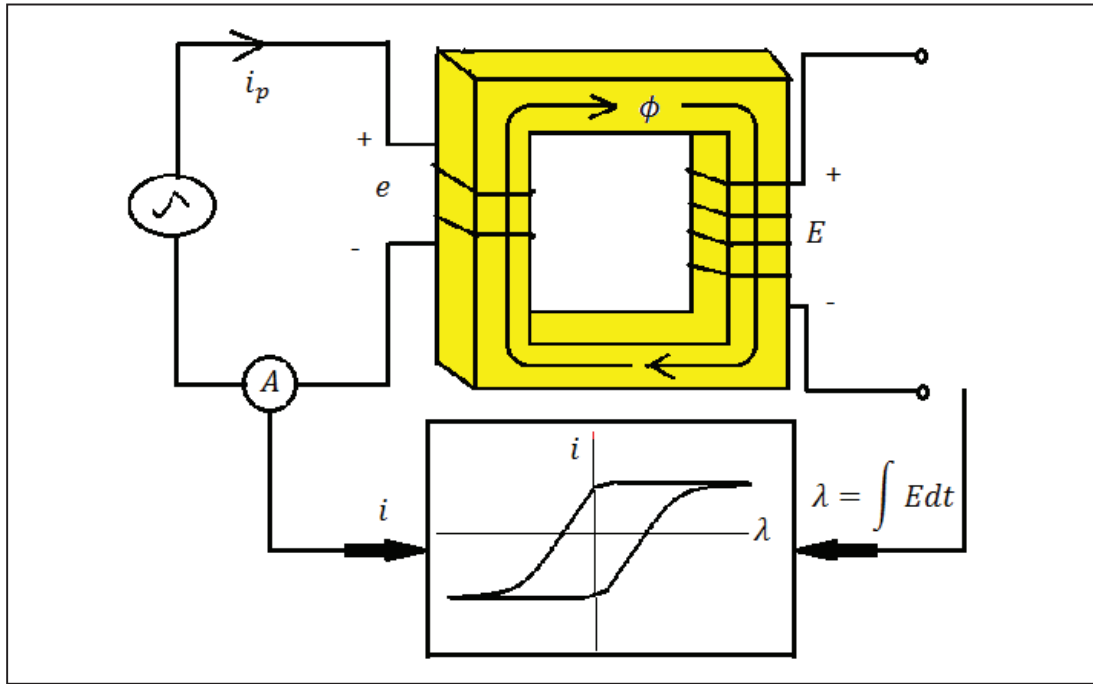


Fig. 4.3: Hysteresis loop; flux linkage and excitation current plot, schematic.

In equation (4.3), a_n and b_n are given by following relations:

$$a_n = \frac{\omega}{\pi} \int_{t_0}^t \lambda(t) \cos(n\omega t) dt \quad (4.4)$$

$$b_n = \frac{\omega}{\pi} \int_{t_0}^t \lambda(t) \sin(n\omega t) dt \quad (4.5)$$

Where t_0 is a random point on time axis and

$$t = t_0 + \left(\frac{2\pi}{\omega}\right) \quad (4.6)$$

$(2\pi/\omega)$ being the time period of the input magnetization current.

Assuming that the nonlinear component is symmetric about axis; equation (4.3) becomes:

$$\lambda(t) = \sum_{n=1}^{\infty} a_n \cos(n\omega t) + \sum_{n=1}^{\infty} b_n \sin(k\omega t) \quad (4.7)$$

$$\approx a_1 \cos(n\omega t) + b_1 \sin(n\omega t)$$

$$\begin{aligned}
 &\approx a_1 \sin(\omega t + 90^\circ) + b_1 \sin(\omega t) \\
 &\approx c_1 \sin(\omega t + \phi) \\
 &\approx c_1 e^{j(\omega t + \phi)}
 \end{aligned} \tag{4.8}$$

Here

$$c_1 \angle \phi = b_1 + ja_1 \tag{4.9}$$

Replacing the value of $(b_1 + ja_1)$ in equation (4.1) gives the gain of nonlinearity as

$$N(E, \omega) = \frac{c_1 \angle \phi}{E} \tag{4.10}$$

4.3 Polynomial fitting of the hysteresis curve

The dynamic hysteresis loop in iron core is composed of two symmetrical parts. The normal magnetizing curve, as the first part marked by "aoc" in Fig. 4.4, is the locus of the mid points of the hysteresis loop. This can be obtained by the measured hysteresis data. The loss part, as the second part marked by distances such as "ef" in Fig. 4.4, represents loss in the hysteresis loop. It is also termed as the "consuming function" because the main part contributes proper shape and area of the hysteresis loop.

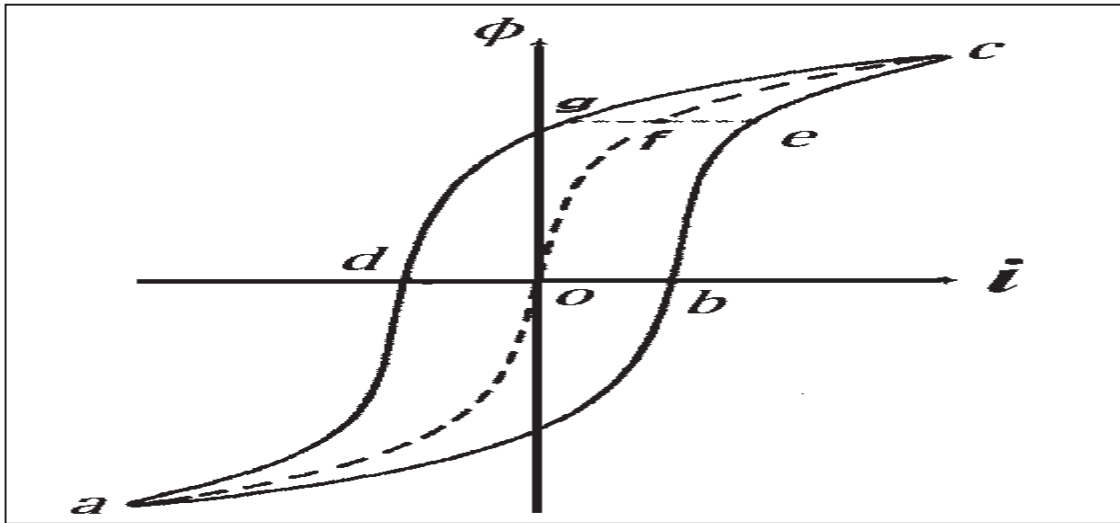


Fig. 4.4: A sample hysteresis loop approximated by four line sections

The distance “ ef ” changes periodically by a half wave symmetry. The periphery of the hysteresis loop is obtained by adding or subtracting the consuming function to the normal magnetizing curve. Usually, for modern transformers, normal magnetizing curve can be approximated by four line sections. The equations of these lines are:

$$i = (i_1 - m_1\phi_1) + m_1\phi \quad \phi_0 < |\phi| < \phi_1 \quad (4.11)$$

$$i = (i_2 - m_2\phi_2) + m_2\phi \quad \phi_1 < |\phi| < \phi_2 \quad (4.12)$$

$$i = (i_3 - m_3\phi_3) + m_3\phi \quad \phi_2 < |\phi| < \phi_3 \quad (4.13)$$

$$i = (i_4 - m_4\phi_4) + m_4\phi \quad \phi_3 < |\phi| < \phi_4 \quad (4.14)$$

Where

$$\phi = \phi_m \cos(\omega t) \quad (4.15)$$

Subscripts 1, 2, 3 and 4 denote for the sampled points of Fig. 4.5 and m is slope of the corresponding line sections.

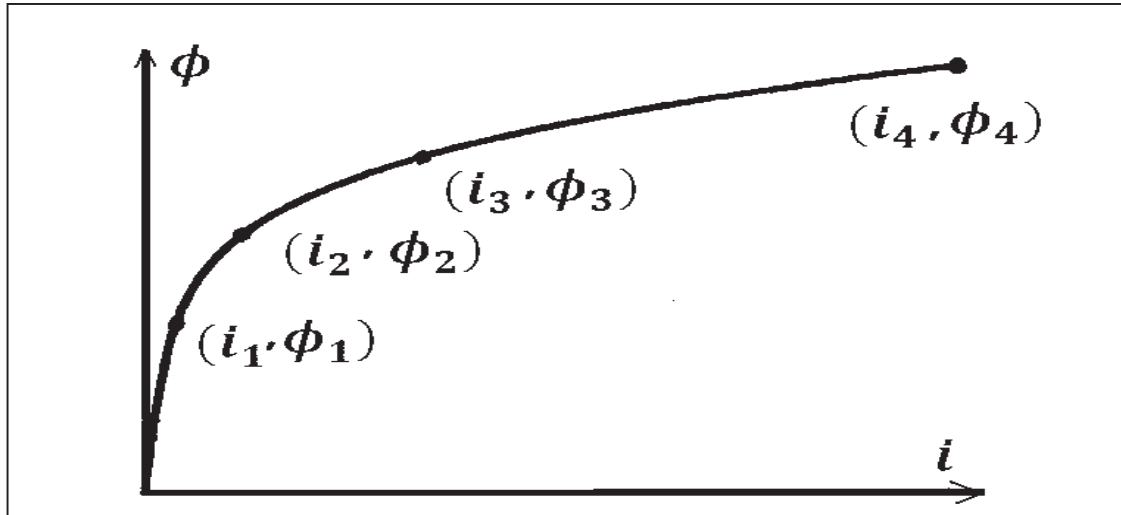


Fig. 4.5: Sampled points on the magnetization curve

The nature of the consuming function is a reverse function of the normal magnetizing curve. It reaches maximum when the normal magnetizing goes to zero, and vice versa. Hence the consuming function can be represented by:

$$f(\phi) = D\left(\frac{d\phi}{dt}\right) \quad (4.16)$$

$$f(\phi) = D\left(\frac{d}{dt}\{\phi_m \cos(\omega t)\}\right) \quad (4.17)$$

$$f(\phi) = -D\omega\phi_m \sin(\omega t) \quad (4.18)$$

$$f(\phi) = -ob \sin(\omega t) \quad (4.19)$$

Where D is a coefficient, and ob is the maximum distance between the mid point locus and the periphery of the hysteresis loop.

The hysteresis loop is represented by combining Equations (4.11-14) and (4.19). By fitting the four line sections into the normal magnetizing curve, the periphery of the hysteresis loop turns out a composition of sixteen line sections. The mathematical expression for the hysteresis loop becomes:

$$i = (i_k - m_k\phi_k) + m_k\phi - ob \sin(\omega t) \quad (4.20)$$

Where

$$\phi_{k-1} < |\phi| < \phi_k \quad k = 1, 2, \dots, 16 \quad (4.21)$$

In a simple magnetic core, the current-flux relationship existing in an unloaded power transformer, may be approximated [30] by a polynomial equation of the form:

$$i = a\phi + b\phi^n \quad (4.22)$$

Where i and ϕ are magnetizing current and core linkage flux respectively.

Constant coefficients a and b respectively impact the linear and saturated regions of the core magnetization characteristic. The curvature of the characteristic in saturation region is mainly deduced based on constant exponent n .

Fig. 4.6 shows how magnetization curve changes with a change in a , b and n of Equation (4.22). The coefficients a , b and n can be derived from the basic information about the machine and experimental magnetization curve.

Let us assume that Fig. 4.7 shows the positive half of such an experimental magnetization curve for a certain transformer. Following information about the recorded curve is tabulated:

- Slope of the linear part = 1700
- At knee point, $(i, \varphi) = (0.002, 1)$
- Maximum flux and maximum current = $(i, \varphi) = (1.3, 0.004)$

By putting all this information in Equation (4.22) gives:

$$0.004 = \frac{1}{1700}(1.3) + b(1.3)^n$$
$$\text{or } b = \frac{0.0032}{(1.3)^n}$$

which gives

$$b = 0.0015 \text{ for } n = 3,$$
$$b = 0.000862 \text{ for } n = 5,$$
$$b = 0.00051 \text{ for } n = 7,$$
$$b = 0.0003 \text{ for } n = 9 \text{ and so on.}$$

Coordinates at the knee point tell us that $i = 0.002$ when $\varphi = 1$. While the polynomial equation is solved for different values of n and corresponding b at $\varphi = 1$; the current obtained is:

$$i = 0.0021 \text{ for } n = 3,$$
$$i = 0.0015 \text{ for } n = 5,$$
$$i = 0.0011 \text{ for } n = 7 \text{ and}$$
$$i = 0.0009 \text{ for } n = 9$$

Hence most suitable fitting of this curve is:

$$i = 0.00059\varphi + 0.0015\varphi^3$$

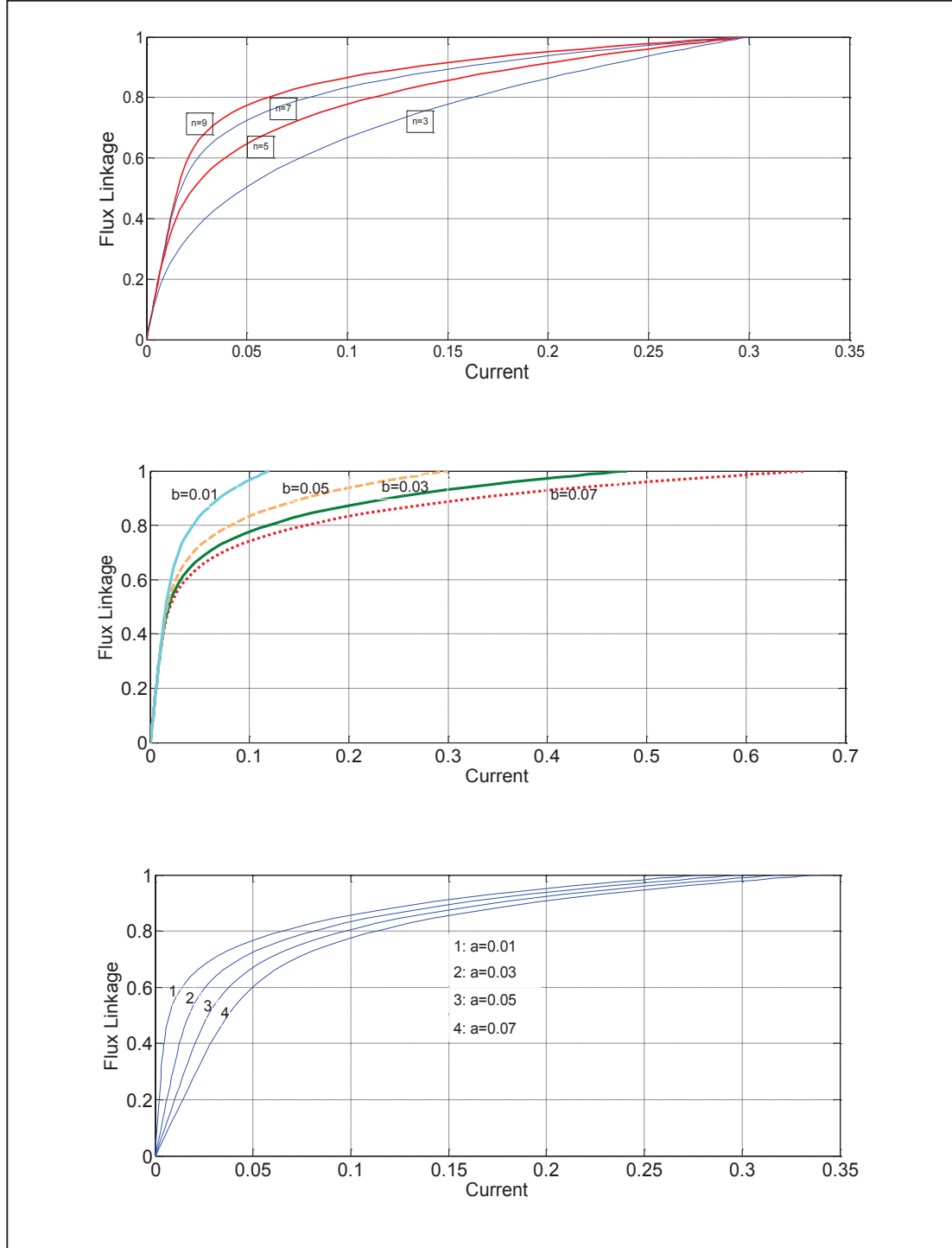


Fig. 4.6: Variation in magnetization curve with a change in a , b and n

For the case of $n=3$, the self and mutual-convolutions in frequency domain may be carried out as:

$$\varphi^2 = \varphi \otimes \varphi \quad (4.23)$$

$$\varphi^3 = \varphi \otimes \varphi^2 \quad (4.24)$$

The reason for the use of polynomial evaluation via repeated convolutions is that it is equivalent to the algebraic approach; at the same time has the advantage of being amenable to efficient computer implementations [28].

Assuming the following voltage excitation,

$$e = E_{\max} \cos \omega t \quad (4.25)$$

and upon integration,

$$\varphi = \frac{E_{\max}}{\omega} \cdot \sin \omega t \quad (4.26)$$

Alternatively, expressing the flux in the form of complex exponential coefficients,

$$\varphi = \frac{E_{\max}}{\omega} \cdot \frac{e^{j\omega t} - e^{-j\omega t}}{2j} \quad (4.27)$$

It should be remembered that,

$$\sin \omega t = \frac{e^{j\omega t} - e^{-j\omega t}}{2j} \quad (4.28)$$

and

$$\cos \omega t = \frac{e^{j\omega t} + e^{-j\omega t}}{2} \quad (4.29)$$

Putting only the complex exponential coefficients from equation (4.27) in equation (4.22), an expression for the current, in terms of complex exponential coefficients, is carried out as follows:

$$i = a \left(\frac{e^{j\omega t} - e^{-j\omega t}}{2j} \right) + b \left(\frac{e^{j\omega t} - e^{-j\omega t}}{2j} \right)^3 \quad (4.30)$$

$$i = j\frac{b}{8} \cdot e^{j3\omega t} + j\left(\frac{a}{2} - \frac{b}{8}\right) \cdot 3e^{j\omega t} - j\left(\frac{a}{2} - \frac{b}{8}\right) \cdot 3e^{-j\omega t} - j\frac{b}{8} \cdot e^{-j3\omega t} \quad (4.31)$$

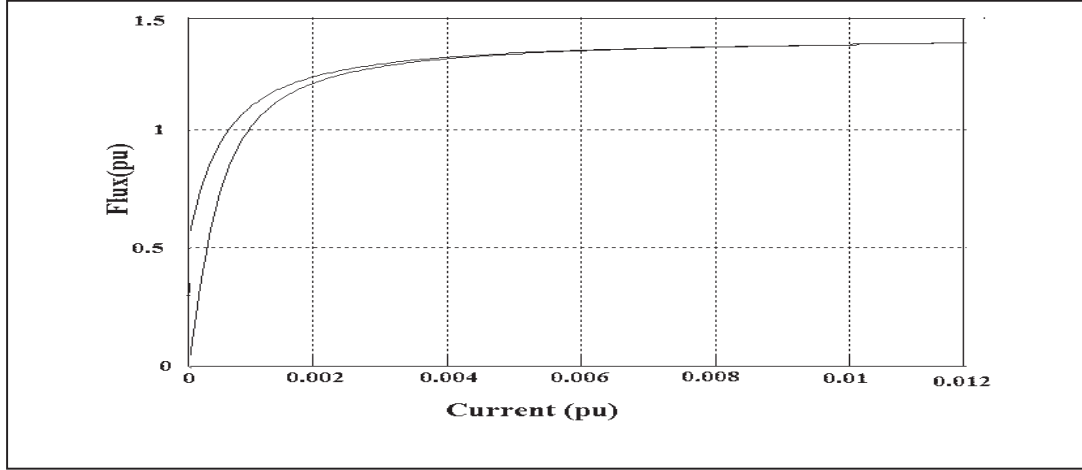


Fig. 4.7: Recorded magnetizing characteristics of the transformer

It should be noticed that although the flux is a pure sinusoid, the current contains higher frequency terms, namely third harmonic. The harmonic contents in the current waveform are as in Table 4.1.

Table 4.1: Harmonic contents in the current given by Equation (4.31)

3 rd	2 nd	1 st	DC	-1 st	-2 nd	-3 rd
$jb/8$	0	$j(a/2-b/8)$	0	$-j(a/2-b/8)$	0	$-jb/8$

The above algebraic procedure is fully equivalent to the graphical procedure shown in Fig. 4.8, which would go accompanied by FFT procedures in order to extract the harmonic content of the current waveform.

Notice that the graphical procedure involves mapping a full-period (only half-period shown) of the flux onto the magnetizing non-linear flux-current characteristic, in order to derive the magnetizing current waveform – which happens to be non-sinusoidal even for an impressed sinusoidal flux, due to non-linear nature of the flux-current characteristic.

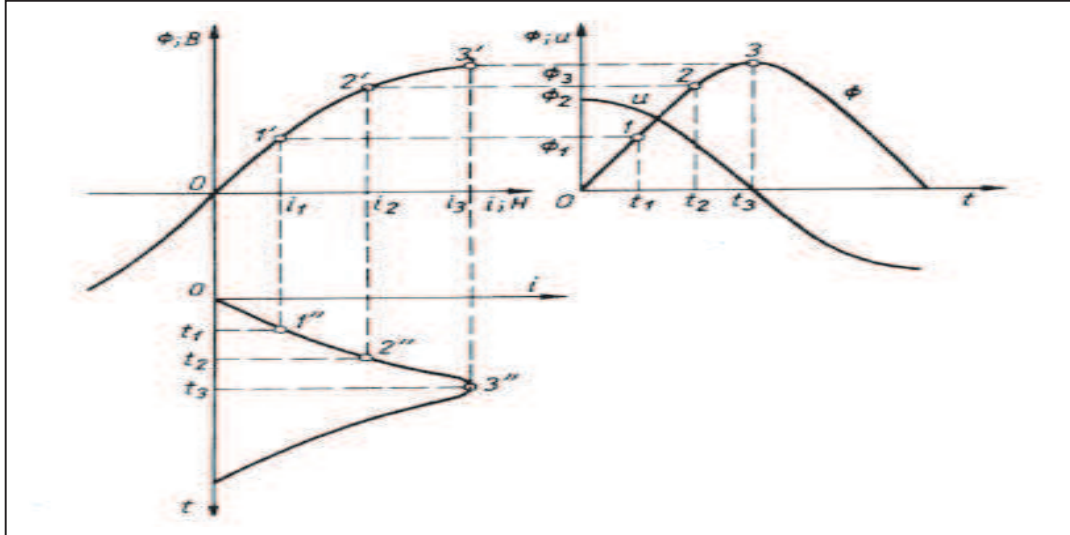


Fig. 4.8: Relation between main flux, supply voltage and no-load magnetizing current [29]

4.4 Norton equivalent for the magnetization branch in harmonic domain

Transformers are usually designed to operate very close to the limit of the linear characteristics and even under small over-excitation, their contribution to harmonic content is often important. The experimental magnetizing curves can be analytically approximated. Fig. 4.9 shows an idealized flux-current characteristic, when hysteresis is neglected and obtained with the transformer operating under no-load.

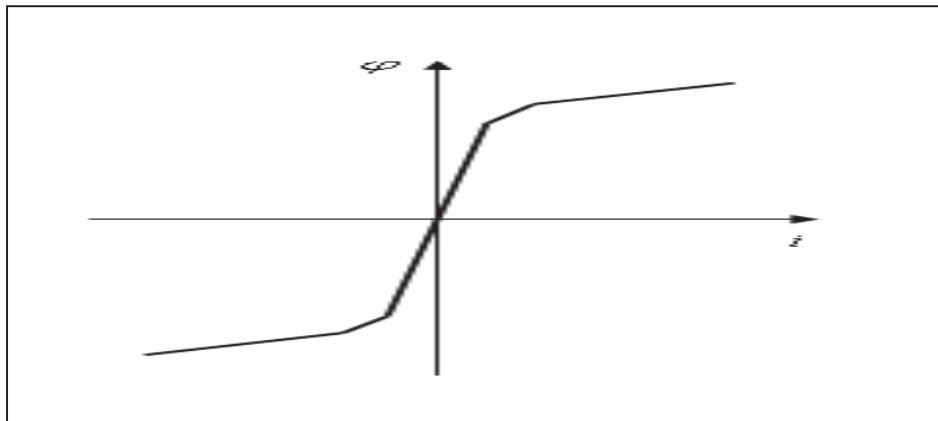


Fig.4.9: An idealized flux-current characteristic curve

For the average upper half of the magnetizing curve, if ϕ_0 and ϕ_1 represent the approximate values of flux in the core against the respective values of current i_0 and i_1 as shown in Fig. 4.10. Then for a certain operating length on the curve

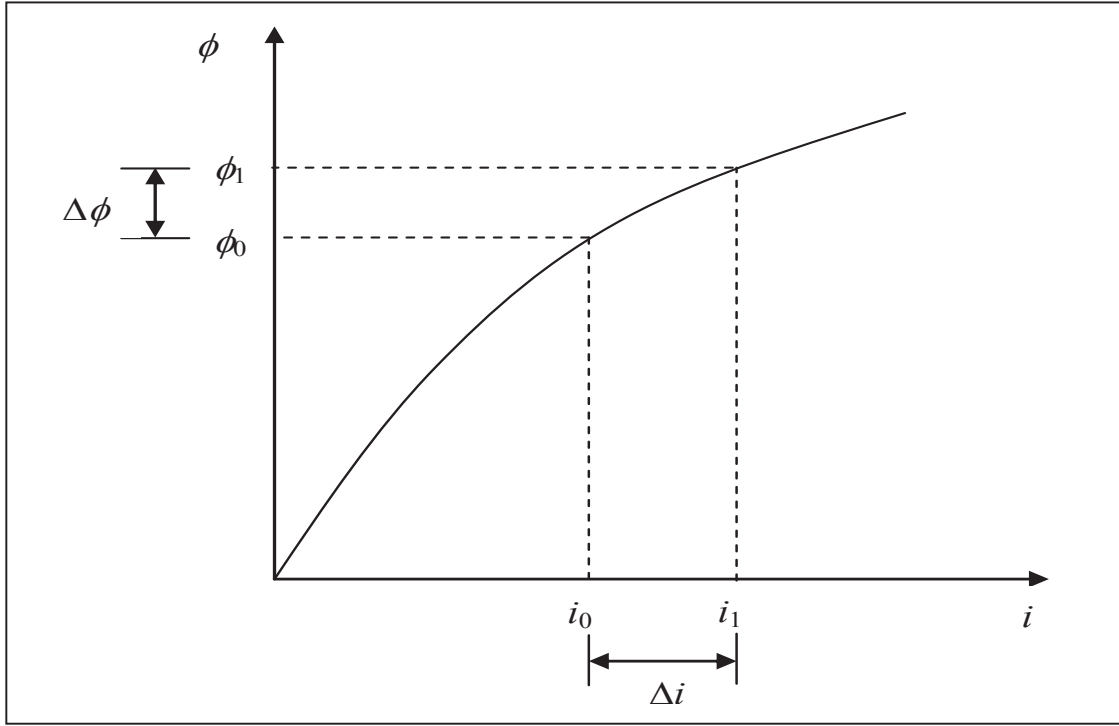


Fig 4.10: Change in flux with change in magnetizing current near operating point

$$\frac{\Delta i}{\Delta \phi} = G \quad (4.32)$$

Where G is the incremental magnetic conductance

$$\Delta i = G \Delta \phi \quad (4.33)$$

Equation (4.33) can also be written as

$$(i_1 - i_0) = G(\phi_1 - \phi_0) \quad (4.34)$$

or

$$i_1 = G(\phi_1 - \phi_0) + i_0$$

$$i_1 = G\phi_1 - G\phi_0 + i_0$$

$$i_1 = G\phi_1 + (i_0 - G\phi_0) \quad (4.35)$$

As we know that time derivative of flux results in the voltage i.e.

$$\begin{aligned}
 \frac{d}{dt}\phi &= V \\
 \Rightarrow jh\omega\phi &= V \\
 \Rightarrow \phi &= \frac{1}{jh\omega}V \\
 \Rightarrow \phi &= D^{-1}(jh\omega)V
 \end{aligned} \tag{4.36}$$

From equation (35) and equation (36), we can write that

$$\begin{aligned}
 I_1 &= GD^{-1}(jh\omega)V + \{i_0 - GD^{-1}(jh\omega)V\} \\
 I_1 &= GD^{-1}(jh\omega)V + I_N \\
 I_1 &= YV + I_N
 \end{aligned} \tag{4.37}$$

Where

$$Y = GD^{-1}(jh\omega)$$

and

$$I_N = i_0 - YV$$

Equation (4.37) may be interpreted as harmonic Norton equivalent for the magnetization branch of the transformer as shown in Fig. 4.11.

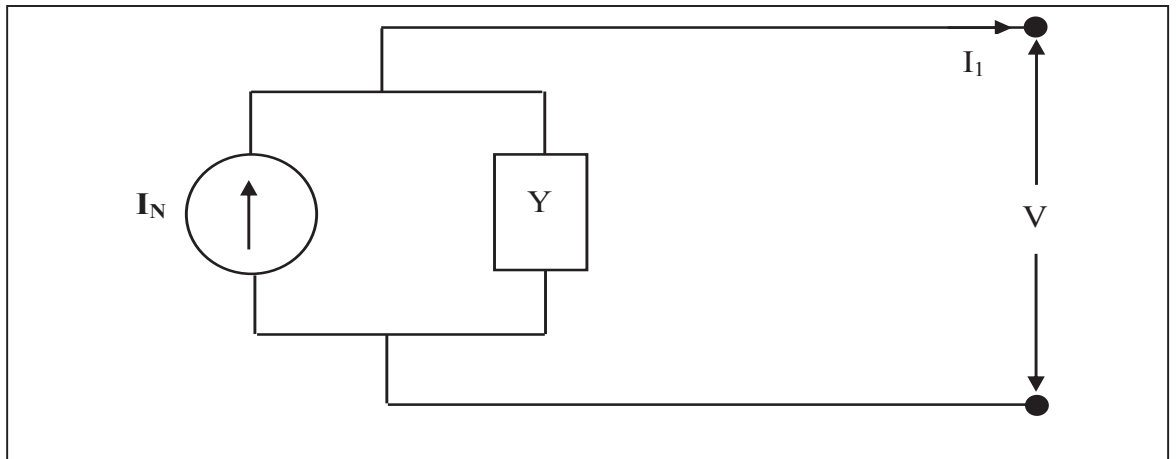


Fig. 4.11: Harmonic Norton equivalent for the magnetization branch

Notice that in the harmonic Norton equivalent, the admittance matrix \mathbf{Y} is a band-diagonal matrix of dimensions $2h+1 \times 2h+1$, where h is the harmonic order; \mathbf{I}_N , \mathbf{I} and \mathbf{V} are harmonic vectors of dimensions $2h+1$.

4.5 Full transformer model in harmonic domain

The circuit of harmonic Norton equivalent for the magnetizing branch of the transformer (Fig. 4.11) is now combined with the rest of the equivalent circuit of single-phase transformer to give a full harmonic representation for the single-phase transformer and is shown in Fig. 4.12.

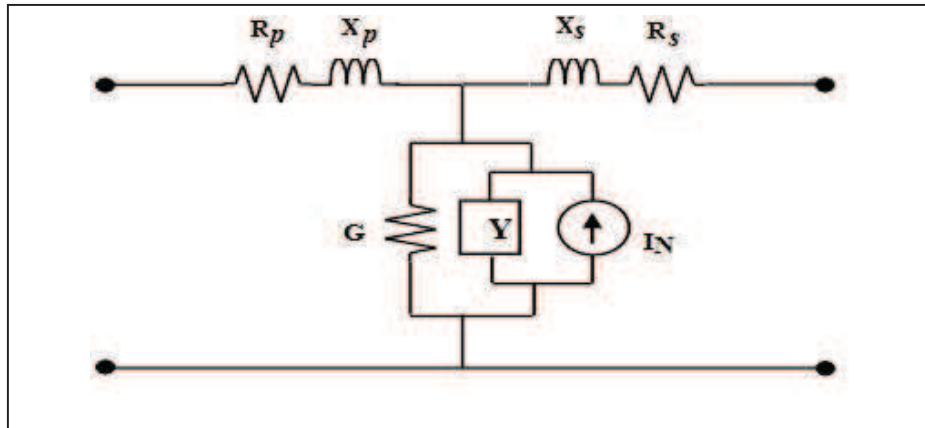


Fig. 4.12: Full harmonic representation of a single-phase transformer

The transformer core is a kind of flux controlled inductance. For high currents the transformer core is driven into saturation where the flux current characteristics are modelled as a polynomial equation (4.22) by using self and mutual convolutions. The magnetic flux is derived according to equation (4.36). The operational derivative matrix (D) is built for this purpose and its inverse is taken to obtain the operational matrix of integration. Notice that the dimensions of this matrix (D) are $((2h + 1) \times 1)$, where h is the harmonic order. Equation (4.37) is put up with the help of G and i_0 where G is a Toeplitz matrix assembled with the harmonic inductance of the magnetizing characteristics, whereas, i_0 is assembled with the coefficients of harmonic current.

4.6 Case study

Using iterations, for harmonic response of the circuit shown in Fig. 4.13 is worked out. The circuit comprises of a voltage source feeding a transmission line via a step up transformer.

The magnetizing branch of the transformer is responsible for producing harmonic current distortion and is assumed to be connected at the high level bus of the transformer (bus 2). The transmission line is modelled by pi-equivalent circuit.

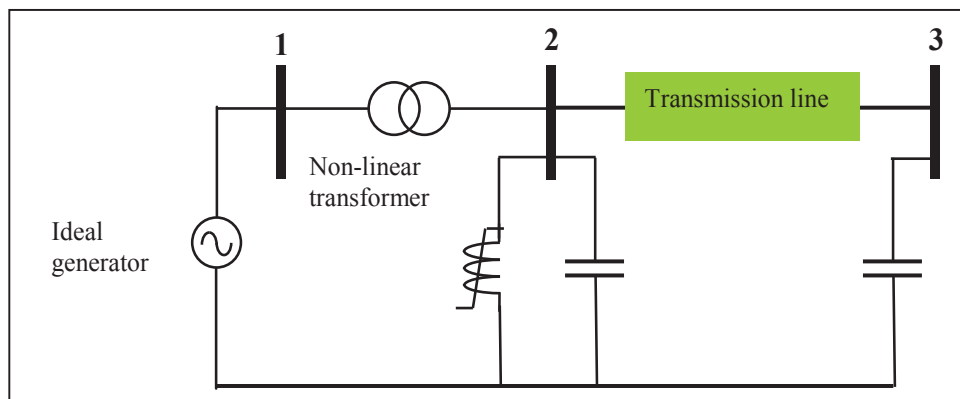


Fig. 4.13: Test circuit

Harmonic values up to 15th term are considered in the simulation. However; the terms above 5th harmonic showed to have negligible small values.

Please notice that in the results shown in Fig. 14-16, harmonic voltage vectors contain positive and negative harmonics as well as the DC term. Further the numerical values are rounded off.

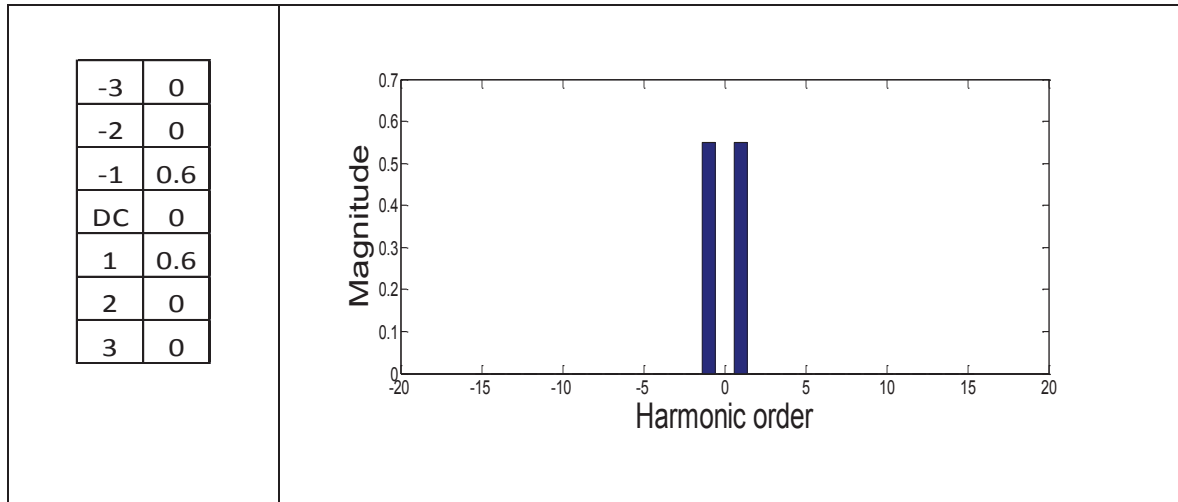


Fig. 4.14: Harmonic Voltage at Node 1, Fig. 4.13

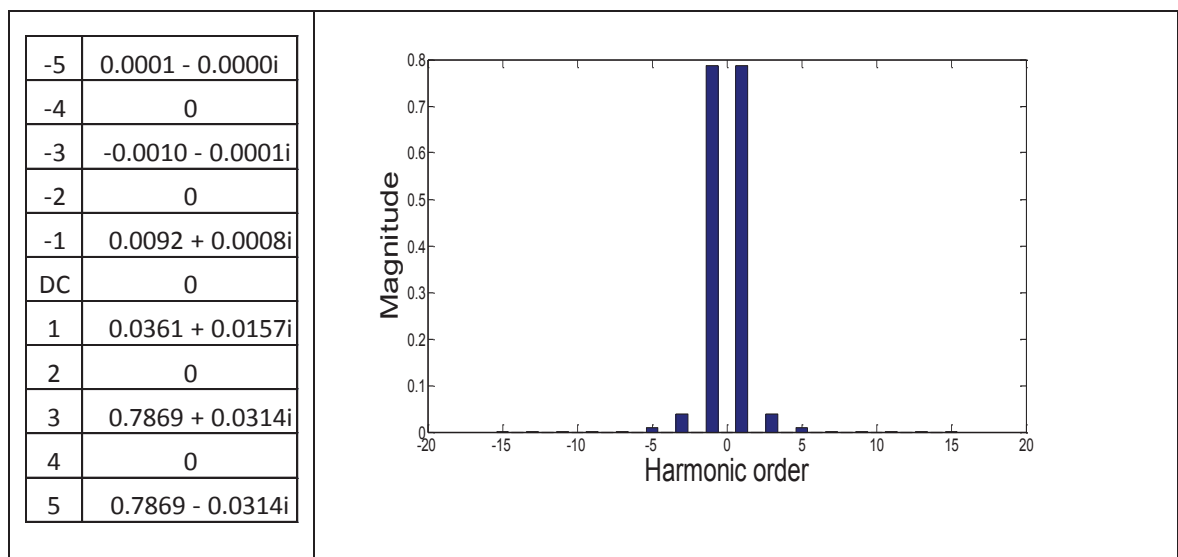


Fig. 4.15: Harmonic Voltage at Node 2, Fig. 4.13

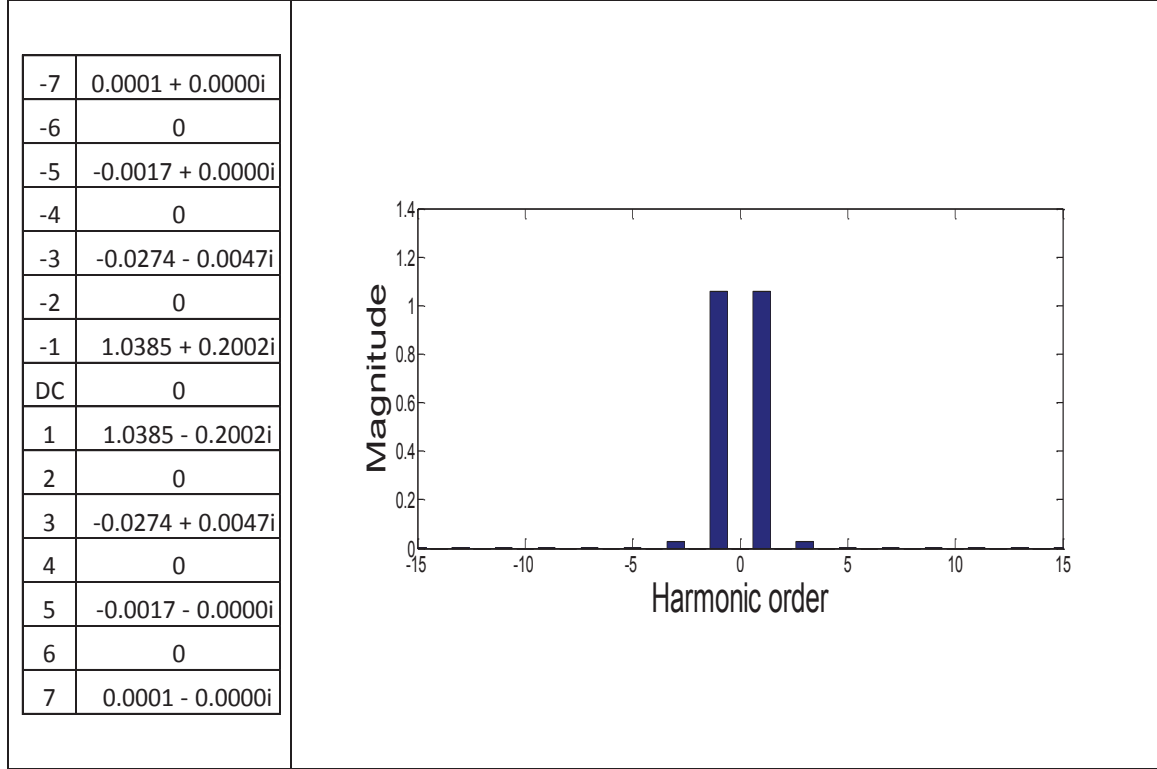


Fig. 4.16: Harmonic Voltage at Node 3, Fig. 4.13

The circuit is solved on the basis of a constant core resistance R and a magnetizing current dependant flux linkage. The characteristic of the nonlinear inductance is based on flux and magnetizing current. The operational matrix for integration is achieved by taking the inverse of operational derivative matrix D which is then multiplied by the voltage to calculate flux linkage (φ).

The programme is initialized by setting the initial conditions (tol, error, iter) and a small (estimated) value of flux linkage to start the iterative process. All the system parameters have been gathered and Norton harmonic equivalent for the magnetization branch is built. A check for the convergence is performed at the end of two successive iterations of harmonic current values. The network nodal harmonic voltages are obtained when the solution is converged. *Appendix I*, shows all the functions used in MATLABTM for the calculation of harmonic voltage magnitudes.

4.7 Generalization to 3-phase transformer

Magnetic circuits have their analogy to the electric circuits. In the electric circuit shown in the electric circuit of Fig. 4.17, the potential difference between point A and B is:

$$V_{AB} = V_A - V_B \quad (4.38)$$

and
$$V = iR \quad (4.39)$$

Where R is the resistance of the conductor i. e. the path for the flow of current, depending upon cross-sectional area and length of the conductor. Similarly, in the symbolic magnetic circuit of Fig. 4.17, the difference in mmf between points A and B is:

$$F_{AB} = F_A - F_B \quad (4.40)$$

Also
$$F = \Phi \mathcal{R} \quad (4.41)$$

Where \mathcal{R} is know as the reluctance of the magnetic path. \mathcal{R} is the counter part of resistance in the electric circuit. The only difference between two circuits in this regard is that in an electric circuit current travels through the path while in a magnetic circuit flux travels through the path provided.

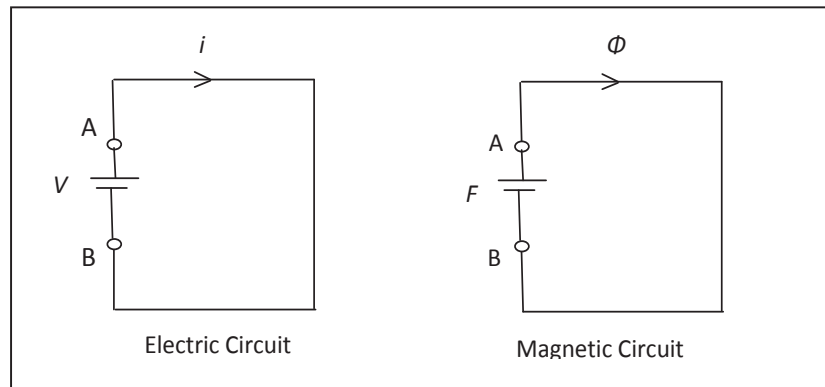


Fig. 4.17: Analogy of electric and magnetic circuit

In equation (4.41), F represents mmf of electro-magnetic source. In transformers and most of other electrical machines

$$F = Ni \quad (4.42)$$

Modelling of Power Transformer in Harmonic Domain

Where N is the numbers of turns of winding conductor and i is the excitation current.

Replacing value of F from equation (4.42) into equation (4.41) yields

$$Ni = \Phi \mathcal{R} \quad (4.43)$$

Now, if the distance between A and B is very small (incremental), equation (4.43) may be written as

$$\Delta F = \mathcal{R} \Delta \Phi \quad (4.44)$$

or

$$\begin{aligned} F_A - F_B &= \mathcal{R}(\Phi_A - \Phi_B) \\ F_B &= \mathcal{R}\Phi_B + F_A - \mathcal{R}\Phi_A \\ F_B &= \mathcal{R}\Phi_B + F_n \end{aligned} \quad (4.45)$$

where

$$F_n = F_A - \mathcal{R}\Phi_A$$

here \mathcal{R} is the incremental reluctance of the magnetic path between points A and B .

Assuming that *mmf* source is attached to point A i.e.

$$F_A = Ni$$

Then equation (4.42) becomes:

$$F_{AB} = Ni - \mathcal{R}\Phi_B - F_n \quad (4.46)$$

Multiplying both sides of equation (4.46) with G , gives:

$$GF_{AB} = GNi - G\mathcal{R}\Phi_B - GF_n \quad (4.47)$$

In equation (47) G is the inverse of \mathcal{R} , know as magnetic conductance. Solving for flux, produces:

$$\Phi_B = GNi - GF_{AB} - GF_n \quad (4.48)$$

In a per unit system, $Ni = i$, so equation (4.48) can be moderated as:

$$\Phi_B = Gi - GF_{AB} - GF_n \quad (4.49)$$

Where al the quantities are phasor quantities. Generalizing equation (4.49) in matrix form so that different branches can be included:

$$\Phi_B = [G]i - [G]F - [G]F_n$$

or

$$\Phi = [G]i - [G]F - F_n \quad (4.50)$$

where

$$F_n = [G]F_n$$

Multiplying both sides of equation (4.50) by $[\mathcal{R}]$ gives:

$$[\mathcal{R}]\Phi = i - F - [\mathcal{R}]F_n \quad (4.51)$$

Multiplying both sides of equation (4.51) by connection matrix $[C]^t$

$$[C]^t[\mathcal{R}]\Phi = [C]^ti - [C]^tF - [C]^t[\mathcal{R}]F_n \quad (4.52)$$

If $[C]^ti = i_N$ and $F = [C]F_N$, equation (4.52) can be written as:

$$[C]^t[\mathcal{R}]\Phi = i_N - [C]^t[C]F_N - [C]^t[\mathcal{R}]F_n$$

Solving for F_N

$$F_N = -\frac{1}{[C]^t[C]} \{[C]^t[\mathcal{R}]\Phi + [C]^t[\mathcal{R}]F_n - i_N\}$$
$$F_N = -[X_1]\{[C]^t[\mathcal{R}]\Phi + [C]^t[\mathcal{R}]F_n - i_N\} \quad (4.53)$$

where

$$[X_1] = \frac{1}{[C]^t[C]}$$

Simultaneously solving equations (4.50) and (4.53) for i gives the out put:

$$i = [X_2]\Phi + X_2F_n + [C][X_1]i_N \quad (4.54)$$

where

$$[X_2] = [\mathcal{R}]\{1 - [C][X_1][C]^t\}$$

Now going back to equation (4.36), putting the value of flux in equation (4.54) generates:

$$i = [X_2]D^{-1}(jh\omega)V + [X_2]F_n + [C][X_1]i_N$$

$$i = [Y]V + \hat{i}_N$$

(4.55)

where

$$[Y] = [X_2]D^{-1}(jh\omega)$$

and

$$\hat{i}_N = [X_2]F_n + [C][X_1]i_N$$

Based on the fact that three single-phase transformers can be connected to achieve a three-phase transformer, method stated in section 4. 4 can be used for the modeling of a three-phase transformer. The three-phase transformer model involves the type of connections as well as the number of limbs in the core.

4.8 Case study

The harmonic response of the circuit of Fig. 4.13 is simulated using iterations, assuming that the circuit is a three-phase one now. The circuit comprises a three phase voltage source feeding a transmission line via a three phase step up transformer.

Again it is assumed that the source is an ideal one and the magnetizing branch of the transformer is responsible for producing harmonic current distortion. It is also assumed to be connected at the high level bus of the transformer (bus 2). The transmission line again is modelled by pi-equivalent circuits as it was in previous case.

As the voltage source is an ideal one, no harmonics are observed at Node 1. Notice that the voltage vector used in simulation is up to 15th harmonic term and harmonic voltages at Node 2 and Node 3 are given in Tabe 4.2 ad Table 4.3 respectively.

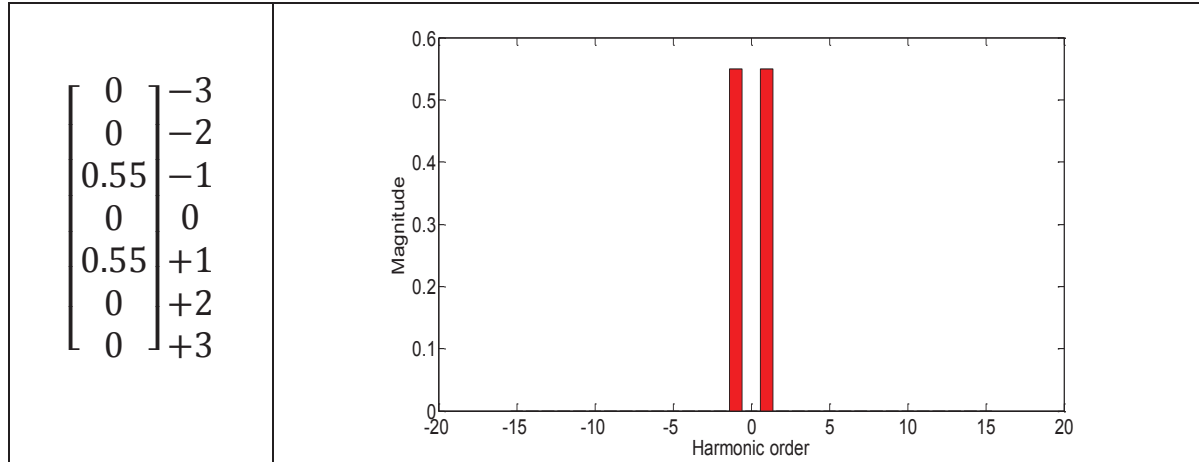


Fig. 4.18: Harmonic Voltage at Node 1. Phase *a*, Fig. 4.13

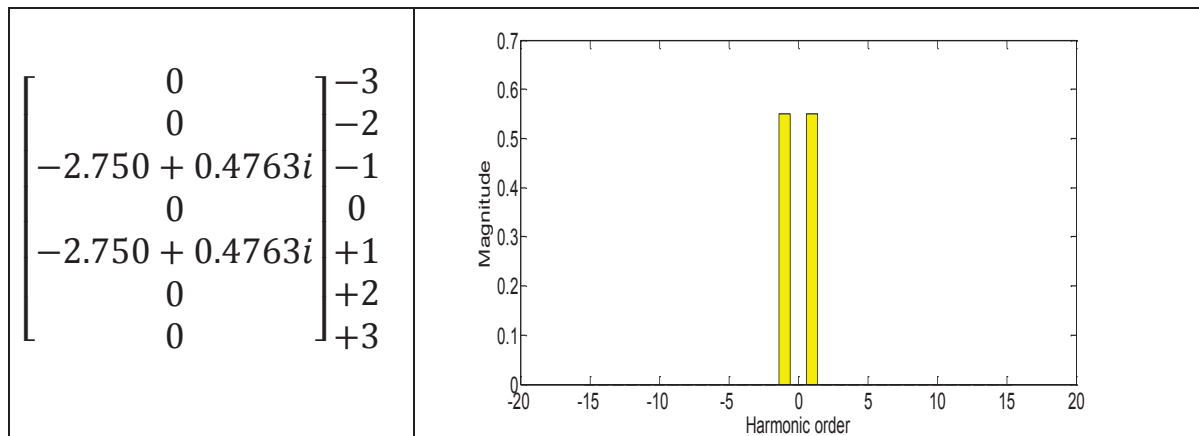


Fig. 4.19: Harmonic Voltage at Node 1. Phase *b*, Fig. 4.13

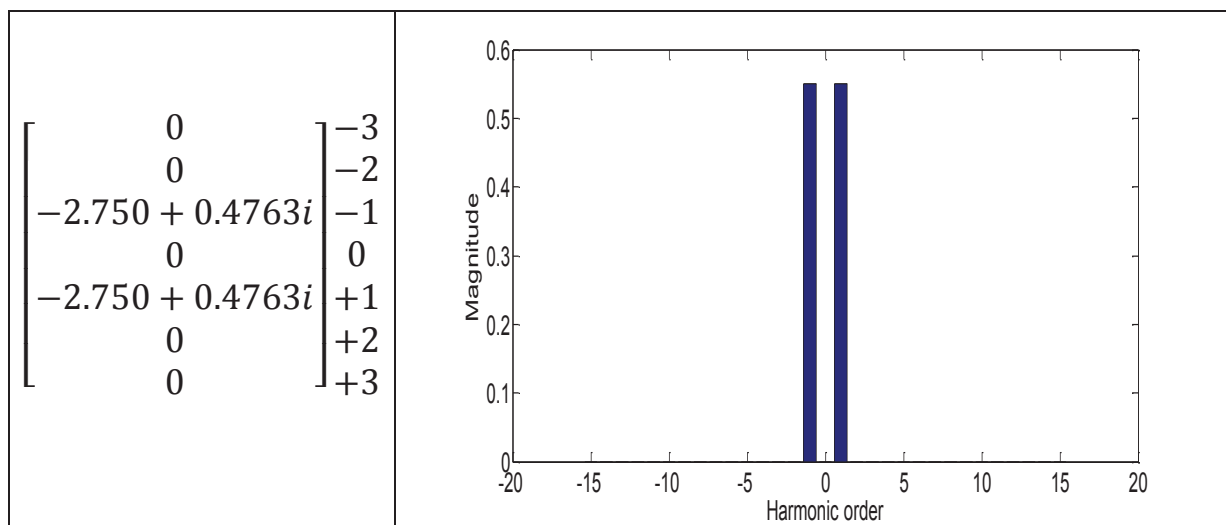


Fig. 4.20: Harmonic Voltage at Node 1. Phase *c*, Fig. 4.13

Table 4.2: Harmonic voltages at Node 2, Fig. 4.13

Harmonic order	V, Phase <i>a</i>	V, Phase <i>b</i>	V, Phase <i>c</i>
-15	-0.0000 + 0.0000i	-0.0000 + 0.0000i	-0.0000 + 0.0000i
-14	0	0	0
-13	0.0000 + 0.0000i	-0.0000 + 0.0000i	-0.0000 - 0.0000i
-12	0	0	0
-11	-0.0000 + 0.0000i	0.0000 + 0.0000i	0.0000 - 0.0000i
-10	0	0	0
-9	0.0001 - 0.0000i	0.0001 - 0.0000i	0.0001 - 0.0000i
-8	0	0	0
-7	-0.0010 - 0.0001i	0.0006 - 0.0008i	0.0004 + 0.0009i
-6	0	0	0
-5	0.0092 + 0.0008i	-0.0039 - 0.0084i	-0.0053 + 0.0076i
-4	0	0	0
-3	0.0361 + 0.0157i	0.0361 + 0.0157i	0.0361 + 0.0157i
-2	0	0	0
-1	0.7869 + 0.0314i	-0.4206 + 0.6657i	-0.3662 - 0.6971i
DC	0	0	0
1	0.7869 - 0.0314i	-0.4206 - 0.6657i	-0.3662 + 0.6971i
2	0	0	0
3	0.0361 - 0.0157i	0.0361 - 0.0157i	0.0361 - 0.0157i
4	0	0	0
5	0.0092 - 0.0008i	-0.0039 + 0.0084i	-0.0053 - 0.0076i
6	0	0	0
7	-0.0010 + 0.0001i	0.0006 + 0.0008i	0.0004 - 0.0009i
8	0	0	0
9	0.0001 + 0.0000i	0.0001 + 0.0000i	0.0001 + 0.0000i
10	0	0	0
11	-0.0000 - 0.0000i	0.0000 - 0.0000i	0.0000 + 0.0000i
12	0	0	0
13	0.0000 - 0.0000i	-0.0000 - 0.0000i	-0.0000 + 0.0000i
14	0	0	0
15	-0.0000 - 0.0000i	-0.0000 - 0.0000i	-0.0000 - 0.0000i

Table 4.3: Harmonic voltages at Node 3, Fig. 4.13

Harmonic order	V, Phase <i>a</i>	V, Phase <i>b</i>	V, Phase <i>c</i>
-15	0.0000 - 0.0000i	0.0000 - 0.0000i	0.0000 - 0.0000i
-14	0	0	0
-13	-0.0000 - 0.0000i	0.0000 - 0.0000i	0.0000 + 0.0000i
-12	0	0	0
-11	0.0000 - 0.0000i	-0.0000 - 0.0000i	-0.0000 + 0.0000i
-10	0	0	0
-9	-0.0000 + 0.0000i	-0.0000 + 0.0000i	-0.0000 + 0.0000i
-8	0	0	0
-7	0.0001 + 0.0000i	-0.0000 + 0.0001i	-0.0000 - 0.0001i
-6	0	0	0
-5	-0.0017 + 0.0000i	0.0008 + 0.0014i	0.0008 - 0.0014i
-4	0	0	0
-3	-0.0274 - 0.0047i	-0.0274 - 0.0047i	-0.0274 - 0.0047i
-2	0	0	0
-1	1.0385 + 0.2002i	-0.6926 + 0.7992i	-0.3459 - 0.9994i
DC	0	0	0
1	1.0385 - 0.2002i	-0.6926 - 0.7992i	-0.3459 + 0.9994i
2	0	0	0
3	-0.0274 + 0.0047i	-0.0274 + 0.0047i	-0.0274 + 0.0047i
4	0	0	0
5	-0.0017 - 0.0000i	0.0008 - 0.0014i	0.0008 + 0.0014i
6	0	0	0
7	0.0001 - 0.0000i	-0.0000 - 0.0001i	-0.0000 + 0.0001i
8	0	0	0
9	-0.0000 - 0.0000i	-0.0000 - 0.0000i	-0.0000 - 0.0000i
10	0	0	0
11	0.0000 + 0.0000i	-0.0000 + 0.0000i	-0.0000 - 0.0000i
12	0	0	0
13	-0.0000 + 0.0000i	0.0000 + 0.0000i	0.0000 - 0.0000i
14	0	0	0
15	0.0000 + 0.0000i	0.0000 + 0.0000i	0.0000 + 0.0000i

4.9 Harmonic domain iterative solution

A devised network comprising of a nonlinear transformer, an ideal voltage source and transmission line has been analyzed using a unified iterative procedure. The main steps of iterative procedure are:

- a) First of all the required parameters have been gathered for iterative solution
- b) The data for different components has been collected and arrays are initialized. A separate programme is run for this purpose
- c) The admittance matrices for different linear network components have been constructed
- d) The functions for operational derivative have been defined. D is the operational matrix for derivation, its inverse is the operational matrix for integration
- e) Harmonic Norton equivalent has been built up for the iterative harmonic solution. Separate programmes are run for this purpose, also separate programmes are run to define self and mutual convolutions functions used
- f) A check for the convergence based on two successive iterations of harmonic current values is made
- g) Network nodal admittance and current matrices have been built up
- h) For nodal harmonic pivots greater than zero, the matrix has been partially inverted
- i) Finally, the nodal voltages at inverted harmonic nodes are determined

Shown in *Appendix II*, are the codes of functions used in MATLABTM for the calculation of harmonic voltage magnitudes.

4.10 Summary

Starting from the historic development in modelling of a transformer, the harmonic domain model for the magnetization branch of the transformer has been derived and presented in this chapter. The various non-linear effects found in the transformer magnetic core are outlined, with the emphasis being placed on core saturation because of its high impact on harmonic generation. The harmonic balance method is used as a frame of reference to assess the harmonic behaviour of the power transformer. Due to the fact that magnetic core saturation can be well presented by polynomial functions and that these are amenable to speedy harmonic evaluations using repeated convolution, then efficient algorithms have been developed.

The transformer's electric and magnetic circuits have been combined together to give a full harmonic electromagnetic representation. The transformer model is interfaced with the rest of the power network and is demonstrated through several examples which are solved using a Newton-type iterative technique. The model can be very helpful in harmonic domain analysis. Because of its simplicity in mathematical expressions, the model therefore has a special advantage over existing models.

4.11 References

- [1] E. Acha, J. Arrillaga, A. Medina, A. Semlyen; "General frame of reference for analysis of harmonic distortion in system with multiple transformer nonlinearities" IEE Proceedings, vol. 136, Pt. C, No. 5, 1989
- [2] M. S Nakhla; J. Vlach; "A piecewise harmonic balance technique for determination of the periodic response of nonlinear systems" IEEE, Transactions on circuits and systems, vol, CAS-23, no. 2, 1976
- [3] G. W. Stagg and A. H. El-Abiad; "Computer Methods in Power System Analysis" McGraw-Hill, London, 1968

- [4] M. S. Chen and W. E. Dillon; “Power System Modelling” IEEE Transactions on “Power Delivery”, vol. 62, no. 7, pp. 901-915, 1974
- [5] H. L. Nakra and T. H. Barton; “Three Phase Transformer Transients” IEEE PES winter meeting, pp. 1810-181, 1973
- [6] J. A. Rosales and F. L. Alvarado; “Nonlinear Frequency Dependant Transformer Model for Electro Magnetic Transient Studies in Power Systems” IEEE transactions on Power Apparatus and Systems, vol. PAS-101, no. 11, pp. 4281-4288, 1982
- [7] J. D. Green and A. C. Grass; “Nonlinear modelling of transformer”, IEEE Transactions on Industry Applications, vol. 24, pp. 434-438, 1988
- [8] A. Semlyen, E. Acha, J. Arrillaga; “Harmonic Norton equivalent for the magnetizing branch of a transformer” IEE Proceedings on Generation, Transmission and Distribution. Vol: 134, Iss: 2, pp- 162 – 169, 1987
- [9] A. Medina and J. Arrillaga; “Simulation of multilimb power transformers in the harmonic domain” IEE Proceedings on Generation, Transmission and Distribution. Vol: 139, Iss: 3, pp-269 – 276, 1992
- [10] A. Medina and J. Arrillaga; “GENERALISED MODELLING OF POWER TRANSFORMERS IN THE HARMONIC DOMAIN”, IEEE Transactions on Power Delivery. Vol: 7; Iss: 3, pp: 1458 - 1465 , 1992
- [11] Wu Dugui, Xu Zheng; “Harmonic Model of Power Transformer” IEEE, Power System Technology, Proceedings, vol. 2, pp. 1045-1049, 1998
- [12] S. R. Huang, S. C. Chung; B. N. Chen; Y. H. Chen; “ A harmonic model for nonlinearities of single-phase transformer with describing functions” IEEE, Transaction on Power Delivery, vol. 18, no. 3, 2003

- [13] J. Arrillaga, B. C. Smith, N. R. Watson and A. R. Wood; "Power System Harmonic Analysis: Wiley, 1997
- [14] A. Semlyen, E. Ach, J. Arrillaga and S. Mem; "Newton-type algorithms for the harmonic phasor analysis of nonlinear power circuits, in periodic steady state with special reference to magnetic non-linearities," IEEE Trans. Power Delivery, vol. 3, pp. 1090-1097, 1988
- [15] A. Medina, J. Arrillaga; "Generalized modelling of power transformer in harmonic domain", IEEE Trans. Power Delivery, vol. 7, issue 3, pp. 1458-1465, 1992
- [16] Task Force on Harmonics Modelling and Simulation, "Modelling and Simulation of the Propagation of Harmonics in Electric Power Networks, Part I: Concepts, Models and Simulation Techniques", IEEE Transactions on Power Delivery, vol . 11, no. 1, pp, 452-465, 1996
- [17] A. Damnjanovic and G. M. J. Parsley; "Modelling of transformer nonlinearities taking hysteresis into account with consuming function and harmonic balance method" IEEE AFRICON, pp. 741-744, 2004
- [18] Wiechowski, W.; Bak-Jensen, B.; Bak, C.L.; Lykkegaard, J.; Poller, M.; 'Transformer Core Nonlinearities Modeled in Harmonic Domain' Transmission and Distribution Conference and Exhibition: Asia and Pacific, 2005 IEEE/PES, Page(s):1 – 8, 2005
- [19] Chang, G.; Hatziadoniu, C.; Xu, W.; Ribeiro, P.; Burch, R.; Grady, W.M.; Halpin, M.; Liu, Y.; Ranade, S.; Ruthman, D.; Watson, N.; Ortmeyer, T.; Wikston, J.; Medina, A.; Testa, A.; Gardinier, R.; Dinavahi, V.; Acram, F.; Lehn, P.; "Modelling devices with nonlinear voltage-current characteristics for harmonic studies", IEEE, Transactions on Power Delivery, Vol: 19 , Iss: 4, pp: 1802 – 1811, 2004

- [20] Holmberg, P. ; Bergqvist, A. ; Engdahl, G. ; “Modelling eddy currents and hysteresis in a transformer laminate”, IEEE Transactions on Magnetics, Volume : 33 , no. 2, pp. 1306 - 1309, 1997
- [21] J. G. Santasmases, J. Ayala and A. H. Cachero, "Analytical Approximation of Dynamic Hysteresis Loop and its Application to a Series Ferroresonant Circuit," PROCEEDINGS OF THE INSTITUTION OF ELECTRICAL ENGINEERS, vol. 117, no. 1, pp, 234-240, 1970
- [22] I. A. Wright and K. Morsztyn, "An Improved Method of Simulating the Transient Performance of Power Systems Transformers, "INTERNATIONAL JOURNAL OF ELECTRICAL ENGINEERING EDUCATION, vol. 6, pp. 499-516, 1969
- [23] M. D. Abrams and D. H. Gillott, "Numerical Analysis of Hysteresis and Eddy-Current Losses in Solid Cylindrical Rods of No. 1010 Steel," IEEE TRANSACTIONS ON POWER APPARATUS AND SYSTEMS, vol. PAS-86, no. 9, pp. 1077-1083, 1967
- [24] Chandrasena, W.; McLaren, P.G.; Annakkage, U.D.; Jayasinghe, R.P.; Dirks, E.; “Simulation of eddy current effects in transformers”, IEEE CCECE. Canadian Conference on “Electrical and Computer Engineering”, vol.1, pp. 122-126, 2002
- [25] De Leon, F.; Semlyen, A.; Time domain modeling of eddy current effects for transformer transients. IEEE Transactions on “Power Delivery”, vol.8, iss. 1, pp. 271-280, 1993
- [26] Sy-Ruen Huang; Chung, S.C.; Bing-Nan Chen; Yi-Hung Chen; “A harmonic model for the nonlinearities of single-phase transformer with describing functions” . IEEE Transactions on “Power Delivery”, vol. 18, no. 3, pp. 815-819, 2003

- [27] Damnjanovic, A.; Parsley, G.M.J.; Modelling transformer nonlinearities taking hysteresis into account with consuming function and the harmonic balance method. . IEEE, 7th African Conference in Africa”, vol. 02, pp. 741-744, 2004
- [28] Acha, E; Madrigal M.; ‘Power Systems Harmonics computer modeling and analysis’ John Wiley, 2001
- [29] Damnjanovic, A.; Parsley, G.M.J.; Modelling transformer nonlinearities taking hysteresis into account with consuming function and the harmonic balance method. . IEEE, 7th African Conference in Africa”, vol. 02, pp. 741-744, 2004
- [30] Z. Emin, B.A.T. Al Zahawi, D.W. Auckland and Y.K. Tong; “Ferroresonance in Electromagnetic Voltage Transformers: A Study Based on Nonlinear Dynamics”, IEE , Generation Transmission and Distrib, vol. 144, no. 4, pp. 383-387, 1997

5. Harmonic Domain Modelling of Synchronous Generator

5.1 Introduction

The modelling of a synchronous generator starts with the development of the synchronous machine's dynamic model, which has been known for more than seventy years. A three-phase, wound field synchronous generator has three identical armature windings symmetrically distributed around the air-gap. There may also be one or more damper windings present in addition to a field winding. Normally the armature windings are placed on the stator and the field and the damper windings on the rotor, however there are cases when armature windings are placed on the rotor and field winding on the stator. This does not affect the machine modeling approach, since only relative motion between the stator and rotor windings is important.

A synchronous machine can be described by a system of ' $n+1$ ' equations, n of which are electrical and one of which is mechanical. The number n of electrical equations is equal to the number of independent electrical variables necessary to describe the machine. These variables can be either currents or flux linkages. Electrical equations are obtained by writing Kirchhoff's voltage law for every winding, i.e. by equating the voltage at the winding's terminal to the sum of the resistive and inductive voltage drops across the winding [1]. Notice that the damper windings, if present, are always short circuited. Therefore, their terminal voltage is equal to zero.

In order to correctly calculate the inductive voltage drop across a winding, the total magnetic flux linked with the winding needs to be evaluated. This is achieved by means of an inductance matrix which relates all the windings' flux linkages to all the windings' currents. When this is done for a salient-pole synchronous machine, an inductance matrix dependent on the rotor position is obtained. This dependence is due to the magnetic asymmetry of the rotor: because of the way the rotor of a salient pole machine is shaped, there exists a preferable magnetic direction. This direction coincides with the direction of the flux produced by the field winding and is defined as the machine's d axis. The machine's q axis is placed at 90 electrical degrees (in a

counterclockwise direction) with respect to the machine's d axis. Then, the rotor position can be expressed by means of an angle, between the magnetic axis of the armature's phase a and the rotor's q axis.

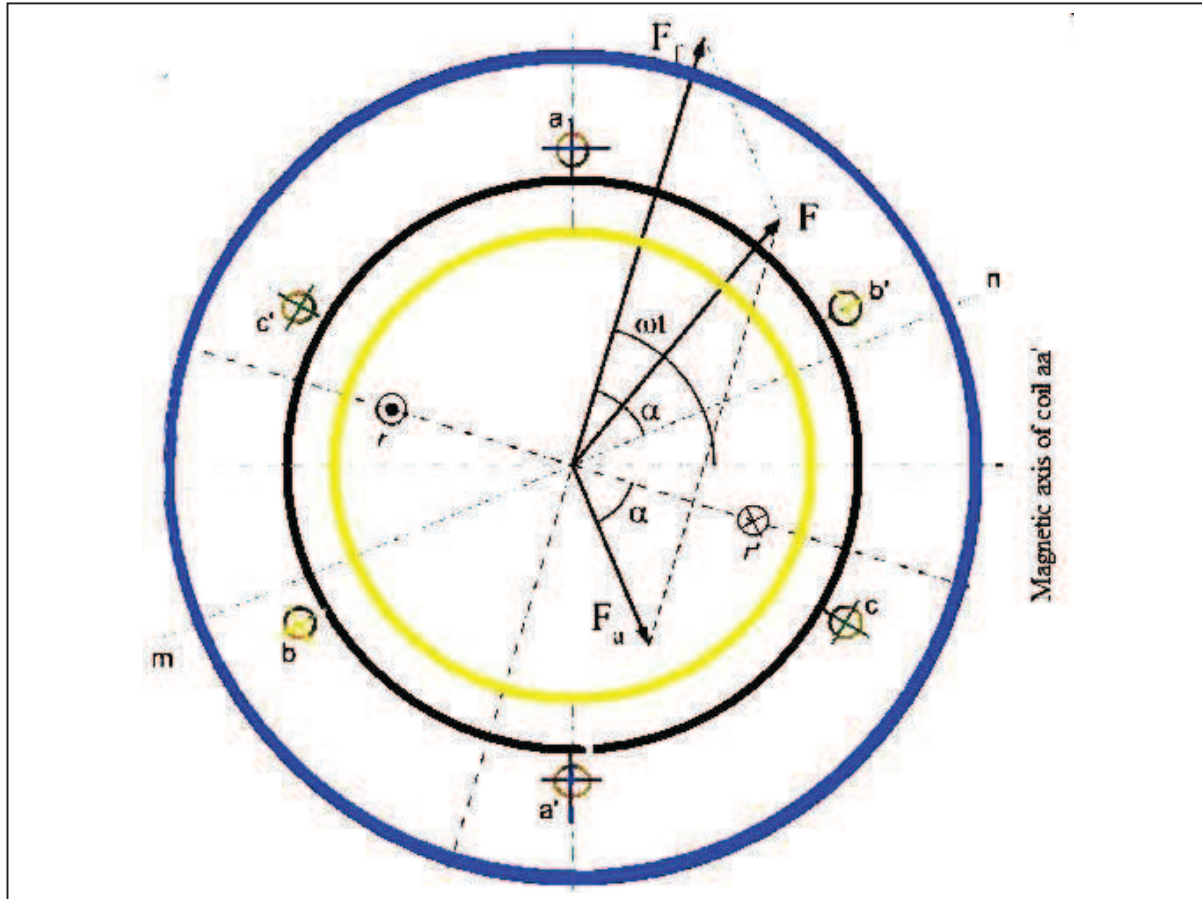


Fig. 5.1: Cross-section of a simple synchronous generator

Dependence of the inductance matrix on the rotor position represents the main difficulty in modeling the synchronous machine. A solution to this problem is to change the reference system, or frame, in which the machine's electrical and magnetic variables are expressed. In an abc reference frame, variables are expressed as they can actually be measured in the machine, but the machine parameters are time variant. In a dq , reference frame, all variables are expressed in a form in which a hypothetical observer placed on the rotor would measure them. Transformation from the abc to the dq reference frame is given by the following transformation matrix:

$$\mathbf{T} = \sqrt{2/3} \begin{bmatrix} \sin \theta & \sin(\theta - \frac{2\pi}{3}) & \sin(\theta + \frac{2\pi}{3}) \\ \cos \theta & \cos(\theta - \frac{2\pi}{3}) & \cos(\theta + \frac{2\pi}{3}) \end{bmatrix} \quad (5.1)$$

Inverse transformation (from the dq to the abc reference frame) is then given by:

$$\mathbf{T}^{-1} = \sqrt{2/3} \begin{bmatrix} \sin \theta & \cos \theta \\ \sin(\theta - \frac{2\pi}{3}) & \cos(\theta - \frac{2\pi}{3}) \\ \sin(\theta + \frac{2\pi}{3}) & \cos(\theta + \frac{2\pi}{3}) \end{bmatrix} \quad (5.2)$$

Any set of three-phase variables f_a , f_b and f_c expressed in the abc reference frame can be transformed in dq reference frame variables f_d and f_q by multiplying them by \mathbf{T} :

$$\begin{bmatrix} f_d \\ f_q \end{bmatrix} = \mathbf{T} \begin{bmatrix} f_a \\ f_b \\ f_c \end{bmatrix} \quad (5.3)$$

Vice versa:

$$\begin{bmatrix} f_a \\ f_b \\ f_c \end{bmatrix} = \mathbf{T}_{inv} \begin{bmatrix} f_d \\ f_q \end{bmatrix} \quad (5.4)$$

Notice that the transformation of variables preserve total system power. In every time instant, power in abc reference frame is equal to power in dq reference frame. Regarding zero variables which generally must be taken into account when variables are transformed into rotor reference frame; for a Y-connected generator without neutral connection, zero variables are always equal to zero. When the machine's electrical equations are transformed from the abc to the dq reference frame, they assume the following form [1, 2]:

For damper

$$0 = R_{kd} i_{kd} - L_{md} \frac{d}{dt} i_d + L_{md} \frac{d}{dt} i_{fd} + (L_{lkd} + L_{md}) \frac{d}{dt} i_{kd} \quad (5.5)$$

$$0 = R_{kq} i_{kq} - L_{mq} \frac{d}{dt} i_q + (L_{lkq} + L_{mq}) \frac{d}{dt} i_{kq} \quad (5.6)$$

For field

$$V_{fd} = R_{fd}i_{fd} - L_{md}\frac{d}{dt}i_d + (L_{lfd} + L_{md})\frac{d}{dt}i_{fd} + L_{md}\frac{d}{dt}i_{kd} \quad (5.7)$$

For armature

$$V_d = -R_s i_d - \omega \lambda_q - (L_{ls} + L_{md})\frac{d}{dt}i_d + L_{md}\frac{d}{dt}i_{fd} + L_{md}\frac{d}{dt}i_{kd} \quad (5.8)$$

$$V_q = -R_s i_q - \omega \lambda_d - (L_{ls} + L_{mq})\frac{d}{dt}i_q + L_{mq}\frac{d}{dt}i_{kq} \quad (5.9)$$

Where $\lambda_d = -(L_{ls} + L_{md})i_d + L_{md}(i_{fd} + i_{kd}) = \text{flux linkage} \quad (5.10)$

and $\lambda_q = -(L_{ls} + L_{mq})i_q + L_{mq}i_{kq} \quad (5.11)$

The equivalent circuits are similar to a transformer equivalent circuit. In each of them, several windings characterized by some resistance and leakage inductance, are coupled through a mutual coupling inductance.

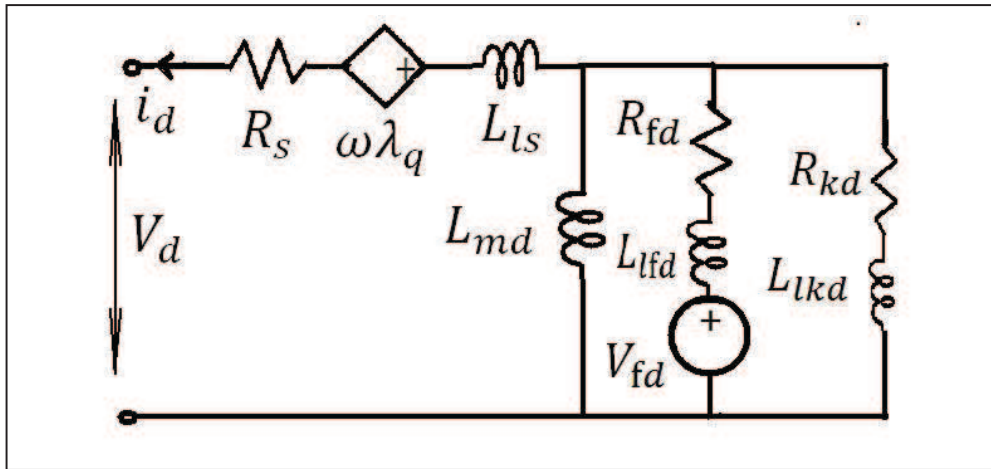


Fig. 5.2: Synchronous generator's equivalent circuit in rotor frame of reference

The difference, compared to the transformer is that, while a transformer's equivalent circuit is an ac circuit, here, when the generator is operating in sinusoidal steady state, all voltages, currents and flux linkages are dc. If the machine has no damper windings, the damper windings branches can be removed from the equivalent circuit. The turns ratio between the rotor and armature is taken into account when the actual values of rotor are of interest.

The mechanical variable in electrical equivalent circuit is represented by rotor speed, and the mechanical equation of the system must be taken into account for a complete model.

The equation corresponding to the equivalent circuit representation also depend upon flux linkages like above shown equations however the determination of parameter values for the model elements, e .g. resistances and inductances becomes difficult. Traditionally open and short-circuit tests of the machine are performed to obtain these parameters. The machine data can be got from machine manufacturers.

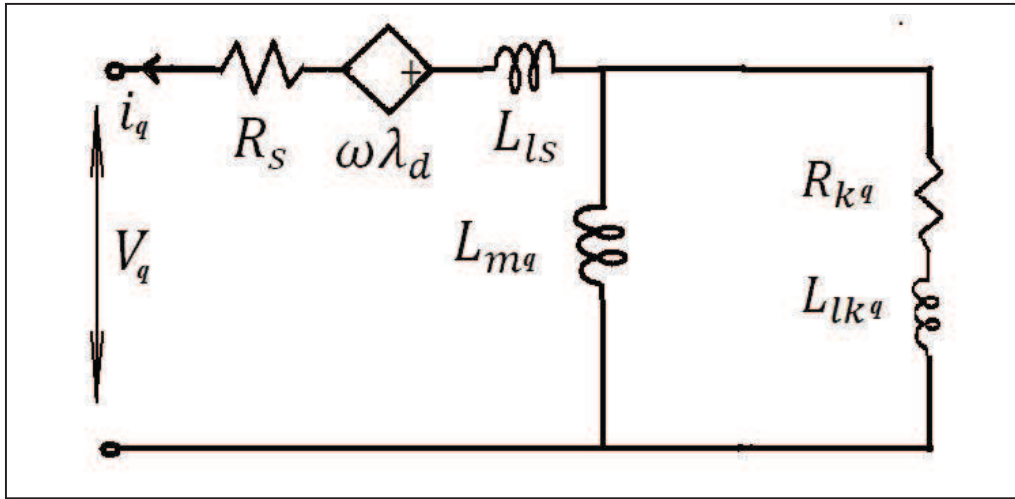


Fig. 5.3: Synchronous generator's equivalent circuit in rotor frame of reference without damper winding

Before the steady state is reached, rotor electrical speed is different from the terminal voltage's angular frequency during which the synchronous generator represents harmonic currents. The supply to an unbalanced, three phase load may also cause harmonic currents in the stator winding. This phenomenon is known as the *frequency conversion effect* [3]. Some harmonic currents are also caused by the non-linear characteristic effect [3, 4] due to magnetic saturation effect.

5.2 Synchronous generator under harmonic conditions in the Fourier harmonic domain

During transient or steady state operation of synchronous generator, the asymmetry of the winding distribution and structure of rotor (in addition to the influence of a set of unbalanced or distorted stator currents) creates *mmfs* in rotor which rotate relative to each other. This process induces unbalanced voltages which result in further stator current distortion. This process is quite frequent at harmonic frequencies.

With only linear loads connected to machine, the currents and voltages of higher order being sequentially generated will be progressively smaller since in this case the rotor reaction field effectively opposes the presence of high frequency flux components. Nonlinear effects or harmonic magnification on the eternal system requires a harmonic balance between load and rotor with no necessarily negligible higher order currents and voltages. In a cylindrical rotor machine, a negative sequence current of order h injected to the stator creates a flux of order $h+1$ in the rotor. This rotor flux induces a negative sequence voltage of order h . In case of a positive sequence h order harmonic current in the stator the rotor flux is of the order $h-1$ which results in positive sequence voltage of the order h .

In a salient pole machine, a negative sequence current of the order h produces two counter rotating fluxes of order $h+1$ in the rotor. One of these fluxes induces a negative sequence voltage of the order h while the other one induces negative sequence voltage of the order $h+2$ in the stator. A positive sequence current of the order h in this type of machine produces two counter rotating fluxes of order $h-1$ in the rotor. One of these fluxes induces a positive sequence voltage of the order h while the other one induces positive sequence voltage of the order $h+2$ in the stator. This process in the stator is similar for the $h-2$ or higher harmonic orders. In general it can be concluded that in phase coordinates any h order harmonic current in the stator produces harmonic voltages of the order $h-2$, h and $h+2$. Presented here is generator's periodic behaviour derived basically from the quantities in dq axes using well known variables and notations [5, 9].

5.2.1 Machine's Fourier harmonic admittance matrix model in $dq0$ axis

The synchronous machine's periodic behaviour is presented here for a cross coupled and multi harmonic three phase model. The set of differential equations describing the nonlinear machine's behaviour is given below

$$-v_d = Ri_d + p(L_d i_d + M_{df} i_f + M_{ds} i_s) - \omega(L_q i_q + M_{qt} i_t) \quad (5.13)$$

$$-v_q = Ri_q + p(L_q i_q + M_{qt} i_t) + \omega(L_d i_d + M_{df} i_f + M_{ds} i_s) \quad (5.14)$$

$$v_f = R_f i_f + p(L_f i_f + M_{df} i_d + M_{fs} i_s) = 0 \quad (5.15)$$

$$v_s = R_s i_s + p(L_s i_s + M_{ds} i_d + M_{fs} i_f) = 0 \quad (5.16)$$

$$v_t = R_t i_t + p(L_t i_t + M_{qt} i_q) = 0 \quad (5.17)$$

The variables s and t represent a closed damper winding in d and q axes respectively. It is assumed that if the applied field voltage is constant no harmonics are produced in field voltage [10] therefore v_f is set to zero. At a particular frequency h , the required variables of equation set (5.13-17) is described in phasor form [11] as:

$$\omega_h = \text{Re}\{W_h e^{j\omega h t}\} \quad (5.18)$$

where phasor W_h is given by the equation:

$$W_h = W'_h + jW''_h \quad (5.19)$$

In harmonic domain as:

$$p = j\omega h \quad (5.20)$$

Writing equation set (5.13-17) in phasor form and solving for dq quantities yields:

$$V_{dq} = \left\{ [Z_{dq}] - [Z_{dq-fst}] [Z_{fst}]^{-1} [Z_{fst-dq}] \right\} I_{dq} \quad (5.21)$$

For harmonic h equation (5.21) can be written as:

$$I_{dq0h} = [Y_{dq0h}]V_{dq0h} \quad (5.22)$$

where

$$Y_{dq0h} = [G + iB] = \left[[Z_{dq}] - [Z_{dqfst}][Z_{fst}]^{-1}[Z_{fst-dq}] \right]^{-1} \quad (5.23)$$

known as Fourier harmonic admittance matrix in $dq0$ axis for harmonic analyses of the machine. G and B respectively represent real and imaginary parts of the matrix. The **Matlab** functions used to obtain Y_{dq0} in Fourier harmonic domain are given in *Appendix III*.

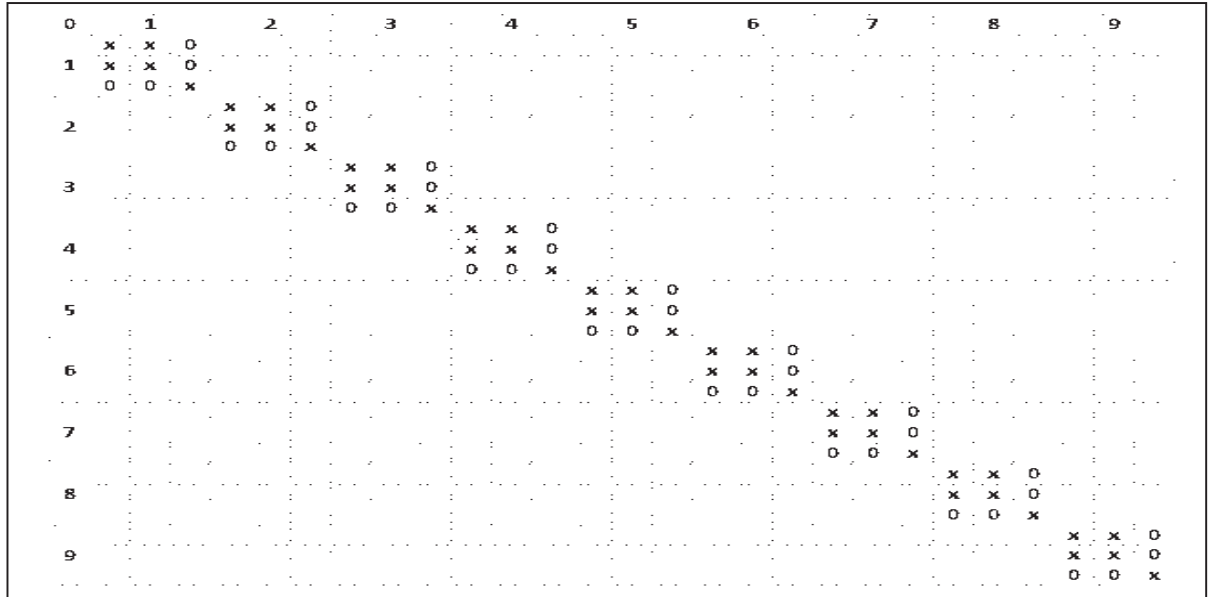


Fig. 5.4 (a): The shape of admittance matrix Y_{dq0} (simulation result)

Fig. 5.4 (a); shows a zoomed view of the admittance matrix Y_{dq0} produced by the code in *Appendix III*. The cross here represent different complex values of the form $a+ib$, where as the spikes in the surface plot of Fig. 5.4 (b), indicate their magnitude. The relationship between variables is represented by the equation (5.22). When solved for unknown variables, sparsity based algorithms are used to optimize the execution time and to minimize the memory requirement, as most of the operations take place only between non-zero elements of the matrices and vectors in equation 5.22. Figures such as Fig. 5.4, not only provide useful

information about the sparsity of the matrices but also indicate if there is any cross coupling. In the case of cross coupling, a zero is replaced by a non-zero.

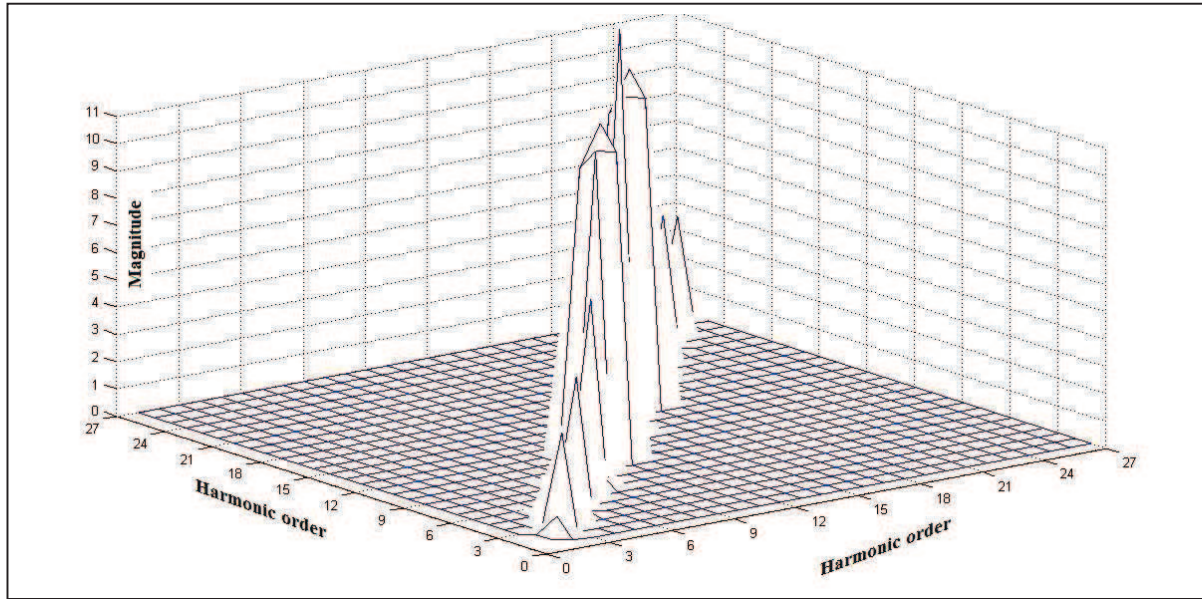


Fig. 5.4 (b): Y_{dq0} , Surface plot

5.2.2 Machine's Fourier harmonic admittance matrix model in $\alpha\beta\gamma$ axis

The relationship between space-stationary, orthogonal dq axis and a three phase winding is determined depending upon whether this winding is stationary or rotating. To account for both conditions a winding transformation has been defined [9] between three phase and two phase windings such that the phase separation between the winding axes remains constant irrespective of winding rotation where α axis is fixed with phase a , while β axis is ninety degrees leading in the direction of rotation. If the three phase winding is stationary $\alpha\beta$ and dq axes are presumed coincident. If the winding is rotating, a second transformation between rotating two-phase $\alpha\beta$ and stationary dq winding is required. The transformation between $\alpha\beta$ and dq components of voltage may be determined with the help of relationships given by:

$$\begin{bmatrix} V_{\alpha_h} \\ V_{\beta_h} \end{bmatrix} = \begin{bmatrix} \cos \omega t & -\sin \omega t \\ \sin \omega t & \cos \omega t \end{bmatrix} \begin{bmatrix} V_{d_h} \\ V_{q_h} \end{bmatrix} \quad (5.24)$$

Phasors V_{d_h} and V_{q_h} can be expressed in trigonometric form of equation (5.18) as:

$$V_{d_h} = V'_{d_h} \cos h\omega t - V''_{d_h} \sin h\omega t \quad (5.25)$$

$$V_{q_h} = V'_{q_h} \cos h\omega t - V''_{q_h} \sin h\omega t \quad (5.26)$$

where

$$\cos h\omega t = \frac{1}{2}(e^{jh\omega t} + e^{-jh\omega t}) \quad (5.27)$$

$$\sin h\omega t = \frac{1}{2j}(e^{jh\omega t} - e^{-jh\omega t}) \quad (5.28)$$

$$e^{jh\omega t} = \cos h\omega t + j \sin h\omega t \quad (5.29)$$

$$e^{-jh\omega t} = \cos h\omega t - j \sin h\omega t \quad (5.30)$$

Similar expressions apply for $\cos \omega t$ and $\sin \omega t$. Respective substitution of equation set (5.25-30) into equation (5.24) and after some tedious algebra gives:

$$V_{\alpha_{h-1}}^h = \frac{1}{2}(V_{d_h} - jV_{q_h}) \quad (5.31)$$

$$V_{\alpha_{h+1}}^h = \frac{1}{2}(V_{d_h} + jV_{q_h}) \quad (5.32)$$

$$V_{\beta_{h-1}}^h = \frac{1}{2}(jV_{d_h} + V_{q_h}) \quad (5.33)$$

$$V_{\beta_{h+1}}^h = \frac{1}{2}(-jV_{d_h} + V_{q_h}) \quad (5.34)$$

The transformation between $\alpha\beta$ and dq quantities can be obtained by assembling together the equation set (5.31-34). In compact form this set of equations can be written as:

$$[V_{\alpha\beta}] = [C] [V_{dq}] \quad (5.35)$$

Similarly

$$[I_{\alpha\beta}] = [C][I_{dq}] \quad (5.36)$$

For a practical harmonic spectrum from $-n$ to $+n$, where n being the number of harmonics to be analyzed, $[V_{\alpha\beta}]$, $[C]$ and $[V_{dq}]$, have the form:

$$[V_{\alpha\beta}] = [V_{\alpha_{-n}}, V_{\beta_{-n}}, \dots, V_{\alpha_{-1}}, V_{\beta_{-1}}, V_{\alpha_0}, V_{\beta_0}, V_{\alpha_1}, V_{\beta_1}, \dots, V_{\alpha_n}, V_{\beta_n}]^T \quad (5.37)$$

$$[V_{dq}] = [V_{d_{-n}}, V_{q_{-n}}, \dots, V_{d_{-1}}, V_{q_{-1}}, V_{d_0}, V_{q_0}, V_{d_1}, V_{q_1}, \dots, V_{d_n}, V_{q_n}]^T \quad (5.38)$$

$$[C] = \frac{1}{2} \begin{bmatrix} \ddots & & & & & & & & \\ & N^* & M^* & & & & & & \\ & & N^* & M^* & & & & & \\ & & & N^* & 2M^* & & & & \\ & & & & N^* & 2M & N & & \\ & & & & & 2M & M & N & \\ & & & & & & M & M & N \\ & & & & & & & & \ddots \end{bmatrix} \quad (5.39)$$

where

$$M = N^* = \begin{bmatrix} 1 & j \\ -j & 1 \end{bmatrix} \quad (5.40)$$

To derive $[Y_{\alpha\beta}]$ the general matrix equation is first written for all harmonics as:

$$[I_{dq}] = [Y_{dq}][V_{dq}] \quad (5.41)$$

Variables V_{dq} and I_{dq} are determined by respective inverse transformation of both the equations in equation set (5.35-36) as:

$$V_{dq} = [C]^*[V_{\alpha\beta}] \quad (5.42)$$

$$\text{and} \quad I_{dq} = [C]^*[I_{\alpha\beta}] \quad (5.43)$$

Substituting equation set (5.42-43) in equation (5.41) gives:

$$[I_{\alpha\beta}] = [Y_{\alpha\beta}][V_{\alpha\beta}] \quad (5.44)$$

where

$$[Y_{\alpha\beta}] = [C][Y_{dq}][C]^* \quad (5.45)$$

Since conversion matrix has the non square form, a direct admittance transformation from two phase $\alpha\beta$ frame of reference to a three phase reference is not possible, thus precluding inversion. This problem is solved by augmenting $[Y_{\alpha\beta}]$ with a zero sequence diagonal matrix of the order equal to the harmonic spectrum analyzed and adding to the transformation matrix defined as T_h for a particular harmonic h , a third row of equal numerical constants. Hence the admittance matrix becomes:

$$[Y_{\alpha\beta\gamma}] = \begin{bmatrix} Y_{\alpha\beta} & 0 \\ 0 & Y_\gamma \end{bmatrix} \quad (5.46)$$

The **Matlab** function used to compute $Y_{\alpha\beta\gamma}$ in Fourier harmonic domain is given in *Appendix III* and the structure of the matrix is shown in Fig. 5.5.

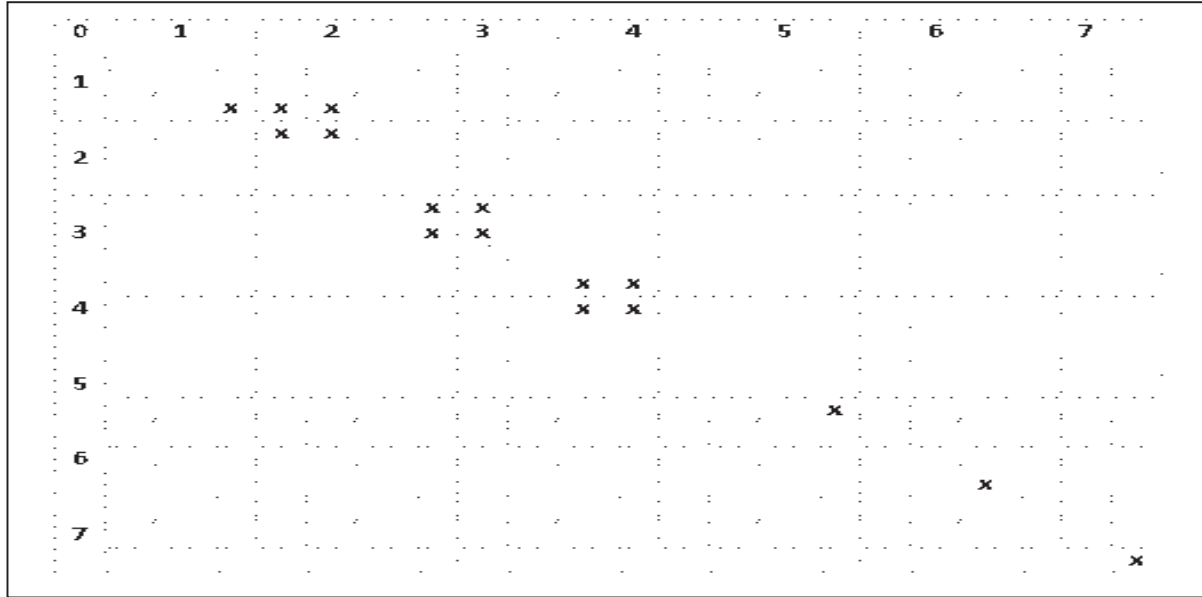


Fig. 5.5 (a): The shape of admittance matrix $Y_{\alpha\beta\gamma}$ (simulation result)

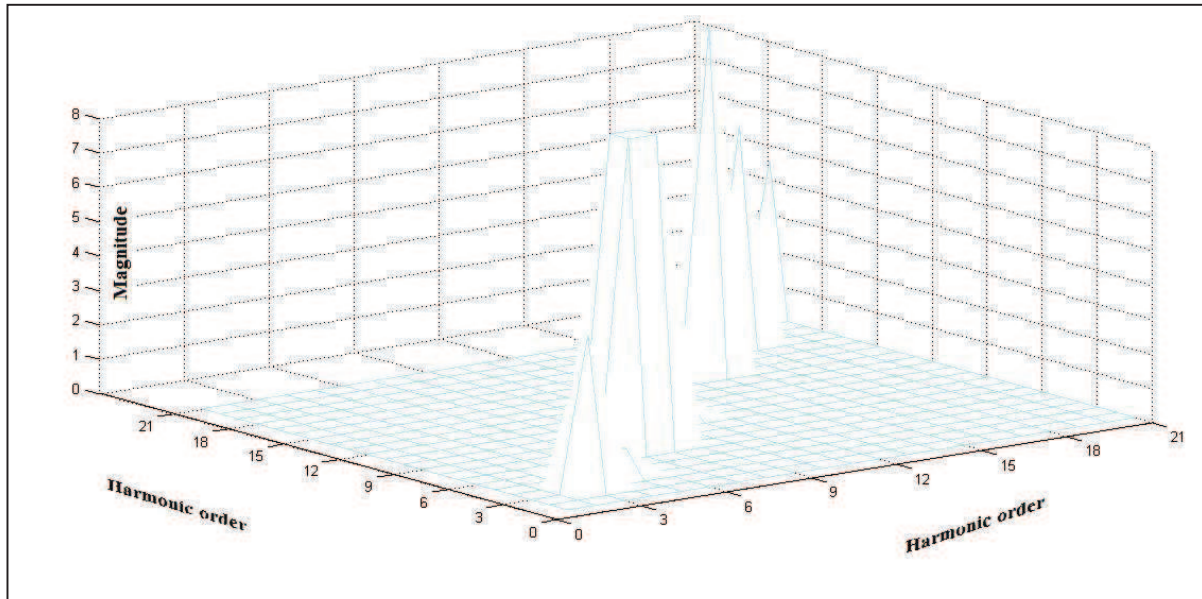


Fig. 5.5 (b): $Y_{\alpha\beta\gamma}$, surface plot

A cross in Fig. 5.5 (a), represents a complex number of the form $a + ib$, where as the horizontal and vertical numbers indicate the index of two dimensional array. All the remaining entries of the admittance matrix are zero.

5.2.3 Machine's Fourier harmonic admittance matrix model in *abc* axis

As mentioned in the previous section with an incorporation of zero sequence diagonal matrix of the order equal to the harmonic spectrum under analysis, the following relation can be established to perform $\alpha\beta\gamma$ to abc transformation for any harmonic h :

$$V_{\alpha\beta\gamma_h} = [T_t]V_{abc_h} \quad (5.47)$$

$$I_{\alpha\beta\gamma_h} = [T_t]I_{abc_h} \quad (5.48)$$

where

$$[T_t] = \begin{bmatrix} 1 & -1/2 & -1/2 \\ 0 & \sqrt{3}/2 & -\sqrt{3}/2 \\ 1/3 & 1/3 & 1/3 \end{bmatrix} \quad (5.49)$$

Equation (5.44) can be written in $\alpha\beta\gamma$ components as

$$I_{\alpha\beta\gamma} = [Y_{\alpha\beta\gamma}]V_{\alpha\beta\gamma} \quad (5.50)$$

Substituting equation (5.50) into equation set (5.47-48) gives:

$$I_{abc} = [Y_{abc}]V_{abc} \quad (5.51)$$

where

$$[Y_{abc}] = [T]^{-1}[Y_{\alpha\beta\gamma}][T] \quad (5.52)$$

is machines admittance matrix in Fourier harmonic domain.

The **Matlab** code used to compute Y_{abc} in Fourier harmonic domain is also given in *Appendix III* and the structure of the matrix is shown in Fig. 5.6.

The structure of matrix Y_{abc} , will change with cross coupling between even and odd harmonics. However, the even harmonics are usually caused by hysteresis effect which is not taken into account here. For single valued symmetrical magnetising curve only odd harmonics will be produced, also the cross coupling between these harmonics will take place.

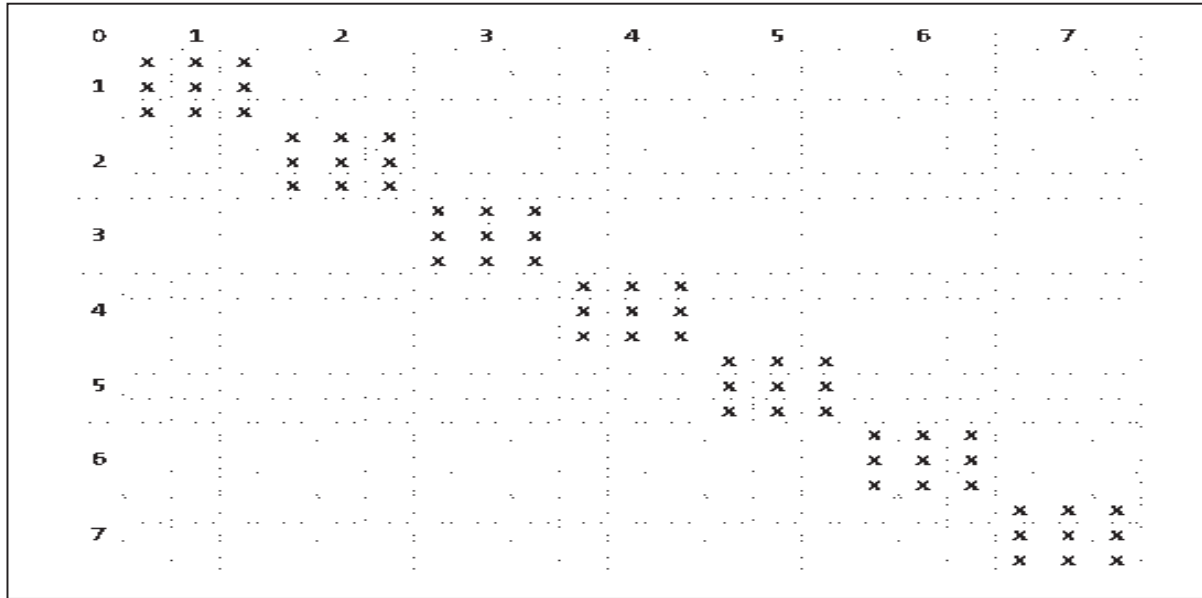


Fig. 5.6 (a): Structure of admittance matrix Y_{abc} (simulation result)

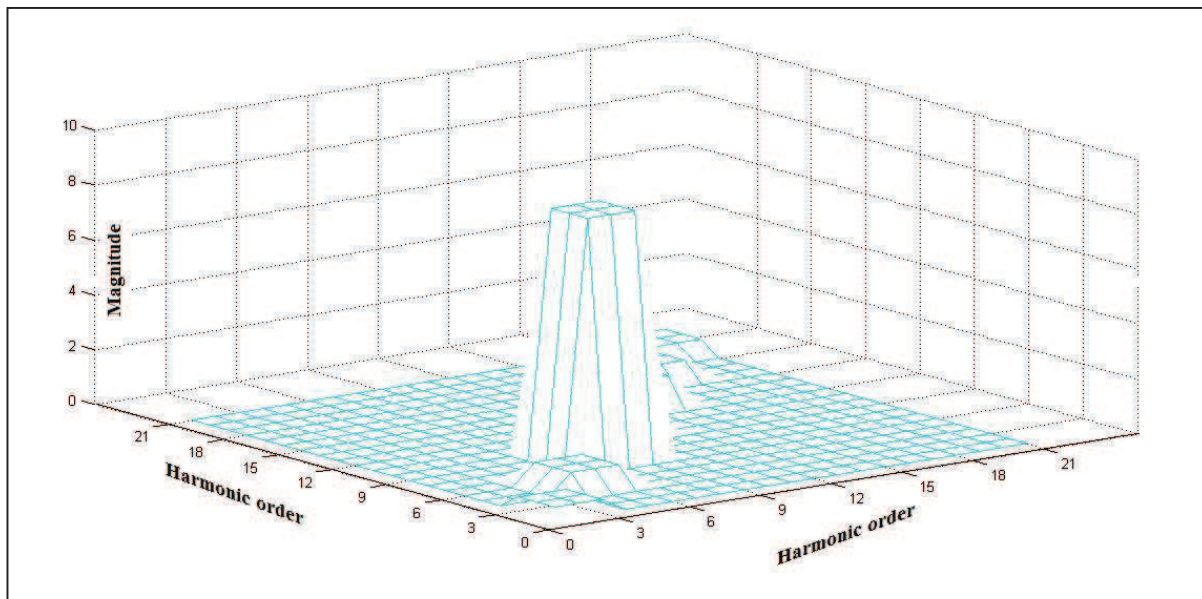


Fig. 5.6 (b): Y_{abc} , surface plot

Similar to the previously mentioned case, cross in Fig. 5.6 (a), represents a complex number of the form $a + ib$, showing that Y_{abc} , is also a diagonal matrix and the order of the matrix depends upon the harmonic order.

5.3 Synchronous generator's harmonic equivalents

Several models have been developed for the representation of magnetic saturation in synchronous machine based on saturation along either d axis or q axis. A model based on the iterative modification of self and mutual inductances on dq axis has been presented [12]. Because of lack of information about saturation in q axis, the common practice is to correct for the saturation in the self-inductance on d axis and neglect this effect on q axis [12, 13].

For large synchronous machines the saturation of direct and quadrature axis is quite different [14, 15]. In a comparison study on different approaches towards the simulation of saturation in synchronous machine, the importance of modelling saturation along q axis is emphasised [16]. More is that the saturation in any one of the d or q axis affects the other [17]. This phenomenon is referred to as cross-magnetising effect [18, 19]. Later it was concluded that saturation depends upon total mmf rather than depending upon separate contribution of d and q axes [20].

5.3.1 Machine's Norton's harmonic equivalent

A method to model saturation is to obtain Norton harmonic equivalent through a linearization process in harmonic domain. The harmonic equivalent at the end of each iteration in the iterative process with the rest of dependent variables. The stator magnetic and electrical parts are presented by the state equations describing the non-linear characteristics of an ideal inductor, that is:

$$v = p\varphi \quad (5.53)$$

$$i = f(\varphi) \quad (5.54)$$

In the harmonic domain the above two equations are respectively linearized as:

$$\Delta V = \{jh\omega\}\Delta\varphi \quad (5.55)$$

and

$$\Delta I = F_g\Delta\varphi \quad (5.56)$$

where

$$\Delta I = I - I_{bg} \quad \text{and} \quad \Delta V = V - V_{bg} \quad (5.57-58)$$

In equation set (5.57-58), I_{bg} is the base current obtained from the magnetising characteristics of the generator where as V_{bg} is the base voltage at generators terminals. Solving the equation set (5.56-58) gives a solution for current which may be generalized in matrix form as:

$$I = [H_g]V + I_N \quad (5.59)$$

Equation (5.59) represents the Norton's harmonic equivalent of the generator stator combining together its electrical parts where I_N and H_g are respectively Norton harmonic current vector and Norton harmonic admittance matrix given by:

$$I_N = I_{bg} - [H_g]V_{bg} \quad (5.60)$$

$$[H_g] = [F_g](j\omega h)^{-1} \quad (5.61)$$

Fig. 5.7 shows the Norton's equivalent representation of synchronous generator in open circuit.

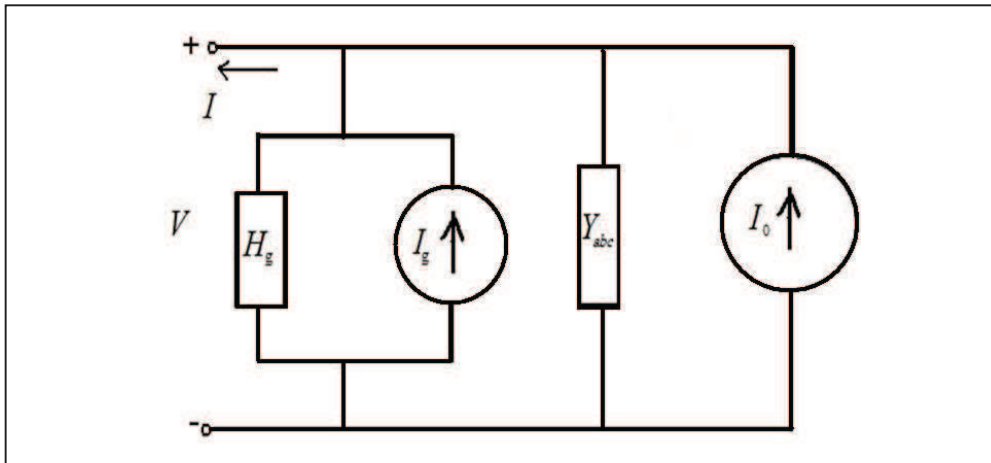


Fig. 5.7: The Norton's harmonic equivalent of synchronous generator.

5.3.2 Machine's Thevni's harmonic equivalent

The synchronous generator can also be represented as Thevni's equivalent. Fig. 5.8 shows the Thevni's equivalent of synchronous generator under an open circuit condition, where

$$Y_{abc}(V_1 - V_2) = I_1 \quad (5.62)$$

$$Y_{abc}(V_1 - V_2) + H_g V_2 = I_2 \quad (5.63)$$

or, arranging these two equations in matrix form

$$\begin{bmatrix} Y_{abc} & -Y_{abc} \\ -Y_{abc} & (Y_{abc} + H_g) \end{bmatrix} \begin{bmatrix} V_1 \\ V_2 \end{bmatrix} = \begin{bmatrix} I_1 \\ I_2 \end{bmatrix} \quad (5.64)$$

If a load having admittance Y_l is connected at the terminals of the generator, the equation (5.64) becomes

$$\begin{bmatrix} Y_{abc} & -Y_{abc} \\ -Y_{abc} & (Y_{abc} + H_g + Y_l) \end{bmatrix} \begin{bmatrix} V_1 \\ V_2 \end{bmatrix} = \begin{bmatrix} I_1 \\ I_2 \end{bmatrix} \quad (5.65)$$

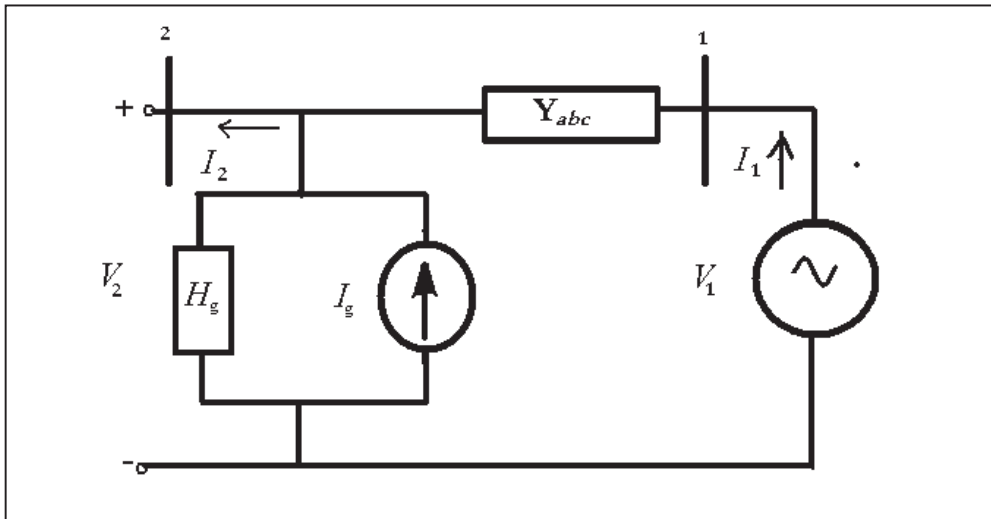


Fig. 5.8: The Thevenin's harmonic equivalent of synchronous generator.

5.4 Synchronous generator under harmonic conditions in the Hartley harmonic domain

With the generator based on Park's equations, waveforms have been analyzed using electromagnetic transient programs (EMTP) and EMTDC [21-25]. Different methods to estimate machine's parameter have been studied by the researchers [26-34]. As stated above there are two main reasons for which the synchronous generators have the harmonics: the frequency conversion effect and the magnetic saturation. The voltages for rotor and stator of a synchronous machine can be given by the following equation

$$v = Ri + \frac{d}{dt}\varphi \quad (5.66)$$

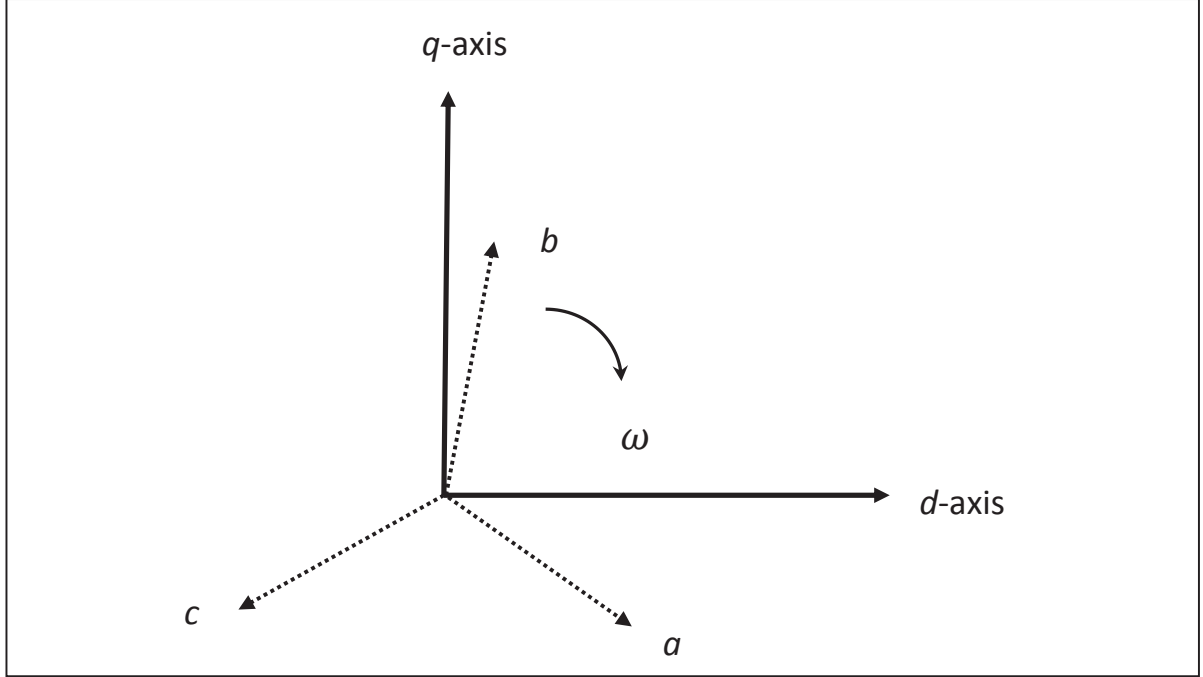


Fig. 5.9: Machine's *abc* and *dq0* axes

5.4.1 Machine's Hartley harmonic admittance matrix model in *dq0* axis

The instantaneous voltage of synchronous generator in terms of flux and current is given by equation (5.66), where R and L are machine's resistance and inductance matrices respectively where as $\varphi = Li$. Equation (5.66) can be expanded into stator and rotor subset equations as:

$$\begin{bmatrix} v_s \\ v_r \end{bmatrix} = \begin{bmatrix} R_s & 0 \\ 0 & R_r \end{bmatrix} \begin{bmatrix} i_s \\ i_r \end{bmatrix} + \omega_r \begin{bmatrix} G_{ss} & G_{sr} \\ G_{rs} & 0 \end{bmatrix} \begin{bmatrix} i_s \\ i_r \end{bmatrix} + \begin{bmatrix} L_{ss} & L_{sr} \\ L_{rs} & L_{rr} \end{bmatrix} \begin{bmatrix} pi_s \\ pi_r \end{bmatrix} \quad (5.67)$$

where $p = d/dt$, $G = dL/d\theta$ and $\omega_r = d\theta/dt$, ω_r being the angular velocity while θ is the angular distance. In *dq* axis equation (5.67) may be expressed as [35-37]:

$$\begin{bmatrix} v_d \\ v_q \\ v_0 \\ v_f \\ v_s \\ v_t \end{bmatrix} = \left\{ \begin{bmatrix} R_d & 0 & 0 & 0 & 0 & 0 \\ 0 & R_q & 0 & 0 & 0 & 0 \\ 0 & 0 & R_0 & 0 & 0 & 0 \\ 0 & 0 & 0 & R_f & 0 & 0 \\ 0 & 0 & 0 & 0 & R_s & 0 \\ 0 & 0 & 0 & 0 & 0 & R_t \end{bmatrix} + p \begin{bmatrix} L_d & 0 & 0 & M_{df} & M_{ds} & 0 \\ 0 & L_q & 0 & 0 & 0 & M_{qt} \\ 0 & 0 & L_0 & 0 & 0 & 0 \\ M_{df} & 0 & 0 & L_f & 0 & 0 \\ M_{ds} & 0 & 0 & 0 & L_s & 0 \\ 0 & M_{qt} & 0 & 0 & 0 & L_t \end{bmatrix} + \omega_r \begin{bmatrix} 0 & -L_q & 0 & 0 & 0 & -M_{qt} \\ L_d & 0 & 0 & M_{df} & M_{ds} & 0 \\ 0 & 0 & 0 & 0 & 0 & 0 \\ 0 & 0 & 0 & 0 & 0 & 0 \\ 0 & 0 & 0 & 0 & 0 & 0 \\ 0 & 0 & 0 & 0 & 0 & 0 \end{bmatrix} \right\} \times \begin{bmatrix} v_d \\ v_q \\ v_0 \\ v_f \\ v_s \\ v_t \end{bmatrix} \quad (5.68)$$

As mentioned afore, damper windings are short circuited therefore their voltages will be zero. If the field voltage has no ripple then $v_f = 0$. Also assuming that field voltage has only dc component; equation (5.68) can be given as:

$$\begin{bmatrix} v_{dq0} \\ 0 \end{bmatrix} = \left\{ \begin{bmatrix} R_{11} & 0 \\ 0 & R_{22} \end{bmatrix} + p \begin{bmatrix} L_{11} & L_{12} \\ L_{21} & L_{22} \end{bmatrix} + \omega_r \begin{bmatrix} J_{11} & J_{12} \\ 0 & 0 \end{bmatrix} \right\} \times \begin{bmatrix} I_{dq0} \\ I_{fst} \end{bmatrix} \quad (5.69)$$

In equation (5.69)

$$R_{11} + pL_{11} + \omega_r J_{11} = Z_{11}$$

$$pL_{12} + \omega_r J_{12} = Z_{12} \quad (5.70-73)$$

$$pL_{21} = Z_{12}$$

and

$$R_{22} + pL_{22} = Z_{22}$$

therefore equation (5.69) may be written as:

$$\begin{bmatrix} v_{dq0} \\ 0 \end{bmatrix} = \begin{bmatrix} Z_{11} & Z_{12} \\ Z_{21} & Z_{22} \end{bmatrix} \times \begin{bmatrix} I_{dq0} \\ I_{fst} \end{bmatrix} \quad (5.74)$$

For a harmonic term $n, p = jn\omega_0$, where ω_0 is the electrical speed for non-sinusoidal steady state analysis. For Hartley harmonic impedance matrices of the machine [38], equations (5.70-73) can be identified as:

$$Z_{11n} = \begin{bmatrix} R_{11} + \omega_r J_{11} & n\omega_0 L_{11} \\ -n\omega_0 L_{11} & R_{11} + \omega_r J_{11} \end{bmatrix}$$

$$Z_{12_n} = \begin{bmatrix} \omega_r J_{12} & n\omega_r L_{12} \\ -n\omega_r L_{12} & \omega_r J_{12} \end{bmatrix}$$

$$Z_{21_n} = \begin{bmatrix} 0 & n\omega_0 L_{21} \\ -n\omega_0 L_{21} & 0 \end{bmatrix}$$

$$Z_{22_n} = \begin{bmatrix} R_{22} & n\omega_0 L_{22} \\ -n\omega_0 L_{22} & R_{22} \end{bmatrix}$$

Equation (5.74) can be solved for a any given harmonic n for I_{dq0} .

$$I_{dq0_n} = Y_{dq0_n} V_{dq0_n} \quad (5.75)$$

where

$$Y_{dq0_n} = (Z_{11_n} - Z_{12_n} Z_{22_n}^{-1} Z_{21_n})^{-1} \quad (5.76)$$

and

$$Y_{dq0_n} = \begin{bmatrix} G_n & -B_n \\ B_n & G_n \end{bmatrix} \quad (5.77)$$

known as the Hartley admittance matrix of the machine. Both G_n and B_n are 3×3 real matrices.

For all the harmonic terms simultaneously equation (5.75) is expressed as:

$$I_{dq0_h} = Y_{dq0_h} V_{dq0_h} \quad (5.78)$$

where Y_{dq0_h} is Hartley admittance matrix for harmonic analysis of the machine. See **Matlab** functions used to obtain Y_{dq0} given in *Appendix IV*.

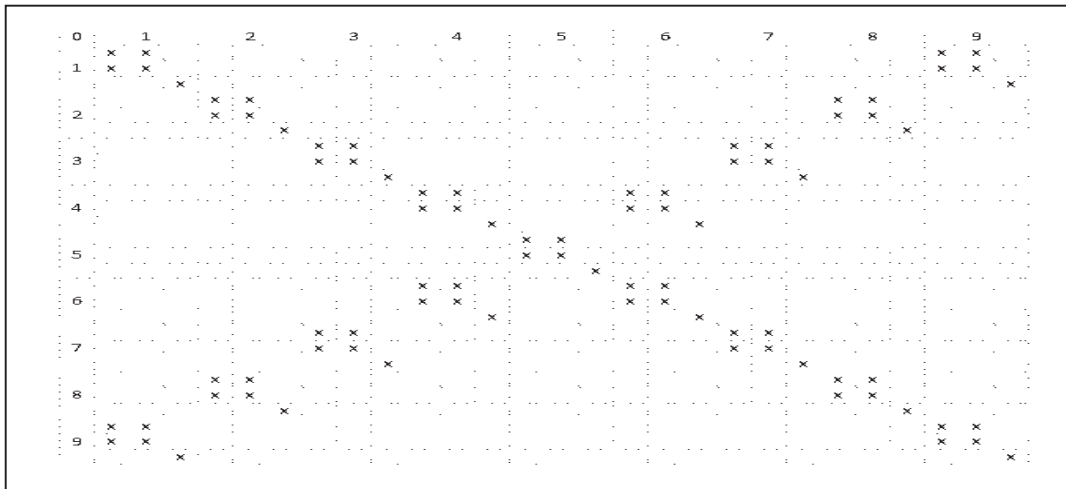


Fig. 5.10 (a): The structure of admittance matrix Y_{dq0} in Hartley harmonic domain.

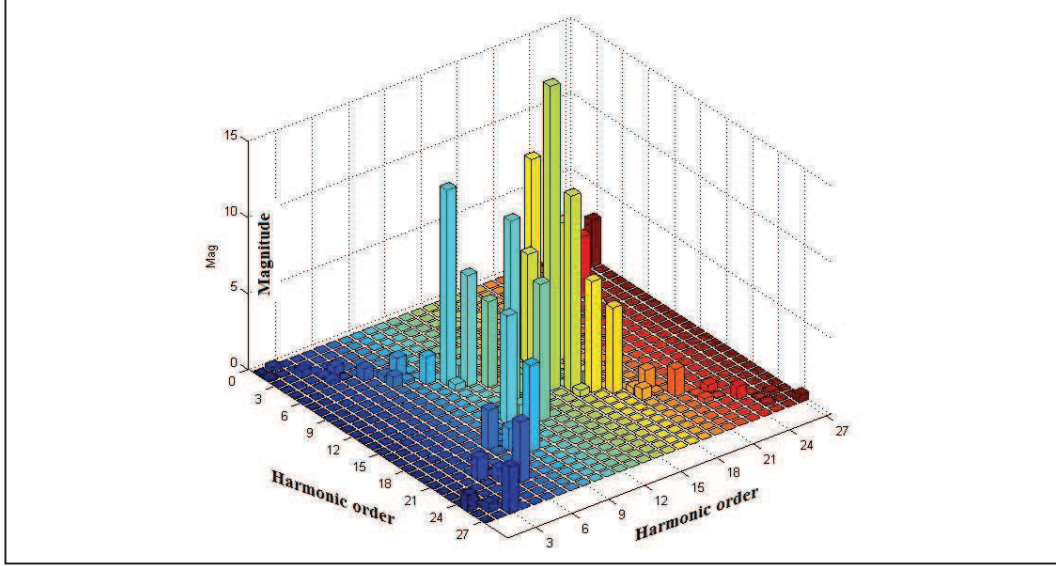


Fig. 5.10 (b): Y_{dq0} in Hartley harmonic domain, Harmonic order Vs Magnitude

The structure of Y_{dq0} , the admittance matrix (Fig. 5.10), in Hartley harmonic domain is well explaining itself. The total number of crosses here has doubled compared to the structure of the Y_{dq0} admittance matrix structure when obtained by using the Fourier transform. However, all the crosses in here (Fig. 5.10), indicate the real numbers only.

5.4.2 Machine's Hartley harmonic admittance matrix model in $\alpha\beta\gamma$ axis

The transformation from $dq0$ axes to $\alpha\beta\gamma$ axes is given by the matrix equation

$$\begin{bmatrix} v_\alpha \\ v_\beta \\ v_\gamma \end{bmatrix} = \begin{bmatrix} \cos \omega_r t & -\sin \omega_r t & 0 \\ \sin \omega_r t & \cos \omega_r t & 0 \\ 0 & 0 & 1 \end{bmatrix} \times \begin{bmatrix} v_d \\ v_q \\ v_0 \end{bmatrix} \quad (5.79)$$

The votages v_d , v_q and v_0 are non-sinusoidal periodic functions which in Hartley harmonic domain are given as:

$$v_d = \sum_{n=-\infty}^{\infty} V_{d_n} \text{cas } n v_0 t \quad (5.80)$$

$$v_q = \sum_{m=-\infty}^{\infty} V_{q_m} \text{cas } m v_0 t \quad (5.81)$$

$$v_0 = \sum_{i=-\infty}^{\infty} V_{0i} \text{cas } i v_0 t \quad (5.82)$$

Therefore

$$v_\alpha = \sum_{k=-\infty}^{\infty} V_{\alpha k} \text{cas } k v_0 t \quad (5.83)$$

$$v_\beta = \sum_{j=-\infty}^{\infty} V_{\beta j} \text{cas } j v_0 t \quad (5.84)$$

$$v_\gamma = \sum_{r=-\infty}^{\infty} V_{\gamma r} \text{cas } r v_0 t \quad (5.85)$$

Replacing ω_r by v_0 and solving equation (5.79) based on equations (5.80-82) gives:

$$v_\alpha = \frac{1}{2} \left\{ \sum_{n=-\infty}^{\infty} V_{d_n} \text{cas } (n+1) v_0 t + \sum_{n=-\infty}^{\infty} V_{d_n} \text{cas } (n-1) v_0 t + \sum_{m=-\infty}^{\infty} V_{q_m} \text{cas } (-m-1) v_0 t + \sum_{m=-\infty}^{\infty} V_{q_m} \text{cas } (-m+1) v_0 t \right\} \quad (5.86)$$

$$v_\beta = -\frac{1}{2} \left\{ \sum_{n=-\infty}^{\infty} V_{d_n} \text{cas } (-n-1) v_0 t + \sum_{n=-\infty}^{\infty} V_{d_n} \text{cas } (-n+1) v_0 t + \sum_{m=-\infty}^{\infty} V_{q_m} \text{cas } (m+1) v_0 t + \sum_{m=-\infty}^{\infty} V_{q_m} \text{cas } (m-1) v_0 t \right\} \quad (5.87)$$

and

$$v_\gamma = \sum_{i=-\infty}^{\infty} V_{0i} \text{cas } i v_0 t \quad (5.88)$$

Comparing equations (5.83-85) term by term with the equation set (5.80-82) leads to the following Hartley harmonic domain vectors:

$$\begin{bmatrix} \vdots \\ V_{\alpha-3} \\ V_{\alpha-2} \\ V_{\alpha-1} \\ V_{\alpha_0} \\ V_{\alpha_1} \\ V_{\alpha_2} \\ V_{\alpha_3} \\ \vdots \end{bmatrix} = \frac{1}{2} \left\{ \begin{bmatrix} \vdots \\ V_{d-4} \\ V_{d-3} \\ V_{d-2} \\ V_{d-1} \\ V_{d_0} \\ V_{d_1} \\ V_{d_2} \\ \vdots \end{bmatrix} + \begin{bmatrix} \vdots \\ V_{d-2} \\ V_{d-1} \\ V_{d_0} \\ V_{d_1} \\ V_{d_2} \\ V_{d_3} \\ V_{d_4} \\ \vdots \end{bmatrix} + \begin{bmatrix} \vdots \\ V_{q_2} \\ V_{q_1} \\ V_{q_0} \\ V_{q-1} \\ V_{q-2} \\ V_{q-3} \\ V_{q-4} \\ \vdots \end{bmatrix} - \begin{bmatrix} \vdots \\ V_{q_4} \\ V_{q_3} \\ V_{q_2} \\ V_{q_1} \\ V_{q_0} \\ V_{q-1} \\ V_{q-2} \\ \vdots \end{bmatrix} \right\} \quad (5.89)$$

$$\begin{bmatrix} \vdots \\ V_{\beta-3} \\ V_{\beta-2} \\ V_{\beta-1} \\ V_{\beta_0} \\ V_{\beta_1} \\ V_{\beta_2} \\ V_{\beta_3} \\ \vdots \end{bmatrix} = -\frac{1}{2} \left\{ \begin{bmatrix} \vdots \\ V_{d_2} \\ V_{d_1} \\ V_{d_0} \\ V_{d-1} \\ V_{d-2} \\ V_{d-3} \\ V_{d-4} \\ \vdots \end{bmatrix} + \begin{bmatrix} \vdots \\ V_{d_4} \\ V_{d_3} \\ V_{d_2} \\ V_{d_1} \\ V_{d_0} \\ V_{d-1} \\ V_{d-2} \\ \vdots \end{bmatrix} + \begin{bmatrix} \vdots \\ V_{q_4} \\ V_{q_3} \\ V_{q_2} \\ V_{q_1} \\ V_{q_0} \\ V_{q-1} \\ V_{q-2} \\ \vdots \end{bmatrix} + \begin{bmatrix} \vdots \\ V_{q-2} \\ V_{q-1} \\ V_{q_0} \\ V_{q_1} \\ V_{q_2} \\ V_{q_3} \\ V_{q_4} \\ \vdots \end{bmatrix} \right\} \quad (5.90)$$

$$\begin{bmatrix} \vdots \\ V_{\gamma-3} \\ V_{\gamma-2} \\ V_{\gamma-1} \\ V_{\gamma_0} \\ V_{\gamma_1} \\ V_{\gamma_2} \\ V_{\gamma_3} \\ \vdots \end{bmatrix} = \begin{bmatrix} \vdots \\ V_{0-3} \\ V_{0-2} \\ V_{0-1} \\ V_{0_0} \\ V_{0_1} \\ V_{0_2} \\ V_{0_3} \\ \vdots \end{bmatrix} \quad (5.91)$$

A general relation based on equations (5.89-91) and a transformation matrix can be derived for $dq0$ to $\alpha\beta\gamma$ axes transformation as:

$$V_{\alpha\beta\gamma_h} = C_h V_{dq0_h} \quad (5.92)$$

In equation (5.92), C_h is the transformation matrix which is singular. In order to remove the singularity either the first row and column or the last row and last column is removed from the original matrix. It can also be proved that:

$$C_h^T C_h = \begin{bmatrix} X & O & O & O & O & O & Y^T \\ O & U & O & O & O & O & O \\ O & O & O & O & O & O & O \\ O & O & O & U & O & O & O \\ O & O & O & O & O & O & O \\ O & O & O & O & O & U & O \\ Y & O & O & O & O & O & X \end{bmatrix}$$

where

$$X = \frac{1}{2} \begin{bmatrix} 1 & 0 & 0 \\ 0 & 1 & 0 \\ 0 & 0 & 2 \end{bmatrix}, \quad U = \begin{bmatrix} 1 & 0 & 0 \\ 0 & 1 & 0 \\ 0 & 0 & 1 \end{bmatrix} \text{ and } Y = \frac{1}{2} \begin{bmatrix} 0 & 1 & 0 \\ -1 & 0 & 0 \\ 0 & 0 & 0 \end{bmatrix}$$

Multiplying equation (5.92) by C^T using the harmonic term $h+1$,

$$C_{(h+1)}^T V_{\alpha\beta\gamma_{(h+1)}} = C_{(h+1)}^T C_{(h+1)} V_{dq0_{(h+1)}} \quad (5.93)$$

In equation (5.93), reducing the affect of harmonic term $h+1$,

$$V_{dq0_h} = C_h^T V_{\alpha\beta\gamma_h} \quad (5.94)$$

Similarly

$$I_{dq0_h} = C_h^T I_{\alpha\beta\gamma_h} \quad (5.95)$$

Replacing the values of V_{dq0_h} and I_{dq0_h} from equation equations (5.94-95) into equation (5.78), gives:

$$I_{\alpha\beta\gamma_h} = Y_{\alpha\beta\gamma_h} V_{\alpha\beta\gamma_h} \quad (5.96)$$

where $Y_{\alpha\beta\gamma_h}$ is Hartley harmonic matrix in $\alpha\beta\gamma$ axes given by:

$$Y_{\alpha\beta\gamma_h} = C_h Y_{dq0_h} C_h^T \quad (5.97)$$

The **Matlab** functions used to obtain $Y_{\alpha\beta\gamma_h}$ is given in *Appendix IV*.

Harmonic Domain Modelling of Synchronous Generator

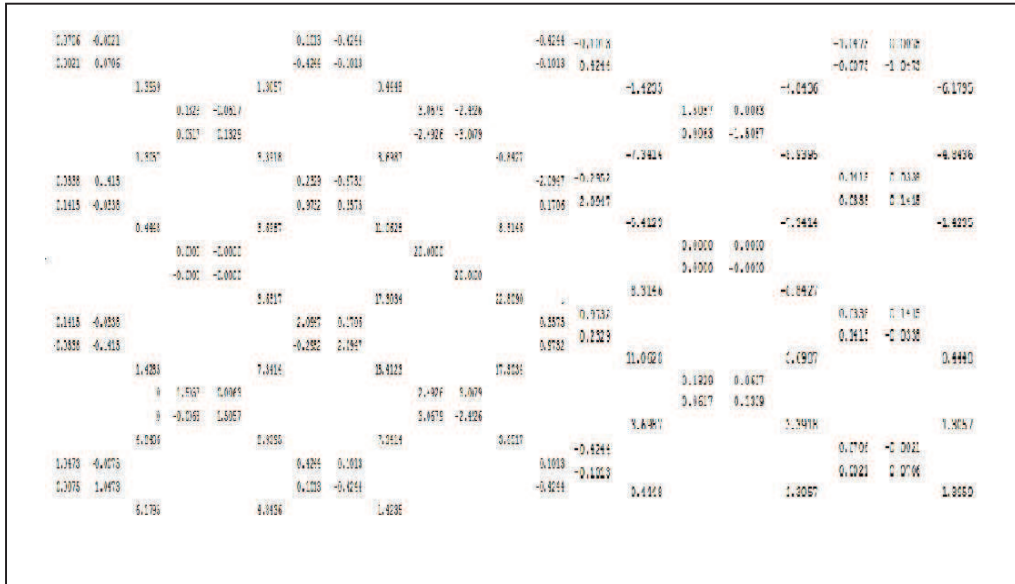


Fig. 5.11 (a): Structure of admittance matrix in $\alpha\beta\gamma$ reference frame

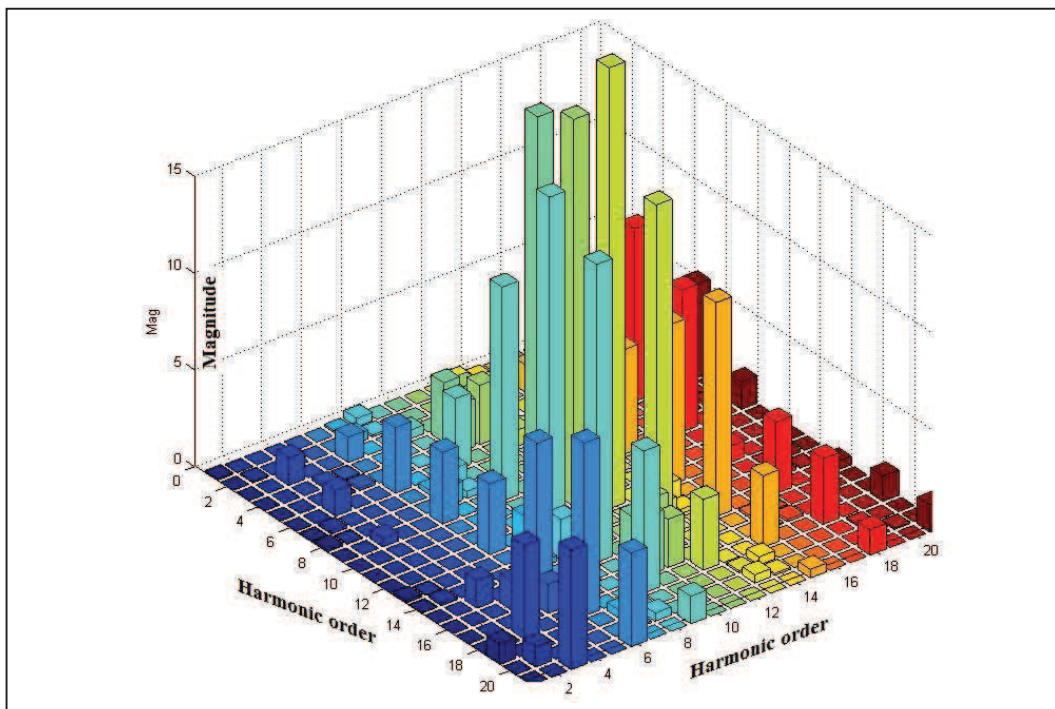


Fig. 5.11 (b): $Y_{\alpha\beta\gamma}$, in Hartley harmonic domain, Harmonic order Vs Magnitude

5.4.3 Machine's Hartley harmonic admittance matrix model in *abc* axis

The transformation from $\alpha\beta\gamma$ to *abc* axes is performed with the help of transformation matrix T_t , given by:

$$T_t = \begin{bmatrix} \sqrt{2/3} & -\sqrt{1/6} & -\sqrt{1/6} \\ 0 & \sqrt{1/2} & -\sqrt{1/2} \\ \sqrt{1/3} & \sqrt{1/3} & \sqrt{1/3} \end{bmatrix}$$

Using transformation matrix T_t , the voltage and current from $\alpha\beta\gamma$ to *abc* axes are transformed respectively as:

$$V_{\alpha\beta\gamma} = T_t V_{abc} \quad (5.98)$$

$$I_{\alpha\beta\gamma} = T_t I_{abc} \quad (5.99)$$

Since $T_t^{-1} = T_t^T$ for h harmonics the transformation matrix becomes:

$$T_{th} = \begin{bmatrix} \ddots & & & \\ & T_t & & \\ & & T_t & \\ & & & T_t \\ & & & & \ddots \end{bmatrix} \quad (5.100)$$

Substituting equation (5.96) in equations (5.98-99) for h harmonics leads to:

$$I_{abc_h} = Y_{abc_h} V_{abc_h} \quad (5.101)$$

where Y_{abc_h} is Hartley harmonic admittance matrix in *abc* frame of reference given by:

$$Y_{abc_h} = T_{th}^T Y_{\alpha\beta\gamma_h} T_{th} \quad (5.102)$$

The **Matlab** functions used to obtain Y_{abc_h} is also given *Appendix IV*.

If we compare the admittance matrices in Fourier's harmonic domain shown in Fig. 5. 4-6 with those in Hartley's harmonic domain shown in Fig. 5.10-12, it may be noticed that a series of differences is present. Most dominant difference is that in Hartley's domain, in all three reference frames the matrices contain only real values. However the structure of the matrices becomes more complex; in particular when saturation and frequency conversion effects are present and inter-harmonics appear in the structure.

5.5 Case study

Fig. 5.13 shows a synchronous generator, directly feeding an assumed ground linear unbalanced load. The load comprises of a purely resistive component in phase a , an inductive reactance in phase b and a capacitive reactance in phase c . It is also assumed that each of the loads has a value of 1.0 p.u. The study is limited up to 7th harmonic. The load represents an extreme unbalance, even though the assumptions make the scenario highly unlikely. However the aim of this test system is to show the ability of synchronous generator to produce harmonic distortion.

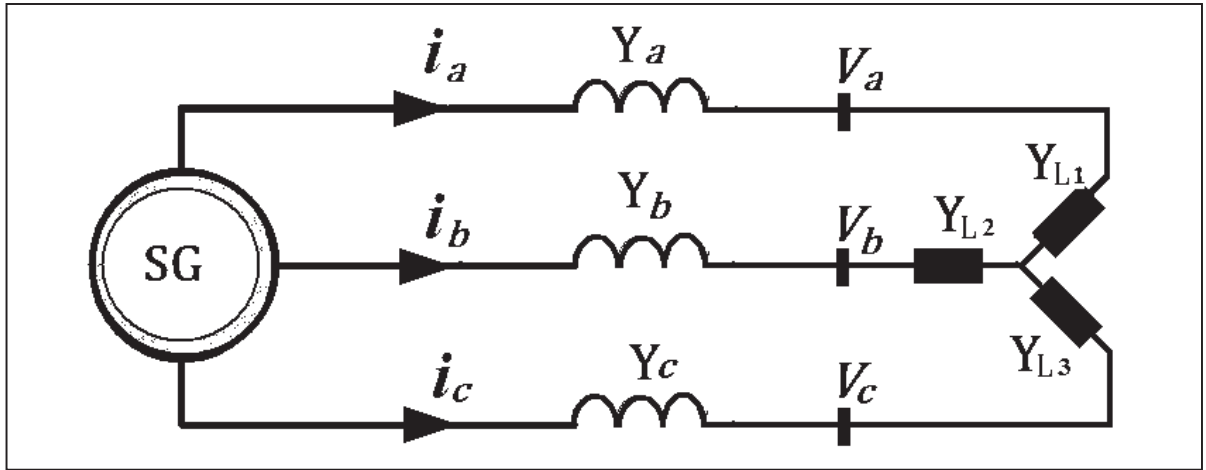


Fig. 5.13: Circuit arrangement for case study

In Fig. 5.13, voltages V_a , V_b and V_c are given by the equation:

$$[i_{abc}] = [Y_{Gen} + Y_{Load}][V_{abc}] \quad (5.103)$$

Fig. 5.14 and Fig. 5.15 show voltage and current waveforms respectively, across the unbalanced load shown in Fig. 5.13. There is not any nonlinear effect present in the system so that no cross coupling between harmonics exists. Hence the harmonic interaction between stator and rotor can not be described. Sinusoidal unbalanced waveforms with zero harmonic contents result with this arrangement. Fig. 5.16 and Fig. 5.17 show the harmonic contents in voltage and current respectively when the process of frequency conversion in the generator is represented in the harmonic domain. The voltage harmonic contents are very high due to load characteristics as shown in Fig. 5.16.

The unbalanced load has a different effect in distortion produced in the current waveform and harmonics seem to be more evenly distributed along the load phases.

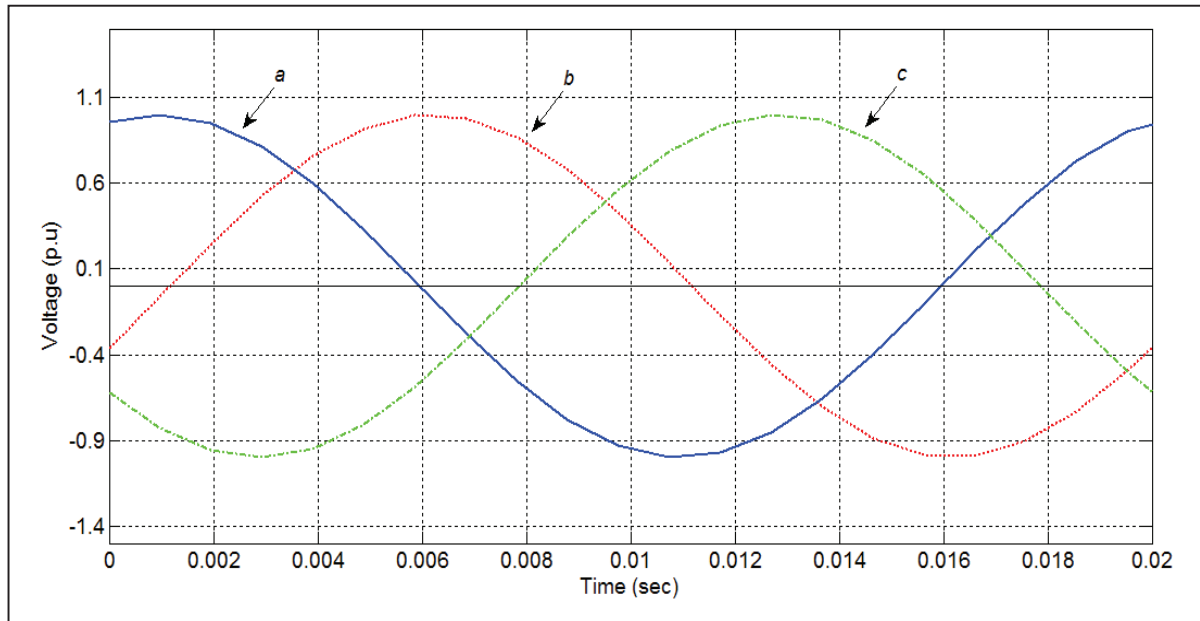


Fig. 5.14: Voltage waveform across unbalanced load (Fig. 5.13)

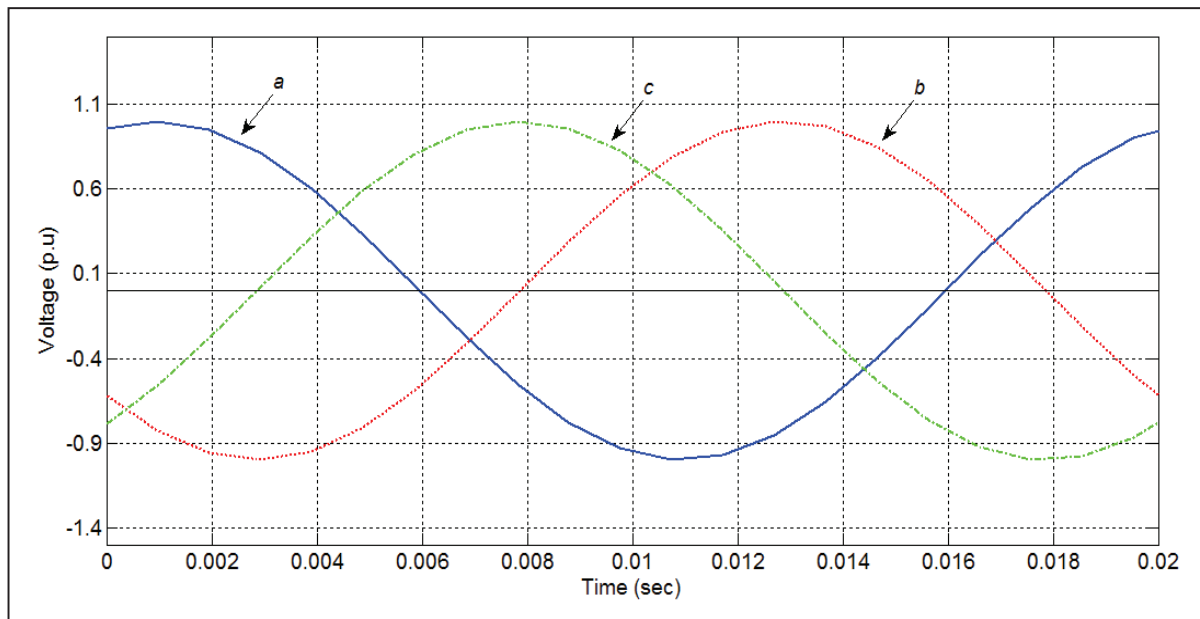


Fig. 5.15: Current waveform across unbalanced load (Fig. 5.13)

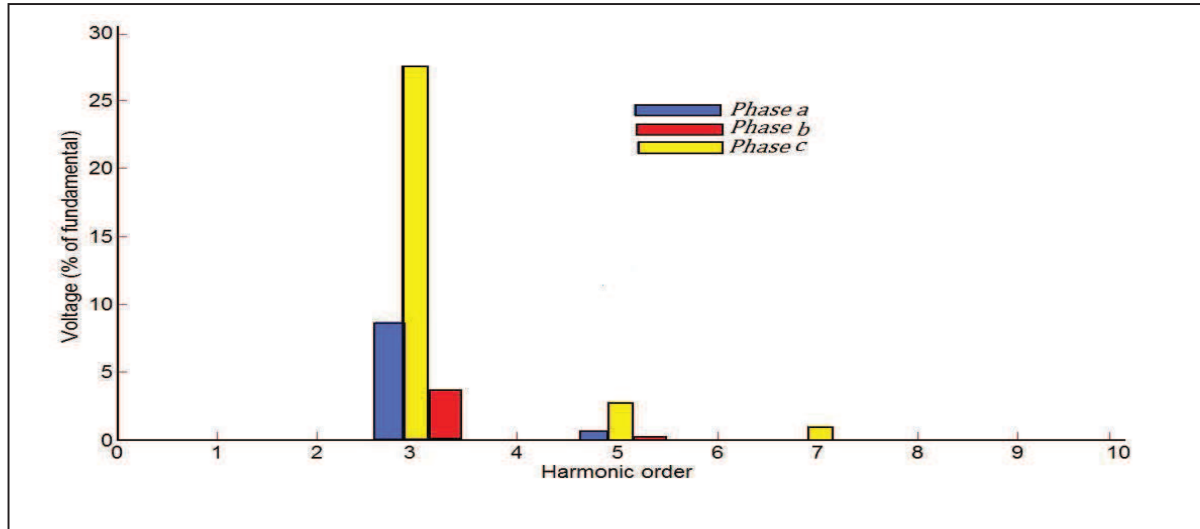


Fig. 5.16: The harmonic voltage content across the load (frequency conversion effect included).

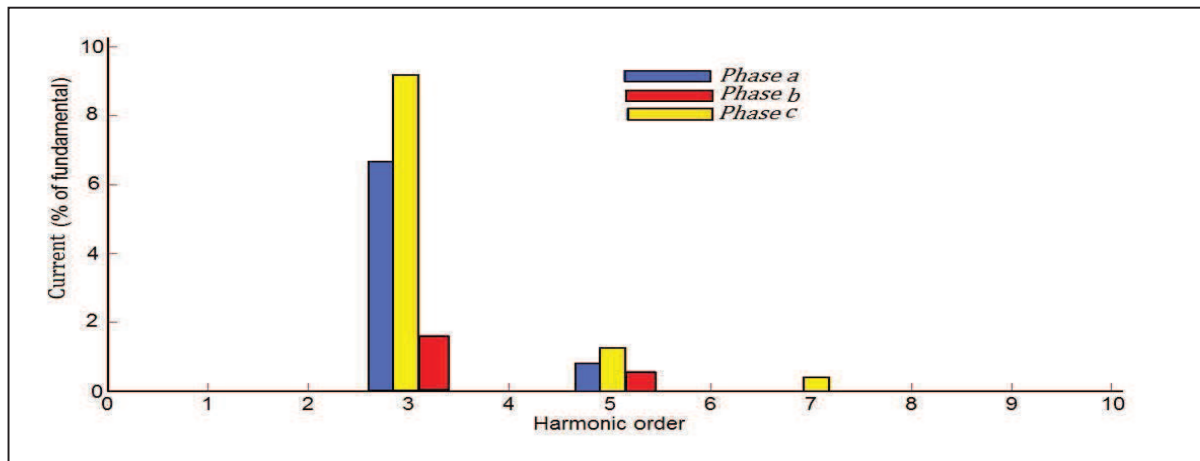


Fig. 5.17: The harmonic currents across the load (frequency conversion effect included).

The bar representing the *phase c*, in the frequency response shown both in Fig. 5.16 and 5.17, shows high distortion and points towards a probable resonance occurring between the inductive machine and the capacitive load around 3rd harmonic.

5.6 A comparison of the Fourier and the Hartley based admittance matrix models of synchronous generator

A general comparison of the Fourier and Hartley series amid at harmonic domain applications is presented in chapter 3. This section covers the main differences in the structure of two models of synchronous generator based on the Fourier and the Hartley. Modelling for the magnetic core saturation is performed based on solving the polynomial equations via repeated convolutions. The synchronous generator's magnetic core saturation model is an extended application of the transformer core saturation model described in chapter 4. Both from execution time and memory requirement point of view, it has already been made clear in section 3.8 that the Hartley based model has better performance in such cases. Therefore, the magnetic core saturation part of the model has better performance in the Hartley harmonic domain.

The algorithm for the construction of Y_{dq0} admittance matrix in both domains is similar. It makes use of equation (5.23) and equation (5.76) for the Fourier and the Hartley domains respectively. The difference occurs when the elements of the matrix are arranged. When using the Fourier, the elements appear along the diagonal in the form of original complex numbers i.e.

$$Y_{dq0} = [G + iB]$$

In the Hartley harmonic domain, the complex numbers are split into two separate groups of real numbers and arranged along the diagonals of the matrix in such a way that all the elements of new matrix are real numbers i.e.

$$Y_{dq0} = \begin{bmatrix} G & -B \\ B & G \end{bmatrix}$$

From sparsity point of view, Y_{dq0} in the Fourier harmonic domain has an edge. However, since Y_{dq0} consists of real numbers only in the Hartley harmonic domain, it has a computational advantage over it's counterpart in the Fourier domain.

The transformation from $dq0$ to $\alpha\beta\gamma$ in the Fourier harmonic domain is achieved indirectly. In the first stage a two-phase transformation from dq to $\alpha\beta$ reference frame is performed with the help of a connection matrix C given by:

$$[C] = \frac{1}{2} \begin{bmatrix} \ddots & & & & & & & & \\ & \ddots & & & & & & & \\ & & N^* & & M^* & & & & \\ & & & N^* & & M^* & & & \\ & & & & N^* & & 2M^* & & \\ & & & & & N^* & & 2M & \\ & & & & & & N & & \\ & & & & & & & M & N \\ & & & & & & & & M & N \\ & & & & & & & & & \ddots \end{bmatrix}$$

where

$$M = N^* = \begin{bmatrix} 1 & j \\ -j & 1 \end{bmatrix}$$

The connection matrix has the non square form; a direct admittance transformation from two phase $\alpha\beta$ frame of reference to a three phase reference is not possible. Therefore, $Y_{\alpha\beta}$ is augmented and Y_γ is added to the new matrix. Thus $Y_{\alpha\beta\gamma}$ is obtained as:

$$[Y_{\alpha\beta\gamma}] = \begin{bmatrix} Y_{\alpha\beta} & 0 \\ 0 & Y_\gamma \end{bmatrix}$$

The transformation from $dq0$ to $\alpha\beta\gamma$ in the Hartley harmonic domain is also performed with the help of a connection matrix C . Although the order of the connection matrix remains the same (as in the Fourier harmonic domain, $2(h+1)+1$ by $2(h+1)+1$) but the structure of the connection matrix is quite different here. The connection matrix for $h=3$, is given by:

$$[C] = \frac{1}{2} \begin{bmatrix} \ddots & & & & & & & & \\ & D & U & & & & M & & \\ & U & D & U & & & M & M' & \\ & & U & D & N & & M' & & \\ & & & N & D & N' & & & \\ & & M & & N' & D & U & & \\ M & & & & & U & D & U & \\ & M' & & & & & U & D & \\ & & & & & & & \ddots \end{bmatrix}$$

Where

$$U = \begin{bmatrix} 1 & 0 & 0 \\ 0 & 1 & 0 \\ 0 & 0 & 0 \end{bmatrix}; M = \begin{bmatrix} 0 & 1 & 0 \\ -1 & 0 & 0 \\ 0 & 0 & 0 \end{bmatrix}; N = \begin{bmatrix} 1 & 1 & 0 \\ -1 & 1 & 0 \\ 0 & 0 & 0 \end{bmatrix}; D = \begin{bmatrix} 0 & 0 & 0 \\ 0 & 0 & 0 \\ 0 & 0 & 2 \end{bmatrix}$$

The order of the connection matrix is then changed to remove singularity.

Exploiting the sparsity of a matrix is a useful tool when building up an algorithm for matrix operation. That is why, $Y_{\alpha\beta\gamma}$ in the Fourier harmonic domain is better than in the Hartley domain for same number of harmonics. However; a less number of operations hence less execution time is required on $Y_{\alpha\beta\gamma}$ in the Hartley's domain, giving it a computational priority.

The transformation from $Y_{\alpha\beta\gamma}$ to Y_{abc} in both the cases is carried out by using well known Clarke's transformation matrix, given as:

$$T_t = \begin{bmatrix} 1 & -1/2 & -1/2 \\ 0 & \sqrt{3}/2 & -\sqrt{3}/2 \\ 1/3 & 1/3 & 1/3 \end{bmatrix}$$

A power-invariant form of this matrix is used in the transformation. Notice that matrix Y_{abc} has to be re-arranged in the Fourier as well as in the Hartley harmonic domain before it can be merged to the external circuit. Similar to $Y_{\alpha\beta\gamma}$, Y_{abc} also has computational priority in Hartley's domain.

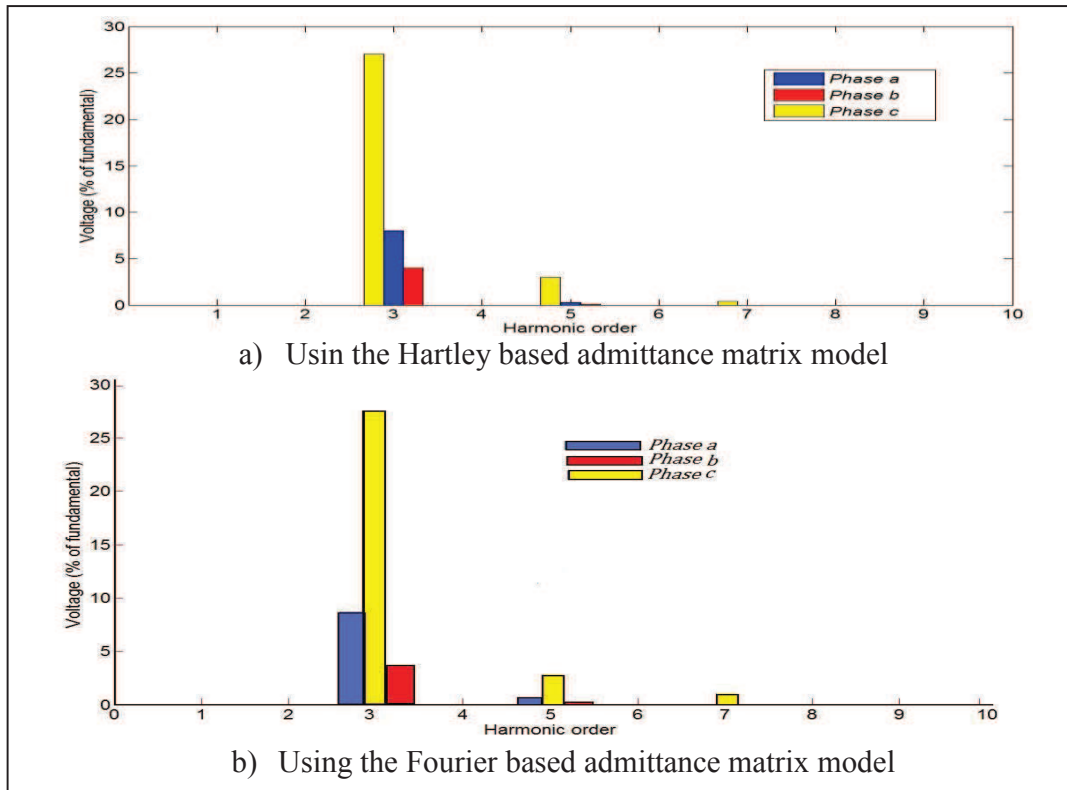


Fig. 5.18: The harmonic voltages in *phase a, b* and *c*, (Fig. 5.13)

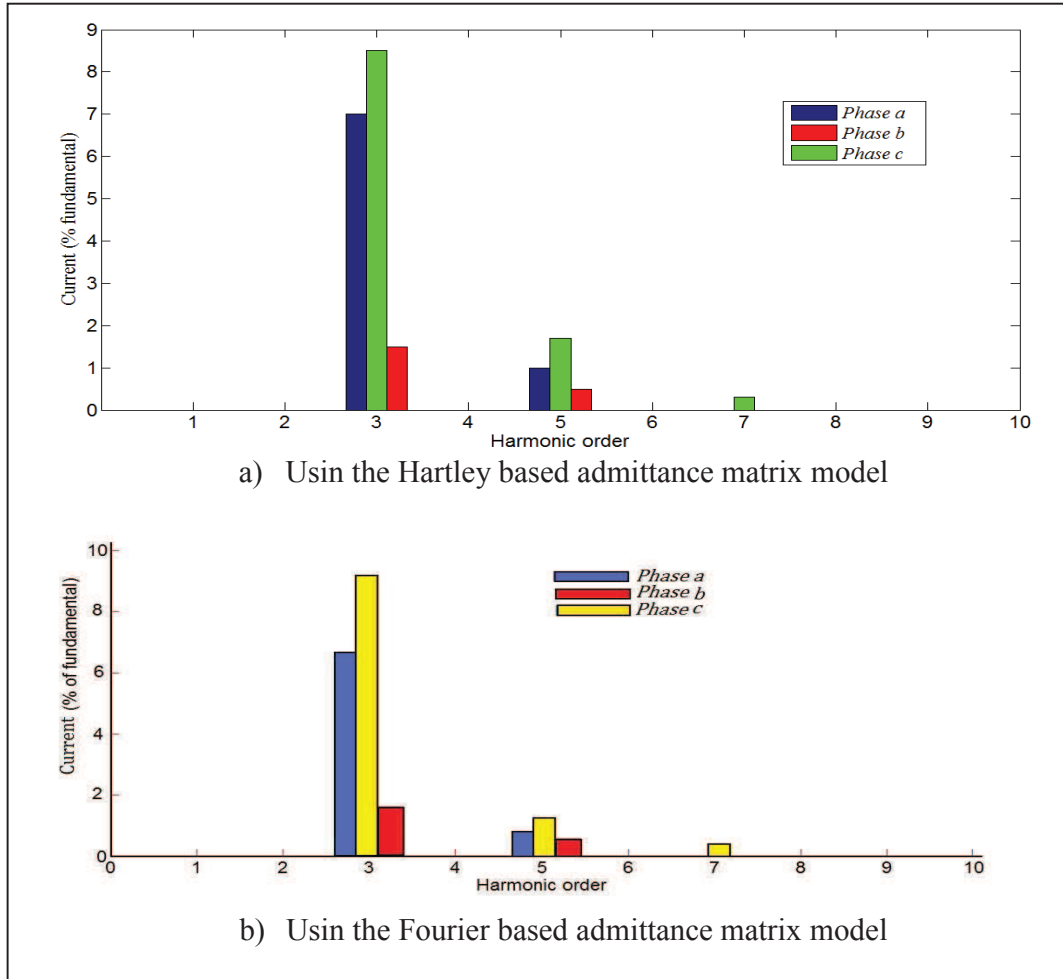


Fig. 5.19: The harmonic currents in *phase a, b* and *c*, (Fig. 5.13)

A comparative study between the Fourier based admittance matrix model and a Hartley based admittance matrix model of the synchronous generator was performed based on case study presented in the previous section. The results show that both the models are well capable of representing the ability of synchronous generator to produce harmonics under unbalanced conditions. The results (shown in Fig. 5.18-19) also indicate that there is hardly any difference in the distortion of either voltage or current for the respective harmonic term. This also confirms the accuracy of the model in both the Fourier and the Hartley's harmonic domains. However, since the Hartley's based algorithms require lesser time and lesser storage; they provide a better choice, in particular when higher number of harmonics is involved and time and memory are important.

5.7 Summary

The synchronous machine's admittance matrix harmonic domain model has been presented in two different ways, the first using the conventional Fourier approach and then using the Hartley harmonic domain. The existing models of synchronous machine for harmonic analysis only account for the harmonics due to unbalanced loading but do not include magnetic core saturation saturation effect, which is an additional source of harmonics. The models presented here, take into account both the frequency conversion phenomenon between stator-rotor and the magnetic saturation effect. The model has a form that allows its representation by either a Norton's or Thevenin's harmonic equivalent.

Since the Hartley's transform uses only 'real functions', it shows efficiency advantages over a comparable model developed using a complex Fourier representation. The harmonic domain model of a synchronous generator has been developed using the Hartley transform, assuming a short-circuited damper winding and taking only the DC component of the field excitation into account. The Hartley admittance matrices of the synchronous generator in the $dq0$ and the $\alpha\beta\gamma$ axes are derived and used to obtain the admittance in abc coordinates by means of transformation matrices. These admittance matrices illustrate, rather well, the frequency conversion effect present in the synchronous generator.

The main points of the results are:

- The important structures of the admittance matrices in the $dq0$, abc and $\alpha\beta\gamma$ frames of reference in both the Fourier and the Hartley harmonic domains.
- The pattern of the admittance matrix in the $\alpha\beta\gamma$ frame is of special interest, as it gives us an insight into the frequency conversion effect present in a synchronous generator, operating under unbalanced conditions. A harmonic voltage of order n ($V_{\alpha\beta\gamma_n}$) can generate harmonic currents of the order n ($I_{\alpha\beta\gamma_n}$), as well as the harmonic currents of the order $n \pm 1$ ($I_{\alpha\beta\gamma_{n\pm 1}}$), which makes the effect of 'frequency conversion' observable. Similar characteristics are exhibited by the admittance matrix Y_{abc} .

- Further, the nonlinear effect in the machine, caused by saturation, is represented by the Norton's harmonic equivalent in the model. For the evaluation of this effect an equal number of operations are required in both the Fourier and the Hartley domain. The evaluation involves convolution operations and multiplications of large vectors and matrices. In addition, the method uses an iterative process, which means a re-evaluation at the end of each iteration in the iterative process. The real operation in the Hartley domain, compared to a corresponding complex operation in the Fourier domain is four times faster because there is a very high number of operations involved in the evaluation of the saturation effect. The time saving aspect of working in the Hartley domain becomes crucial and gives it a priority in such applications.
- Finally, the harmonic studies were carried out by connecting an unbalanced linear load at the generators terminals to assess the effect of the detailed representation of the machine. The frequency conversion effect in a synchronous machine is further excited by saturation.

A simple model, linearly dependant with the frequency, can not represent either the frequency conversion effect or the impact of magnetic saturation on the process of frequency conversion based on the cross-coupling existing between harmonics of different order. The model described here works rather well and represents the complex process of harmonic conversion and catalyst role played by saturation in this process.

5.8 References

- [1] P. C. Krause, O. Wasynczuk, and S. D. Sudhoff; "Analysis of Electric Machinery," New York: IEEE Press, 1994. McGraw Hill, 1986
- [2] A. E. Fitzgerald, C. Kingsley, Jr., S. D. Umans; "Electric Machinery." McGraw Hill, 1990
- [3] E. Acha, M. Madrigal; "Power Systems Harmonics computer modeling and analysis" John Wiley 2001

- [4] J. Arrillaga, B. C. Smith, N. R. Watson, A. R. Wood; "Power System Harmonic Analysis". John Wiley, 1997
- [5] D. O'Kelly, S. Simmons; "Introduction to Generalized Machine Theory" McGraw Hill, London, 1968
- [6] M. S. Sarma; "Synchronous Machines (their theory, stability and excitation system)" Gordon and Breach, London, Paris, New York, 1979
- [7] P. C. Krause, O. Wasynczuk, S. D. Sudhoff, "Analysis of Electric Machinery" IEEE Press, New York, 1994
- [8] G. T. Heydt; "System Analysis Using Hartley Impedance" IEEE, transactions on power delivery, vol. 8, no. 2, pp. 518-523, 1993
- [9] E. Clarke; "Circuit Analysis of AC Power Systems" vol. 2, John Wiley & Sons, London, 1950
- [10] J. D. Rorak and C. A. Fross; "Unbalanced synchronous machine analysis using frequency domain methods" IEEE/PES, 1978
- [11] A. Semlyen, J. F. Eggleston and J. Arrillaga; "Admittance matrix model of a synchronous machine for harmonic analysis", IEEE, Transaction on Power Systems, pp. 833-840, 1987
- [12] P. M. Anderson and A. A. Foud; "Power System Control and Stability", IOWA State University press, IOWA, 1977
- [13] G. R. Slemon. "Analytical models for saturated synchronous machines", IEEE, Transactions on Power Apparatus and Systems, vol. PAS-90, no. 2, pp. 409-417, 1971

- [14] G. Shackshaft and P. B. Henser; "Results of stability tests on an under excited 120 MW generator", IEE, vol. 119, no. 2, pp. 759-763, 1979
- [15] G. Shackshaft and G. Neilson; "Model of generator saturation for use I power system studies", IEE, vol. 126, no. 8, pp. 175-188, 1972
- [16] R. G. Harley, D. J. N. Limbeer and E. Chrricozzi; "Comparison study of saturation methods in synchronous machine models", IEE, vol. 127, no. 1, pp. 1-7, 1980
- [17] B. Adkins and R. G. Harley; "The general theory of alternating current machines", Chapman and Hall, London, 1975
- [18] A. M. El-Sherafi, A. S. Abdallah, M. K. El-sherbiny and E. H. Badawy; "Experimental study of Saturation and Cross-magnetizing Phenomenon in Saturated Synchronous Machines", IEEE, Transactions on Energy Conversion, vol. 3, no. 4, pp. 815-823, 1988
- [19] V. Brandwajin; "Representation of Magnetic Saturation in Synchronous Machine Model in an Electro-Magnetic Transient Program", IEEE, Transaction on Power Apparatus and Systems, 1980
- [20] W. Xu, J. R. Marti and H. W. Dommel; "A Multiphase Harmonic Load Flow Solution", IEEE, Transactions on Power Apparatus and Systems, vol. 6, no. 1, pp. 174-182, 1991
- [21] H. W. Dommel, "Digital computer solution of electromagnetic transients in single and multiphase networks," IEEE Trans. Power Apparatus and Systems, Vol. PAS-88, no.4, pp. 388-399, 1969
- [22] H. Dommel, "A method for solving transient phenomena in multiphase systems," Proc. 2nd Power System Computation Conference 1966, (Stockholm Sweden) Rept. 5.8, 1996
- [23] D. A. Woodford, A. M. Gole, R. W. Menzies, "Digital Simulation of dc links and ac machines," IEEE Trans. Power Apparatus and Systems, Vol. PAS-102, no.6, pp. 1616-1623, 1983

- [24] R. H. Park, "Two-reaction theory of synchronous machines-Part 1: Generalized method of analysis," AIEE Trans. Vol. 48, pp. 716-730, 1929
- [25] Nhut-Quang Dinh; Arrilaga, J.; "A salient-pole generator model for harmonic analysis", IEEE Trans. Power Systems. Vol. 16. Issue. 4, pp. 609-615, 2001
- [26] A. M. El-Serafi, A. S. Abdallah, M. K. El-Sherbiny, and E. H. Badawy, "Experimental study of the saturation and the cross magnetizing phenomenon in saturated synchronous machines," IEEE Trans. on Energy Conversion, vol. EC-3, pp. 815–823, 1988
- [27] C. T. Huang, Y. T. Chen, C. L. Chang, C. Yi, H. D. Chiang, and J. C. Wang, "On-line measurements-based model parameter estimation for synchronous generators: Model development and identification schemes," IEEE Trans. on Energy Conversion, vol. 9, pp. 330–336, 1994
- [28] J. Ma, B. W. Hogg, N. Zhiyuan, and Y. Yihan, "On line decoupled identification of transient and sub-transient generator parameters," IEEE Trans. on Power Systems, vol. 9, no. 4, pp. 1908–1914, Nov. 1994
- [29] H. Tsai, A. Keyhani, J. A. Demcko, and R. G. Farmer, "Online synchronous machine parameter estimation from small disturbance operating data," *IEEE Trans. on Energy Conversion*, vol. 10, no. 1, pp. 25–36, 1995
- [30] A. Keyhani, S. Hao, and R. P. Schulz, "Maximum likelihood estimation of generator stability constants using SSFR test data," IEEE Trans. On Energy Conversion, vol. 6, no.1, pp. 140–154, 1991
- [31] I. M. Canay, "Determination of model parameters of machines from reactance operators $x_d(p)$, $x_q(p)$: Evaluation of standstill frequency responses tests," *IEEE Trans. on Energy Conversion*, vol. 8, no. 1, pp. 272–279, 1993

- [32] J. L. Kirtley, "On turbine-generator rotor equivalent circuit structures for empirical modeling of turbine generators," *IEEE Trans. on Energy Conversion*, vol. PWR-9, no.1 pp. 269–271, 1994
- [33] I. Kamwa, P. Viarouge, and J. Dickinson, "Identification of generalized models of synchronous machines from time domain tests," *IEE Proceedings Part C*, vol. 138, no. 6, pp. 485–498, 1991
- [34] J. Jesús Rico Melgoza, Gerald Thomas Heydt, Ali Keyhani, L. Agrawal, and Douglas Selin, "Synchronous Machine Parameter Estimation Using the Hartley Series" *IEEE Trans. Energy Conversion*, vol. 16, no. 1, 2001
- [35] D. O'Kelly, S. Simmons; "Introduction to Generalized Machine Theory" McGraw Hill, London, 1968
- [36] M. S. Sarma; "Synchronous Machines (their theory, stability and excitation system)" Gordon and Breach, London, Paris, New York, 1979
- [37] P. C. Krause, O. Wasynczuk, S. D. Sudhoff, "Analysis of Electric Machinery" IEEE Press, New York, 1994
- [38] G. T. Heydt; "System Analysis Using Hartley Impedance" *IEEE, transactions on power delivery*, vol. 8, no. 2, pp. 518-523, 1993

6. INDUCTION GENERATOR MODEL FOR WIND-FARM APPLICATIONS

6.1 Introduction to wind-based power

Renewable energy sources provide a great deal of electrical energy in many countries, thus providing a large percentage of the world's energy demand. There are many types of renewable energy devices. For example wind energy systems, biomass energy systems and photovoltaic energy systems. But more experience is required to precisely forecast the future energy requirements. The earliest known use of wind energy was in a sail boat, but windmills for grinding purpose have a history going back more than three thousand years [1]. By the mid-ages, windmills were in common use around the Mediterranean. At end of 19th century about twenty thousand wind-based generators were in use only in the Netherlands and Britain [2].

In terms of the total installed capacity, the wind power in the world has shown a growth rate of more than thirty percent in the last few years [3]. In spite of the present worldwide economic crises, the total world capacity for electrical power has reached about 200 thousand MW [3]. The share of wind energy was only 0.54% of the world's electric power in 2005 [4], which has increased to about 2% in 2010. Depending upon the wind speed, wind projects simply cannot control the wind in the same way that a conventional facility can control its fuel delivery. Electric power generated by wind is better used locally rather than being transmitted. It is argued that a micro-grid is a good choice for the efficient use of wind based electric power. A micro-grid can provide an improved electric service giving quality and reliability to the consumer and it may also provide dispatchable loads [5] for use during peak power conditions.

INDUCTION GENERATOR MODEL FOR WIND-FARM APPLICATIONS

Wind energy is also an indirect form of solar energy produced by heating of the earth's surface. As a power source, it is lesser predictable compared to solar power but it is available for more hours in a given day. Wind sources are influenced by the land surface, altitude and the physical distance from the sea, etc. The power from a wind source is given by:

$$P_w = \frac{1}{2} \rho A V^3 \quad (6.1)$$

Where ρ is the air density, A is the area of wind parcel and V represents the speed of the wind.

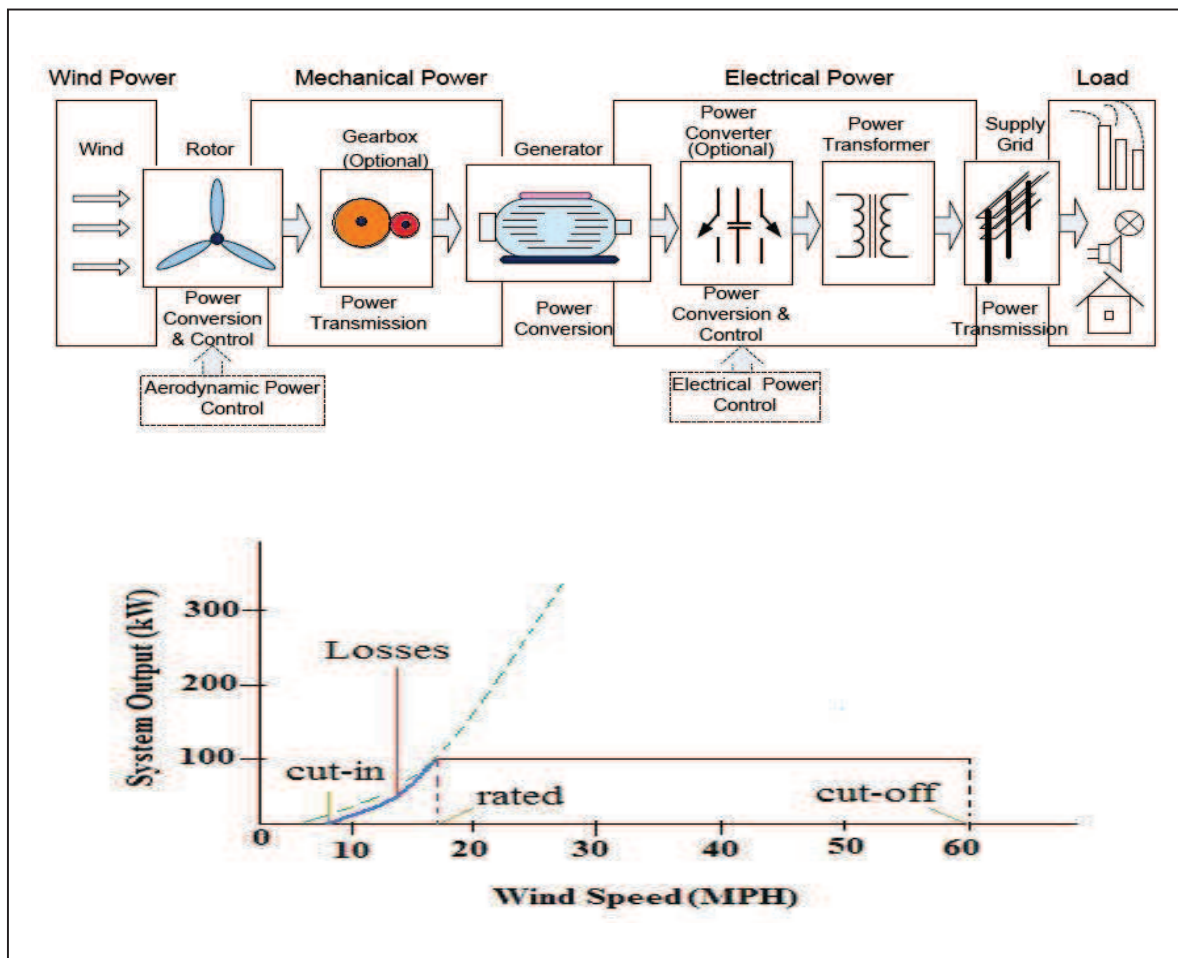


Fig. 6.1: A schematic of a wind energy conversion system and wind turbine generator output Vs wind speed plot [6]

INDUCTION GENERATOR MODEL FOR WIND-FARM APPLICATIONS

The wind speed, sufficient to generate electric power in a certain system, is known as the cut-in wind speed. There is actually enough mechanical power in the wind turbine at slightly lower speed than cut-in speed, but that counts for different losses in the system. At rated wind speed the power input to the wind turbine will reach the limit for continuous operation. When the wind speed exceeds this level the extra power in the wind turbine is discarded by suitable design of the blades. When the speed of of wind exceeds a certain (cut-off) value, the turbine is shut down.

6.1.1 Types of wind turbines

There are two main types of wind turbines classified on the basis of their axis of rotation.

6.1.1.1 Horizontal axis wind turbines

The horizontal axis wind turbines are most famous type of the wind turbines in use. There are many arrangements in which this type of wind turbine can be used depending upon the application and location. The generators used with this type of wind turbine are usually self starting and have a low cost. However the main disadvantage is that this type of turbine must be reoriented with the change in the direction of the wind. The generator, gear box and all the control are all above the ground, making the maintenance of these equipments inconvenient.

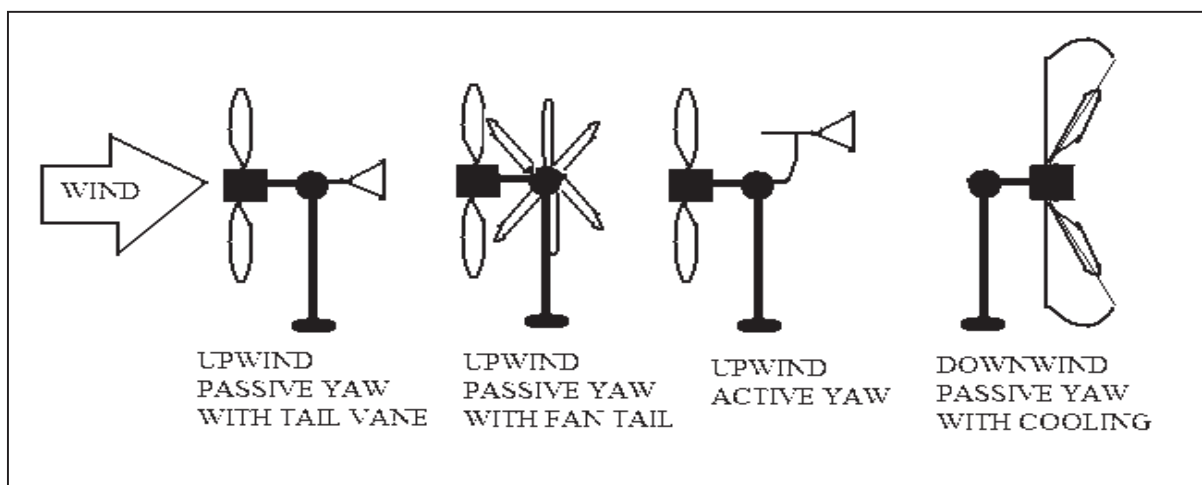


Fig. 6.2: The horizontal axis wind turbine arrangements

6.1.1.2 Vertical axis wind turbines

Vertical axis wind turbines are not as commonly used as the horizontal ones are used because of certain design issues. The benefit of such arrangement is that there is no additional cost on changing the direction of turbine when the direction of the wind changes. Another advantage is that the coupled generator, gear box and associated control are all on the ground, so the maintenance cost is low compared to horizontal axis wind turbines.

The fixed speed operation means that maximum coefficient of performance would be available simply at one particular wind speed, and if wind speed is different from this particular one the turbine will not be operating at highest coefficient hence the output power lesser. Another technique to improve the average coefficient of performance at fixed speed is the operation of turbine at a variable pitch. However this technique increases the mechanical design complexity as well as the cost of turbine.

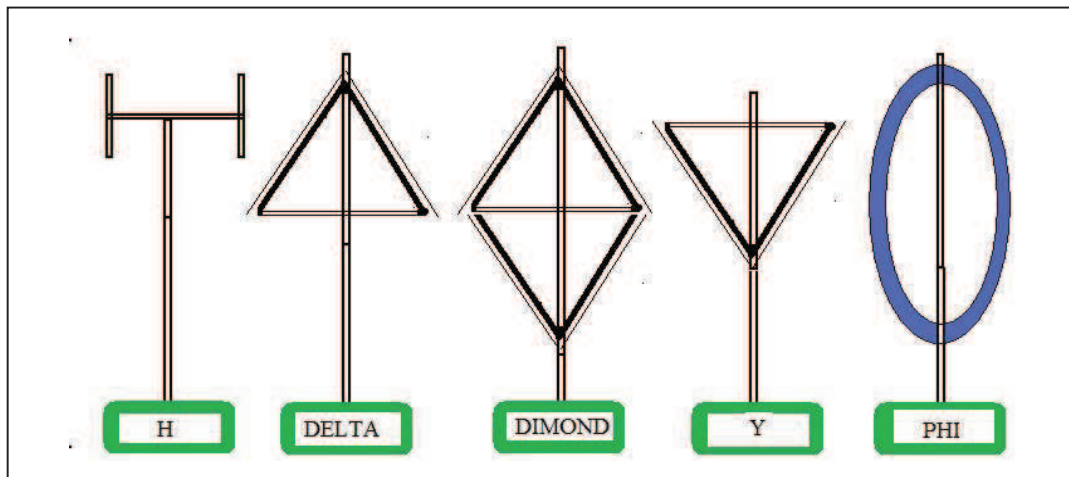


Fig. 6.3: The vertical axis wind turbine arrangements

A comparison has been made [7] between the horizontal axis wind turbine generators and the vertical axis wind turbine generators in Table 6.1. Most wind turbines operate at a fixed speed apart from starting and stopping which helps to avoid the mechanical resonance that might destroy the turbine.

INDUCTION GENERATOR MODEL FOR WIND-FARM APPLICATIONS

Table 6.1: Comparison between horizontal axis and vertical axis wind turbine generators

Item	Horizontal axis turbine generators	Vertical axis turbine generators
Output power range	Wide	Narrow
Starting	Self start	Need starting means
Efficiency	High	Low
Cost	Low	High
With a change in wind direction	Need to be reoriented	Do not need to be reoriented
Installation of generator and gear box	Mounted on tower	At the ground level
Maintenance	Inconvenient	Relatively convenient

6.1.2 Anatomy of wind turbine

Main parts and important controls of a horizontal axis wind turbine are shown in Fig. 6.4. Following is a brief description of these parts

1. Blade

The ratio between the speed of the blade tips and the speed of the wind is called tip speed ratio (λ). High efficiency 3-blade-turbines have tip speed/wind speed ratios of 6 to 7. Modern wind turbines are designed to spin at varying speeds. Use of aluminum and composite materials in their blades has contributed to low rotational inertia, which means that newer wind turbines can accelerate quickly if the winds pick up, keeping the tip speed ratio near to constant.

It is generally understood that noise increases with higher blade tip speeds. To increase tip speed without increasing noise would allow reduction the torque into the gearbox and generator and reduce overall structural loads, thereby reducing cost. The reduction of noise is linked to the detailed aerodynamics of the blades, especially factors those reduce abrupt stalling.

INDUCTION GENERATOR MODEL FOR WIND-FARM APPLICATIONS

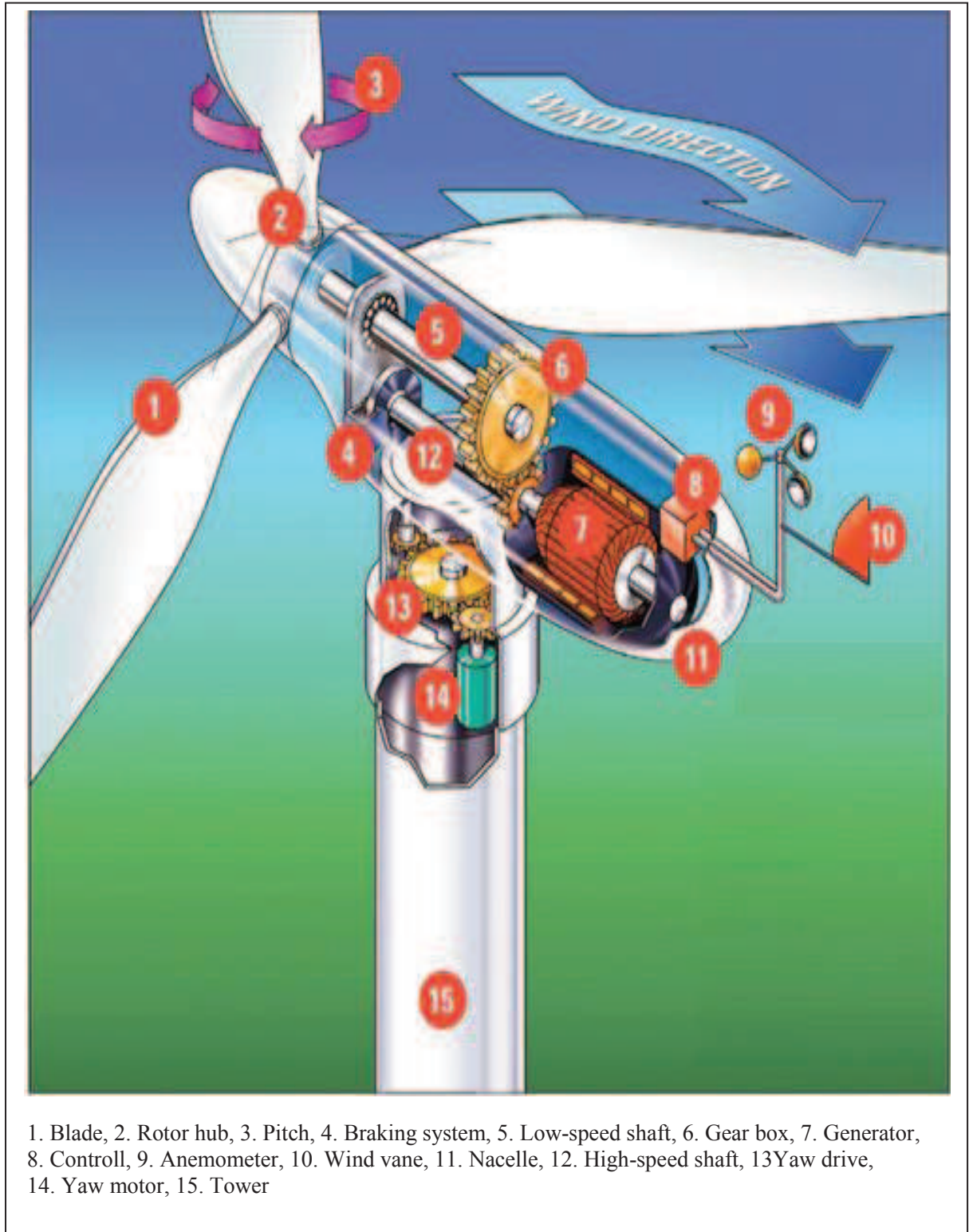


Fig. 6.4: Main parts and different controls of a wind-turbine[35]

The inability to predict stall, restricts the development of aggressive aerodynamic concepts [8]. A blade can have a lift-to-drag ratio of 120 compared to 70 for a sailplane and 15 for an airliner [9-10]

2. Rotor hub

In simple designs, the blades are directly bolted to the hub and hence are stalled. In other more sophisticated designs, they are bolted to the pitch mechanism, which adjusts their angle of attack according to the wind speed to control their rotational speed. The pitch mechanism is itself bolted to the hub. The hub is fixed to the rotor shaft which drives the generator through a gearbox. Direct drive wind turbines (also called gearless) are constructed without a gearbox.

3. Gearbox

Usually the rotational speed of the wind turbine is slower than the equivalent rotation speed of the electrical network - typical rotation speeds for a wind generators are 5-20 rpm while a directly connected machine will have an electrical speed between 750-3600 rpm. Therefore, a gearbox is inserted between the rotor hub and the generator. This also reduces the generator cost and weight.

Enercon has produced gearless wind turbines with separately excited generators for many years [11], and Siemens produces a gearless "inverted generator" 3MW model [12-13]. In conventional wind turbines, the blades spin a shaft that is connected through a gearbox to the generator. The gearbox converts the turning speed of the blades 15 to 20 rotations per minute for a large, one-megawatt turbine into the faster 1,800 rotations per minute that the generator needs to generate electricity [14].

The studies show that the reliability of gearboxes is not the main problem in a wind turbine. Reliability of direct drive turbines offshore is still not known, since the sample size is so small. A geared generator with permanent magnets uses 25 kg/MW of the rare earth element Neodymium, while a gearless may use 250 kg/MW. Direct-drive turbines require 600 kg of PM material per megawatt, which translates to several hundred

INDUCTION GENERATOR MODEL FOR WIND-FARM APPLICATIONS

kilograms of rare earth content per megawatt, as Neodymium content is estimated to be 31% of magnet weight. Hybrid drive trains (intermediate between direct drive and traditional geared) use significantly less rare earth materials. While PM wind turbines only account for about 5% of the market outside of China, their market share inside of China is estimated at 25% or higher. Demand for neodymium in wind turbines is estimated to be 1/5 of that in electric vehicles [15].

4. Braking system

Braking of a small wind turbine can be done by dumping energy from the generator into a resistor bank, converting the kinetic energy of the turbine rotation into heat. This method is useful if the kinetic load on the generator is suddenly reduced or is too small to keep the turbine speed within its allowed limit.

Cyclical braking causes the blades to slow down, which increases the stalling effect, reducing the efficiency of the blades. This way, the turbine's rotation can be kept at a safe speed in faster winds while maintaining (nominal) power output. This method is usually not applied on large grid-connected wind turbines.

A mechanical drum brake or disk brake is used to hold the turbine at rest for maintenance. Such brakes are usually applied only after blade furling and electromagnetic braking have reduced the turbine speed, as the mechanical brakes would wear quickly if used to stop the turbine from full speed. There can also be a stick brake.

5. Generator

The interfacing of wind energy with utility network requires high frequency and voltage stability. There are number of ways in which the synchronous power from wind turbine generators can be achieved [16]. Each method of generating synchronous power from a wind turbine has specific advantages and disadvantages which should be considered at the design stage for a specific application. These methods are summarized in Table 6.2.

INDUCTION GENERATOR MODEL FOR WIND-FARM APPLICATIONS

A variable pitch turbine is able to operate at a good coefficient of performance over a range of wind speed when turbine's angular velocity is fixed. However a variable pitch turbine is much more expensive than a fixed pitch turbine.

Case 4, is a variable speed constant frequency system. Here turbine drives a DC generator which runs a DC motor at synchronous speed. The disadvantage of this system over some other systems is that it requires additional machines hence increasing the cost. Since all this is to be mounted on tower therefore it creates maintenance difficulties.

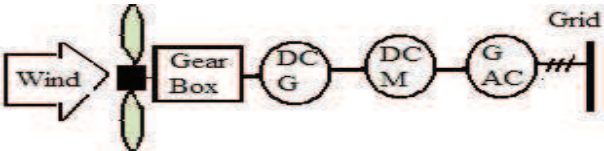
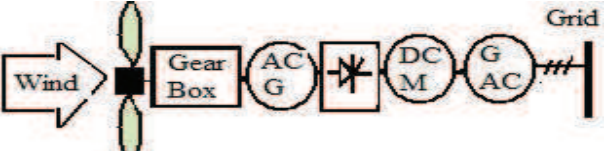

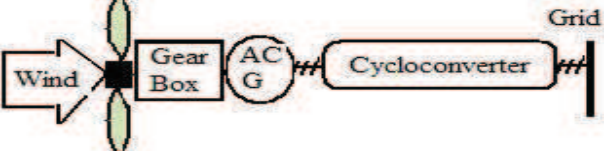
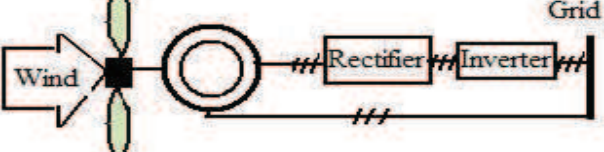
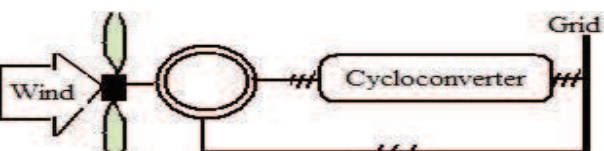
System 5, shows a combination of an AC generator and a rectifier which may be lesser expensive and more reliable compared to system 4. The reliability is very important because maintenance at the top of the tower can be quite hard.

Table 6.2: Techniques for the generation of synchronous power from wind

No	Rotor	Generator	The conversion system
1	Constant speed variable pitch fixed ratio gear box	AC	
2	Constant speed variable pitch two-stage gear box	AC	
3	Constant speed variable pitch variable ratio gear box	AC	
Continued			

INDUCTION GENERATOR MODEL FOR WIND-FARM APPLICATIONS

Table: 6.2, continued from previous page

4	Variable speed fixed pitch	DC generator/ DC motor/ AC generator	
5	Variable speed fixed pitch	AC generator/ Rectifier/ DC motor/ AC generator	
6	Variable speed fixed pitch	AC generator/ Rectifier/ Inverter	
7	Variable speed fixed pitch	Direct AC converter (matrix converter)	
8	Variable speed fixed pitch (Wound rotor)	Induction gen.	
9	Variable speed fixed pitch (Wound rotor)	Induction gen. Cycloconverter in rotor circuit	

INDUCTION GENERATOR MODEL FOR WIND-FARM APPLICATIONS

At No. 6, the conversion of wind turbine output power into DC power by an AC generator and solid state rectifier is shown. The direct current is then converted into AC by an inverter.

Modern solid state inverters became available in 1970s and allowed this system to supply synchronous power from a wind energy system to the electric utility grid. In system 7, the output of AC generator is synchronized in one step to constant frequency constant voltage using a cycloconverter.

Last two cases in the Table 6.2; represent variable speed constant frequency systems where slip ring induction generator has been used. The stator frequency can be maintained constant over a wide speed range if the rotor circuit is supplied with slip frequency voltage. The system can work in sub-synchronous or super-synchronous speeds. In the former case the slip power will subtract from the rotor circuit while in the later case the power is supplied to the rotor [17]. Depending on how converter feeds generator and generator's connection to grid; wind generators can mainly be categorized in three different ways:

- i. Direct drive synchronous generators
- ii. Fixed speed squirrel cage induction generators
- iii. Variable speed double fed (wound-rotor) induction generators

i. Direct drive synchronous generators

The power loss in the gear box accounts for a fairly high proportion of the total system loss, and thus reduces competence [18-19]. For this reason, interest by wind turbine manufacturers is returning to directly driven generators. The weight of the direct drive generators are much higher as expected, than for generators driven through a gear box. In spite of the larger weight and higher cost of the direct drive system, the trend of the wind turbine market shows that the direct drive generators are becoming a favored choice.

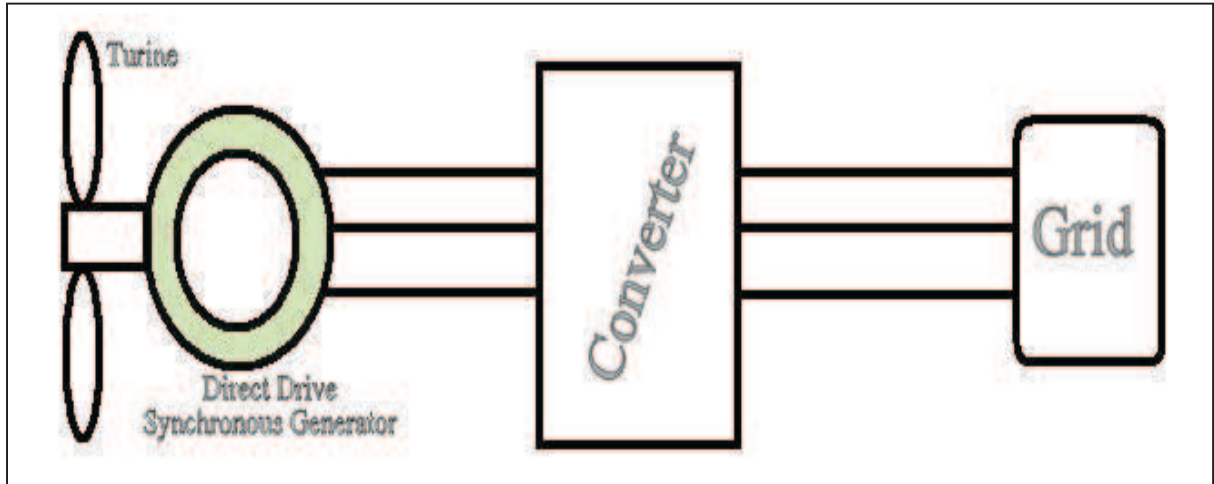


Fig. 6.5: Direct drive synchronous generators

ii. Fixed-speed squirrel cage induction generators

Fixed-speed squirrel cage induction generators do not need the complex and expensive power electronics convertors and are highly efficient. Although these generators undergo high mechanical stresses during variations in wind, they are the simplest therefore have lowest maintenance cost. The rotor speed can not be varied and have very low power factor.

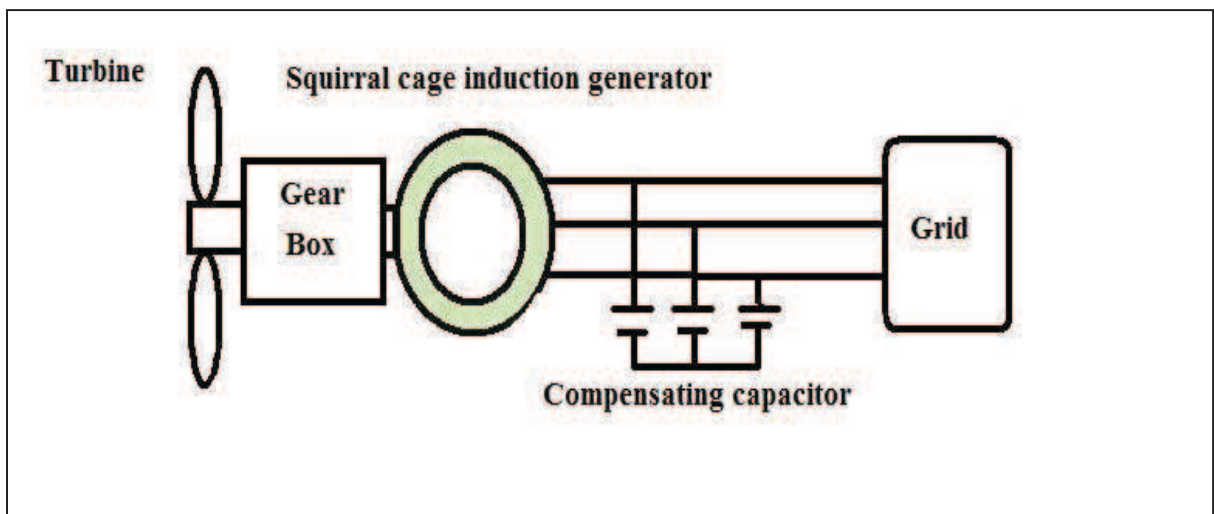


Fig. 6.6: Fixed-speed squirrel cage induction generators

iii. Variable speed double-fed (wound rotor) induction generators

Variable speed induction generators also need a gear box and are less efficient compared fixed-speed counter parts. As discussed in the previous section, because of pole mounted arrangements, such a machine is difficult and inconvenient for maintenance hence expensive. As indicated by the name, since the speed of these generators can be adjusted there fore maximum power output can be achieved at different wind speeds by adjusting the rotor speed.

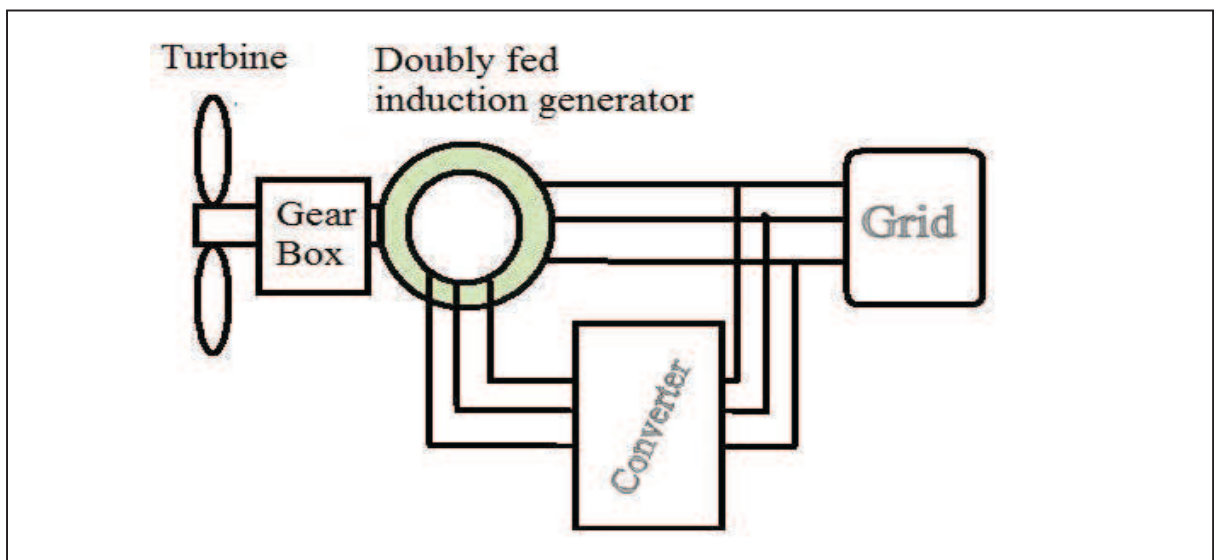


Fig. 6.7: Variable speed double-fed (wound rotor) induction generators

6. Anemometer

Wind turbines need to be steered into the wind direction with the blades controlled according to wind speed to ensure maximum efficiency. To ensure this, an anemometer is placed at the top of wind turbine forming a key control function for the wind turbine. As wind farms are often located on remote areas, it is very important to select an anemometer for the wind turbine that is accurate and reliable with little to no maintenance required.

INDUCTION GENERATOR MODEL FOR WIND-FARM APPLICATIONS

Wind turbines must be protected from ice accumulation. It can make anemometer readings inaccurate and which can cause high structure loads and damage. Latest designed anemometers for wind turbines remain ice free in most freezing weather conditions, with a robust stainless steel construction and the ability to measure a wind speed up to 75 meters per second (nearly 170 miles per hour).

7. Nacelle

A nacelle is a cover housing that houses all of the generating components in a wind turbine, including the generator, gearbox, drive train, and brake assembly. It is usually made of fiberglass that protects the internal components from the environment. The nacelle cover is fastened to the main frame, which also supports all the other components inside the nacelle. The main frames are large metal structures that must be able to withstand large fatigue loads. It also contains the blade pitch control, a hydraulic system that controls the angle of the blades, and the yaw drive, which controls the position of the turbine relative to the wind.

8. Yaw (wind orientation) control

Modern large wind turbines are typically actively controlled to face the wind direction measured by a wind vane situated on the back of the nacelle. By minimizing the yaw angle (the misalignment between wind and turbine pointing direction), the power output is maximized and non-symmetrical loads minimized. However, since the wind direction varies quickly the turbine will not strictly follow the direction and will have a small yaw angle on average.

9. Tower

The floating and land-based towers are used for wind turbines. Wind velocities increase at higher altitudes due to surface aerodynamic drag and the viscosity of the air. The variation in velocity with altitude, called wind shear, is most dramatic near the surface. To avoid buckling, doubling the tower height generally requires doubling the diameter of the tower as well, increasing the amount of material by a factor of at least four. At night

INDUCTION GENERATOR MODEL FOR WIND-FARM APPLICATIONS

time, or when the atmosphere becomes stable, wind speed close to the ground usually subsides whereas at turbine hub altitude it does not decrease that much or may even increase. As a result the wind speed is higher and a turbine will produce more power than expected. Doubling the altitude may increase wind speed by twenty to sixty per cent.

10. Access system

The internal access to the generator and nacelle is through the tower. It is usually a ladder with capability of withstanding small weights. Many times the generation system on the top of the tower has to be accessed externally by a crane or sometimes using a helicopter. Therefore while designing the wind turbine and planning its location, access must be kept in mind

11. Connection to the grid

The main components for the grid connection of the wind turbine are the transformer and the substation with the circuit breaker and the electricity meter inside it. Because of the high losses in low voltage lines, each of the turbines has its own transformer from the voltage level of the wind turbine (400 or 690 V) to the medium voltage line. The transformers are located directly beside the wind turbine to avoid long low-voltage cables. Only for small wind turbine generators, it is possible to connect them directly to the low voltage line of the grid without a transformer or, in a wind farm of small wind turbine, to connect some of the small wind turbine to one transformer.

12. Foundation

The foundations for a conventional engineering structure are designed mainly to transfer the vertical load (dead weight) to the ground, this generally allows for a comparatively unsophisticated arrangement to be used. However in the case of wind turbines, due to the high wind and environmental loads experienced there is a significant horizontal dynamic load that needs to be appropriately restrained.

6.1.3 Modelling of wind turbine

As shown in Fig. 6.6 and Fig. 6.7, for the modeling of the three-phase induction generator coupled to a wind turbine and feeding power to a substation, requires a separate model for the wind turbine. Following is the main procedure which may be adopted for this model. The power available in wind is given by equation 6.1; however, all available wind power (P_{wind}) can not be converted to mechanical power (P_m) by the turbine blades. The power coefficient determines the maximum power that can be extracted from the wind-flow as shown in Fig. 6.1. The power coefficient is given by:

$$C_p = \frac{P_{mechanical}}{P_{wind}} < 59.3\% \quad (6.2)$$

Hence, the actual mechanical power utilized by the wind turbine can be given as:

$$P_{mechanical} = \frac{1}{2} \rho A V^3 C_p \quad (6.3)$$

From manufacturer's curve, one may read the value of tip speed ratio (λ), given against the corresponding wind speed which provides the highest value of power coefficient.

The blade pitch angle (β) can also be determined from manufacturer's provided data for a chosen value of (λ), such that power output of the turbine is maximum. The power coefficient is a function of λ and β [31] and defined as:

$$C_p = C_1 \times \left\{ \frac{C_2}{\lambda_i} - \beta C_3 - C_4 \right\} e^{\left(-\frac{C_5}{\lambda_i} \right)} + C_6 \lambda \quad (6.4)$$

$$\text{where } \lambda_i = \frac{1}{\lambda + 0.08\beta} - \frac{0.035}{\beta^3 + 1} \quad (6.5)$$

The coefficients C_1 through C_6 are constant coefficients, given by $C_1 = 0.5176$, $C_2 = 116$, $C_3 = 0.4$, $C_4 = 5$, $C_5 = 21$ and $C_6 = 0.0068$. The relation between the speed of wind turbine (V_t) and the wind-speed is given by:

$$V_t = \frac{\lambda \times V_{wind}}{r_t} \quad (6.6)$$

where r_t is the radius to the tip of the rotor.

For a known value of the wind speed (V_{wind}), turbine speed can be determined using the manufacturer supplied curves for maximum extraction of wind power. Then exact value of C_p can be calculated with the help of equations 6.4 and equation 6.5. In turn when this value is used (6.6), one can obtain the maximum mechanical power developed by the wind turbine for any particular value of wind speed. See *Appendix V* for the Matlab functions used.

6.2 Induction generator modelling

Induction generator is better suited for isolated location that's why it is widely used in wind-based electricity systems. The induction generator is supplied magnetising current either from a bank of capacitors connected across its terminal or it draws magnetising current from the grid it is connected. If the slip of the generator is zero, the stator draws magnetising from the grid where rotor does not draw any current. When the speed increases slightly above the synchronous speed *emf* and *current* of slip frequency are induced in the rotor conductors. The current in the rotor gives rise to a magnetic field rotating at slip speed relative to the rotor. Thus the rotor *mmf* moves around in the air gap with the same speed as the stator magnetic field, which means that rotor current has line frequency relative to stator and regardless of the magnitude of the slip the primary current has the frequency that correspond to the rotating magnetic field determined by the frequency of the system to which the induction generator is connected.

Fig. 6.8 shows a general per phase equivalent circuit of an induction generator. Hysteresis, Eddy currents, winding and friction losses all are included in R_m . X_m , is the magnetising reactance whereas R_s and R_r are the statotor and rotor resistances respectively. X_s and X_r are the leakage reactances of the stator and rotor respectively. s denotes the slip and R represents the equivalent source of power.

If the generator is to be excited by a bank of capacitors, the bank is connected at terminals otherwise the machine draws magnetising current from the system.

INDUCTION GENERATOR MODEL FOR WIND-FARM APPLICATIONS

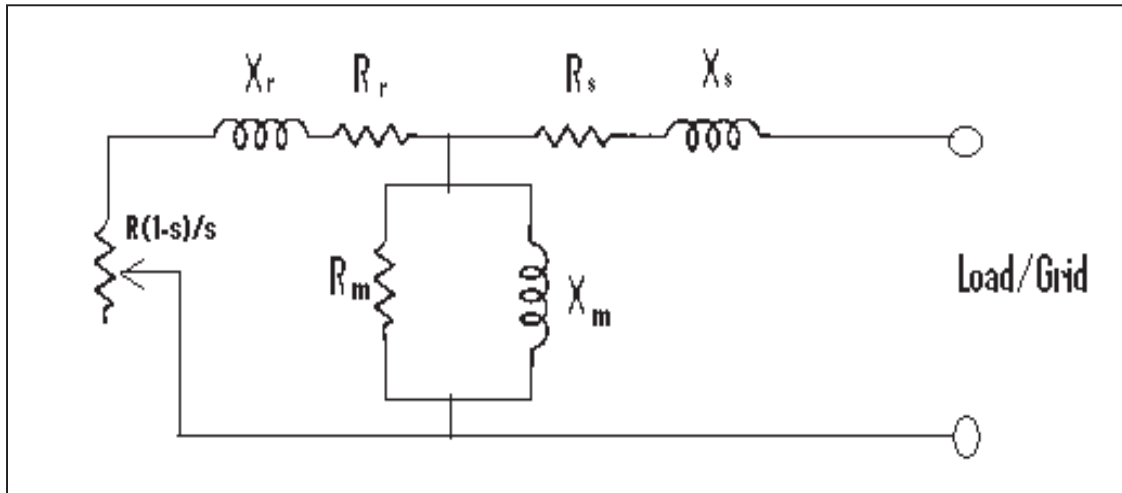


Fig. 6.8: A general per phase equivalent circuit of an induction generator.

Traditional wind turbines are equipped with induction generators. Unfortunately, induction generators require reactive power from the grid to operate and some capacitor compensation is often used. Because reactive power varies with the output power, the capacitor compensation is adjusted as the output power varies. The interactions among the wind turbine, the power network, and the capacitor compensation are important aspects of wind generation.

Self-excitation may occur in a fixed-speed wind turbine equipped with an induction generator. Fixed capacitors are the most commonly used method of reactive power compensation in a fixed-speed wind turbine. Induction generators alone cannot self excite. They require reactive power from the grid to operate normally. The grid dictates the voltage and frequency of the induction generator. Although self-excitation does not occur during normal grid-connected operation, it can occur during off-grid operation.

For instance, if a wind turbine operating in normal mode becomes disconnected from the power line due to a sudden fault or disturbance in the line feeder, the capacitors

INDUCTION GENERATOR MODEL FOR WIND-FARM APPLICATIONS

connected to the induction generator will provide reactive power compensation. However, the voltage and the frequency are determined by the balancing of the systems.

One disadvantage to self-excitation is the safety aspect. Because the generator is still generating voltage, it may compromise the safety of the personnel inspecting or repairing the line or generator. Another disadvantage is that the generator's operating voltage and frequency are determined by the balance between the system's real power and the reactive power. Thus, if sensitive equipment is connected to the generator during self-excitation, the equipment may be subjected to an over or an under voltage and frequency operation.

In spite of the disadvantages of operating the induction generator in self-excitation, some people use self-excitation for dynamic braking to help control the rotor speed during an emergency such as a grid loss condition. Thus, with the proper choice of capacitance and resistor load (to dump the energy from the wind turbine), the wind turbine can be brought to a safe operating speed during grid loss and mechanical brake malfunctions.

In an isolated operation, the conservation of real and reactive power must be preserved. The equation governing the system can be simplified by looking at the impedance or admittance of the induction machine. To operate in an isolated fashion, the total admittance of the induction machine and the rest of the connected load must be zero. The voltage of the system is determined by the flux and frequency of the system. Thus the level of saturation is important in sustaining or collapsing the self-excitation process [20].

Consider the power network, shown in Fig. 6.9. It shows a simple system consisting of a wind turbine, an induction generator, the compensation capacitor, a transformer, locally connected load and a line feeding to a grid.

INDUCTION GENERATOR MODEL FOR WIND-FARM APPLICATIONS

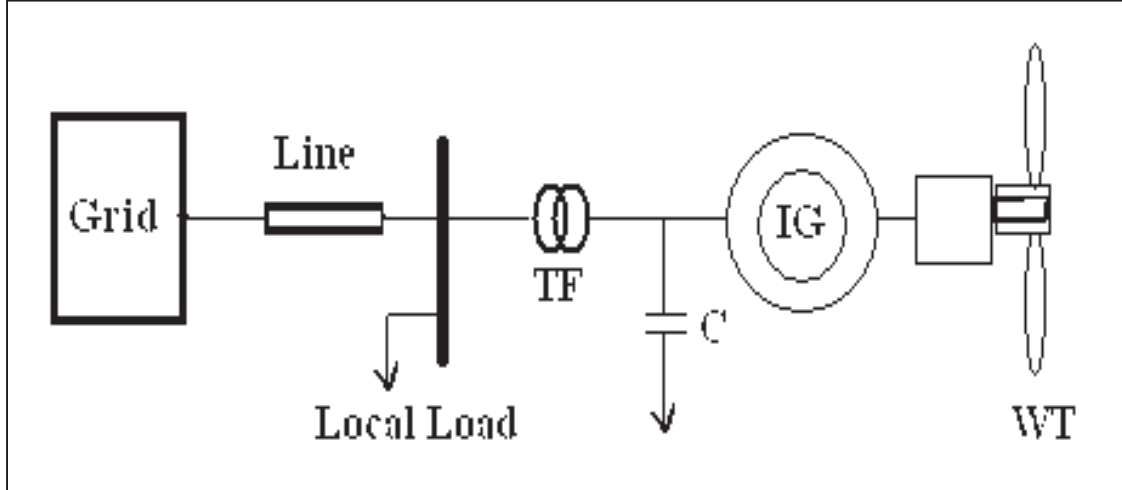


Fig. 6.9: An induction generator feeding to local load and grid.

Fig. 6.10, represents a per phase equivalent circuit of the circuit for harmonic representation of the circuit components. In this circuit representation, the harmonics is denoted with h to indicate the higher harmonics multiples of say 50 Hz. Thus $h=5$ indicates the 5th harmonic (250 Hz). In wind turbine applications, the induction generator, transformer, and capacitors are three phases and either Wye or Delta is connected. Thus, the flow of even harmonics, the third, and its multiples do not exist ($h = 5, 7, 11, 13, 17 \dots$ etc only).

The grid and the line feeder connecting the wind turbine to the substation are represented by a simple Thevenin's equivalent of a larger power system network. Therefore these are represented by a simple RL line. A three-phase transformer with standard impedance is considered. The magnetizing inductance of a large transformer is usually very high compared to the leakage inductance, therefore only the leakage inductance is considered. Assuming the efficiency of the transformer is ninety eight to ninety nine percent at full load, and that the copper losses are equal to the core losses (general assumption for an efficient, large transformer), the winding resistance can be approximated, which is generally very small for an efficient transformer.

INDUCTION GENERATOR MODEL FOR WIND-FARM APPLICATIONS

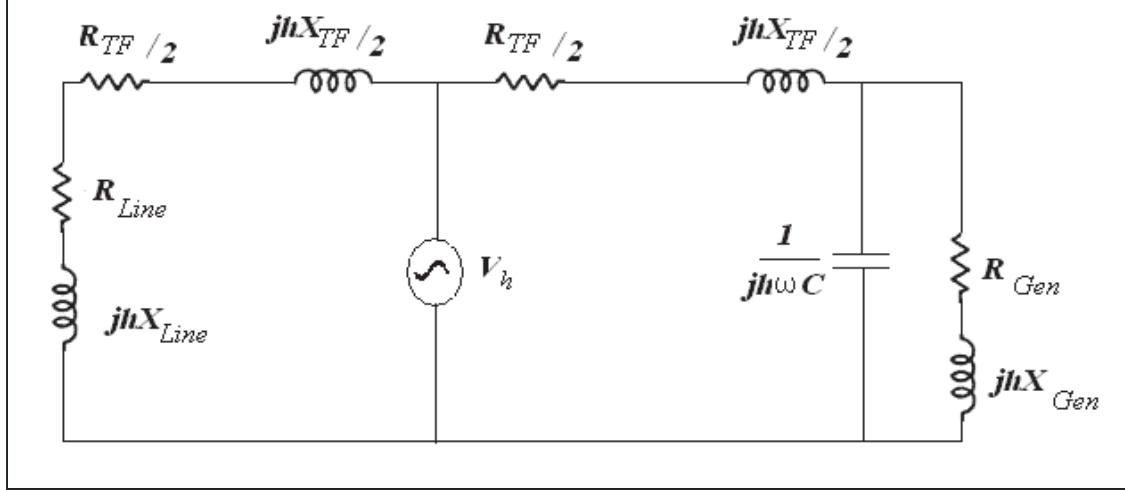


Fig. 6.10: Equivalent circuit for the model system shown in Fig.6.8

The capacitors representing the compensation of the wind turbine are switched capacitors. Although the manufacturer usually set the wind turbine with only a few hundred kVAR for reactive power compensation, the wind turbines are provided with additional reactive power compensation. The wind turbine is compensated at different levels of compensation depending on the level of generation. The capacitor is represented by the capacitance C . In case there are some losses in the capacitor, a resistor may be included in series with the capacitance. As the losses in capacitor are usually very small for a good quality capacitor, the series resistance is not shown in the circuit.

The operating slip of the induction generator at fundamental frequency is around 1%. The slip of induction generator at harmonic frequency can be computed by the relation:

$$S_h = \frac{h\omega_s - h\omega_r}{h\omega_s} \quad (6.7)$$

where S_h = slip for h^{th} harmonics , h = harmonics order , ω_s = synchronous speed of the generator and ω_r = rotor speed of the generator.

INDUCTION GENERATOR MODEL FOR WIND-FARM APPLICATIONS

Thus for higher harmonics (5^{th} and higher) the slip is close to one ($S_h = 1$) and for practical purposes may assumed to be one. From the circuit diagram we can compute the impedance seen by the harmonic source as:

$$Z_h = \frac{\left(Z_{Line} + \frac{1}{2}Z_{TF}\right) \times \left(\frac{1}{2}Z_{TF} + \frac{Z_C Z_{Gen}}{Z_C + Z_{Gen}}\right)}{\left(Z_{Line} + Z_{TF} + \frac{Z_C Z_{Gen}}{Z_C + Z_{Gen}}\right)} \quad (6.8)$$

The admittance can be calculated from the impedance:

$$Y_h = \frac{1}{Z_h} \quad (6.9)$$

The admittance corresponds to the harmonic current for a given harmonic voltage excitation. Because the data in the field only consists of the total harmonic distortion, and does not provide information about individual harmonics, one can only compare the trends shown by the admittance. When the size of the capacitor compensation is increased, the circuit admittance or the total harmonic distortion shows resonance at different higher harmonics. The circuit will resonate at different higher harmonics when that particular harmonics presents or excites the circuit.

The source of harmonics can be traced back from the saturation level of the magnetizing branch of the transformer, creating a nonlinear magnetizing inductance and a distorted line current. The deviation of the line current from sinusoidal wave shape may excite the harmonics circuit created by the combination of line inductances and capacitance of the capacitor compensation in the collector system network. There are many others sources of harmonics and issues related to power quality that need to be address such as flicker, faults, start-up transients etc., but, this chapter is confined only to harmonics.

The voltage at each turbine within the wind power plant varies independently because of the difference in wind speeds, the line impedances, and compensations among the wind turbines. However, the most important point is the point of common coupling (PCC) that provides a gateway for the wind power plant to the real world. The reactive power

INDUCTION GENERATOR MODEL FOR WIND-FARM APPLICATIONS

compensation affects the voltage behavior of a very large area consisting of many wind power plants. When studying a relatively large wind power plant the plant as a single turbine can not be represented. A very large wind power plant should be represented by groups of wind turbines representing its unique characteristics with respect to the location, the type of turbines, the control setting, and the line impedance.

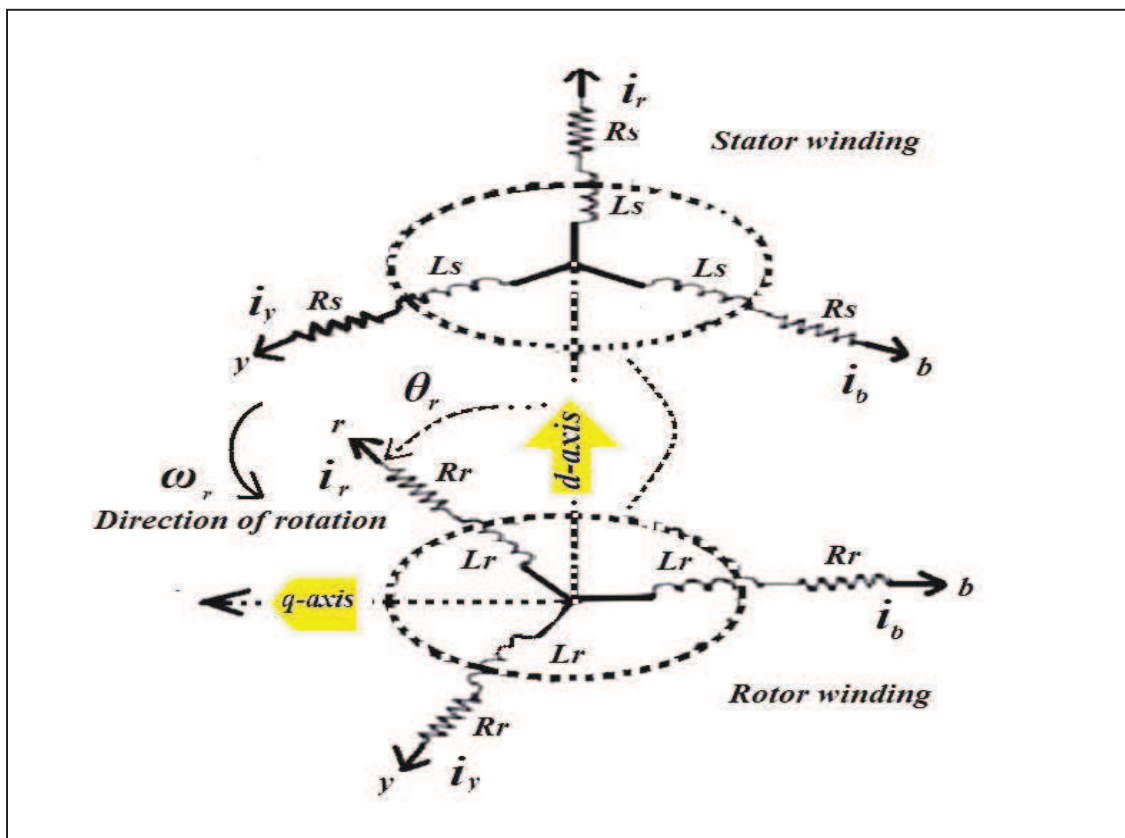


Fig. 6.11: Relative position of rotor and stator in an induction machine.

Fig. 6.11 shows the relative position of rotor and stator in an induction generator. This model [21] is based on following assumptions:

- The air-gap between rotor and stator is uniform
- The windings of rotor and stator are balanced and with sinusoidal mmf
- Inductance and rotor position is sinusoidal

INDUCTION GENERATOR MODEL FOR WIND-FARM APPLICATIONS

- Saturation and parameter changes are neglected

In terms of flux linkages, the 3-phase stator terminal voltages (V_{as} , V_{bs} , V_{cs}) are given as:

$$V_{as} = -i_{as}R_s + \frac{d\lambda_{as}}{dt} \quad (6.10)$$

$$V_{bs} = -i_{bs}R_s + \frac{d\lambda_{bs}}{dt} \quad (6.11)$$

$$V_{cs} = -i_{cs}R_s + \frac{d\lambda_{cs}}{dt} \quad (6.12)$$

Similarly, the rotor voltages (V_{ar} , V_{br} , V_{cr}) in terms of flux linkages are given by:

$$V_{ar} = i_{ar}R_s + \frac{d\lambda_{ar}}{dt} \quad (6.13)$$

$$V_{br} = i_{br}R_s + \frac{d\lambda_{br}}{dt} \quad (6.14)$$

$$V_{cr} = i_{cr}R_s + \frac{d\lambda_{cr}}{dt} \quad (6.15)$$

The flux linkages are given by following matrix equation in terms of stator and rotor winding [22]:

$$\begin{bmatrix} \lambda_s^{abc} \\ \lambda_r^{abc} \end{bmatrix} = \begin{bmatrix} L_{ss}^{abc} & L_{sr}^{abc} \\ L_{rs}^{abc} & L_{rr}^{abc} \end{bmatrix} \begin{bmatrix} i_s^{abc} \\ i_r^{abc} \end{bmatrix} \quad \text{Wb.Turn} \quad (6.16)$$

where

$$[\lambda_s^{abc}] = \begin{bmatrix} \lambda_{as} \\ \lambda_{bs} \\ \lambda_{cs} \end{bmatrix}; [\lambda_r^{abc}] = \begin{bmatrix} \lambda_{ar} \\ \lambda_{br} \\ \lambda_{cr} \end{bmatrix} \quad (6.17)$$

and

$$[i_s^{abc}] = \begin{bmatrix} i_{as} \\ i_{bs} \\ i_{cs} \end{bmatrix}; [i_r^{abc}] = \begin{bmatrix} i_{ar} \\ i_{br} \\ i_{cr} \end{bmatrix} \quad (6.18)$$

INDUCTION GENERATOR MODEL FOR WIND-FARM APPLICATIONS

The sub matrices of self and mutual inductances of stator to stator and rotor to rotor given by the following matrix equation:

$$[L_{ss}^{abc}] = \begin{bmatrix} L_s + L_{ss} & L_{sm} & L_{sm} \\ L_{sm} & L_s + L_{ss} & L_{sm} \\ L_{sm} & L_{sm} & L_s + L_{ss} \end{bmatrix} \quad (6.19)$$

$$[L_{rr}^{abc}] = \begin{bmatrix} L_r + L_{rr} & L_{rm} & L_{rm} \\ L_{rm} & L_r + L_{rr} & L_{rm} \\ L_{rm} & L_{rm} & L_r + L_{rr} \end{bmatrix} \quad (6.20)$$

In equation set (6.19-20), L_s is per phase stator winding leakage inductance, L_{ss} is stator winding self inductance, L_{sm} is mutual inductance between two stator windings, L_r is per phase rotor winding leakage inductance, L_{rr} is rotor winding self inductance and L_{rm} is mutual inductance between two stator windings. The mutual inductances from stator to rotor are dependant on rotor angle i.e.

$$[L_{sr}^{abc}] = [L_{rs}^{abc}] = \begin{bmatrix} \cos \theta_r & \cos \left(\theta_r + \frac{2\pi}{3} \right) & \cos \left(\theta_r - \frac{2\pi}{3} \right) \\ \cos \left(\theta_r - \frac{2\pi}{3} \right) & \cos \theta_r & \cos \left(\theta_r + \frac{2\pi}{3} \right) \\ \cos \left(\theta_r + \frac{2\pi}{3} \right) & \cos \left(\theta_r - \frac{2\pi}{3} \right) & \cos \theta_r \end{bmatrix} \quad (6.21)$$

6.2.1 Reference frame transformation of induction generator

The two most frequently used reference frames for induction machines are the stationery reference frame and the synchronous rotating reference frames. Both reference frames have associated advantages. In a stationery reference frame dq variables used are the same as those used for the supply network where as in the synchronous rotating frame of reference the dq variables are steady in steady-state. This is an important factor when deriving the small signal model about a selected operating point.

The synchronous reference frame can be determined by substituting ω with ω_s , the synchronous angular speed after developing a model in an arbitrary rotating reference frame, ω is arbitrary speed of rotation [23]. By applying a transformation, T , for transformation of three phase variables abc to two axis $qd0$ reference frame rotating at , the relation for the variables becomes:

$$\begin{bmatrix} f_q \\ f_d \\ f_0 \end{bmatrix} = [T_{qdo}(\theta)] \begin{bmatrix} f_a \\ f_b \\ f_c \end{bmatrix} \quad (6.22)$$

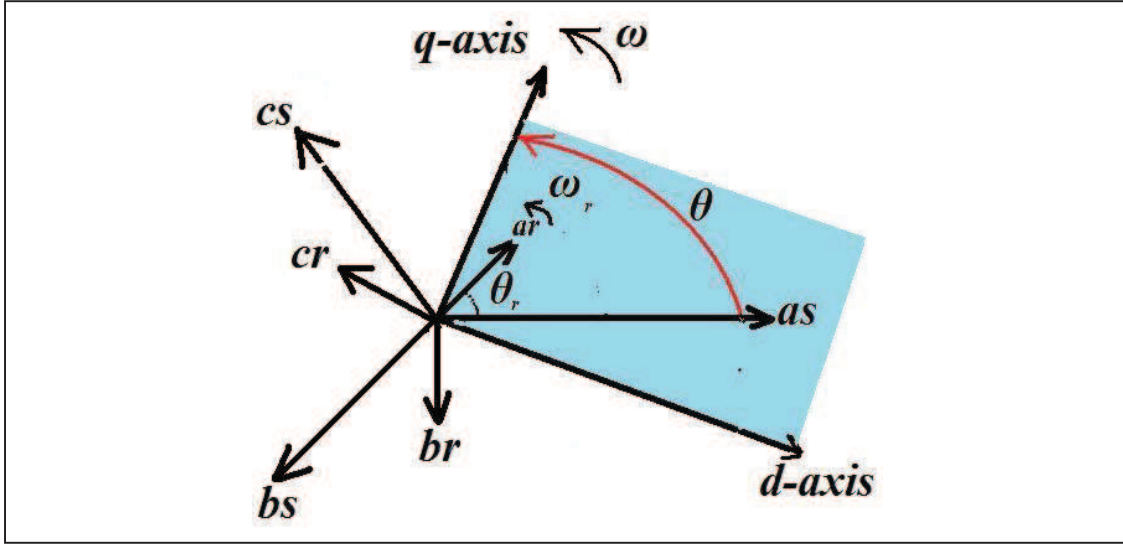


Fig. 6.12: Transformation of reference frame in an induction machine

In equation (6.22), f can be any of phase voltages, flux linkages or currents. The transformation angle(θ_t), is given by:

$$\theta_t = \int_0^t \omega_{(t)} dt + \theta(0) \quad (6.23)$$

Similarly, the rotor angle θ_r , between the axes of the stator and the rotor's a-phases, for a rotor rotating with speed ω_r , can be given as:

$$\theta_r = \int_0^t \omega_{r(t)} dt + \theta_r(0) \quad (6.24)$$

In equations (6.23) and (6.24), $\theta(0)$ and $\theta_r(0)$ respectively are the initial values of the angles at the beginning of time t . Resolving the sum of components of phase variables ($f(a, b, c)$) on q and d axes, the transformation matrix ($[T_{qdo}(\theta)]$) is given by following equation:

$$[T_{qdo}(\theta)] = \begin{bmatrix} \cos \theta & \cos(\theta - 2\pi/3) & \cos(\theta + 2\pi/3) \\ \sin \theta & \sin(\theta - 2\pi/3) & \sin(\theta + 2\pi/3) \\ 1/2 & 1/2 & 1/2 \end{bmatrix} \quad (6.25)$$

The inverse is given by:

$$[T_{qd0(\theta)}]^{-1} = \begin{bmatrix} \cos \theta & \sin \theta & 1 \\ \cos(\theta - 2\pi/3) & \sin(\theta - 2\pi/3) & 1 \\ \cos(\theta + 2\pi/3) & \sin(\theta + 2\pi/3) & 1 \end{bmatrix} \quad (6.26)$$

Equation set (6.10-6.12) can be summarised in matrix form for the stator voltages as:

$$V_s^{abc} = p\lambda_s^{abc} - R_s^{abc} R_s^{abc} \quad (6.27)$$

Where $p = d/dt$. Applying transformation $[T_{qd0(\theta)}]$, to the voltage, flux linkage and current; the equation (6.27) becomes:

$$V_s^{qd0} = [T_{qd0(\theta)}] p [T_{qd0(\theta)}]^{-1} [\lambda_s^{abc}] - [T_{qd0(\theta)}] r_s^{abc} [T_{qd0(\theta)}]^{-1} [i_s^{qd0}] \quad (6.28)$$

The time derivative term ($p [T_{qd0(\theta)}]^{-1} [\lambda_s^{abc}]$) in equation (6.28) is given by:

$$p [T_{qd0(\theta)}]^{-1} [\lambda_s^{abc}] = \begin{bmatrix} -\sin \theta & \cos \theta & 0 \\ -\sin(\theta - 2\pi/3) & \cos(\theta - 2\pi/3) & 0 \\ \sin(\theta + 2\pi/3) & \cos(\theta + 2\pi/3) & 0 \end{bmatrix} \frac{d\theta}{dt} \lambda_s^{qd0} + [T_{qd0(\theta)}]^{-1} [p\lambda_s^{dq0}] \quad (6.29)$$

Replacing the term $p [T_{qd0(\theta)}]^{-1} [\lambda_s^{abc}]$ in equation (6.28) with right hand side of equation (6.29) and rearranging, gives the expression for stator voltage in $qd0$ frame of reference as:

$$V_s^{qd0} = \omega \begin{bmatrix} 0 & 1 & 0 \\ -1 & 0 & 0 \\ 0 & 0 & 0 \end{bmatrix} \lambda_s^{qd0} + p\lambda_s^{qd0} - R_s^{qd0} i_s^{qd0} \quad (6.30)$$

where

$$p = \frac{d}{dt}, \quad \omega = \frac{d\theta}{dt}, \quad \text{and} \quad R_s^{qd0} = \begin{bmatrix} 1 & 0 & 0 \\ 0 & 1 & 0 \\ 0 & 0 & 1 \end{bmatrix}$$

The rotor phase quantities $f(a, b, c)$, can be transformed using transformation angle $(\theta - \theta_r)$. With $T_{qd0(\theta-\theta_r)}$ transformation, the rotor's voltage equations may be transformed into $qd0$ reference frame voltage equations as follows:

$$V_r^{qd0} = (\omega - \omega_r) \begin{bmatrix} 0 & 1 & 0 \\ -1 & 0 & 0 \\ 0 & 0 & 0 \end{bmatrix} \lambda_r^{qd0} + p\lambda_r^{qd0} + R_r^{qd0} i_r^{qd0} \quad (6.31)$$

6.2.2 Flux linkages

The flux linkages of stator are obtained by multiplying transformation matrix $[T_{qd0(\theta)}]$ to the phase quantities of flux linkages as follows:

$$\lambda_s^{qd0} = [T_{qd0(\theta)}][L_s^{abc} i_s^{abc} + L_{sr}^{abc} i_r^{abc}] \quad (6.32)$$

Using the inverse transformation to replace the abc stator currents by respective $qd0$ currents, the above equation becomes:

$$\begin{aligned} \lambda_s^{qd0} &= [T_{qd0(\theta)}] L_s^{abc} [T_{qd0(\theta)}]^{-1} i_s^{qd0} + [T_{qd0(\theta)}] L_{sr}^{abc} [T_{qd0(\theta-\theta_r)}]^{-1} i_r^{qd0} \\ &= \begin{bmatrix} L_{ls} + \frac{3}{2} L_{ss} & & \\ & L_{ls} + \frac{3}{2} L_{ss} & \\ & & L_{ls} + \frac{3}{2} L_{ss} \end{bmatrix} i_s^{qd0} + \begin{bmatrix} L_{ls} + \frac{3}{2} L_{ss} & & \\ & L_{ls} + \frac{3}{2} L_{ss} & \\ & & L_{ls} + \frac{3}{2} L_{ss} \end{bmatrix} i_r^{qd0} \end{aligned} \quad (6.34)$$

Where L_{ls} and L_{ss} , respectively are leakage and self inductances of the stator. Similarly the flux linkages for rotor are given as:

$$\begin{aligned} \lambda_r^{qd0} &= [T_{qd0(\theta-\theta_r)}] L_{rs}^{abc} [T_{qd0(\theta)}]^{-1} i_s^{qd0} + [T_{qd0(\theta-\theta_r)}] L_{rr}^{abc} [T_{qd0(\theta-\theta_r)}]^{-1} i_r^{qd0} \\ &= \begin{bmatrix} \frac{3}{2} L_{sr} & 0 & 0 \\ 0 & \frac{3}{2} L_{sr} & 0 \\ 0 & 0 & 0 \end{bmatrix} i_s^{qd0} + \begin{bmatrix} L_{lr} + \frac{3}{2} L_{rr} & & \\ & L_{lr} + \frac{3}{2} L_{rr} & \\ & & L_{lr} + \frac{3}{2} L_{rr} \end{bmatrix} i_r^{qd0} \end{aligned} \quad (6.35)$$

In equation (6.36), L_{lr} and L_{rr} , leakage and self inductances of the rotor. The relationship for the flux linkage between stator and rotor can be expressed as:

$$\begin{bmatrix} \lambda_{qs} \\ \lambda_{ds} \\ \lambda_{0s} \\ \lambda'_{qr} \\ \lambda'_{dr} \\ \lambda'_{0r} \end{bmatrix} = \begin{bmatrix} L_{sr} + L_m & & & & & \\ & L_{sr} + L_m & & & & \\ & & L_{sr} + L_m & & & \\ & & & L'_{sr} + L_m & & \\ & & & & L'_{sr} + L_m & \\ & & & & & L'_{sr} + L_m \end{bmatrix} \begin{bmatrix} i_{qs} \\ i_{ds} \\ i_{0s} \\ i'_{qr} \\ i'_{dr} \\ i'_{0r} \end{bmatrix} \quad (6.37)$$

INDUCTION GENERATOR MODEL FOR WIND-FARM APPLICATIONS

For a balanced machine, equation (6.37) may be reduced to

$$\begin{bmatrix} \lambda_{qs} \\ \lambda_{ds} \\ \lambda'_{qr} \\ \lambda'_{dr} \end{bmatrix} = \begin{bmatrix} L_{sr} + L_m & & & \\ & L_{sr} + L_m & & \\ & & 0 & \\ & & & L'_{sr} + L_m \\ & & & & L'_{sr} + L_m & \\ & & & & & 0 \end{bmatrix} \begin{bmatrix} i_{qs} \\ i_{ds} \\ i'_{qr} \\ i'_{dr} \end{bmatrix} \quad (6.38)$$

In above equations, different rotor variables referred to stator according to following relations:

$$\lambda'_{qr} = \frac{N_s}{N_r} \lambda_{qr}, \quad \lambda'_{dr} = \frac{N_s}{N_r} \lambda_{dr}, \quad i'_{qr} = \frac{N_r}{N_s} i_{qr}, \quad i'_{dr} = \frac{N_r}{N_s} i_{dr} \text{ and } L'_{lr} = \left(\frac{N_s}{N_r}\right)^2 L_{lr}$$

The magnetizing inductance on the stator side is given as:

$$L_m = \frac{3}{2} L_s = \frac{3}{2} \frac{N_s}{N_r} L_{sr} = \frac{3}{2} \frac{N_s}{N_r} L_{rr} \quad (6.39)$$

6.2.3 Equations of an induction machine in arbitrary reference frame

$$V_{qs} = -R_s i_{qs} + \omega \lambda_{ds} + \frac{d\lambda_{qs}}{dt} \quad (6.40)$$

$$V_{ds} = -R_s i_{ds} + \omega \lambda_{qs} + \frac{d\lambda_{ds}}{dt} \quad (6.41)$$

$$V_{0s} = -R_s i_{0s} + \frac{d\lambda_{0s}}{dt} \quad (6.42)$$

With rotor values referred to stator (primed variables in above equations), following equations may be written:

$$V'_{qr} = \frac{d}{dt} \lambda'_{qr} + (\omega - \omega_r) \lambda'_{dr} + R_r i'_{qr} \quad (6.43)$$

$$V'_{dr} = \frac{d}{dt} \lambda'_{dr} + (\omega - \omega_r) \lambda'_{qr} + R_r i'_{dr} \quad (6.44)$$

$$V'_{0r} = \frac{d}{dt} \lambda'_{0r} + R_r i'_{0r} \quad (6.45)$$

6.2.4 Induction machine in synchronous rotating reference frame

Substituting ω by ω_s , in above stated arbitrary rotor and stator equations (6.40-45), the following synchronous rotating frame stator and rotor equations are derived [24-25].

$$V_{qs} = -R_s i_{qs}^e + \omega_s \lambda_{ds}^e + \frac{d}{dt} \lambda_{qs}^e \quad (6.46)$$

$$V_{ds} = -R_s i_{ds}^e - \omega_s \lambda_{qs}^e + \frac{d}{dt} \lambda_{ds}^e \quad (6.47)$$

$$V_{0s} = -R_s i_{0s}^e + \frac{d}{dt} \lambda_{0s}^e \quad (6.48)$$

Similarly for rotor

$$\begin{aligned} V_{qr}' &= \frac{d}{dt} \lambda_{qr}'^e + (\omega_s - \omega_r) \lambda_{dr}'^e + R_r i_{qr}'^e \\ &= \frac{d}{dt} \lambda_{qr}'^e + S(\omega_s) \lambda_{dr}'^e + R_r i_{qr}'^e \end{aligned} \quad (6.49)$$

$$\begin{aligned} V_{dr}' &= \frac{d}{dt} \lambda_{dr}'^e - (\omega_s - \omega_r) \lambda_{qr}'^e + R_r i_{dr}'^e \\ &= \frac{d}{dt} \lambda_{dr}'^e - S(\omega_s) \lambda_{qr}'^e + R_r i_{dr}'^e \end{aligned} \quad (6.50)$$

$$V_{0r}' = \frac{d}{dt} \lambda_{0r}'^e + R_r i_{0r}'^e \quad (6.51)$$

Equation (6.48) and equation (6.51) can be neglected for a balanced machine. The relationship amongst different variables can be symbolized by the circuit diagrams shown in Fig. 6.13, where $\psi = \lambda$ = flux linkage and $\omega = \omega_s$ represents the synchronous angular speed, V is the voltage, ψ is the flux, the subscripts q and d for quadrature and direct axis and subscripts r and s represent rotor and stator currents respectively.

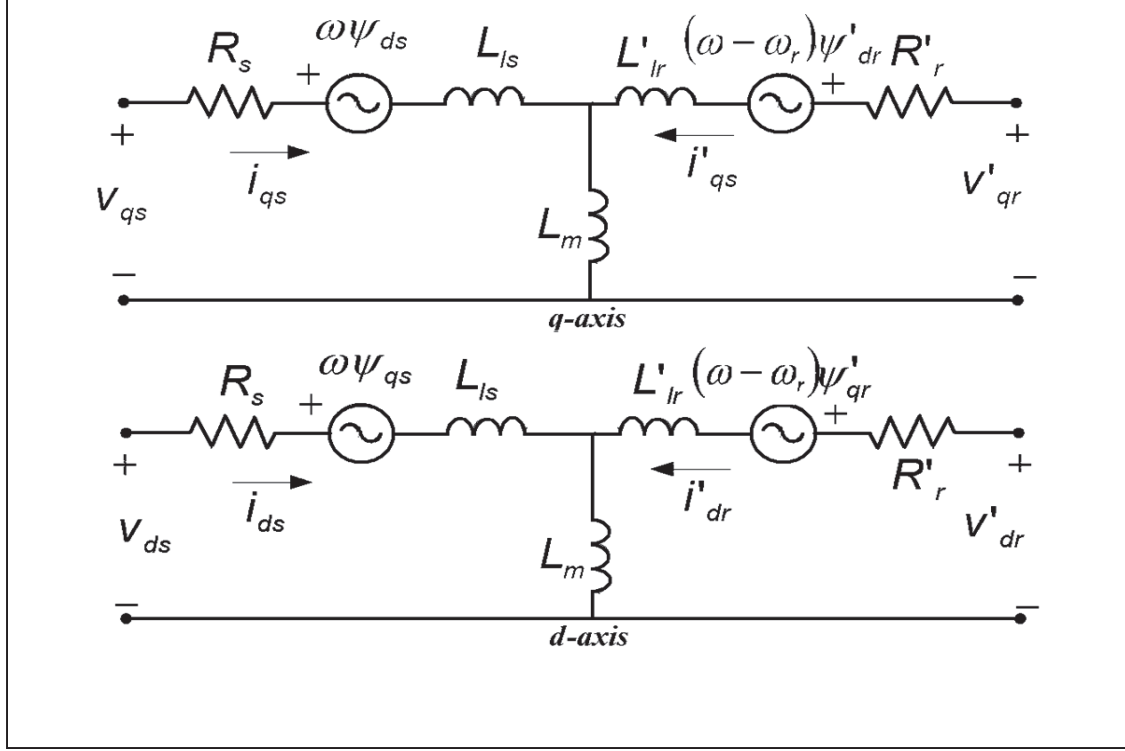


Fig. 6.13: Induction generator in synchronous rotating frame

6.2.5 The dynamic equations of induction generator

As mentioned earlier, for a balanced squirrel cage induction machine in synchronous rotating frame the zero sequence voltages can be neglected [27-30]. Dropping the primes from the equation set (6.46-51), neglecting the zero sequence voltages and rearranging these equations:

$$V_{qs} = \frac{d}{dt} \lambda_{qs} + \omega_s \lambda_{ds} - R_s i_{qs} \quad (6.52)$$

$$V_{ds} = \frac{d}{dt} \lambda_{ds} - \omega_s \lambda_{qs} - R_s i_{ds} \quad (6.53)$$

And for rotor

$$V_{qr} = \frac{d}{dt} \lambda_{qr} + S(\omega_s) \lambda_{dr} + R_r i_{qr} \quad (6.54)$$

$$V_{dr} = \frac{d}{dt} \lambda_{dr} - S(\omega_s) \lambda_{qr} + R_r i_{dr} \quad (6.55)$$

INDUCTION GENERATOR MODEL FOR WIND-FARM APPLICATIONS

In equation set (6.52-55), the flux linkages can be given in terms of currents and inductances as below:

$$\lambda_{ds} = -L_s i_{ds} + L_m i_{dr} \quad (6.56)$$

$$\lambda_{qs} = -L_s i_{qs} + L_m i_{qr} \quad (6.57)$$

$$\lambda_{dr} = L_r i_{dr} - L_m i_{ds}$$

$$\text{or} \quad i_{dr} = \frac{\lambda_{dr} + L_m i_{ds}}{L_r} \quad (6.58)$$

$$\lambda_{qs} = L_r i_{qs} - L_m i_{ds}$$

$$\text{or} \quad i_{dr} = \frac{\lambda_{dr} + L_m i_{ds}}{L_r} \quad (6.59)$$

6.2.6 The model

An induction generator is either delta or ungrounded star connected, which means under balanced conditions there is not any zero sequence current flow. The positive and negative sequence equivalent circuit of the generator is shown in Fig. 6.14. All the rotor side parameters are referred to the stator side. The parameters R_s and R_r are stator and rotor resistances, L_{sl} and L_{rl} are the stator and rotor leakage inductances, L_m is the magnetizing inductance, and ω_s and ω_r are the synchronous and rotor angular speeds. The sequence machine slip s , is the slip of the machine during normal operating conditions and $s_i = s_{0,1,2}$ corresponds to the respective sequence component.

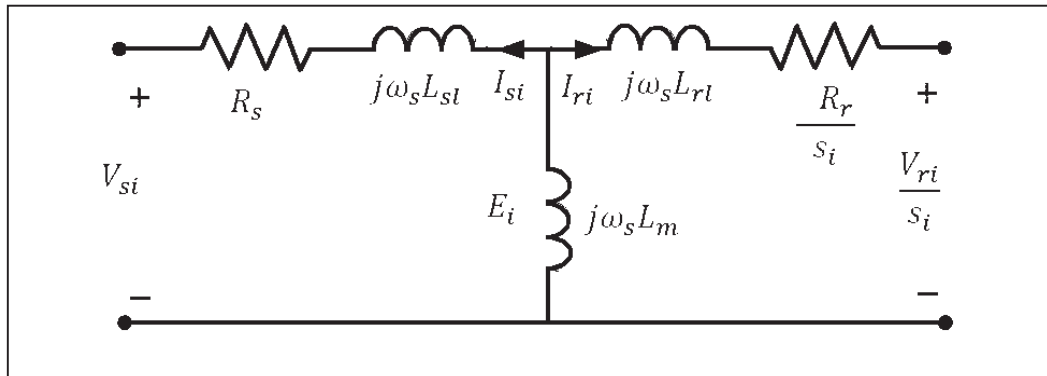


Fig. 6.14: A steady state equivalent circuit of a wound rotor induction machine

INDUCTION GENERATOR MODEL FOR WIND-FARM APPLICATIONS

The zero, positive and negative sequence slip values of the machine are given as [32]:

$$s_{0,1,2} = \begin{bmatrix} s_0 \\ s_1 \\ s_2 \end{bmatrix} = \begin{bmatrix} 0 \\ s \\ 2-s \end{bmatrix} = \begin{bmatrix} 0 \\ \frac{1}{\omega_s}(\omega_s - \omega_r) \\ \frac{1}{\omega_s}(\omega_s + \omega_r) \end{bmatrix} \quad (6.60)$$

For each sequence network, at the stator frequency, the impedances are given as:

$$\text{Stator} \quad Z_{s_{0,1,2}} = R_s + j\omega_s L_{sl} \quad (6.61)$$

$$\text{Rotor} \quad Z_{r_{0,1,2}} = \frac{R_r}{s_{0,1,2}} + j\omega_s L_{sr} \quad (6.62)$$

$$\text{Magnetization} \quad Z_{m_{0,1,2}} = j\omega_s L_{sm} \quad (6.63)$$

The induced voltage for respective sequence can be calculated using the nodal equation as:

$$E_{0,1,2} = \frac{\left(\frac{V_{s_{0,1,2}}}{Z_{s_{0,1,2}}}\right) + \left(\frac{V_{r_{0,1,2}/s_{0,1,2}}}{Z_{r_{0,1,2}}}\right)}{(1/Z_{s_{0,1,2}} + 1/Z_{r_{0,1,2}} + 1/Z_{m_{0,1,2}})} \quad (6.64)$$

The stator and rotor currents are calculated by:

$$I_{s_{0,1,2}} = \frac{V_{s_{0,1,2}} - E_{0,1,2}}{Z_{s_{0,1,2}}} \quad \text{And} \quad I_{r_{0,1,2}} = \frac{(V_{r_{0,1,2}/s_{0,1,2}} - E_{0,1,2})}{Z_{r_{0,1,2}}} \quad (6.65)$$

The real power flow at the rotor frequency, through the rotor slip-rings is $P_{r_{0,1,2}}$ which may be calculated as:

$$P_{r_{0,1,2}} = \text{real}\{V_{r_{0,1,2}} \cdot I_{r_{0,1,2}}^*\} \quad (6.66)$$

The stator's power can also be calculated by the similar relation using corresponding values of voltage and current. With the help of wind turbine model presented in section 6.1 and using the procedure demonstrated by equation set 6.60-66, the state of an induction generator can be determined whether it is operating under the steady state condition or not. The sequence quantities can then be transformed into actual phase quantities using reference frame transformation.

A Matlab programme is given in *Appendix V* for the induction generator model, the compiled results are summarized in the Table 6.3. The model uses the machine

INDUCTION GENERATOR MODEL FOR WIND-FARM APPLICATIONS

parameters and wind turbine data given in reference [34] with minor changes for simplicity.

Table 6.3: Results of induction generator model

Turbine	Stator	Rotor
Speed of wind = 15 m/s	$V_a = 1385 + j25.05$	$V_a = 37.03 - j40.33$
$\omega_r = 157.08$ rad/s	$V_b = -671.0 - j1212.3$	$V_b = -53.27 - j11.91$
$\beta = 0.200$	$V_c = -714.4 + j1187.3$	$V_c = 16.24 + j52.23$
$\lambda_i = 11.301$	$I_a = 66.97 - j3739.1$	$I_a = -55.52 + j3677.8$
$C_1 = 0.5176$	$I_b = -3271.7 + j1927.4$	$I_b = 3212.8 - j1791.0$
$C_2 = 116$	$I_c = 3204.7 + j1927.4$	$I_c = -3157.3 - j1886.8$
$C_3 = 0.4$	$P_a = -900.8403$	$P_a = -1.5038e5$
$C_4 = 5$	$P_b = -1070.7$	$P_b = -1.4982e5$
$C_5 = 21$	$P_c = -1086.5$	$P_c = -1.4982e5$
$C_6 = 0.0068$	$Q_a = 5.2e6$	$Q_a = -1.3396e5$
$C_p = 0.4736$	$Q_b = 5.2e6$	$Q_b = -1.3365e5$
Power = -2.1323e+006	$Q_c = 5.2e6$	$Q_c = -1.3429e5$

The VSC model has been ignored here but this does not effect the over all generator model. The wind turbine model receives the wind speed, pitch angle and generator speed as inputs and in turn computes and applies mechanical power to the rotor shaft of the induction generator.

6.3 Summary

This chapter starts with an introduction to the history and fundamentals of wind based electrical power, and also gives a comparison between the different types of wind turbines. The main parts of wind-generator and the essential controls are outlined. Possible methods to obtain synchronous power from the wind are discussed. Based on the manufacturers provided data, the wind speed (V_{wind}), the power coefficient (C_p), the tip

speed ratio (λ) and the blade pitch angle (β), an efficient algorithm is developed to determine the input mechanical power provided by a wind turbine.

A new three-phase model of an induction generator has been derived for a wind-based electrical power system. The model includes the wind turbine model as a sub model and has the compatibility with an unbalanced three-phase distribution system. The model also covers the analytical representation of its major components, mainly the wind turbine and the wound-rotor induction generator. The set of nonlinear equations has been used in the model for the active and the reactive power introduced at the point of common coupling (PCC). This induction generator model may be used in an iteration based load flow algorithm and provides a new path to determining the harmonic analysis of wind based distribution systems.

6.4 References

- [1] J. F. Walker and N. Jenkins; “Wind Energy Technology”, John Wily and Sons, 1997
- [2] J. Musgrove; “Wind energy conversion and introduction”, IEE, Proceedings, vol. 130, no. 9, pp. 506-517, 1983
- [3] World Wind Energy Association (WWEA), “World Wind Energy Report 2009”
- [4] Cristina L. Archer; Mark Z. Jacobson.: “Evaluation of global wind power” Journal of Geophysical Research, vol. 110, D12110, doi: 10.1029/2004JD005462, 2005
- [5] Xuan Liu; Bin Su: “Microgrids – “An Integration of Renewable Energy Technologies” IEEE, International Conference on Electricity Distribution, pp: 1-7, 2008
- [6] Dr. Gary L. Johnson; “Wind Energy System”, Prentice-Hall, 2001. © Dr. Gary L. Johnson. (The book is available free in pdf), 2001

INDUCTION GENERATOR MODEL FOR WIND-FARM APPLICATIONS

- [7] P. Gipe; “Wind Energy Comes of Age”, JW & Sons, 1995
- [8] Alan T. Zehnder and Zellman Warhaft, July 2011. ([http:// www.sustainablefuture. cornell.edu/](http://www.sustainablefuture.cornell.edu/)). Cornell University Atkinson Center for a Sustainable Future. Link visited 27/02/2012
- [9] Jamieson, P. “Innovation in Wind Turbine Design”, John *Wiley & Sons*, 2011
- [10] Kroo, I. NASA Green Aviation Summit ([http:// www. aeronautics. nasa. gov/pdf/ 23_kroo_green_aviation_summit. pdf](http://www.aeronautics.nasa.gov/pdf/23_kroo_green_aviation_summit.pdf)) p9, *NASA*, September 2010. Visited: 27/02/ 2012
- [11] Anatomy of an Enercon direct drive wind turbine ([http:// www. wwindea. org](http://www.wwindea.org)), link visited 27/02/2012
- [12] Fairly, P. “Wind Turbines Shed Their Gears” ([http:// www. technologyreview. com/ energy/ 25188/](http://www.technologyreview.com/energy/25188/)) *Technology Review*, 27 April 2010, link visited 27/02/2012
- [13] S. Wittrup; First Siemens gearless ([http:// ing. dk/ artikel/ 110879-gearloese-moeller-fra-siemens-bliver-solgt-for-foerste-gang](http://ing.dk/artikel/110879-gearloese-moeller-fra-siemens-bliver-solgt-for-foerste-gang)) *Ing.dk*), August 2010, link visited 28/02/2012
- [14] Next generation wind turbine; How It Works: Gearless wind Turbine ([http:// www. popsci. com/ technology/ article/ 2010-03/ next-gen-wind-turbine](http://www.popsci.com/technology/article/2010-03/next-gen-wind-turbine)), link visited 28/02/2012
- [15] Steven Chu. “Critical Materials Strategy” ([http://energy.gov/sites/prod/files/ DOE_CMS_2011. pdf](http://energy.gov/sites/prod/files/DOE_CMS_2011.pdf)), link visited 28/12/2012
- [16] G. L. Johnson; “Wind energy system”, Prentice-hall, England, 1985
- [17] Cardirci and M. Ermis; “Double output induction generator operating at synchronous and sub synchronous speeds: steady state performance, optimization and wind energy recovery”, IEE, vol. 139 (Proc-B), no. 9. 1992

INDUCTION GENERATOR MODEL FOR WIND-FARM APPLICATIONS

- [18] Henk Polinder, Frank F. A. Van der Pijl, Gert-Jan de Vilder and Perter J. Tavner, “ Comparison of Direct-Drive and Geared Generator Concepts for Wind Turbines“, IEEE Transactions on Energy Conversion, Vol. 21, No. 3, pp. 725-33, 2006
- [19] Detlef Schulz, Rolf Hanitsch, Karim Mountawakkil and Christoph Saniter, “Power Quality Behavior of Large Wind Parks with Variable Speed Wind Energy Converter”, 17th International Conference on Electricity Distribution, paper No. 28, Barcelona, 2003
- [20] Muljadi, E.; Butterfield, C.P.; Romanowitz, H.; Yinger, R.; “Self-Excitation and Harmonics in Wind Power Generation,” Transactions of ASME, *Journal of Solar Energy Engineering*, Vol. 127, pp. 581-587. 2005
- [21] Tleis, N. “Power System modelling and fault analysis-Theory and Practice”, Newness/Elsevier Ltd, 2008
- [22] C. M. Ong, “Dynamic Simulation of Electric Machinery using Matlab/Simulink”, Prentice Hall PTR (Pearson Education), 1998
- [23] R. Krishnan, “Electric Motor Drives – Modelling, Analysis, and Control”, Prentice Hall 2001
- [24] C. M. Ong; “Dynamic Simulation of Electric Machinery using Matlab/Simulink”, Prentice Hall, PTR (Pearson Education), 1998
- [25] P. Vas; “Electrical Machines and Drives – A Space Vector Theory Approach”, Oxford Science publications, 1992
- [26] R. Krishnan, “Electric Motor Drives – Modelling, Analysis, and Control”, Prentice Hall, 2001
- [27] J.B. Ekanayake, L. Holdsworth, and N. Jenkins, “Comparison of 5th Order and 3rd Order Machine Models for Doubly Fed Induction Generator (DFIG) Wind

INDUCTION GENERATOR MODEL FOR WIND-FARM APPLICATIONS

- Turbines”, Electric Power Systems Research 67(2003)207-215, available online at www.sciencedirect.com, link visited 05/03/2012
- [28] L. S. Barros, W.S. Mota, and D.F.P. Moura, “Matrix Method to Linearization and State Space Representation of Power Systems Containing Doubly Fed Induction Machines Operating as Wind Generators”, IEEE/PES, Transmission & Distribution Conference and Exposition; Latin America, TDC '06, 2006
 - [29] P. Ledesma, “Doubly Fed Induction Generator Model for Transient Stability Analysis”, IEEE Transactions on Energy Conversion, Vol. 20, No.2, 2005
 - [30] Almeida. R, Lopes. J. A, and Barreiros. J.A; “Improving Power System Dynamic Behaviour Through Double Fed Induction Machines Controlled by Static Converter Using Fuzzy Control”; IEEE, Transactions on Power Systems, vol. 19, no. 4, 2004
 - [31] Burton. T, Sharpe. D, Jenkins. N and Bossanyi. E; “Wind Energy Hand Book”, John Wiley & Sons, 2001
 - [32] W. H. Kersting and W. H. Phillips; “Phase frame analysis of the effect of voltage unbalance on an induction machine” IEEE, Transactions on Industry Application, vol. 33, no. 2, pp. 415-420, 1997
 - [33] I. Boldea, “Variable Speed Generators”, CRC, 2006
 - [34] The Mathworks Inc., “Simpower system™ 5 Reference”, 2009
 - [35] www.michellehenry.fr/windfarm.htm

7. CONCLUSIONS AND FUTURE WORK

7.1 Conclusions

- An obvious advantage of fast-microprocessor is the availability to use advanced numerical techniques on a laptop computer and this has accelerated the developments in the field of digital simulation models. The need for accurate predictions of harmonic distortion in the power system has required the development of simulation models for the complete electric network. On the other hand the increased demand of electricity has called for new renewable energy sources. The compatibility of these new sources with the existing power network is a major issue today. A general overview of network harmonics and distributed energy networks is presented in the introductory chapter of this thesis.
- The effect of connecting a new wind based power plant to a local substation can cause adverse effects. At the point of common coupling (PCC), severe harmonic voltage distortion can be caused. Wind generators connected to the PCC by means of electronic power converters inject harmonics, whereas the direct drives create trouble by trying to shift the system frequency. Therefore, it is extremely important to have all the aspects of harmonic impedance defined for such an inter-connections. A concise overview about harmonic impedance, at the point of common coupling, has been given in a preliminary chapter (chapter 2) of this thesis. The analysis however is limited to low and medium voltage levels, thus aiming at the modelling of small wind based microgrids.
- The combination of different periodic functions has to be approximated to for harmonic domain analysis by using trigonometric functions. The Fourier series is probably the best technique to build up this combination. However, in certain

CONCLUSIONS AND FUTURE WORK

circumstances, there are some other methods which can provide faster and better solution. A brief discussion on the topic is given in chapter 3.

- In order to incorporate the transformer's periodic nonlinear behaviour in the analysis of power systems, the effect of magnetic saturation must be precisely calculated. At the same time, the transformer model should also provide a convenient interface to the external network. In case of a three-phase transformer, the model should have the choice of representation for the 'star' (Wye) and 'delta' (Δ) winding connections. More importantly, the derived model should fit easily into a computer programme which can be compiled, executed and run in a reasonable period of time. A synchronous generator model in the harmonic domain should bear all the afore mentioned characteristics. Additionally, this model should also stand for the frequency conversion effect, which is the other key phenomenon of harmonic interaction between the stator and the rotor, besides saturation. Covering all these aspects a generalised harmonic domain model for each of these power system network components has been presented in chapter 4 and chapter 5 respectively.
- The integration of wind-based units with the distribution systems has become one the most important aspect in recent years. If properly modelled, an induction generator is probably the most feasible choice in a wind-based application. Other than previously stated requirements, an induction generator model should have a separate wind turbine model slotted inside the induction generator model, which can counter the change in physical parameters like variable wind speed and blade pitch angle. Chapter 6 describes a model of the induction generator for wind-farm applications, which takes account of these requirements.

7.2 Future work

This present research work is anticipated as a significant step forward towards a detailed harmonic domain model of the fundamental components in 'wind-based power'. It is expected that the basis has already been set in the harmonic domain, that will allow it to

CONCLUSIONS AND FUTURE WORK

be expanded in several directions. The author hopes that these suggestions offered for further research will result in interesting material for future contributions. The following may be a way forward and important directions are suggested:

- It has been shown that the position of the knee point in the magnetising characteristic of a power transformer has considerable effect on the over all harmonic distortion produced. In fact, it can significantly reduce the harmonic content. This point should be taken into account at the early design stage. With the power systems already in operation, the replacement of a transformer would be costly, therefore alternative options should be investigated first. The author recommends real-time monitoring of the harmonic domain results, to check whether a transformer or any other machine with a magnetic nonlinearity is operating in ‘deep’ saturation. If so, a re-distribution of the harmonic flows can be investigated to minimise the effect at critical nodes.
- The computation time for harmonic domain solutions depends upon the number of iterations for convergence and the arithmetic calculations during the iterative process. Any numerical technique which can better handle matrix manipulation, will speed-up the iterative process and reduce the convergence difficulties present in the harmonic domain.
- A synchronous generator is inductive in nature. In a real network, the different admittance matrix models need to be carefully checked for any capacitive loads attached to the generator, such that the level of harmonic distortion due to a possible resonant condition between the generator and the capacive load attached can be properly analysed. The reader has the choice to use either the ‘Fourier domain’ or the ‘Hartley domain’ admittance matrices for this purpose.
- The base induction generator model can be extended to enable a variable-speed induction generator model. Although the induction generator model takes the input from a wind turbine model, it does not however include the power electronic

CONCLUSIONS AND FUTURE WORK

converter model. A harmonic domain model for power electronic equipment used in wind units is the next step towards a complete set of solutions. These rotating machines and transformers, together with power electronic converter models, when added to harmonic domain model of the high voltage transmission lines will confirm a new software-based simulation facility to assess wind generation-based electrical power systems and their micro – grids.

APPENDIX I

MATLAB™ programme for the calculation of harmonic voltage magnitudes used to analyse study case described in *Chapter 4, Section 4.6*

Main

```
%
tol = 1e-12 ;
error = 1 ;
iter = 0;
harmonic_data_sp*1;
[YT] = build_up_Y*2(0,+0.0326,h);
[YL] = build_up_Y(0.0265,0.0626,h);
[YC] = build_up_Y(0,-0.2373,h);
[U] = build_up_Z*3(1,0,h);
[O] = build_up_Z(0,0,h);
[o] = zeros(2*h+1,1);
[D] = build_up_D*4(w,h);
while error == 1
    if iter > 0
        [Ynl,In,F] = harmonic_norton_equivalent*5(h,a,b,n,V2,D);
        if norm(F-F0) < tol ;
            error=0 ; break ;
        end
        F0 = F;
    end
    Ynetwork = [YT -YT O ; -YT (YT+Ynl+YL+YC) -YL ; O -YL (YL+YC) ];
    Inetwork = [V1 ; -In ; o ];
    pivot = [0 1 1];
    [Ynetwork] = Invert_matrix*6(Ynetwork,3,h,pivot);
    Vnetwork = Ynetwork*Inetwork;
    V2 = Vnetwork((2*h+1)+1:2*(2*h+1));
```

```

        iter = iter + 1;
    end
    iter
    V1
    V2
    V3 = Vnetwork(2*(2*h+1)+1:3*(2*h+1))

```

*1 *Harmonic Data (Single-phase Transformer)*

```

%
h = 15;
a = 0.03 ; b = 0.03 ; n = 9;
K = zeros(2*h+1,1) ; K(h+1) = a;
w = 1 ; f = 1 ; Emax = 1.1 ;
V1 = zeros(2*h+1,1) ; V1(h) = Emax'/2 ; V1(h+2) = Emax/2;
V2 = V1 ; V3 = V2;
Ynetwork = zeros(3*(2*h+1),3*(2*h+1));
Vnetwork = zeros(3*(2*h+1),1);
Inetwork = zeros(3*(2*h+1),1);
F0 = zeros(2*h+1,1);
In = zeros(2*h+1,1);
Ynl = zeros(2*h+1,2*h+1);

```

*2 *Admittance Matrix Y (Single-phase Transformer)*

```

%
function [Y] = build_up_Y(R,X,h)
Y = zeros(2*h+1,2*h+1);
n = 1;
for k = -h : h
    Z = R+i*k^(sign(X))*X;
    if (k == 0) && (R == 0);
        Y(n,n) = i*1e9;
    end
    n = n + 1;
end

```



```

else
    Y(n,n) = 1/Z;
end
n = n + 1;
end

```

*3 *Impedance Matrix Z (Sigle-phase Transformer)*

```

%
function [Z] = build_up_Z(R,X,h)
Z = zeros(2*h+1,2*h+1);
n = 1;
for k = -h : h
    Z(n,n) = R + i*k^(sign(X))*X;
    n = n + 1;
end
Z(h+1,h+1) = R + 1e-9;

```

*4 *Operational Derivative Matrix D (Single-phase Transformer)*

```

%
function [D] = build_up_D(w,h)
D = zeros(2*h+1,1);
n = 1;
for k = -h : h
    D(n,n) = i*k^(sign(w))*w;
    n = n + 1;
end
D(h+1,h+1) = i*1e-9;

```

*5 *Harmonic Norton Equivalent (Single-phase Transformer)*

```
%
function [Ynl,In,F] = harmonic_norton_equivalent(h,a,b,n,V2,D)
K = zeros(2*h+1,1) ; K(h+1) = a;
%
psi1 = inv(D)*V2;
[psi2] = self_convolution*7(psi1,h);
[psi4] = self_convolution(psi2,h);
[psi8] = self_convolution(psi4,h);
[psi9] = mutual_convolution*8(psi1,psi8,h);
F = a*psi1 + b*psi9;
DF = K + b*n*psi8;
DF = Toeplitz_matrix*9(DF,h);
Ynl = DF*inv(D);
In = (F-Ynl*V2);
```

*6 *Invert Matrix (Single-phase Transformer)*

```
%
function [A] = Invert_matrix(A,N,h,pivot)
for ii = 1 : N
    if pivot(ii) > 0
        A1 = A((ii-1)*(2*h+1)+1:ii*(2*h+1),(ii-1)*(2*h+1)+1:ii*(2*h+1));
        A1 = inv(A1);
        A((ii-1)*(2*h+1)+1:ii*(2*h+1),(ii-1)*(2*h+1)+1:ii*(2*h+1)) = A1;
    for jj = 1 : N
        if ii ~= jj
            A2 = A((jj-1)*(2*h+1)+1:jj*(2*h+1),(ii-1)*(2*h+1)+1:ii*(2*h+1));
            A2 = A2*A1;
            A((jj-1)*(2*h+1)+1:jj*(2*h+1),(ii-1)*(2*h+1)+1:ii*(2*h+1)) = A2;
        for kk = 1 : N
```

```

        if kk ~= ii
            A3 = A((jj-1)*(2*h+1)+1:jj*(2*h+1),(kk-1)*(2*h+1)+1:kk*(2*h+1));
            Aa = A((ii-1)*(2*h+1)+1:ii*(2*h+1),(kk-1)*(2*h+1)+1:kk*(2*h+1));
            A3 = A3 - A2*Aa;
            A((jj-1)*(2*h+1)+1:jj*(2*h+1),(kk-1)*(2*h+1)+1:kk*(2*h+1)) = A3;
        end
    end
end
end
for jj = 1 : N
    if ii ~= jj
        A4 = A((ii-1)*(2*h+1)+1:ii*(2*h+1),(jj-1)*(2*h+1)+1:jj*(2*h+1));
        A4 = -A1*A4;
        A((ii-1)*(2*h+1)+1:ii*(2*h+1),(jj-1)*(2*h+1)+1:jj*(2*h+1)) = A4;
    end
end
end
end
end

```

*7 *Self Convolution (Single-phase Transformer)*

```

%
function [Vec2] = self_convolution(Vec,h)
Vec1 = Vec;
[Tpz] = Toeplitz_matrix(Vec1,h);
Vec2 = Tpz*Vec;

```

*8 *Mutual Convolution (Single-phase Transformer)*

```

%
function [Vec3] = mutual_convolution(Vec1,Vec2,h)
[Tpz] = Toeplitz_matrix(Vec1,h);
Vec3 = Tpz*Vec2;

```

*9 *Toeplitz Matrix (Single-phase Transformer)*

```

%
function [Tpz] = Toeplitz_matrix(Vec,h)
Tpz(2*h+1,2*h+1) = zeros;
jj = h+1;
for ii = 1 : h+1
    ll = jj;
    for kk = 1 : jj
        Tpz(ii,kk) = Vec(ll);
        ll = ll - 1;
    end
    jj = jj + 1;
end
jj = 2;
for ii = h+2 : 2*h+1
    ll = 2*h+1;
    for kk = jj : 2*h+1
        Tpz(ii,kk) = Vec(ll);
        ll = ll - 1;
    end
    jj = jj + 1;
end
end

```

APPENDIX II

The functions in MATLABTM for the calculation of harmonic voltage magnitudes used in the analyses of study case described in *Section 4.8, Chapter 4*.

Main

```
%
tol = 1e-12 ;
error = 1 ;
iter = 0;
harmonic_data_tp*10;
[z] = zeros(3*(2*h+1),1);
[O] = build_up_Z*11(0,0,h);
[YT] = build_up_Y*12(0,+0.0326,h);
[Yt] = [YT O O ; O YT O ; O O YT];
[YL] = build_up_Y(0.0265,0.0626,h);
[Yl] = [YL O O ; O YL O ; O O YL];
[YC] = build_up_Y(0,-0.2373,h);
[Yc] = [YC O O ; O YC O ; O O YC];
[o] = [O O O ; O O O ; O O O];
[D] = build_up_D*13(w,h);
while error == 1
    if iter > 0
        [Ynl,In,F] = harmonic_norton_equivalent_tp*14(h,a,b,n,V2,D);
        if norm(F-F0) < tol ; error=0 ; break ; end
        F0 = F;
    end
    Ynetwork = [Yt -Yt o ; -Yt (Ynl+Yt+Yl+Yc) -Yl ; o -Yl (Yl+Yc) ];
    Inetwork = [V1 ; -In ; z ];
    pivot = [0 1 1];
    [Ynetwork] = Invert_matrix_tp*15(Ynetwork,3,h,pivot);
```

```

Vnetwork = Ynetwork*Inetwork;
V2 = Vnetwork(3*(2*h+1)+1:6*(2*h+1));
iter = iter + 1;
end
iter
V1
V2
V3 = Vnetwork(6*(2*h+1)+1:9*(2*h+1))
V1_Phase_a = V1(1:31);
V1_Phase_b = V1(32:62);
V1_Phase_c = V1(63:93);
V2_Phase_a= V2(1:31);
V2_Phase_b= V2(32:62);
V2_Phase_c = V2(63:93);
V3_Phase_a = V3(1:31);
V3_Phase_b = V3(32:62);
V3_Phase_c = V3(63:93);

```

*10 ***Harmonic Data (Three-phase Transformer)***

```

%
h = 15;
w = 1 ; f = 1;
a(1) = 0.03 ; b(1) = 0.03 ; n(1) = 9;
K1 = zeros(2*h+1,1) ; K1(h+1) = a(1);
a(2) = 0.03 ; b(2) = 0.03 ; n(2) = 9;
K2 = zeros(2*h+1,1) ; K2(h+1) = a(2);
a(3) = 0.03 ; b(3) = 0.03 ; n(3) = 9;
K3 = zeros(2*h+1,1) ; K3(h+1) = a(3);
Emax1 = 1.1;
Emax2 = 1.1*(cos(240*pi/180)+i*sin(240*pi/180));
Emax3 = 1.1*(cos(120*pi/180)+i*sin(120*pi/180));

```

```

V1 = zeros(3*(2*h+1),1);
V1(h) = Emax1'/2 ; V1(h+2) = Emax1/2;
V1((2*h+1)+h) = Emax2'/2 ; V1((2*h+1)+(h+2)) = Emax2/2;
V1(2*(2*h+1)+h) = Emax3'/2 ; V1(2*(2*h+1)+(h+2)) = Emax3/2;
V2 = V1 ; V3 = V2;
Ynetwork = zeros(3*3*(2*h+1),3*3*(2*h+1));
Vnetwork = zeros(3*3*(2*h+1),1);
Inetwork = zeros(3*3*(2*h+1),1);
F = zeros(3*(2*h+1),1);
F0 = zeros(3*(2*h+1),1);
In = zeros(3*(2*h+1),1);
Ynl = zeros(3*(2*h+1),3*(2*h+1));

```

*11 *Impedance Matrix Z (Three-phase Transformer)*

```

%
function [Z] = build_up_Z(R,X,h)
Z = zeros(2*h+1,2*h+1);
n = 1;
for k = -h : h
    Z(n,n) = R + i*k^(sign(X))*X;
    n = n + 1;
end
Z(h+1,h+1) = R + 1e-9;

```

*12 *Admittance Matrix Y ((Three-phase Transformer)*

```

%
function [Y] = build_up_Y(R,X,h)
Y = zeros(2*h+1,2*h+1);
n = 1;
for k = -h : h
    Z = R+i*k^(sign(X))*X;

```

```

if (k == 0) && (R == 0);
    Y(n,n) = i*1e9;
else
    Y(n,n) = 1/Z;
end
n = n + 1;
end

```

*13 ***Operational Derivative Matrix D (Three-phase Transformer)***

```

%
function [D] = build_up_D(w,h)
D = zeros(2*h+1,1);
n = 1;
for k = -h : h
    D(n,n) = i*k^(sign(w))*w;
    n = n + 1;
end
D(h+1,h+1) = i*1e-9;

```

*14 ***Harmonic Norton Equivalent for Three-phase Transformer***

```

%
function [Ynl,In,F] = harmonic_norton_equivalent_tp(h,a,b,n,V2,D)
F = zeros(3*(2*h+1),1) ; In = zeros(3*(2*h+1),1) ;
Ynl = zeros(3*(2*h+1),3*(2*h+1));
for ii = 1 : 3
    K = zeros(2*h+1,1) ; V = K;
    psi1 = K ; psi2 = K ; psi4 = K ; psi8 = K ; psi9 = K;
    F1b = K ; DF1b = K ; DFm = zeros(2*h+1,2*h+1);
    K(h+1) = a(ii);
    V = V2((ii-1)*(2*h+1)+1:ii*(2*h+1));
    psi1 = inv(D)*V;

```



```

[psi2] = self_convolution*16(psi1,h);
[psi4] = self_convolution(psi2,h);
[psi8] = self_convolution(psi4,h);
[psi9] = mutual_convolution*17(psi1,psi8,h);
F1b = a(ii)*psi1 + b(ii)*psi9;
F((ii-1)*(2*h+1)+1:ii*(2*h+1)) = F1b;
DF1b = K + b(ii)*n(ii)*psi8;
[DFm] = Toeplitz_matrix*18(DF1b,h);
Ynl((ii-1)*(2*h+1)+1:ii*(2*h+1),(ii-1)*(2*h+1)+1:ii*(2*h+1)) = DFm*inv(D);
In((ii-1)*(2*h+1)+1:ii*(2*h+1)) = (F1b-DFm*inv(D)*V);
end

```

^{*15} *Invert Matrix (Three-phase Transformer)*

```

%
function [A] = Invert_matrix_tp(A,N,h,pivot)
for ii = 1 : N
    if pivot(ii) > 0
        A1 = A(3*(ii-1)*(2*h+1)+1:3*ii*(2*h+1),3*(ii-1)*(2*h+1)+1:3*ii*(2*h+1));
        A1 = inv(A1);
        A(3*(ii-1)*(2*h+1)+1:3*ii*(2*h+1),3*(ii-1)*(2*h+1)+1:3*ii*(2*h+1)) = A1;
        for jj = 1 : N
            if ii ~= jj
                A2 = A(3*(jj-1)*(2*h+1)+1:3*jj*(2*h+1),3*(ii-1)*(2*h+1)+1:3*ii*(2*h+1));
                A2 = A2*A1;
                A(3*(jj-1)*(2*h+1)+1:3*jj*(2*h+1),3*(ii-1)*(2*h+1)+1:3*ii*(2*h+1)) = A2;
            for kk = 1 : N
                if kk ~= ii
                    A3 = A(3*(jj-1)*(2*h+1)+1:3*jj*(2*h+1),3*(kk-1)*(2*h+1)+1:3*kk*(2*h+1));
                    Aa = A(3*(ii-1)*(2*h+1)+1:3*ii*(2*h+1),3*(kk-1)*(2*h+1)+1:3*kk*(2*h+1));
                    A3 = A3 - A2*Aa;
                    A(3*(jj-1)*(2*h+1)+1:3*jj*(2*h+1),3*(kk-1)*(2*h+1)+1:3*kk*(2*h+1)) = A3;
                end
            end
        end
    end
end

```

```

        end
    end
end
end
for jj = 1 : N
    if ii ~= jj
        A4 = A(3*(ii-1)*(2*h+1)+1:3*ii*(2*h+1),3*(jj-1)*(2*h+1)+1:3*jj*(2*h+1));
        A4 = -A1*A4;
        A(3*(ii-1)*(2*h+1)+1:3*ii*(2*h+1),3*(jj-1)*(2*h+1)+1:3*jj*(2*h+1)) = A4;
    end
end
end
end
end

```

*16 *Self Convolution (Three-phase Transformer)*

```

%
function [Vec2] = self_convolution(Vec,h)
Vec1 = Vec;
[Tpz] = Toeplitz_matrix(Vec1,h);
Vec2 = Tpz*Vec;

```

*17 *Mutual Convolution (Three-phase Transformer)*

```

%
function [Vec3] = mutual_convolution(Vec1,Vec2,h)
[Tpz] = Toeplitz_matrix(Vec1,h);
Vec3 = Tpz*Vec2;

```

*18 *Toeplitz Matrix (Three-phase Transformer)*

```

%
function [Tpz] = Toeplitz_matrix(Vec,h)
Tpz(2*h+1,2*h+1) = zeros;

```

```
jj = h+1;
for ii = 1 : h+1
    ll = jj;
    for kk = 1 : jj
        Tpz(ii,kk) = Vec(ll);
        ll = ll - 1;
    end
    jj = jj + 1;
end
jj = 2;
for ii = h+2 : 2*h+1
    ll = 2*h+1;
    for kk = jj : 2*h+1
        Tpz(ii,kk) = Vec(ll);
        ll = ll - 1;
    end
    jj = jj + 1;
end
```

APPENDIX III

MATLAB™ functions used to compute synchronous generator admittance matrices; Y_{dq0} , $Y_{\alpha\beta\gamma}$ and Y_{abc} , in Fourier harmonic domain, with referenc to *Section 5.2, Chapter 5*.

Main

```
%  
function [Ydq0] = calc_Ydq0(data*19,h)  
h=3;  
hh=h+1;  
Ydq0 = zeros(hh*2+1, hh*2+1);  
[G,B]= calc_GB*20(0,data);  
Ydq0 = form_A*21(Ydq0,G+1i*B, hh+1, hh+1);  
for j=1:hh,  
    [G,B]= calc_GB(j,data);  
    Ydq0 = form_A(Ydq0,G+1i*B, hh+1-j, hh+1-j);  
    Ydq0 = form_A(Ydq0,G+1i*B, hh+1+j, hh+1+j);  
end  
Ydq0;
```

^{*19} Data (Synchronous Machine Ydq0)

```
%  
function data=dat_maql  
Rd=0.05; Rq=0.06; Ro=0.07;  
Rf=0.02; Rs=0.01; Rt=0.01;  
Ld=1.0; Lq=0.8; Lo=0.07;  
Lf=1.2; Ls=1.0; Lt=0.831;  
Mdf=0.9; Mds=1.0; Mqt=0.6; Mfs=1.0;  
data=[Rd,Rq,Ro,Rf,Rs,Rt,Ld,Lq,Lo,Lf,Ls,Lt,Mdf,Mds,Mqt,Mfs];  
data;
```

***20 Formation of Synchronous Machines Matrices Y (Admittance),
 G (Conductance) and B (Suceptance)**

```
%
function [G,B]=calc_GB(h,data)
Rd=data(1); Rq=data(2); Ro=data(3); Rf=data(4); Rs=data(5); Rt=data(6);
Ld=data(7); Lq=data(8); Lo=data(9); Lf=data(10); Ls=data(11); Lt=data(12);
Mdf=data(13); Mds=data(14); Mqt=data(15);
Mfs=data(16);
wr=1; w=1;
R11 = [Rd 0 0 ; 0 Rq 0 ; 0 0 Ro];
R22 = [Rf 0 0 ; 0 Rs 0 ; 0 0 Rt];
O = [0 0 0 ; 0 0 0 ; 0 0 0 ];
L11=[Ld 0 0 ; 0 Lq 0 ; 0 0 Lo];
L12=[Mdf Mds 0 ; 0 0 Mqt ; 0 0 0];
L21=[Mdf 0 0 ; Mds 0 0 ; 0 Mqt 0];
L22=[Ls Mfs 0 ; Mfs Ls 0 ; 0 0 Lt];
J11=[0 -Lq 0 ; Ld 0 0 ; 0 0 0];
J12=[0 0 -Mqt ; Mdf Mds 0 ; 0 0 0];
Z11=[R11+wr*J11+1i*(h*w*L11)];
Z12=[wr*J12+1i*(h*w*L12)];
Z21=[0+1i*(h*w*L21)]
Z22=[R22+1i*(h*w*L22)]
Y=inv(Z11-Z12*inv(Z22)*Z21)
G=real(Y)
B=imag(Y)
```

***21 Allocation of Matrix Elements**

```
%
function A=form_A(A,a,i,j)
I=(i-1)*3;
```

```

J=(j-1)*3;
A(I+1,J+1)=a(1,1);
A(I+1,J+2)=a(1,2);
A(I+1,J+3)=a(1,3);
A(I+2,J+1)=a(2,1);
A(I+2,J+2)=a(2,2);
A(I+2,J+3)=a(2,3);
A(I+3,J+1)=a(3,1);
A(I+3,J+2)=a(3,2);
A(I+3,J+3)=a(3,3);

```

22 *Synchronous Generator Admittance Matrix in $\alpha\beta\gamma$ Reference Frame (Fourier)

```

%
function Yabg=calc_Yabg(Ydq0,h)
hh=h+1;
C=zeros(hh*2+1, hh*2+1);
M=[1 1i 0; -1i 1 0; 0 0 0];
N=[1 -1i 0; 1i 1 0; 0 0 0];
D=[0 0 0; 0 0 0; 0 0 2];
C=form_A(C,D,1,1);
C=form_A(C,D,hh*2+1,hh*2+1);
C=form_A(C,D,hh+1,hh+1);
for j= 1:hh-1
    C=form_A(C,D,hh+1+j,hh+1+j);
    C=form_A(C,D,hh+1-j,hh+1-j);
    C=form_A(C,M,hh+1+j+1,hh+1+j+1);
    C=form_A(C,N,hh+1-j+1,hh+1-j+1);
end
C=C/2;

```

```
Yabg=C*Ydq0*(C');
Yabg = Yabg(4:hh*2*3,4:hh*2*3)
```

23 *Synchronous Generator Admittance Matrix in abc Reference Frame (Fourier)

```
%
function Yabc=calc_Yabc(Yabg,h,connection)
%connection: 0 for star, 1 for delta
% Form matrix T
a=1/2 ; b=sqrt(3)/2 ; c=1/3 ;
% d=sqrt(2/3) ;
Ti=[1 -a -a ; 0 b -b ; c c c];
T=zeros(2*h+1,2*h+1);
for j=1:2*h+1
    T=form_A(T,Ti,j,j);
end
% Form matrix Yabc
Yabc=(T')*Yabg*T;
% Change order of matrix Yabc
for j=1:3
    c=0;
    for k=j:2*h+j
        Y(k+(2*h)*(j-1),1:(2*h+1)*3)=Yabc(j+c,1:(2*h+1)*3);
        c=c+3;
    end
end
for j=1:3
    c=0;
    for k=j:2*h+j
        Yy(1:(2*h+1)*3,k+(2*h)*(j-1))=Y(1:(2*h+1)*3,j+c);
```

```

        c=c+3;
    end
end

```

For *Delta* Connection

```

% if connection==1
%   U=zeros(2*h+1,2*h+1);
%   for j=1:2*h+1
%       U(j,j)=1;
%   end
%   Q=[U -U 0*U ; 0*U U -U ; -U 0*U U];
%   Yabc=Q*Yy*Q;
% end
Yabc

```


APPENDIX IV

MATLABTM functions used to compute synchronous generator admittance matrices; Y_{dq0} , $Y_{\alpha\beta\gamma}$ and Y_{abc} , in the Hartley harmonic domain, with referenc to *Section 5.4, Chapter 5*.

Main

```
%  
function [Ydq0] = calc_Ydq0(data*19,h)  
hh=h+1;  
Ydq0 = zeros(hh*2+1, hh*2+1);  
[G,B]= calc_GB*24(0,data);  
Ydq0 = form_A*25(Ydq0,G+B,hh+1,hh+1);  
for j=1:hh,  
    [G,B]= calc_GB(j,data);  
    Ydq0 = form_A(Ydq0,G,hh+1-j,hh+1-j);  
    Ydq0 = form_A(Ydq0,G,hh+1+j,hh+1+j);  
    Ydq0 = form_A(Ydq0,-B,hh+1-j,hh+1+j);  
    Ydq0 = form_A(Ydq0,B,hh+1+j,hh+1-j);  
end
```

^{*24} ***Formation of Synchronous Machines Matrics Y (Admittance),***

G (Conductance) and B (Suceptance)

```
%  
function [G,B]=calc_GB(h,data)  
Rd=data(1); Rq=data(2); Ro=data(3);  
Rf=data(4); Rs=data(5); Rt=data(6);  
Ld=data(7); Lq=data(8); Lo=data(9);  
Lf=data(10); Ls=data(11); Lt=data(12);  
Mdf=data(13); Mds=data(14); Mqt=data(15);  
Mfs=data(16);  
wr=1; w=1;
```

```

R11 = [Rd 0 0 ; 0 Rq 0 ; 0 0 Ro];
R22 = [Rf 0 0 ; 0 Rs 0 ; 0 0 Rt];
O = [0 0 0 ; 0 0 0 ; 0 0 0 ];
L11=[Ld 0 0 ; 0 Lq 0 ; 0 0 Lo];
L12=[Mdf Mds 0 ; 0 0 Mqt ; 0 0 0];
L21=[Mdf 0 0 ; Mds 0 0 ; 0 Mqt 0];
L22=[Ls Mfs 0 ; Mfs Ls 0 ; 0 0 Lt];
J11=[0 -Lq 0 ; Ld 0 0 ; 0 0 0];
J12=[0 0 -Mqt ; Mdf Mds 0 ; 0 0 0];
Z11=[R11+wr*J11 h*w*L11 ; -h*w*L11 R11+wr*J11];
Z12=[wr*J12 h*w*L12 ; -h*w*L12 wr*J12];
Z21=[O h*w*L21 ; -h*w*L21 O];
Z22=[R22 h*w*L22 ; -h*w*L22 R22];
Y=inv(Z11-Z12*inv(Z22)*Z21);
G=Y(1:3,1:3);
B=Y(4:6,1:3);

```

*25 *Allocation of Matrix Elements*

```

%
function A=form_A(A,a,i,j)
I=(i-1)*3;
J=(j-1)*3;
A(I+1,J+1)=a(1,1);
A(I+1,J+2)=a(1,2);
A(I+1,J+3)=a(1,3);
A(I+2,J+1)=a(2,1);
A(I+2,J+2)=a(2,2);
A(I+2,J+3)=a(2,3);
A(I+3,J+1)=a(3,1);
A(I+3,J+2)=a(3,2);
A(I+3,J+3)=a(3,3);

```

***26 Synchronous Generator Admittance Matrix in $\alpha\beta\gamma$ Reference Frame (Hartley)**

```
%
function Y $\alpha\beta\gamma$ =calc_Y $\alpha\beta\gamma$ (Ydq0,h)
h=3;
hh=h+1;
C=zeros(hh*2+1,hh*2+1);
U=[1 0 0;0 1 0;0 0 1];
M = [0 1 0;-1 0 0; 0 0 0];
N=U+M;
D=[0 0 0;0 0 0;0 0 2];
C=form_A(C,D,1,1);
C=form_A(C,D,hh*2+1,hh*2+1);
C=form_A(C,D,hh+1,hh+1);
for j= 1:hh-1
    C=form_A(C,D,hh+1+j,hh+1+j);
    C=form_A(C,D,hh+1-j,hh+1-j);
    C=form_A(C,U,hh+1+j+1,hh+1+j);
    C=form_A(C,U,hh+1-j,hh+1-j-1);
    C=form_A(C,U,hh+1+j,hh+1+j+1);
    C=form_A(C,U,hh+1-j-1,hh+1-j);
    C=form_A(C,M',hh+1-j,hh+1+j+1);
    C=form_A(C,M',hh+1+j+1,hh+1-j);
    C=form_A(C,M,hh+1+j,hh+1-j-1);
    C=form_A(C,M,hh+1-j-1,hh+1+j);
end
C=form_A(C,N,hh+1,hh+1-1);
C=form_A(C,N,hh+1-1,hh+1);
C=form_A(C,N',hh+1,hh+1+1);
C=form_A(C,N',hh+1+1,hh+1);
```

```

C=C/2;
Y $\alpha\beta\gamma$  = C*Ydq0*(C');
Y $\alpha\beta\gamma$  = Y $\alpha\beta\gamma$ (4:hh*2*3,4:hh*2*3);

```

27 *Synchronous Generator Admittance Matrix in abc Reference Frame (Hartley)

```

%
h=3;
a=1/2 ; b=sqrt(3)/2 ; c=1/sqrt(2) ; d=sqrt(2/3) ;
Ti=d*[1 -a -a ; 0 b -b ; c c c];
T=zeros(2*h+1,2*h+1);
for j=1:2*h+1
    T=form_A(T,Ti,j,j);
end
Yabc=(T')*Yabg*T;
for j=1:3
    c=0;
    for k=j:2*h+j
        Y(k+(2*h)*(j-1),1:(2*h+1)*3)=Yabc(j+c,1:(2*h+1)*3);
        c=c+3;
    end
end
for j=1:3
    c=0;
    for k=j:2*h+j
        Yy(1:(2*h+1)*3,k+(2*h)*(j-1))=Y(1:(2*h+1)*3,j+c);
        c=c+3;
    end
end
end

```

APPENDIX V

MATLABTM functions used to calculate the total active and reactive power of a wind turbine using an induction generator; *Section 6.2, Chapter 6.*

Main

%

function Model_IG

global Vsa Vsb Vsc Vs0 Vs1 Vs2 Zero Pos Neg Zero0 Pos0 Neg0 Vr0 Vr1 Vr2 p P Fs
Rs Rr Lm Xm Zs Zs0 Zs1 Zs2 Ws Xr Xs s s0 s1 s2 Zr0 Zr1 Zr2 Zm Zn Zm0 Zm1 Zm2
Lg Xg Is0 Is1 Is2 Ir0 Ir1 Ir2 E0 E1 E2 Pm0 Pm1 Pm2 aseq Pm012 Wind_speed Wr bitta
Pm_3ph Vstator1 Vstator2 Vstator3

Wind_speed = 15; Wr = 1500*(2*pi/60); bitta = 0.2;

Windturbine_Model^{*28}

Pm012=Pm_3ph/3

Sbase = 1.5e6 ; Vbase = 2400 ; p = 4 ; P = 2*p ; Fs = 50 ; Rs = 0.03; Rr = 0.02;

Lls = 0.23/377 ; Llr = 0.23/377 ; Lm = 13.04/377 ; Lg = 0.345/377 ;

Xs=2*pi*50*Lls ; Xr = 2*pi*50*Llr ; Xm = 2*pi*50*Lm ; Xg = 2*pi*50*Lg ;

Zn = 0 ; Zm = 0 ;

Ws = 2*pi*Fs/p ;

s = (Ws-Wr)/Ws ; s0 = s ; s1 = s ; s2 = 2-s;

aseq = 1*(cos(2*pi/3)+ 1j*sin(2*pi/3)) ;

Vstator1 = 1 *(cos(1.036*(2*pi/360)) + 1j*sin(1.036*(2*pi/360))) ;

Vstator2 = 1 *(cos((1.036-120)*(2*pi/360))+ 1j*sin((1.036-120)*(2*pi/360))) ;

Vstator3 = 1 *(cos((1.036+120)*(2*pi/360))+1j*sin((1.036+120)*(2*pi/360))) ;

Vstator_Vbus_pu=[abs(Vstator1) , angle(Vstator1)*360/(2*pi); abs(Vstator2) ,
angle(Vstator2)*360/(2*pi) ; abs(Vstator3) ,angle(Vstator3)*360/(2*pi)]

Vsa = ((abs(Vstator1))*(Vbase/sqrt(3)))*complex(cos(angle(Vstator1)),sin(angle(Vstator1))) ;

Vsb = ((abs(Vstator2))*(Vbase/sqrt(3)))*complex(cos(angle(Vstator2)),sin(angle(Vstator2))) ;

Vsc = ((abs(Vstator3))*(Vbase/sqrt(3)))*complex(cos(angle(Vstator3)),sin(angle(Vstator3)));

Vsabc_SI = [abs(Vsa) ,angle(Vsa)*360/(2*pi); abs(Vsb),angle(Vsb)*360/(2*pi);abs(Vsc) ,
angle(Vsc)*360/(2*pi)]

```

Vs0 = (1/3)* ( Vs0 + Vs1 + Vs2 ) ;
Vs1 = (1/3)* ( Vs0 + (aseq*Vs2) + ((aseq^2)*Vs0) ) ;
Vs2 = (1/3)* ( Vs0 + ((aseq^2)*Vs2) + aseq*Vs0 ) ;
Vs012_SI = [abs(Vs0),angle(Vs0)*(360/(2*pi));abs(Vs1),
            angle(Vs1)*(360/(2*pi));abs(Vs2),angle(Vs2)*(360/(2*pi))] ;

Zs = Rs + 1i * Xs ;
Zs0 = Zs + 3*Zn + 3*Zm ; Zs1 = Zs - Zm ; Zs2 = Zs - Zm ;
Zr0 = complex(Rr/s0,Xr) + 3*Zn + 3*Zm ;
Zr1 = complex(Rr/s1,Xr)- Zm ;
Zr2 = complex(Rr/s2,Xr) - Zm ;
Zm0 = j*Xm + 3*Zn + 3*Zm ; Zm1 = j*Xm - Zm ; Zm2 = j*Xm - Zm ;
options = optimset ('Display','iter');
Zero0 = [-1e-5 , -1e-6 ]; Pos0 = [37.032 -40.229]; Neg0 = [-1e-4 , -0.1] ;
X0 = [-1e-5 , -1e-6 , 37.032 -40.229, -1e-4 , -0.1] ;
[X,fval] = fsolve( @myfunfr012^29, X0 , options);
Zero(1) = X(1);Zero(2) = X(2);
Pos(1) = X(3);Pos(2) = X(4);
Neg(1) = X(5);Neg(2) = X(6);
Vr0 = Zero(1)+ i * Zero(2); Vr1 = Pos(1) + i * Pos(2); Vr2 = Neg(1) + i * Neg(2);
Vs0 ;Is0 ; Ir0 ; E0 ; Vr0 ;
Vs1 ;Is1 ; Ir1 ; E1 ; Vr1 ;
Vs2 ;Is2 ; Ir2 ; E2 ; Vr2 ;
Vr_012 = [abs(Vr0), angle(Vr0)*(360/(2*pi));abs(Vr1),
          angle(Vr1)*(360/(2*pi));abs(Vr2), angle(Vr2)*(360/(2*pi))]
Vs_012 = [abs(Vs0),angle(Vs0)*(360/(2*pi));abs(Vs1),
          angle(Vs1)*(360/(2*pi));abs(Vs2),angle(Vs2)*(360/(2*pi))]
E_012 = [abs(E0),angle(E0)*(360/(2*pi));abs(E1),
          angle(E1)*(360/(2*pi));abs(E2),angle(E2)*(360/(2*pi))]
Ir_012 = [abs(Ir0),angle(Ir0)*(360/(2*pi));abs(Ir1),angle(Ir1)*(360/(2*pi));
          abs(Ir2),angle(Ir2)*(360/(2*pi))]

```

$$\begin{aligned}
Is_012 &= [abs(Is0), angle(Is0)*(360/(2*pi)); abs(Is1), angle(Is1)*(360/(2*pi)) ; \\
&\quad abs(Is2) , angle(Is2)*(360/(2*pi))] \\
Vsa &= Vs0 + Vs1 + Vs2 ; \\
Vsb &= Vs0 + Vs1 *(aseq^2) + Vs2 * aseq ; \\
Vsc &= Vs0 + Vs1 * aseq + Vs2 *(aseq^2) ; \\
Vsabc &= [abs(Vsa) , angle(Vsa)*(360/(2*pi)); abs(Vsb) , angle(Vsb)*(360/(2*pi)) ; \\
&\quad abs(Vsc) , angle(Vsc)*(360/(2*pi))] ; \\
Vra &= Vr0 + Vr1 + Vr2 ; \\
Vrb &= Vr0 + Vr1 * (aseq^2) + Vr2 * aseq ; \\
Vrc &= Vr0 + Vr1 * aseq + Vr2 *(aseq^2) ; \\
Vr_abc &= [abs(Vra) , angle(Vra)*(360/(2*pi)); \\
&\quad abs(Vrb) , angle(Vrb)*(360/(2*pi)) ; abs(Vrc) , angle(Vrc)*(360/(2*pi))] \\
Ira &= Ir0 + Ir1 + Ir2 ; \\
Irb &= Ir0 + (aseq^2*Ir1) + (aseq*Ir2) ; \\
Irc &= Ir0 + (aseq*Ir1) + ((aseq^2)*Ir2) ; \\
Ir_abc &= [abs(Ira) , angle(Ira)*(360/(2*pi)); abs(Irb) , angle(Irb)*(360/(2*pi)) ; \\
&\quad abs(Irc) , angle(Irc)*(360/(2*pi))] \\
Isa &= Is0 + Is1 + Is2 ; \\
Isb &= Is0 + (aseq^2*Is1) + (aseq*Is2) ; \\
Isc &= Is0 + (aseq*Is1) + ((aseq^2)*Is2) ; \\
Is_abc &= [abs(Isa) , angle(Isa)*(360/(2*pi)); abs(Isb) , angle(Isb)*(360/(2*pi)) ; \\
&\quad abs(Isc) , angle(Isc)*(360/(2*pi))] \\
Pm0 &= ((abs(Ir0)^2)*Rr)*((1-s0)/(s0))-(real(Vr0*conj(Ir0))*((1-s0)/(s0))); \\
Pm1 &= ((abs(Ir1)^2)*Rr)*((1-s1)/(s1))-(real(Vr1*conj(Ir1))*((1-s1)/(s1))); \\
Pm2 &= ((abs(Ir2)^2)*Rr)*((1-s2)/(s2))-(real(Vr2*conj(Ir2))*((1-s2)/(s2))); \\
Pm0_Pm1_Pm2 &= [Pm0 , Pm1 , Pm2] \\
Psa &= real (Vsa *conj(Isa)) ; Psb = real (Vsb *conj(Isb)) ; Psc = real(Vsc *conj(Isc)); \\
Qsa &= imag (Vsa *conj(Isa)) ; Qsb = imag (Vsb *conj(Isb)) ; Qsc = imag(Vsc *conj(Isc)); \\
Pra &= real (Vra *conj(Ira)) ; Prb = real (Vrb *conj(Irb)) ; Prc = real(Vrc *conj(Irc)); \\
Qra &= imag (Vra *conj(Ira)) ; Qrb = imag (Vrb *conj(Irb)) ; Qrc = imag(Vrc *conj(Irc)); \\
P_a &= Psa + Pra ; P_b = Psb + Prb ; P_c = Psc + Prc ;
\end{aligned}$$

```

Q_a = Qsa + Qra ; Q_b = Qsb + Qrb ; Q_c = Qsc + Qrc ;
P3ph_abc = P_a + P_b + P_c ;
Q3ph_abc = Q_a + Q_b + Q_c ;
S3ph_abc = P3ph_abc + j*Q3ph_abc ;
P_Q_abc_si = [P_a , Q_a , P_b , Q_b , P_c , Q_c ]
end

```

^{*28}***Turbine Model***

```

%
function [Pm_3ph] = Windturbine_Model (Wind_speed,Vr,bitta )
v_actual = Wwind_speed ;
Vr_actual = Vr ;
bitta = bitta ;
Pmec = 1500e3;
Pelec = 1500e3/0.9;
v_base = 12;
Vr_base = (1800) * (2*pi/60);
Vt_base = 1.2 * Vr_base;
Pmec_max_base_wind=0.73*Pmec ;
Pem = 1.01054 ;
lambda_base = 8.10 ;
Cp_base = 0.48 ;
c1 = 0.5176 ; c2 = 116 ; c3 = 0.4 ; c4 = 5 ; c5 = 21 ; c6 = 0.0068;
Vr_pu = Vr_actual / Vr_base ;
Vt_pu = Vr_pu *Vr_base / Vt_base ;
v_pu = v_actual / v_base ;
lambda_pu = Vt_pu / v_pu ;
lambda_actual = lambda_pu * lambda_base ;
lambda_i = 1/(1/(lambda_actual+0.08*bitta)-0.035/(bitta^3+1));
Cp_actual = c1*(c2/lambda_i-c3*bitta-c4)*exp(-c5/lambda_i)+c6*lambda_actual ;
Cp_pu = Cp_actual / Cp_base ; Pwind_pu = (v_pu)^3 ; Pmec_pu = Cp_pu * Pwind_pu ;

```



```

Pelec_pu = Pmec_pu * ( Pmec_max_base_wind / Pelec ) ;
Pelec_actual = (-1) * Pelec_pu * Pelec ;
Pm_3ph = Pem*Pelec_actual; Pm_1ph = Pm_3ph/3;
Vr = Vr_actual ;

```

****29 Function for Power Balance***

```

%
function F = myfunfr012(X)
global Vs0 Rs Rr Zs0 s0 Zr0 Zm0 Is0 Ir0 E0 Vr0 Vs1 Rs Rr Zs1 s1 Zr1 Zm1 Is1 Ir1 E1
Vs2 Rs Rr Zs2 s2 Zr2 Zm2 Is2 Ir2 E2 Pm012
Zero(1)= X(1); Zero(2)= X(2); Pos(1) = X(3); Pos(2) = X(4);
Neg(1) = X(5); Neg(2) = X(6);
Vr0 = Zero(1) + 1i * Zero(2);
E0 = ((Vs0/Zs0)+((Vr0/s0)/Zr0)) / ((1/Zs0) + (1/Zr0) + (1/(Zm0)));
Ir0 = ((Vr0/s0)-E0) / Zr0 ;
Is0 = (Vs0-E0) / Zs0 ;
Vr1 = Pos(1) + 1i * Pos(2);
E1 = ((Vs1/Zs1)+((Vr1/s1)/Zr1)) / ((1/Zs1) + (1/Zr1) + (1/(Zm1)));
Ir1 = ((Vr1/s1)-E1) / Zr1 ;
Is1 = (Vs1-E1) / Zs1 ;
Neg(1)
Neg(2)
Vr2 = Neg(1) + 1i * Neg(2);
E2 = ((Vs2/Zs2)+((Vr2/s2)/Zr2)) / ((1/Zs2) + (1/Zr2) + (1/(Zm2)));
Ir2 = ((Vr2/s2)-E2) / Zr2 ;
Is2 = (Vs2-E2) / Zs2 ;
F = (real(Vs0*conj(Is0))+ real(Vs1*conj(Is1)) + real(Vs2*conj(Is2)));
F = F - (abs (Is0)^2 * Rs + abs (Is1)^2 * Rs + abs (Is2)^2 * Rs) ;
F = F - ( abs (Ir0)^2 * Rr + abs (Ir1)^2 * Rr + abs (Ir2)^2 * Rr ) ;
F = F + (real((Vr0)*conj(Ir0)) + real((Vr1)*conj(Ir1))+ real((Vr2)*conj(Ir2)));
F = F - ((Pm012)) ;

```